2013

# Sensitivity and stability analysis of nonlinear Kalman filters with application to aircraft attitude estimation

Matthew Brandon Rhudy
*West Virginia University*

# SENSITIVITY AND STABILITY ANALYSIS OF NONLINEAR KALMAN FILTERS WITH APPLICATION TO AIRCRAFT ATTITUDE ESTIMATION

**by**
**Matthew Brandon Rhudy**
**Dissertation submitted to the**
**Benjamin M. Statler College of Engineering and Mineral Resources**
**at West Virginia University**
**in partial fulfillment of the requirements**
**for the degree of**

**Doctor of Philosophy**
**in**
**Aerospace Engineering**

**Approved by**

**Dr. Yu Gu, Committee Chairperson**
**Dr. John Christian**
**Dr. Gary Morris**
**Dr. Marcello Napolitano**
**Dr. Powsiri Klinkhachorn**

**Department of Mechanical and Aerospace Engineering**

**Morgantown, West Virginia**
**2013**

**Keywords: Attitude Estimation, Extended Kalman Filter, GPS/INS Sensor Fusion, Stochastic Stability**

## Abstract

**SENSITIVITY AND STABILITY ANALYSIS OF NONLINEAR KALMAN FILTERS WITH APPLICATION TO AIRCRAFT ATTITUDE ESTIMATION**

**by Matthew B. Rhudy**

State estimation techniques are important tools for analyzing systems that contain states that are not directly measureable. If the estimated states are used, for example, in place of the true states in a feedback controller, the accuracy and stability of the estimates becomes crucial for the safe and effective execution of the controller. This is especially important in aircraft control applications, where safety is an essential concern. Because of this, the stability characteristics of the state estimation are investigated. Additionally, two different nonlinear Kalman filters are considered and compared with respect to various design parameters.

This work considers the sensitivity and stability characteristics of nonlinear state estimation through the aircraft attitude estimation problem. This problem is approached using sensor information from Global Positioning System (GPS) and Inertial Navigation System (INS) in order to obtain estimates of the aircraft attitude angles. This case study uses experimentally collected flight data from subscale aircraft to derive estimation results. The goal of this work is to obtain a better understanding of the properties of nonlinear Kalman filters in order to make more informed decisions regarding the selection and tuning of these filters for different real-world applications.

## ACKNOWLEDGMENTS

This research was partially supported by NASA grant # NNX07AT53A, grant # NNX10AI14G, grant # NNX12AM56A, and NASA West Virginia Space Grant Consortium Graduate Fellowship.

I would like to thank my research advisor, Dr. Yu Gu, for his guidance and support throughout this project. Dr. Gu, your insight and technical advice provided me with great opportunities to succeed and really learn to think about various research problems. I greatly appreciate your time and effort spent providing me with both technical and career advice.

I would like to thank the other faculty members of the Flight Control Systems Laboratory, Dr. Marcello Napolitano, Dr. Srikanth Gururajan, Dr. Brad Seanor, and Dr. Haiyang Chao. Your assistance, particularly with the flight testing program, was invaluable to my research and professional growth.

I would also like to thank my committee members Dr. John Christian, Dr. Powsiri Klinkhachorn, and Dr. Gary Morris. Your discussions and feedback regarding this work were very helpful in improving its quality.

Current and former students of the research group, Frank Barchesky, Matteo Dariol, Giovanni DeNunzio, Jason Gross, Matteo Guerra, Tanmay Mandal, Kyle Lassak, Kerri Phillips, Daniele Tancredi, Amanda McGrail, your collaborative effort has helped me to become a better group member, leader, and mentor. Thank you. I would particularly like to acknowledge the contribution of Jason Gross, who offered a fantastic introduction into this research area, as well as many productive discussions allowing us to both further our understanding.

Finally, I would like to thank my wife, Stephanie, for supporting me throughout this process. Thank you for your love and support.

## TABLE OF CONTENTS

## LIST OF TABLES

## LIST OF FIGURES

## NOMENCLATURE

Acronyms

| | |
|---|---|
| BIBO | Bounded-Input Bounded-Output |
| CG | Center of Gravity |
| DCM | Direction Cosine Matrix |
| EKF | Extended Kalman Filter |
| EKO | Extended Kalman Observer |
| GPS | Flight Control Systems Laboratory |
| GPS | Global Positioning System |
| IMU | Inertial Measurement Unit |
| INS | Inertial Navigation System |
| LKF | Linear Kalman Filter |
| LTI | Linear Time-Invariant |
| MEMS | Micro-Electro-Mechanical Systems |
| NED | North-East-Down |
| UKF | Unscented Kalman Filter |
| WVU | West Virginia University |

English Symbols

| | |
|---|---|
| $\mathbf{K}$ | Kalman Gain Matrix |
| $\mathbf{P}$ | State Error Covariance Matrix |
| $\mathbf{Q}$ | Assumed Process Noise Covariance Matrix |
| $\mathbf{R}$ | Assumed Measurement Noise Covariance Matrix |
| $a_x$ | Acceleration in Aircraft Body x-direction |
| $a_y$ | Acceleration in Aircraft Body y-direction |
| $a_z$ | Acceleration in Aircraft Body z-direction |
| $p$ | Aircraft Body Roll Rate |
| $q$ | Aircraft Body Pitch Rate |
| $r$ | Aircraft Body Yaw Rate |
| $\mathbf{u}$ | Input Vector |
| $\mathbf{x}$ | State Vector |
| $\mathbf{y}$ | Output Vector |
| $\mathbf{z}$ | Measurement Vector |

Greek Symbols

| | |
|---|---|
| $\phi$ | Roll Angle |
| $\theta$ | Pitch Angle |
| $\psi$ | Yaw Angle |

# 1.0 INTRODUCTION

In many engineering applications, it is common for the mathematical system model to contain states that are not directly measureable. Because of this, state observers or state estimators become a necessary component of the system for applications such as full state feedback control [1], where it is essential for the estimation algorithm to be stable in order to achieve stable system response, although the system stability still may not be guaranteed. The stability of a state estimator is typically defined in terms of the convergence of the state estimate to the true state, or, in other words, the state estimate error converges to zero, or becomes bounded within some region near zero. This work investigates the stability of a nonlinear state estimator through the context of a particular application problem.

The Linear Kalman Filter (LKF) [2] is a commonly used state estimator for linear systems. This method has been proven to have exponentially stable state estimation error by various authors [3-7]. However, state estimators for nonlinear systems introduce additional difficulties, and therefore the stability is not as clearly defined. The current industry standard for nonlinear state estimation is the Extended Kalman Filter (EKF) [8]. As its name suggests, this method is an extension of the linear Kalman filtering framework, which utilizes a first order analytical linearization to handle the nonlinearities in the state. In many applications, the accuracy and stability of the EKF is sufficient. However, in some cases, typically those involving strong nonlinearity, the first order

linearization of the EKF is insufficient [9]. Because of this issue, the Unscented Kalman Filter (UKF) [10] was introduced in order to handle the nonlinearity using a statistical linearization method. Various simulation studies [10-13] establish the theoretical advantage of the UKF statistical linearization over the EKF analytical linearization for strong nonlinear equations. However, for practical applications, the advantage is not as clear, due to mixed results from different research groups.

Because of the inconsistencies in the existing research, a detailed comparison and sensitivity analysis was desired. Various work was done by the Flight Control Systems Laboratory (FCSL) and the Interactive Robotics Laboratory (IRL) at West Virginia University (WVU) regarding the comparison [14], sensitivity [15-17], and other theoretical analyses [18,19] investigating the differences between the EKF and UKF. Some of these results are also presented in Chapter 5 of this dissertation. While these results offered some insight into the differences in these two nonlinear filters, further work was necessary in order to analyze and evaluate the stability characteristics on the nonlinear state estimation problem.

Early stability analysis work for recursive filtering started with the work of Kalman, who introduced a minimum-variance linear estimator, which later came to be referred to as the Kalman filter [2]. The first Kalman filter stability proof was provided by Kalman, who derived the conditions for stability of the homogeneous filter equations for continuous systems [3]. Additionally for continuous time systems, Fitzgerald investigated the different causes of divergence in the linear Kalman filter [20]. Following the effort by Kalman for continuous time systems, Sorenson derived lower and upper bounds on the error covariance matrix for discrete-time systems, but did not present any

stability analysis [21]. Deyst and Price derived the sufficient conditions for uniform asymptotic stability of the discrete homogeneous linear minimum-variance estimation [4]. Jazwinski also presented a proof of the asymptotic stability of the discrete-time minimum variance linear estimator if certain controllability and observability conditions are met [6]. Following the work of Hitz *et al.* [22] who pointed out an error in the effort in [4,6] to establish estimation error covariance bounds, and Tse [23] who questioned the stability results, Deyst proposed a correction paper to address these issues [5]. Crassidis and Junkins provided a Lyapunov-based stability proof of the linear discrete-time Kalman filter [7].

Some other authors have also considered the stability and related issues for the linear Kalman filter. Guo established the convergence and stability properties of the linear stochastic time-varying parameter identification problem using a Kalman filter based technique [24]. Chan *et al.* discussed the convergence properties of solutions to the algebraic Riccati equation and the Riccati difference equation [25]. Costa and Astolfi provide the conditions for stability of the discrete-time Kalman filter for linear time-invariant (LTI) systems with respect to perturbations in the initial error covariance [26]. Moore and Anderson demonstrated techniques for handling singular state transition matrices for linear time-varying estimation and control stability analyses [27].

Using the linear Kalman filter stability work as a basis, various work has been done on the topic of Extended Kalman Filter (EKF) stability. Ljung analyzed, using techniques derived in [28], the asymptotic behavior of the EKF for continuous-time parameter identification of a linear system [29]. Baras *et al.* presented a method to derive dynamic observers as asymptotic limits of recursive filters for both linear and nonlinear

systems with no inputs and linear observations in continuous time [30]. Song and Grizzle provided a proof that the Kalman filter is a global observer for discrete-time linear time-varying systems, and expanded this result to show that the EKF is a quasi-local asymptotic observer [31] for deterministic discrete-time nonlinear systems with no inputs [32]. La Scala *et al.* expanded upon the work of Song and Grizzle [32], giving sufficient conditions for stability of the discrete-time EKF for a no input nonlinear system with linear observation equations. The frequency tracking problem was used as an example to demonstrate the bounds on the tracking error [33]. Boutayeb *et al*. presented a convergence analysis of the EKF for deterministic discrete-time nonlinear systems with inputs [34]. In [34], the deterministic case was considered, *i.e.*, no process or measurement noise, and therefore presented results in terms of an arbitrary „**R**" matrix, and introduced two additional matrices that are used to control the stability and convergence of the EKF. Xiong *et al*. presented a stability analysis of the UKF [35], which was later pointed out by Wu *et al*. [36] to apply to a more general set of filters, including the EKF. These results were extended by Xu *et al*. to handle correlated noise [37].

Several influential works on EKF stability were published in the late 1990"s by Konrad Reif with various co-authors [38-42]. First, Reif *et al*. proposed a modification to the continuous-time EKF that introduced an additive term of instability which is used to assign the degree of stability and effectively treat the nonlinearity [38]. Reif *et al*. later expanded this work and added a proof to show that the proposed observer was in fact an exponential observer using Lyapunov"s direct method [39]. In 1999, Reif *et al*. provided a detailed stability proof of the discrete-time EKF. This paper also provides a method for

calculating the required bounds on the initial state error and noise terms in order to maintain stability. It was shown and stated in this work that these bounds are very conservative, and may not be practical in application [40]. Reif and Unbehauen also presented a proof using the Lyapunov direct method that the EKF is an exponential observer for deterministic systems [41]. Reif *et al*. also provided a companion paper to [40] which offered similar stochastic stability discussion, however pertaining to the continuous-time EKF [42]. In a more recent paper, Kluge, Reif and Brokate reanalyzed the discrete-time EKF stochastic stability using the same principles as [40], but now consider the effect of intermittent observations, non-additive noise, and singular system Jacobian matrix [43].

Other authors have also considered the stability of the EKF with certain modifications [38,39]. Song and Speyer designed the modified gain EKF, which was shown to be globally stable. This filter was developed assuming a system with linear stochastic system dynamics, but a nonlinear stochastic measurement equation. Results were presented for this new filter as applied to the bearings only measurement problem [44]. Babacan *et al.* showed that under certain conditions the projection-based discrete-time EKF with equality constrained states is an exponential observer for deterministic systems, and also presented a modification to the EKF that increases the degree of stability and convergence speed [45]. Boutayeb and Aubry analyzed the stability of a strong tracking Extended Kalman Observer (EKO), where the deterministic case was considered, and the importance of the „**Q**“ and „**R**“ matrices as design parameters was emphasized [46].

## 1.1 OBJECTIVE

The objective of this study is to analyze the sensitivity and stability of nonlinear state estimation using the EKF through the example of attitude estimation using GPS/INS sensor fusion. First, the sensitivity of different design parameters is considered to obtain a better understanding of the problem. This analysis is then extended to investigate the convergence and stability characteristics of the algorithms. This work utilizes previous stability work of other authors as well as existing stability theory, in particular Lyapunov‟s direct method, in order to develop a new set of conditional requirements to ensure the stability of the state estimation. The primary goal of this work is to obtain a realistic set of stability requirements for the system that can be achieved with a real measurement system for practical application. This produces a confidence in the accuracy of the estimated states so that they can safely and reliably be used for various purposes including feedback control. This work aims to derive techniques for stability analysis that can be applied to any nonlinear state estimation problem using the EKF, with results presented in the context of the particular example application of attitude estimation.

## 1.2 ORGANIZATION

The rest of this dissertation is organized as follows. Chapter 2 presents the necessary background information for this work including a thorough review of stability theory and definitions, as well as an introduction to state estimation and the existing

corresponding stability analyses for both linear and nonlinear Kalman filtering. Chapter 3 introduces the studied application of nonlinear state estimation, attitude estimation using GPS/INS sensor fusion. Chapter 4 describes the details of the considered experimental flight testing platform, including an analysis and summary of the selected flight data. Chapter 5 presents a comparison and sensitivity analysis which studies the different effects of the Extended Kalman Filter (EKF) and Unscented Kalman Filter (UKF). Chapter 6 represents the core work of this dissertation, with a detailed analysis of the stability of the considered application of nonlinear state estimation. Finally, Chapter 7 summarizes and concludes this work, with some additional discussion regarding future directions of this research topic.

# 2.0 BACKGROUND INFORMATION

This chapter presents an outline of the necessary background information for this research study. First, the basic definitions of stability for continuous-time systems are discussed, followed by discussion of both linear and nonlinear continuous-time stability theory, including both of Lyapunov‟s methods: linearization and direct. Next, the corresponding theory is presented for linear and non-linear discrete-time systems. Then, the problem of nonlinear state estimation is presented, followed by sections detailing the linear discrete-time Kalman filter, Extended Kalman Filter (EKF), and Unscented Kalman Filter (UKF), including a detailed description of the current stability theory for these recursive filters.

## 2.1 STABILITY OF CONTINUOUS-TIME SYSTEMS

A simple but general form of a nonlinear dynamic system can be described by

$$\dot{\mathbf{x}}(t) = \mathbf{f}\left(\mathbf{x}(t), t\right) \tag{1}$$

where $\mathbf{x}$ is the ($n_x \times 1$) state vector and $\mathbf{f}$ is an ($n_x \times 1$) vector valued function. The explicit dependence on the continuous time variable, $t$, defines this system in general as a non-autonomous or time-varying system. Conversely, if the system is not an explicit function of time, it is called an autonomous or time-invariant system. Thus, the autonomous form of (1) is given by

$$\dot{\mathbf{x}}(t) = \mathbf{f}\left(\mathbf{x}(t)\right) \tag{2}$$

Although this form of system does not include a dependence on a control input, **u**, if this control input is determined through a set of control laws such that

$$\mathbf{u}(t) = \mathbf{g}\left(\mathbf{x}(t), t\right) \tag{3}$$

then the system can be rewritten in the form of (1). In the following paragraphs, the stability of the autonomous system (2) is discussed [47].

A state of the system, $\mathbf{x}^*$, is defined as an equilibrium state or point if it satisfies the equation

$$\mathbf{f}\left(\mathbf{x}^*(t)\right) = \mathbf{0} \tag{4}$$

where **0** is an ($n_x$ × 1) vector of zeros. A given system can have multiple equilibrium points. In fact certain systems, such as the system defining the motion of a simple pendulum, have an infinite number of equilibrium points [47].

The zero solution of the system, $\mathbf{x}(t) \equiv \mathbf{0}$, is a commonly considered equilibrium point for many systems, and is used as a basis for the discussion of stability. The zero solution is said to be Lyapunov stable if the state trajectory stays bounded within an $n_x$ dimensional hypersphere of radius $\delta$, *i.e.*, $\left\|\mathbf{x}(t)\right\|_2 < \delta$, given that the initial state is bounded within an $n_x$ dimensional hypersphere of radius $\varepsilon$, *i.e.*, $\left\|\mathbf{x}(0)\right\|_2 < \varepsilon$, where $\left\|\cdot\right\|_2$ is the $L_2$ norm of the vector [48], as calculated using

$$\left\|\mathbf{v}\right\|_2 = \sqrt{\sum_{i=1}^{n} v_i^2}, \quad \mathbf{v} = \begin{bmatrix} v_1 & v_2 & \dots & v_n \end{bmatrix}^T \tag{5}$$

In other words, the zero solution is considered Lyapunov stable if starting from a point sufficiently close to the origin, the state trajectory stays arbitrarily close to the origin.

Lyapunov stability is also sometimes referred to as "stable in the sense of Lyapunov" or "marginally stable" [49]. A further classification of stability that extends this concept is asymptotic stability. In addition to the requirement of Lyapunov stability, asymptotic stability requires that the state trajectory approaches the origin as time goes to infinity. A 2-dimensional qualitative example of these different types of stability is shown in Figure 1.

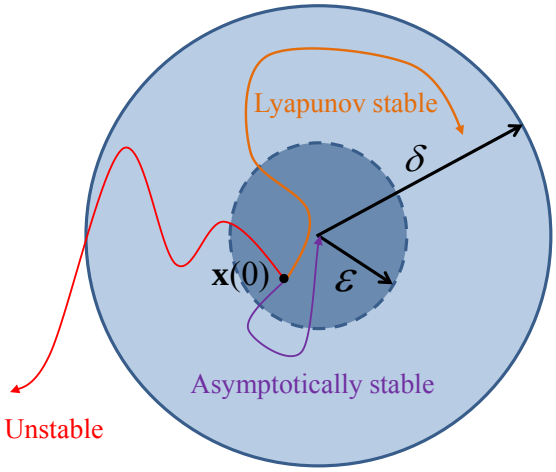


Figure 1. 2-D Illustration of Types of Local Stability

An even further classification of stability was defined for applications to systems where the rate of the state trajectory approaching the origin is important. This type of stability is called exponential stability, and exists for systems which satisfy

$$\|\mathbf{x}(t)\|_2 \leq \alpha \|\mathbf{x}(0)\|_2 e^{-\beta t}, \quad \alpha > 0, \quad \beta > 0 \tag{6}$$

This means that in order to have exponential stability, the state trajectory of the system must converge to the origin at a rate faster than that of an exponential function. A 1-dimensional example showing exponential stability is given in Figure 2. The classifications of stability up to this point describe local stability, *i.e.*, the behavior of the

system starting from an initial state close to the origin. Additionally, if a system is asymptotically or exponentially stable for any initial state, then this system is said to be globally asymptotically or exponentially stable [47,50,51].

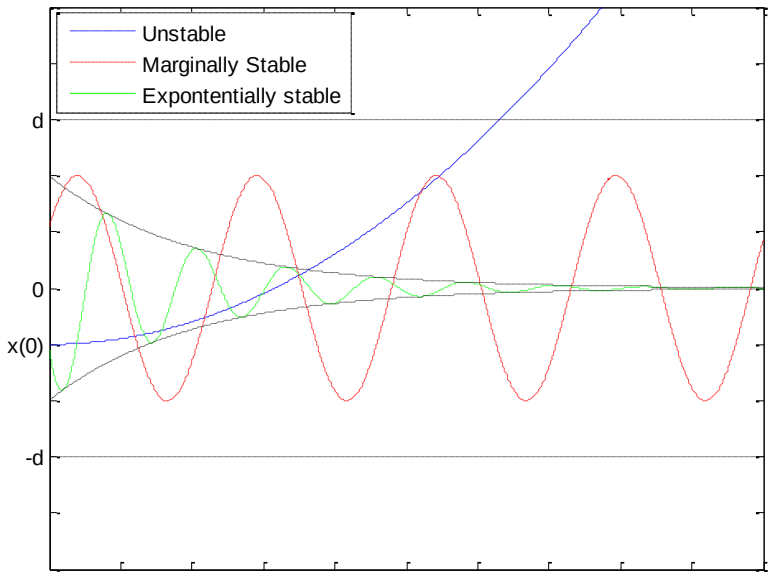


Figure 2. 1-D Illustration of Types of Local Stability

### 2.1.1 Stability of Continuous-Time Linear Systems

The standard format for a continuous-time linear state space system is given by

$$\begin{aligned} \dot{\mathbf{x}}(t) &= \mathbf{A}(t)\mathbf{x}(t) + \mathbf{B}(t)\mathbf{u}(t) \\ \mathbf{y}(t) &= \mathbf{C}(t)\mathbf{x}(t) + \mathbf{D}(t)\mathbf{u}(t) \end{aligned} \tag{7}$$

where **x** is the state vector, **y** is the output vector, **u** is the input vector, and **A**, **B**, **C**, and **D** are matrices describing the system. Although the **A**, **B**, **C**, and **D** matrices can in general be time varying, for linear time-invariant (LTI) systems they are constant. The stability of LTI systems is often separated into two components. The first consideration

is sometimes referred to as internal stability [49], and is defined by stability of the zero-input response of the system, *i.e.*, the response of

$$\dot{\mathbf{x}}(t) = \mathbf{A}\mathbf{x}(t) \tag{8}$$

to a nonzero initial condition x(0), whose solution is given by

$$\mathbf{x}(t) = e^{\mathbf{A}t}\mathbf{x}(0) \tag{9}$$

where $e^{\mathbf{A}t}$ is the matrix exponential, which is defined through its infinite series as

$$e^{\mathbf{A}t} = \mathbf{I} + \sum_{n=1}^{\infty} \frac{\mathbf{A}^n t^n}{n!} = \mathbf{I} + \mathbf{A}t + \frac{\mathbf{A}^2 t^2}{2!} + \frac{\mathbf{A}^3 t^3}{3!} + \ldots \tag{10}$$

where **I** is the identity matrix [52]. It is clear from (9) that for single state systems (or scalar systems) the solution will be exponentially stable if Re(**A**) < 0, and Lyapunov stable for Re(**A**) = 0, where Re(.) denotes the real part of a generally complex number. To extend this result to higher state dimensions, the matrix **A** is diagonalized using a similarity transformation [48]. To do this, the eigenvalues and eigenvectors of the matrix are calculated, then the matrix can be written as

$$\mathbf{A} = \mathbf{X}\mathbf{\Lambda}\mathbf{X}^{-1} \tag{11}$$

where **X** is the matrix of eigenvectors of **A**, and **Λ** is a diagonal matrix of the corresponding eigenvalues of **A**. Using (11), it can be shown that any polynomial of **A**, $p(\mathbf{A})$, can be expressed as

$$p(\mathbf{A}) = \mathbf{X}p(\mathbf{\Lambda})\mathbf{X}^{-1} \tag{12}$$

given that

$$\mathbf{A}^k = \prod_{i=1}^{k} \mathbf{A} = \mathbf{AA}...\mathbf{A} = \left(\mathbf{X}\Lambda\mathbf{X}^{-1}\right)\left(\mathbf{X}\Lambda\mathbf{X}^{-1}\right)...\left(\mathbf{X}\Lambda\mathbf{X}^{-1}\right) = \mathbf{X}\Lambda^k\mathbf{X}^{-1} \tag{13}$$

Therefore, since $e^{\mathbf{A}t}$ can be expressed as a polynomial of **A**, as in (10), using (12) it is clear that

$$e^{\mathbf{A}t} = \mathbf{X}e^{\Lambda t}\mathbf{X}^{-1} \tag{14}$$

A useful property of the matrix exponential is that diagonal matrix, **Λ**, the matrix exponential is simply a diagonal matrix of exponentials of the terms of **Λ** as in

$$\mathbf{\Lambda} = \begin{bmatrix} \lambda_1 & 0 & ... & 0 \\ 0 & \lambda_2 & 0 & ... \\ 0 & 0 & ... & 0 \\ 0 & ... & 0 & \lambda_n \end{bmatrix}, \qquad e^{\Lambda t} = \begin{bmatrix} e^{\lambda_1} & 0 & ... & 0 \\ 0 & e^{\lambda_2} & 0 & ... \\ 0 & 0 & ... & 0 \\ 0 & ... & 0 & e^{\lambda_n} \end{bmatrix} \tag{15}$$

Using this property, (8) can be shown to be marginally stable if all of the eigenvalues of **A** have zero or negative real part, and exponentially stable if all of the eigenvalues of **A** have strictly negative real part [49]. This type of matrix is called negative definite. The definiteness properties of matrices are discussed next.

An ($n \times n$) matrix **A** is said to be positive definite if [48]

$$\mathbf{x}^T\mathbf{A}\mathbf{x} > 0, \quad \mathbf{x} \neq \mathbf{0} \tag{16}$$

The positive definiteness of a matrix is also guaranteed if all of its eigenvalues are positive [49]. Similar matrix properties can be defined, and for simplicity are summarized in Table 1.

Table 1. Matrix Definiteness Properties

| Matrix Property | Definition | Eigenvalues |
|---|---|---|
| Positive Definite | $\mathbf{x}^T\mathbf{A}\mathbf{x} > 0, \quad \mathbf{x} \neq \mathbf{0}$ | Positive |
| Positive Semi-Definite | $\mathbf{x}^T\mathbf{A}\mathbf{x} \geq 0, \quad \mathbf{x} \neq \mathbf{0}$ | Non-Negative |
| Negative Definite | $\mathbf{x}^T\mathbf{A}\mathbf{x} < 0, \quad \mathbf{x} \neq \mathbf{0}$ | Negative |
| Negative Semi-Definite | $\mathbf{x}^T\mathbf{A}\mathbf{x} \leq 0, \quad \mathbf{x} \neq \mathbf{0}$ | Non-Positive |
| Indefinite | $\mathbf{x}^T\mathbf{A}\mathbf{x}\left(><=\right)^{?} 0, \quad \mathbf{x} \neq \mathbf{0}$ | Some Positive<br>Some Negative |

The definitions in Table 1 are given in the quadratic form [53]. A similar form is given by $\mathbf{B}^T\mathbf{A}\mathbf{B}$, where **B** is some ($n \times m$) matrix with $n \leq m$. If **B** has rank $n$ and **A** is positive definite, then $\mathbf{B}^T\mathbf{A}\mathbf{B}$ is also a positive definite matrix [49]. This property is an important tool for determining positive definiteness of various matrix operations.

An alternative approach to analyzing the zero-input stability of an LTI system uses the Lyapunov equation

$$\mathbf{A}^T\mathbf{M} + \mathbf{M}\mathbf{A} = -\mathbf{N} \tag{17}$$

where **N** is any given positive definite symmetric matrix. All eigenvalues of **A** have negative real part if and only if (17) has a unique symmetric solution **M**, and **M** is also positive definite. If all of the eigenvalues of A have negative real parts, then the solution of (17) can be given by

$$\mathbf{M} = \int_0^\infty e^{\mathbf{A}^T t}\mathbf{N}e^{\mathbf{A}t}dt \tag{18}$$

which is shown to be positive definite using

$$\mathbf{x}^T\mathbf{M}\mathbf{x} = \int_0^\infty \mathbf{x}^T e^{\mathbf{A}^T t}\tilde{\mathbf{N}}^T\tilde{\mathbf{N}}e^{\mathbf{A}t}\mathbf{x}dt = \int_0^\infty \left(\tilde{\mathbf{N}}e^{\mathbf{A}t}\mathbf{x}\right)^T\left(\tilde{\mathbf{N}}e^{\mathbf{A}t}\mathbf{x}\right)dt = \int_0^\infty \left\|\tilde{\mathbf{N}}e^{\mathbf{A}t}\mathbf{x}\right\|_2^2 dt > 0 \tag{19}$$

where **N** was decomposed into

$$\mathbf{N} = \tilde{\mathbf{N}}^T \tilde{\mathbf{N}} \tag{20}$$

which is valid since **N** is given as positive definite. Although (18) is a solution to the equation, (17) is more commonly solved by rearranging into a standard linear algebraic equation [49].

Another important consideration for LTI systems is the bounded-input bounded-output (BIBO) stability of the system, which is given by the zero-state response of (7). This form of stability is often analyzed through the input-output transfer matrix of the system, $\mathbf{G}(s)$, given by

$$\mathbf{G}(s) = \mathbf{C}(s\mathbf{I} - \mathbf{A})^{-1}\mathbf{B} + \mathbf{D} \tag{21}$$

where $s$ is the complex variable defined by the Laplace transform [54]

$$F(s) = \mathcal{L}\left[ f(t) \right] = \int_0^\infty f(t) e^{-st} dt \tag{22}$$

If all of the poles of $\mathbf{G}(s)$ have negative real part, then the zero-state response of (7) is BIBO stable. Since every pole of $\mathbf{G}(s)$ is an eigenvalue of **A**, if the system is asymptotically stable, it is also BIBO stable, although the opposite is not necessarily true due to possible pole-zero cancellations in $\mathbf{G}(s)$ [49].

### 2.1.2 Lyapunov's Linearization Method for Continuous-Time Systems

When discussing nonlinear system stability, an important result from Lyapunov is the linearization method, which is useful because it uses the existing linear system theory in order to derive conclusions about a nonlinear system. Considering the general autonomous nonlinear system given by (2), and additionally assuming that **f** is

continuously differentiable and that **0** is an equilibrium point of the system, the system can be linearized about this equilibrium point by calculating the Jacobian matrix [49]

$$\mathbf{A} = \left.\frac{\partial \mathbf{f}}{\partial \mathbf{x}}\right|_{\mathbf{x}=\mathbf{0}} \tag{23}$$

Using this Jacobian matrix, the linearized system is written as

$$\dot{\mathbf{x}}(t) = \mathbf{A}\mathbf{x}(t) \tag{24}$$

Note that this equation represents a linear system, and therefore the analysis of this system follows the same linear system theory as previously discussed [55].

When analyzing the stability of an equilibrium point of a nonlinear system using the linearization method, first the stability of the linearized system must be determined. This is typically done by determining the eigenvalues of the Jacobian matrix, **A**. Some useful conclusions can be drawn about the nonlinear system stability using this information about the linear system. If the linearized system about a given equilibrium point is asymptotically (or exponentially) stable, then this equilibrium point is also asymptotically (or exponentially) stable for the nonlinear system. Conversely, if the linearized system is unstable, the equilibrium point is unstable for the nonlinear system. However, if the linearized system is marginally stable, then no conclusion can be drawn about the nonlinear system (*i.e.* the system could be asymptotically stable, marginally stable, or unstable) [47].

Although the linearization method is relatively simple to use, it only provides information about the local stability of the equilibrium point. It is often desired to understand the global stability of the system. In order to discuss this form of stability, Lyapunov‟s direct method can be used.

### 2.1.3 Lyapunov's Direct Method for Continuous-Time Systems

The basic premise behind Lyapunov"s direct method is defining a generalized energy function of the system that is zero at the equilibrium point and positive elsewhere [55]. If this energy function is dissipated continuously, it can be shown that the response must eventually converge to an equilibrium point [47]. An advantage of this method is that the stability can be discussed without any knowledge or calculation of the solution of the system equation [56]. Lyapunov"s direct method is sometimes referred to as the second method of Lyapunov.

To discuss the stability of an autonomous nonlinear system of the form (2), a generalized energy function, *V*, which is referred to as a Lyapunov function, must be defined. The properties of this function are used to determine the stability characteristics of the system. In particular, if there exists a Lyapunov function, *V*, such that the following characteristics are met

$$\begin{aligned} &V(\mathbf{0}) = 0 \\ &V(\mathbf{x}) > 0 \quad for \quad \mathbf{x} \neq \mathbf{0} \\ &\dot{V}(\mathbf{x}) = \frac{\partial V}{\partial \mathbf{x}} \mathbf{f}(\mathbf{x}) \leq 0 \end{aligned} \tag{25}$$

then the origin is a Lyapunov stable equilibrium point of the system. Additionally, if

$$\dot{V}(\mathbf{x}) = \frac{\partial V}{\partial \mathbf{x}} \mathbf{f}(\mathbf{x}) < 0 \tag{26}$$

then the origin is an asymptotically stable equilibrium point. In other words, the origin will be a Lyapunov stable equilibrium point if the Lyapunov function is positive definite and its time derivative is negative semi-definite, and asymptotically stable if the Lyapunov function is positive definite and its time derivative is negative definite [47].

For systems with negative semi-definite time derivative of the Lyapunov function, using invariant set theorems [47,50] it is possible to prove asymptotic stability of the system if certain additional conditions are met. To prove exponential stability, an additional set of inequalities must be satisfied [50]

$$\begin{aligned} &\alpha, \beta, \varepsilon, p \in \mathbb{R} \\ &\varepsilon > 0 \quad p \geq 1 \\ &\alpha \|\mathbf{x}\|_2^p \leq V(\mathbf{x}) \leq \beta \|\mathbf{x}\|_2^p \\ &\dot{V}(\mathbf{x}) = \frac{\partial V}{\partial \mathbf{x}} \mathbf{f}(\mathbf{x}) \leq -\varepsilon V(\mathbf{x}) \end{aligned} \tag{27}$$

A detailed proof is not shown here, but can be found in [50].

If the previous discussed properties of the Lyapunov function hold within a bounded hypersphere in the state space, the discussed stability refers to the local stability of the equilibrium point. In order to determine the global stability of the system, the properties of the Lyapunov function must hold for all possible values of $\mathbf{x}$ in the state space. Also, an additional property must hold for the Lyapunov function in order to claim global stability of the equilibrium point

$$V(\mathbf{x}) \longrightarrow \infty \quad as \quad \|\mathbf{x}\| \longrightarrow \infty \tag{28}$$

If the Lyapunov function, $V$, satisfies (28), it is said to be proper or radially unbounded [47,50].

When considering non-autonomous systems as in (1), an additional classification of stability is defined. Uniform stability is defined if the system is stable for any initial time. This is guaranteed if the Lyapunov function is decrescent [47,57]. In order to define a decrescent function, a definition of a class of functions is required. A continuous

function $\alpha$ is said to be of class $K$ if the function is non-decreasing and additionally [47,50]

$$\begin{aligned} &\alpha(0) = 0 \\ &\alpha(x) > 0, \quad x > 0 \end{aligned} \tag{29}$$

A non-autonomous system is said to be uniformly Lyapunov stable if there exists a scalar function, $V$, and class $K$ functions $\alpha$, $\beta$, and $\gamma$ such that

$$\begin{aligned} &0 < \alpha\left(\|\mathbf{x}\|_2\right) \le V(\mathbf{x},t) \le \beta\left(\|\mathbf{x}\|_2\right) \\ &\dot{V}(\mathbf{x},t) \le -\gamma\left(\|\mathbf{x}\|_2\right) \end{aligned} \tag{30}$$

Similar definitions of uniform asymptotic, exponential, global, etc. stability can be defined [47]. Unlike for autonomous systems, the invariant set theorems cannot be applied to non-autonomous systems. However, using Barbalat‟s lemma [58] it is possible to prove the asymptotic stability of non-autonomous systems that do not strictly satisfy the time derivative inequality in (30) [47,50]. The stability of non-autonomous nonlinear systems (sometimes using Barbalat‟s lemma) is a fundamental component of adaptive control theory [59,60].

## 2.2 STABILITY OF DISCRETE-TIME SYSTEMS

Discrete-time stability theory closely parallels the theory of continuous-time stability, and is therefore not presented in as much detail. The general form of an autonomous discrete-time system is given by

$$\mathbf{x}(k+1) = \mathbf{f}\left(\mathbf{x}(k)\right) \tag{31}$$

where $k$ is the discrete time index, and **f** is an ($n_x$ × 1) vector valued function. The definitions of Lyapunov, asymptotic, and global stability are the same as continuous-time systems. A parallel to exponential stability for discrete-time systems is geometric stability, which is defined for the zero solution if there exist positive constants $\alpha$, $\beta$, and $\varepsilon$ such that if $\|\mathbf{x}(0)\|_2 < \varepsilon$, then

$$\|\mathbf{x}(k)\|_2 \le \alpha \|\mathbf{x}(0)\|_2 \beta^{-k}, \quad \alpha > 0, \quad \beta > 1 \tag{32}$$

First, the stability of discrete-time linear systems is discussed, followed by the application of Lyapunov"s direct method to nonlinear discrete-time systems [50].

### 2.2.1 Stability of Discrete-Time Linear Systems

The standard format for a discrete-time linear time-invariant state space system is given by

$$\begin{aligned} \mathbf{x}(k+1) &= \mathbf{A}\mathbf{x}(k) + \mathbf{B}\mathbf{u}(k) \\ \mathbf{y}(k) &= \mathbf{C}\mathbf{x}(k) + \mathbf{D}\mathbf{u}(k) \end{aligned} \tag{33}$$

where **x** is the state vector, **y** is the output vector, **u** is the input vector, and **A**, **B**, **C**, and **D** are matrices describing the system. The internal or zero-input response of this system is given by the solution to

$$\mathbf{x}(k+1) = \mathbf{A}\mathbf{x}(k) \tag{34}$$

which is given by

$$\mathbf{x}(k) = \mathbf{A}^k \mathbf{x}(0) \tag{35}$$

Therefore, (34) is considered marginally stable if the magnitudes of all eigenvalues of **A** are less than or equal to 1, and asymptotically stable if the magnitudes of all eigenvalues of **A** are strictly less than 1. Similar to continuous-time systems, the BIBO stability is defined for discrete-time system by analyzing the poles of the input-output transfer matrix, which is defined using the *z*-transform instead of the Laplace transform [49].

### 2.2.2 Lyapunov's Direct Method for Discrete-Time Systems

For nonlinear systems of the form (31), if there exists a continuous function, *V*, such that

$$\begin{aligned} &V(\mathbf{0}) = 0 \\ &V(\mathbf{x}) > 0, \quad \mathbf{x} \neq \mathbf{0} \\ &V\left(\mathbf{f}(\mathbf{x})\right) - V(\mathbf{x}) \leq 0 \end{aligned} \tag{36}$$

then the zero solution of (31) is Lyapunov stable. Additionally, if

$$V\left(\mathbf{f}(\mathbf{x})\right) - V\left(\mathbf{x}\right) < 0 \tag{37}$$

then the zero solution is asymptotically stable. As for continuous time systems, there are invariant set theorems which can be used to prove asymptotic stability of autonomous discrete-time systems without satisfying (37) [50]. If the following conditions are met

$$\begin{aligned} &\alpha, \beta, \rho, p \in \mathbb{R} \\ &\beta > 0 \quad \rho > 1 \quad p \geq 1 \\ &\alpha \|\mathbf{x}\|_2^p \leq V(\mathbf{x}) \leq \beta \|\mathbf{x}\|_2^p \\ &\rho V\left(\mathbf{f}(\mathbf{x})\right) \leq V(\mathbf{x}) \end{aligned} \tag{38}$$

then the zero solution is geometrically stable. If (28) is satisfied in addition to (37) or (38), then the zero solution is globally asymptotically stable or globally geometrically stable [50].

Consider non-autonomous systems of the form

$$\mathbf{x}(k+1) = \mathbf{f}\left(\mathbf{x}(k), k\right) \tag{39}$$

Lyapunov stability is defined for the system if there exist a continuous function $V$ and a class $K$ function $\alpha$ such that

$$\begin{aligned} &V(\mathbf{0}, k) = 0 \\ &\alpha\left(\|\mathbf{x}\|_2\right) \leq V(\mathbf{x}, k) \\ &\Delta V(\mathbf{x}, k) \leq 0 \end{aligned} \tag{40}$$

If additionally there exist a class $K$ function $\beta$ such that

$$V(\mathbf{x}, k) \leq \beta\left(\|\mathbf{x}\|_2\right) \tag{41}$$

then the system is uniformly Lyapunov stable. Uniform asymptotic stability is defined if additionally there exist a class $K$ function $\gamma$ such that

$$\Delta V(\mathbf{x}, k) \leq -\gamma\left(\|\mathbf{x}\|_2\right) \tag{42}$$

Uniform geometric stability is defined if there exists a continuous function $V$ such that

$$\begin{aligned} &\alpha \|\mathbf{x}\|_2^p \leq V(\mathbf{x}, k) \leq \beta \|\mathbf{x}\|_2^p \\ &\Delta V(\mathbf{x}, k) \leq -\gamma \|\mathbf{x}\|_2^p \end{aligned} \tag{43}$$

for some positive constants $\alpha$, $\beta$, $\gamma$, and $p$, with $p \geq 1$ [50].

## 2.3 NONLINEAR STATE ESTIMATION

A general discrete nonlinear system is described as follows:

$$\begin{aligned} \mathbf{x}_k &= \mathbf{f}(\mathbf{x}_{k-1}, \mathbf{u}_k, \mathbf{w}_k) \\ \mathbf{y}_k &= \mathbf{h}(\mathbf{x}_k, \mathbf{d}_k, \mathbf{v}_k) \end{aligned} \tag{44}$$

where **f** is the vector valued discrete state prediction function, **h** is the vector valued discrete observation function, **x** is the state vector, **y** is the output vector, **u** and **d** are input vectors, **w** is the process noise vector, **v** is the measurement noise vector, and $k$ is the discrete time index. The dimensions of **x**, **u**, **w**, **y**, **d**, and **v**, are $n_x$, $n_u$, $n_w$, $n_y$, $n_d$, and $n_v$, respectively. In general, **f** and **h** are nonlinear multivariate vector valued functions of dimension $n_x$ and $n_y$ respectively. A diagram illustrating the state estimation process of this general nonlinear system with a Kalman filter is shown in Figure 3.

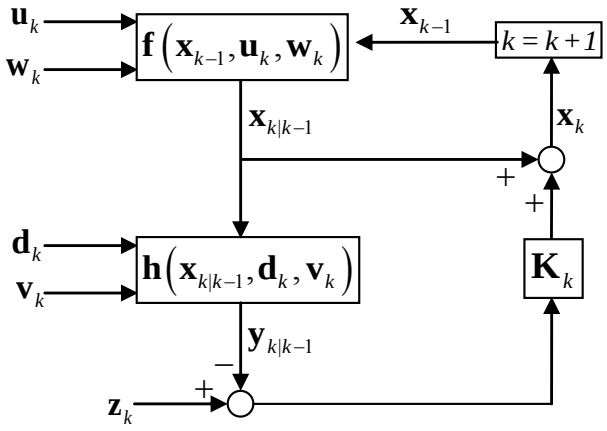


Figure 3. Conceptual Representation of Nonlinear State Estimation

In Figure 3, **K** is the Kalman gain matrix which is calculated from the equations of a nonlinear Kalman filter. First a solution of the linear state estimation problem is presented, followed by the nonlinear extension of this theory.

## 2.4 DISCRETE-TIME LINEAR KALMAN FILTER

In 1960, Kalman introduced a recursive solution to the discrete-time linear filtering problem [2]. This technique has since been named the Kalman filter, and is the basis of much of the current work in recursive estimation problems. This discrete-time linear Kalman filter considers a system with the following properties

$$\begin{aligned} \mathbf{x}_k &= \mathbf{A}_{k-1}\mathbf{x}_{k-1} + \mathbf{B}_{k-1}\mathbf{u}_{k-1} + \mathbf{w}_{k-1} \\ \mathbf{y}_k &= \mathbf{H}_k\mathbf{x}_k + \mathbf{v}_k \end{aligned} \tag{45}$$

where **w** and **v** are the process and measurement noise processes, which are assumed white, uncorrelated, and zero-mean with known covariance matrices **Q** and **R** respectively

$$\begin{aligned} &\mathbf{w}_k \sim (0, \mathbf{Q}_k), \quad E\left[\mathbf{w}_k \mathbf{w}_j^T\right] = \mathbf{Q}_k \delta_{kj} \\ &\mathbf{v}_k \sim (0, \mathbf{R}_k), \quad E\left[\mathbf{v}_k \mathbf{v}_j^T\right] = \mathbf{R}_k \delta_{kj} \\ &E\left[\mathbf{v}_k \mathbf{w}_j^T\right] = 0 \end{aligned} \tag{46}$$

where $\delta$ is the Kronecker delta function [61]

$$\delta_{kj} = \begin{cases} 1 & k = j \\ 0 & k \neq j \end{cases} \tag{47}$$

The initial conditions for the filter are

$$\begin{aligned}\hat{\mathbf{x}}_0 &= E\left[\mathbf{x}_0\right] \\ \mathbf{P}_0 &= E\left[\left(\mathbf{x}_0 - \hat{\mathbf{x}}_0\right)\left(\mathbf{x}_0 - \hat{\mathbf{x}}_0\right)^T\right]\end{aligned} \tag{48}$$

The first step in the Kalman filter is to obtain predictions of the current state and covariance matrix based on information from the previous time step

$$\begin{aligned}\hat{\mathbf{x}}_{k|k-1} &= \mathbf{A}_{k-1}\hat{\mathbf{x}}_{k-1} + \mathbf{B}_{k-1}\mathbf{u}_{k-1} \\ \mathbf{P}_{k|k-1} &= \mathbf{A}_{k-1}\mathbf{P}_{k-1}\mathbf{A}_{k-1}^T + \mathbf{Q}_{k-1}\end{aligned} \tag{49}$$

Next, the Kalman gain matrix, **K**, is calculated

$$\mathbf{K}_k = \mathbf{P}_{k|k-1}\mathbf{H}_k^T\left(\mathbf{H}_k\mathbf{P}_{k|k-1}\mathbf{H}_k^T + \mathbf{R}_k\right)^{-1} \tag{50}$$

Finally, the Kalman gain matrix is used to update the predicted state and covariance matrix using information from the measurement

$$\begin{aligned}\hat{\mathbf{x}}_k &= \hat{\mathbf{x}}_{k|k-1} + \mathbf{K}_k\left(\mathbf{z}_k - \mathbf{H}_k\hat{\mathbf{x}}_{k|k-1}\right) \\ \mathbf{P}_k &= \left(\mathbf{I} - \mathbf{K}_k\mathbf{H}_k\right)\mathbf{P}_{k|k-1} = \left(\mathbf{P}_{k|k-1}^{-1} + \mathbf{H}_k^T\mathbf{R}_k^{-1}\mathbf{H}_k\right)^{-1}\end{aligned} \tag{51}$$

where **z** is the measurement of the output, **y**, and **I** is an identity matrix [62,63].

### 2.4.1 Discrete-Time Linear Kalman Filter Stability

Deyst [4,5] and Price [4] provided a proof of the stability of the discrete-time linear Kalman filter. For this stability proof, the following no input stochastic system is considered

$$\begin{aligned}
&\mathbf{x}(k+1) = \mathbf{\Phi}(k+1,k)\mathbf{x}(k) + \mathbf{w}(k) \\
&\mathbf{z}(k) = \mathbf{H}(k)\mathbf{x}(k) + \mathbf{v}(k) \\
&\mathbf{w}(k) \sim \left(0, \mathbf{Q}(k)\right), \quad \mathbf{v}(k) \sim \left(0, \mathbf{R}(k)\right)
\end{aligned} \tag{52}$$

It is assumed that this system meets the following definition of stochastic controllability and observability

$$\begin{aligned}
&\alpha_2 \mathbf{I} \le \sum_{i=k-N}^{k-1} \mathbf{\Phi}(k,i+1)\mathbf{Q}(i)\mathbf{\Phi}^T(k,i+1) \le \alpha_1 \mathbf{I} \\
&\beta_1 \mathbf{I} \le \sum_{i=k-N}^{k} \mathbf{\Phi}^T(i,k)\mathbf{H}^T(i)\mathbf{R}(i)^{-1}\mathbf{H}(i)\mathbf{\Phi}(i,k) \le \beta_2 \mathbf{I} \\
&\alpha_1, \alpha_2, \beta_1, \beta_2, N \in \mathbb{R} \\
&0 < \alpha_2 < \alpha_1 < \infty \\
&0 < \beta_1 < \beta_2 < \infty
\end{aligned} \tag{53}$$

where $N$ is some fixed finite nonnegative integer, and the state transition matrix, $\mathbf{\Phi}$, satisfies the following properties

$$\begin{aligned}
&\mathbf{\Phi}(k,i) = \mathbf{\Phi}(k,k-1)\mathbf{\Phi}(k-1,k-2)...\mathbf{\Phi}(i+1,i) = \mathbf{A}_{k-1}\mathbf{A}_{k-2}...\mathbf{A}_i \\
&\mathbf{\Phi}(i,k) = \mathbf{\Phi}(k,i)^{-1} \\
&\mathbf{\Phi}(k,k) = \mathbf{I}
\end{aligned} \tag{54}$$

If the stochastic controllability and observability conditions are met, then the error covariance matrix is bounded as follows

$$\frac{1}{\beta_2 + 1/\alpha_2}\mathbf{I} \le \mathbf{P}_k \le \left(\frac{1}{\beta_1} + N\frac{\beta_2^2\alpha_1}{\beta_1^2}\right)\mathbf{I} \tag{55}$$

It is shown in [4] that these are sufficient conditions for uniform asymptotic stability in the large for the homogeneous system [57].

Crassidis and Junkins also provided a stability proof of the linear discrete-time Kalman filter using Lyapunov's direct method [7]. The details of this proof are briefly presented. Consider a Lyapunov candidate function of the form

$$V(\boldsymbol{\xi}) = \boldsymbol{\xi}_k^T \mathbf{P}_k^{-1} \boldsymbol{\xi}_k \tag{56}$$

where $\boldsymbol{\xi}_k \equiv \hat{\mathbf{x}}_{k|k-1} - \mathbf{x}_k$ represents the error in the *a priori* state estimate, although this is not explicitly stated in [7]. Since the covariance, $\mathbf{P}_k$, is a positive definite matrix, its inverse exists and is also positive definite, and therefore by definition $V(\boldsymbol{\xi}) > 0$. From (45), (49), and (51), the error dynamics can be defined by

$$\boldsymbol{\xi}_{k+1} = \mathbf{A}_k\left(\mathbf{I} - \mathbf{K}_k\mathbf{H}_k\right)\boldsymbol{\xi}_k + \mathbf{A}_k\mathbf{K}_k\mathbf{v}_k - \mathbf{w}_k \tag{57}$$

For stability, only the homogeneous part of (57) is considered

$$\boldsymbol{\xi}_{k+1} = \mathbf{A}_k\left(\mathbf{I} - \mathbf{K}_k\mathbf{H}_k\right)\boldsymbol{\xi}_k \tag{58}$$

To prove stability, the increment of the Lyapunov function must be negative, as in (37). For the considered Lyapunov candidate function, this increment is given by

$$\Delta V(\boldsymbol{\xi}) = \boldsymbol{\xi}_{k+1}^T \mathbf{P}_{k+1}^{-1} \boldsymbol{\xi}_{k+1} - \boldsymbol{\xi}_k^T \mathbf{P}_k^{-1} \boldsymbol{\xi}_k \tag{59}$$

Substituting (58) in (59) gives the following necessary condition for stability

$$\boldsymbol{\xi}_k^T \left[\left(\mathbf{I} - \mathbf{K}_k\mathbf{H}_k\right)^T \mathbf{A}_k^T \mathbf{P}_{k+1}^{-1} \mathbf{A}_k \left(\mathbf{I} - \mathbf{K}_k\mathbf{H}_k\right) - \mathbf{P}_k^{-1}\right] \boldsymbol{\xi}_k < 0 \tag{60}$$

This condition reduces to showing that the bracketed matrix is negative definite. Using (49) and (51), the condition can be simplified to the following form

$$-\left(\mathbf{A}_k\mathbf{K}_k\mathbf{R}_k\mathbf{K}_k^T\mathbf{A}_k^T+\mathbf{Q}_k\right)\left[\mathbf{A}_k^{-T}\left(\mathbf{I}-\mathbf{K}_k\mathbf{H}_k\right)^{-T}\mathbf{P}_k^{-1}\left(\mathbf{I}-\mathbf{K}_k\mathbf{H}_k\right)^{-1}\mathbf{A}_k^{-1}\right]<0 \tag{61}$$

Again, since $\mathbf{P}_k^{-1}$ is a positive definite matrix, so is the entire bracketed matrix, therefore reducing the condition to

$$\mathbf{A}_k\mathbf{K}_k\mathbf{R}_k\mathbf{K}_k^T\mathbf{A}_k^T+\mathbf{Q}_k>0 \tag{62}$$

If $\mathbf{R}_k$ is positive definite and $\mathbf{Q}_k$ is positive semi-definite, this condition is satisfied [7]. This proof shows the asymptotic stability of the *a priori* state error of a deterministic linear discrete-time Kalman filter. However, since this system is in general non-autonomous, without showing that the Lyapunov function is a decrescent function, uniform stability is not guaranteed [47]. This proof also does not consider the stochastic stability of the filter [64,65], therefore only the stability of the deterministic system has been shown. These stability issues for the linear discrete-time Kalman filter are discussed further in Section 6.2.

## 2.5 EXTENDED KALMAN FILTER

In order to apply the previously derived linear recursive filtering tools to nonlinear systems, Kalman and Bucy introduced the Extended Kalman Filter (EKF) [8]. This has since become a standard method for nonlinear filtering problems. The EKF considers nonlinear systems of the form (44). The process and measurement noise terms are considered to be uncorrelated, white, and Gaussian with zero mean and known covariance matrices **Q** and **R** respectively

$$\begin{aligned}
&\mathbf{w}_k \sim N(\mathbf{0}, \mathbf{Q}_k) \\
&\mathbf{v}_k \sim N(\mathbf{0}, \mathbf{R}_k) \\
&E\left[\mathbf{w}_k \mathbf{v}_j^T\right] = 0
\end{aligned} \tag{63}$$

The EKF utilizes an analytical linearization method to handle the nonlinearity in the equations. This analytical linearization involves the calculation of Jacobian matrices of the nonlinear prediction and observation functions with respect to both the state and the corresponding noise terms

$$\begin{aligned}
\mathbf{A}_k &= \left.\frac{\partial \mathbf{f}}{\partial \mathbf{x}}\right|_{\hat{\mathbf{x}}_{k-1}}, \quad \mathbf{L}_k = \left.\frac{\partial \mathbf{f}}{\partial \mathbf{w}}\right|_{\hat{\mathbf{x}}_{k-1}} \\
\mathbf{H}_k &= \left.\frac{\partial \mathbf{h}}{\partial \mathbf{x}}\right|_{\hat{\mathbf{x}}_{k|k-1}}, \quad \mathbf{M}_k = \left.\frac{\partial \mathbf{h}}{\partial \mathbf{v}}\right|_{\hat{\mathbf{x}}_{k|k-1}}
\end{aligned} \tag{64}$$

Using these Jacobian matrices, the EKF algorithm is given by [62]

$$\begin{aligned}
\hat{\mathbf{x}}_{k|k-1} &= \mathbf{f}\left(\hat{\mathbf{x}}_{k-1}, \mathbf{u}_{k-1}, \mathbf{0}\right) \\
\mathbf{P}_{k|k-1} &= \mathbf{A}_{k-1}\mathbf{P}_{k-1}\mathbf{A}_{k-1}^T + \mathbf{L}_{k-1}\mathbf{Q}_{k-1}\mathbf{L}_{k-1}^T \\
\mathbf{K}_k &= \mathbf{P}_{k|k-1}\mathbf{H}_k^T\left(\mathbf{H}_k\mathbf{P}_{k|k-1}\mathbf{H}_k^T + \mathbf{M}_k\mathbf{R}_k\mathbf{M}_k^T\right)^{-1} \\
\hat{\mathbf{x}}_k &= \hat{\mathbf{x}}_{k|k-1} + \mathbf{K}_k\left[\mathbf{z}_k - \mathbf{h}\left(\hat{\mathbf{x}}_{k|k-1}, \mathbf{d}_k, \mathbf{0}\right)\right] \\
\mathbf{P}_k &= \left(\mathbf{I} - \mathbf{K}_k\mathbf{H}_k\right)\mathbf{P}_{k|k-1}
\end{aligned} \tag{65}$$

Note that these equations include Jacobian matrices **L** and **M** which are taken with respect to the process and measurement noise terms respectively. For additive noise, which is commonly assumed in many situations, these matrices become identity matrices.

### 2.5.1 Extended Kalman Filter Stability

Various authors have approached the stability issues of the EKF [32-34,38-41,44,45], sometimes discussing a modified version of the EKF [38,39,44,45], or by

reducing the most general nonlinear estimation problem by assuming a deterministic system [34,41,45], no inputs [32,33], linear dynamics [44], or a linear observation [33]. Reif *et al*., however, presented a thorough stability analysis which considered a general formulation of the EKF. This is an important work because it derives the necessary conditions for stability in terms of calculable bounds on the initial state error and noise disturbances. Some of the details of this work are presented [40].

Consider the following nonlinear discrete-time system

$$\begin{aligned} \mathbf{x}_{k+1} &= \mathbf{f}(\mathbf{x}_k, \mathbf{u}_k) + \mathbf{G}_k \mathbf{w}_k \\ \mathbf{y}_k &= \mathbf{h}(\mathbf{x}_k) + \mathbf{D}_k \mathbf{v}_k \end{aligned} \tag{66}$$

where $\mathbf{w}$ and $\mathbf{v}$ are uncorrelated zero-mean white noise processes with identity covariance. Applying the EKF to this problem, the errors due to linearization are determined from

$$\begin{aligned} \mathbf{f}(\mathbf{x}_k, \mathbf{u}_k) - \mathbf{f}(\hat{\mathbf{x}}_k, \mathbf{u}_k) &= \mathbf{A}_k(\mathbf{x}_k - \hat{\mathbf{x}}_k) + \boldsymbol{\varphi}(\mathbf{x}_k, \hat{\mathbf{x}}_k, \mathbf{u}_k) \\ \mathbf{h}(\mathbf{x}_k) - \mathbf{h}(\hat{\mathbf{x}}_k) &= \mathbf{H}_k(\mathbf{x}_k - \hat{\mathbf{x}}_k) + \boldsymbol{\chi}(\mathbf{x}_k, \hat{\mathbf{x}}_k) \end{aligned} \tag{67}$$

where $\boldsymbol{\varphi}$ and $\boldsymbol{\chi}$ are the prediction and observation linearization errors respectively. Thus, the estimation error and its dynamics can be written in the following form

$$\begin{aligned} \tilde{\mathbf{x}}_k &= \mathbf{x}_k - \hat{\mathbf{x}}_k \\ \tilde{\mathbf{x}}_{k+1} &= (\mathbf{A}_k - \mathbf{K}_k \mathbf{H}_k)\tilde{\mathbf{x}}_k + \mathbf{r}_k + \mathbf{s}_k \\ \mathbf{r}_k &= \boldsymbol{\varphi}(\mathbf{x}_k, \hat{\mathbf{x}}_k, \mathbf{u}_k) - \mathbf{K}_k \boldsymbol{\chi}(\mathbf{x}_k, \hat{\mathbf{x}}_k) \\ \mathbf{s}_k &= \mathbf{G}_k \mathbf{w}_k - \mathbf{K}_k \mathbf{D}_k \mathbf{v}_k \end{aligned} \tag{68}$$

The matrix $\mathbf{A}_k$ must be nonsingular for all $k$, and the following bounds are assumed on various matrices

$$\begin{aligned}
&\left\|\mathbf{A}_k\right\| \le a_2 \\
&\left\|\mathbf{H}_k\right\| \le h_2 \\
&p_1\mathbf{I} \le \mathbf{P}_k \le p_2\mathbf{I} \\
&q_1\mathbf{I} \le \mathbf{Q}_k \\
&r_1\mathbf{I} \le \mathbf{R}_k
\end{aligned} \tag{69}$$

for some positive real numbers $a_2$, $h_2$, $p_1$, $p_2$, $q_1$, $r_1 > 0$. The norm of a matrix in this context is defined as the spectral norm, or the largest singular value of the matrix, as in

$$\left\|\mathbf{A}\right\| = \sqrt{\lambda_{\max}\left(\mathbf{A}^*\mathbf{A}\right)} \tag{70}$$

where $\mathbf{A}^*$ is the complex conjugate transpose of the matrix $\mathbf{A}$. Lastly, it is assumed that the linearization errors are bounded by

$$\begin{aligned}
&\left\|\boldsymbol{\varphi}(\mathbf{x}_k, \hat{\mathbf{x}}_k, \mathbf{u}_k)\right\|_2 \le \kappa_\varphi \left\|\mathbf{x}_k - \hat{\mathbf{x}}_k\right\|_2^2, \quad \left\|\mathbf{x}_k - \hat{\mathbf{x}}_k\right\| \le \varepsilon_\varphi \\
&\left\|\boldsymbol{\chi}(\mathbf{x}_k, \hat{\mathbf{x}}_k)\right\|_2 \le \kappa_\chi \left\|\mathbf{x}_k - \hat{\mathbf{x}}_k\right\|_2^2, \quad \left\|\mathbf{x}_k - \hat{\mathbf{x}}_k\right\| \le \varepsilon_\chi
\end{aligned} \tag{71}$$

for some positive real numbers $\kappa_\varphi, \kappa_\chi, \varepsilon_\varphi, \varepsilon_\chi > 0$. If these conditions are satisfied, then the estimation error is exponentially stable as long as the initial estimation error and noise are bounded as follows

$$\begin{aligned}
&\left\|\tilde{\mathbf{x}}_0\right\|_2 \le \varepsilon \\
&\mathbf{G}_k\mathbf{G}_k^T \le \delta\mathbf{I} \\
&\mathbf{D}_k\mathbf{D}_k^T \le \delta\mathbf{I}
\end{aligned} \tag{72}$$

where the positive constants $\varepsilon, \delta > 0$, are determined from the following series of calculations

$$
\begin{aligned}
\alpha &= 1-\left(1+\frac{q_1}{p_2\left(a_2+a_2p_2h_2/r_1\right)^2}\right)^{-1}\\
\varepsilon' &= \min\left(\varepsilon_\varphi,\varepsilon_\chi\right)\\
\kappa' &= \kappa_\varphi+\frac{a_2p_2h_2}{r_1}\kappa_\chi\\
\kappa_{nonl} &= \frac{\kappa'}{p_1}\left[2\left(a_2+\frac{a_2p_2h_2}{r_1}h_2\right)+\kappa'\varepsilon'\right]\\
\kappa_{noise} &= \frac{q}{p_1}+\frac{a_2^2h_2^2p_2^2m}{p_1r_1^2}\\
\varepsilon &= \min\left(\varepsilon',\frac{\alpha}{2p_2\kappa_{nonl}}\right)\\
\delta &= \frac{\alpha\tilde{\varepsilon}^2}{2p_2\kappa_{noise}},\quad \tilde{\varepsilon}<\varepsilon
\end{aligned}
\tag{73}
$$

where $q$ and $m$ are the number of rows in **G** and **D** respectively [40].

Another interesting work is that of La Scala *et al*. [33], in which the stability of the EKF is analyzed using the Total Stability Theorem [66]. A difference between this work and other works is that the stochastic terms are bounded absolutely, as opposed to the more common bounding of covariance. The specific case of a linear observation was assumed. A summary of the application of this work is provided here. This work considers estimation error in the following form

$$
\begin{aligned}
\tilde{\mathbf{x}}_k &= \mathbf{x}_k-\hat{\mathbf{x}}_k\\
\tilde{\mathbf{x}}_k &= (\mathbf{I}-\mathbf{K}_k\mathbf{H}_k)\mathbf{A}_{k-1}\tilde{\mathbf{x}}_{k-1}+\mathbf{r}_k+\mathbf{s}_k\\
\mathbf{r}_k &= (\mathbf{I}-\mathbf{K}_k\mathbf{H}_k)\boldsymbol{\kappa}_f\left(\mathbf{x}_{k-1},\tilde{\mathbf{x}}_{k-1}\right)\\
\mathbf{s}_k &= (\mathbf{I}-\mathbf{K}_k\mathbf{H}_k)\mathbf{w}_k-\mathbf{K}_k\mathbf{v}_k
\end{aligned}
\tag{74}
$$

where $\boldsymbol{\kappa}_f$ is the linearization error term given by

$$
\boldsymbol{\kappa}_f\left(\mathbf{x}_{k-1},\tilde{\mathbf{x}}_{k-1}\right)=\mathbf{f}\left(\mathbf{x}_{k-1}-\tilde{\mathbf{x}}_{k-1}\right)-\mathbf{f}\left(\mathbf{x}_{k-1}\right)+\frac{\partial\mathbf{f}}{\partial\mathbf{x}}\left(\mathbf{x}_{k-1}\right)\tilde{\mathbf{x}}_{k-1}
\tag{75}
$$

Assume that the following assumptions hold for the system

$$
\begin{aligned}
&\mathbf{f} \in C^3\left(\mathbb{R}^n, \mathbb{R}^n\right) \\
&\left|\frac{\partial \mathbf{f}}{\partial \mathbf{x}}(\mathbf{x})\right| \neq 0 \qquad \forall \mathbf{x} \in \mathbb{R}^n \\
&\left\|\mathbf{x}_k\right\| \leq r_x \\
&\left\|\mathbf{H}_k\right\| \leq \rho_5 \\
&E\left[\mathbf{w}_k \mathbf{w}_k^T\right] = \mathbf{Q}_k \geq \delta_1 \mathbf{I}, \quad \left\|\mathbf{w}_k\right\| \leq w_{\max} < \infty \\
&E\left[\mathbf{v}_k \mathbf{v}_k^T\right] = \mathbf{R}_k \geq \delta_2 \mathbf{I}, \quad \left\|\mathbf{v}_k\right\| \leq v_{\max} < \infty
\end{aligned}
\tag{76}
$$

Additionally, it is assumed that $N$ and $\varepsilon_r$ can be found such that the stochastic controllability and observability conditions (53) are satisfied for the linearized system for all $\zeta_k$, $\left\|\zeta_k\right\| \leq \varepsilon_r$, evaluated along the trajectory $\mathbf{x}_k - \zeta_k$. Due to the assumption that $\mathbf{f} \in C^3\left(\mathbb{R}^n, \mathbb{R}^n\right)$, the following derivative terms exist, and can be bounded by positive constants $\rho_i$ as in

$$
\begin{aligned}
&\left\|\frac{\partial^i \mathbf{f}}{\partial \mathbf{x}^i}(\mathbf{x})\right\| \leq \rho_i, \quad i = 1,2,3 \\
&\left\|\frac{\partial \mathbf{f}}{\partial \mathbf{x}}(\mathbf{x}_1) - \frac{\partial \mathbf{f}}{\partial \mathbf{x}}(\mathbf{x}_2) - \frac{\partial^2 \mathbf{f}}{\partial \mathbf{x}^2}(\mathbf{x}_2)(\mathbf{x}_1 - \mathbf{x}_2)\right\| \leq \frac{1}{2}\rho_4 \left\|\mathbf{x}_1 - \mathbf{x}_2\right\|^2
\end{aligned}
\tag{77}
$$

From the assumed bounds, a set of constants are defined for notational convenience

$$
\begin{aligned}
p &\triangleq \alpha_1 + \frac{1}{\beta_1} \\
q &\triangleq \frac{1}{\alpha_2} + \beta_2 \\
s &\triangleq \frac{1}{\alpha_2} + \beta_2 + \frac{\rho_1^2}{\delta_1} \\
\varepsilon_z &\triangleq \min\left\{ \varepsilon_r, \sqrt{\frac{2}{\rho_4}} \left( -\rho_1 + \sqrt{\rho_1^2 + \frac{1}{q}\left( \frac{1}{sp^2} - \gamma \right)} \right)^{\frac{1}{2}} \right\} \\
0 &< \gamma < \frac{1}{sp^2} \\
\alpha &= \sqrt{1 - \frac{\gamma}{q}} \\
\beta &= \sqrt{pq} \\
\zeta_{\bar{z}} &\triangleq \delta_k \rho_5 \rho_1 \varepsilon_z \\
\delta_k &\triangleq \delta_p \rho_5 \delta_2^{-1} \left( 1 + s\rho_5^2 \delta_2^{-1} \right) \\
\delta_p &\triangleq 2\rho_1 \rho_2 p \\
\eta &\triangleq \max\left\{ \begin{array}{l} pq\left( w_{\max} + \frac{1}{2}\rho_4 \varepsilon_r^2 \right) + p\rho_5 \delta_2^{-1} v_{\max}, \\ \delta_k \left( \rho_5 w_{\max} + v_{\max} + \frac{1}{2}\rho_4 \rho_5 \varepsilon_r^2 \right) + 2pq\rho_1 \end{array} \right\} \\
\zeta &\triangleq 2\rho_1 \rho_5 \delta_k + \rho_1 \rho_5 \delta_{k2} \varepsilon_r \\
\left\| \frac{\partial \mathbf{K}_{\bar{z}}}{\partial \mathbf{z}} \right\| &\le \delta_{k2}
\end{aligned}
\tag{78}
$$

With these assumed and calculated bounds, if the following condition is satisfied

$$
\begin{aligned}
&\beta\left(\zeta + \eta\right) + \alpha < 1 \\
&\beta\zeta_{\bar{z}} + \alpha < 1 \\
&\left\| \tilde{\mathbf{x}}_0 \right\| < \varepsilon_z \left( pq \right)^{-1/2}
\end{aligned}
\tag{79}
$$

then the estimation error of the EKF is bounded by

$$\left\|\tilde{\mathbf{x}}_k\right\| \le \beta\alpha^k \left\|\tilde{\mathbf{x}}_0\right\| + \beta\left(\alpha+\zeta\beta\right)^k \left\|\tilde{\mathbf{x}}_0\right\| + \frac{\beta\eta\left(r_x - \beta\varepsilon_z\right)}{1-\left(\alpha+\zeta\beta\right)} \le \varepsilon_r \tag{80}$$

[33].

While the work of Reif *et al*. [40] and La Scala *et al*. [33] consider additive linearization error as in (67) and (75), the work of Boutayeb *et al.* [34,46] as well as Xiong *et al*. [35] formulate the linearization error using an unknown diagonal matrix, $\boldsymbol{\beta}$, as in

$$\mathbf{f}(\mathbf{x}_k, \mathbf{u}_k) - \mathbf{f}(\hat{\mathbf{x}}_k, \mathbf{u}_k) = \boldsymbol{\beta}_k \mathbf{A}_k (\mathbf{x}_k - \hat{\mathbf{x}}_k) \tag{81}$$

This matrix is then assumed bounded with some upper and lower limits, which are then used to derive the conditions for stability.

## 2.6 UNSCENTED KALMAN FILTER

The Unscented Kalman Filter (UKF) uses the unscented transformation [10] to obtain the *a posteriori* estimates of mean and covariance. The first step of the UKF implementation is to calculate $2l+1$ sigma points based on the square-root of the state covariance matrix:

$$\boldsymbol{\chi}_{k-1} = \begin{bmatrix} \hat{\mathbf{x}}_{k-1} & \hat{\mathbf{x}}_{k-1} + \eta\sqrt{\mathbf{P}_{k-1}} & \hat{\mathbf{x}}_{k-1} - \eta\sqrt{\mathbf{P}_{k-1}} \end{bmatrix} \tag{82}$$

where $l$ is the dimension of the state vector, $\boldsymbol{\chi}$ is a matrix of state sigma points, and $\eta$ is the sigma point spread parameter, given by [11]:

$$\eta = \sqrt{l + \lambda} \tag{83}$$

$$\lambda = l\left(\alpha^2 - 1\right) \tag{84}$$

where $\lambda$ is the compound sigma point parameter, and $\alpha$ is the primary sigma point scaling parameter, which is suggested to vary between 0.001 and 1 [11].

The prediction step for the UKF consists of passing each sigma point through the state prediction equations:

$${}^{i}\boldsymbol{\chi}^{x}_{k|k-1} = \mathbf{f}({}^{i}\boldsymbol{\chi}_{k-1}, \mathbf{u}_k), \qquad i = 0,1,...,2l \tag{85}$$

where the superscript $i$ denotes the $(i+1)^{\text{th}}$ column of the matrix. Then, the state mean and covariance are predicted using a weighted average of the transformed sigma points using:

$$\hat{\mathbf{x}}_{k|k-1} = \sum_{i=0}^{2l} \mathbf{w}_m^i \, {}^{i}\boldsymbol{\chi}_{k|k-1} \tag{86}$$

$$\mathbf{P}_{k|k-1} = \mathbf{Q}_k + \sum_{i=0}^{2l} \mathbf{w}_c^i \left({}^{i}\boldsymbol{\chi}_{k|k-1} - \hat{\mathbf{x}}_{k|k-1}\right)\left({}^{i}\boldsymbol{\chi}_{k|k-1} - \hat{\mathbf{x}}_{k|k-1}\right)^T \tag{87}$$

where $\mathbf{w}_m$ and $\mathbf{w}_c$ are weight vectors [11], and $\mathbf{Q}$ is the process noise covariance matrix.

For the update step of the UKF, first the output sigma points, $Y$, are calculated using the current state sigma points in the observation equations:

$${}^{i}\mathbf{Y}_{k|k-1} = \mathbf{h}\left({}^{i}\boldsymbol{\chi}^{x}_{k|k-1}, \mathbf{u}_k\right), \qquad i = 0,1,...,2l \tag{88}$$

Next, the output and output covariance matrix are estimated using:

$$\hat{\mathbf{y}}_{k|k-1} = \sum_{i=0}^{2l} \mathbf{w}_m^i \, {}^i\mathbf{Y}_{k|k-1} \tag{89}$$

$$\mathbf{P}_{\hat{\mathbf{y}}_{k|k-1}} = \mathbf{R}_k + \sum_{i=0}^{2l} \mathbf{w}_c^i \left( {}^i\mathbf{Y}_{k|k-1} - \hat{\mathbf{y}}_{k|k-1} \right) \left( {}^i\mathbf{Y}_{k|k-1} - \hat{\mathbf{y}}_{k|k-1} \right)^T \tag{90}$$

where **R** is the measurement noise covariance matrix. Next, the covariance matrix between the state prediction and output estimate is calculated using:

$$\mathbf{P}_{\hat{\mathbf{x}}_{k|k-1}\hat{\mathbf{y}}_{k|k-1}} = \sum_{i=0}^{2l} \mathbf{w}_c^i \left( {}^i\boldsymbol{\chi}_{k|k-1}^x - \mathbf{x}_{k|k-1} \right) \left( {}^i\mathbf{Y}_{k|k-1} - \mathbf{y}_{k|k-1} \right)^T \tag{91}$$

leading to the Kalman gain matrix:

$$\mathbf{K}_k = \frac{\mathbf{P}_{\hat{\mathbf{x}}_{k|k-1}\hat{\mathbf{y}}_{k|k-1}}}{\mathbf{P}_{\hat{\mathbf{y}}_{k|k-1}}} \tag{92}$$

Finally, using the Kalman gain matrix, the state and state covariance predictions are updated using the GPS measurement vector, **z**:

$$\hat{\mathbf{x}}_k = \hat{\mathbf{x}}_{k|k-1} + \mathbf{K}_k \left( \mathbf{z}_k - \hat{\mathbf{y}}_{k|k-1} \right) \tag{93}$$

$$\mathbf{P}_k = \mathbf{P}_{k|k-1} - \mathbf{K}_k \mathbf{P}_{\hat{\mathbf{y}}_{k|k-1}} \mathbf{K}_k^T \tag{94}$$

### 2.6.1 Linearization of the UKF for Non-Additive Noise

The assumptions on the noise characteristics of the system are important aspects of the nonlinear state estimation problem. For a general nonlinear system of the form (44), modifications can be made to the linearization technique employed by the UKF to accommodate non-additive noise processes. The UKF handles non-additive noise assumptions for process noise through the augmentation of the state vector with the process noise vector, and correspondingly for covariance:

$$\mathbf{x}_k^a = \begin{bmatrix} \mathbf{x}_k \\ \mathbf{w}_k \end{bmatrix} \tag{95}$$

$$\mathbf{P}_k^a = \begin{bmatrix} \mathbf{P}_k & 0 \\ 0 & \mathbf{Q}_k \end{bmatrix} \tag{96}$$

where the superscript *a* denotes augmentation. Using this augmented system, the sigma points used in the unscented transformation have components corresponding to the state and process noise:

$$\boldsymbol{\chi}_k^a = \begin{bmatrix} \boldsymbol{\chi}_k^x \\ \boldsymbol{\chi}_k^w \end{bmatrix} \tag{97}$$

Therefore, these sigma points can be used in (44) directly, as in:

$$\boldsymbol{\chi}_k^x = \mathbf{f}(\boldsymbol{\chi}_{k-1}^x, \mathbf{u}_k, \boldsymbol{\chi}_{k-1}^w) \tag{98}$$

Similar modifications for the UKF can be made to handle non-additive noise in the output equations.

### 2.6.2 Unscented Kalman Filter Stability

The stability of the UKF was analyzed in [35] by building upon the previous estimation stability work for the EKF [40]. This analysis used a similar method to [40], with a distinct difference in the linearization error model. Instead of using the additive noise model from (67), the linearization error is described using an unknown instrumental diagonal matrix, $\boldsymbol{\beta}_k$, as in (81). This diagonal matrix provides a multiplicative representation of the linearization error, where the identity matrix indicates perfect linearization. Bounds on this term are considered such that

$$\beta_{\min}^2 \mathbf{I} \leq \boldsymbol{\beta}_k \boldsymbol{\beta}_k^T \leq \beta_{\max}^2 \mathbf{I} \tag{99}$$

Using this instrumental matrix, a similar analysis as [40] is used to demonstrate the stability of the UKF under certain conditions using the stochastic stability lemma. For full details of the stability proof, see [35]. For this stability analysis, modifications were considered to the standard UKF to incorporate an extra positive definite matrix in the assumed process noise. This matrix serves to improve the stability characteristics of the system, but introduces a tradeoff between stability and accuracy of the estimation. It was stated in [36] that these results apply to a more general class of filters, including the EKF. Further work by Xu *et al.* extended this analysis to incorporate correlated noise terms [37].

# 3.0 AIRCRAFT ATTITUDE ESTIMATION

This work analyzes nonlinear state estimation in the context of a particular application problem, aircraft attitude estimation. This particular application was selected as it is an important nonlinear estimation problem in the aerospace community, especially because of the increased interests in subscale flight testing. Many uses of subscale aircraft require a method of accurately estimating the attitude of the aircraft [67,68]. For example, remote sensing is a popular application that requires accurate attitude estimates. Some example remote sensing applications include 3-D mapping with direct geo-referencing [69] and constructing large mosaics [70]. Because of cost and weight restrictions which are typical for subscale aircraft applications [71,72], high quality military grade inertial navigation systems may not be practical [72,73]. Therefore, attitude estimation using low-cost sensors is an important consideration for civilian applications of subscale aircraft. A common approach to this problem is now discussed.

## 3.1 GPS/INS SENSOR FUSION

A common approach to the attitude estimation problem involves the fusing of information from an onboard Inertial Navigation System (INS) with Global Positioning System (GPS) [74,75]. This process is referred to as GPS/INS sensor fusion. The motivation for this method is that inertial sensors tend to produce results that drift with time when integrated for navigation purposes. GPS, however, does not provide any

direct attitude information, but can be used to regulate the error growth of the INS estimates by providing non-drifting measurements.

There are two different classifications of GPS/INS sensor fusion, which is based on the type of information provided by the GPS to the estimation algorithm: "tightly-coupled" and "loosely-coupled" [74]. A tightly-coupled GPS/INS sensor fusion algorithm uses pseudorange and carrier phase data from each satellite individually in the algorithm. This allows for the use of information from any number of satellites, including situations where the GPS cannot obtain a "fix" in order to calculate a position and velocity solution. On the other hand, a loosely-coupled GPS/INS sensor fusion algorithm uses only position and velocity solutions provided by the GPS receiver. This is limited to situations where the GPS has a fix, but is easier to implement and understand. Only loosely-coupled GPS/INS sensor fusion algorithms are considered in this dissertation.

For both tightly-coupled and loosely-coupled GPS/INS sensor fusion algorithms, different state estimation filters can be used. Kalman-based filters are a commonly used technique due to their optimal observer gains and reasonable computational requirements [62]. Particle filters [76,77] are also a powerful tool for nonlinear state estimation problems, including GPS/INS sensor fusion. The statistical approach used for particle filters involves the generation and propagation of a large number of particles. This allows for very good approximations on nonlinearities and non-Gaussian noise assumptions. However, due to the nature of this method, a large computational load is required, thus making it currently impractical for on-line implementation in real-world

engineering systems. Because of this, only Kalman-based filters are considered in this dissertation.

## 3.2 LOOSELY-COUPLED GPS/INS SENSOR FUSION FORMULATIONS

There are multiple ways to formulate the loosely-coupled GPS/INS sensor fusion problem, *e.g.* [14,16,78,79], and a few of these formulations are presented in the following sections. Each of these formulations uses the state space framework necessary for Kalman-based filters. First, the necessary inertial navigation equations are presented followed by descriptions of the considered GPS/INS sensor fusion formulations. Then, a few alternative methods of attitude estimation are discussed.

### 3.2.1 Inertial Navigation Equations

An important consideration for inertial navigation is the necessary coordinate frames. In general, there are two coordinate frames of interest. The first coordinate frame is the aircraft body coordinate (ABC) frame which is fixed to the aircraft body. This coordinate system is useful, because strap-down sensors such as an inertial measurement unit (IMU) are fixed to the aircraft, and therefore record measurements with respect to the aircraft body. Standard aircraft convention designates the origin of this frame at the center of gravity (CG) of the aircraft, with $x$-axis pointing toward the nose, $y$-axis pointing toward the right wing, and the $z$-axis pointing down. Since GPS information is utilized, it is also important to consider a local Earth-fixed frame with a

specified origin, *e.g.*, a North-East-Down (NED) coordinate frame. Since this problem involves two different coordinate frames, the relationship between the two becomes important. This relationship is determined using the Direction Cosine Matrix (DCM) [80]

$$\mathbf{DCM}(\phi,\theta,\psi)=\begin{bmatrix}\cos\theta\cos\psi & -\cos\phi\sin\psi+\sin\phi\sin\theta\cos\psi & \sin\phi\sin\psi+\cos\phi\sin\theta\cos\psi\\ \cos\theta\sin\psi & \cos\phi\cos\psi+\sin\phi\sin\theta\sin\psi & -\sin\phi\cos\psi+\cos\phi\sin\theta\sin\psi\\ -\sin\theta & \sin\phi\cos\theta & \cos\phi\cos\theta\end{bmatrix} \tag{100}$$

where $\phi$, $\theta$, $\psi$, are the Euler (roll, pitch, and yaw) angles of the aircraft. Therefore, this coordinate frame rotation can be used to establish the relationship between the ABC accelerations as measured by the IMU, and the acceleration in the fixed frame

$$\begin{bmatrix}\dot{V}_x\\ \dot{V}_y\\ \dot{V}_z\end{bmatrix}=\mathbf{DCM}(\phi,\theta,\psi)\begin{bmatrix}a_{\tilde{x}}\\ a_{\tilde{y}}\\ a_{\tilde{z}}\end{bmatrix}+\begin{bmatrix}0\\ 0\\ g\end{bmatrix} \tag{101}$$

where the tilde (~) superscript is used to denote the ABC frame. The acceleration due to gravity, $g$, is included since the accelerometers measure the absolute acceleration of the object, *i.e.*, relative to free fall. A similar coordinate transformation must be used in order to relate the aircraft body angular rates ($p$, $q$, $r$) to the Euler angular rates [81]

$$\begin{bmatrix}\dot{\phi}\\ \dot{\theta}\\ \dot{\psi}\end{bmatrix}=\begin{bmatrix}1 & \sin\phi\tan\theta & \cos\phi\tan\theta\\ 0 & \cos\phi & -\sin\phi\\ 0 & \sin\phi\sec\theta & \cos\phi\sec\theta\end{bmatrix}\begin{bmatrix}p\\ q\\ r\end{bmatrix} \tag{102}$$

Since digital measurement systems can only record discrete-time measurements, these theoretical continuous-time relationships must be discretized. This is done using a first order approximation [1]. The resulting discrete-time form of (101) and (102) using this approximation is given below

$$\begin{bmatrix} V_{x,k} \\ V_{y,k} \\ V_{z,k} \end{bmatrix} = \begin{bmatrix} V_{x,k-1} \\ V_{y,k-1} \\ V_{z,k-1} \end{bmatrix} + T_s^y \left( \mathbf{DCM}\left(\phi_{k-1}, \theta_{k-1}, \psi_{k-1}\right) \begin{bmatrix} a_{\tilde{x},k} \\ a_{\tilde{y},k} \\ a_{\tilde{z},k} \end{bmatrix} + \begin{bmatrix} 0 \\ 0 \\ g \end{bmatrix} \right) \tag{103}$$

$$\begin{bmatrix} \phi_k \\ \theta_k \\ \psi_k \end{bmatrix} = \begin{bmatrix} \phi_{k-1} \\ \theta_{k-1} \\ \psi_{k-1} \end{bmatrix} + T_s^x \begin{bmatrix} 1 & \sin\phi_{k-1}\tan\theta_{k-1} & \cos\phi_{k-1}\tan\theta_{k-1} \\ 0 & \cos\phi_{k-1} & -\sin\phi_{k-1} \\ 0 & \sin\phi_{k-1}\sec\theta_{k-1} & \cos\phi_{k-1}\sec\theta_{k-1} \end{bmatrix} \begin{bmatrix} p_k \\ q_k \\ r_k \end{bmatrix} \tag{104}$$

### 3.2.2 Acceleration Vector Attitude Estimation

An Acceleration Vector Attitude Estimation (AVAE) algorithm was developed for direct attitude estimation following the dynamic tilt sensor concept [14]. The AVAE algorithm uses GPS acceleration in a local NED frame obtained through numerical differentiation of GPS velocity measurements, and accelerometer measurements obtained in the ABC frame. The aircraft Euler angles, roll, pitch, and yaw ($\phi$, $\theta$, $\psi$), relate the velocity in the two coordinate frames through the DCM defined by (100)

$$\begin{bmatrix} a_x \\ a_x \\ a_z \end{bmatrix} = \mathbf{DCM}\left(\phi, \theta, \psi\right) \begin{bmatrix} a_{\tilde{x}} \\ a_{\tilde{y}} \\ a_{\tilde{z}} \end{bmatrix} + \begin{bmatrix} 0 \\ 0 \\ g \end{bmatrix} \tag{105}$$

where $a$ is acceleration and $g$ is the acceleration due to gravity. Note that the NED coordinates are represented by $x$, $y$, $z$, while the ABC coordinates are distinguished using (~). With measurements from both GPS and accelerometers, the projection of the local gravity vector on the three aircraft body-axes in terms of the three Euler angles can then be solved, as demonstrated by Kingston and Beard [82].

To reduce the matrix relationship shown in (105), the yaw angle, $\psi$, is approximated by the aircraft heading angle which is obtained using the instantaneous

four-quadrant inverse tangent (*i.e.* atan2) to the aircraft trajectory using GPS velocity measurements in the *x* and *y* axes within the local NED coordinate frame:

$$\hat{\psi} = \tan^{-1}\left(\frac{V_y^{GPS}}{V_x^{GPS}}\right) \tag{106}$$

The two remaining aircraft Euler angles are then estimated by considering sequential Euler rotations. Specifically, by considering the rotation through the heading angle, an intermediate acceleration vector, denoted with subscript $\psi$, is defined as

$$\begin{bmatrix} a_{x,\psi} \\ a_{y,\psi} \\ a_{z,\psi} \end{bmatrix} = \begin{bmatrix} a_x \cos\hat{\psi} + a_y \sin\hat{\psi} \\ a_y \cos\hat{\psi} - a_x \sin\hat{\psi} \\ a_z - g \end{bmatrix} \tag{107}$$

which leads to the following algebraic equations:

$$\begin{bmatrix} a_{\tilde{x}} \\ a_{\tilde{y}} \\ a_{\tilde{z}} \end{bmatrix} = \begin{bmatrix} \cos\theta & 0 & -\sin\theta \\ \sin\phi\sin\theta & \cos\phi & \sin\phi\cos\theta \\ \cos\phi\sin\theta & -\sin\phi & \cos\phi\cos\theta \end{bmatrix} \begin{bmatrix} a_{x,\psi} \\ a_{y,\psi} \\ a_{z,\psi} \end{bmatrix} \tag{108}$$

The first equation of the above set can be solved to obtain an estimate of the pitch angle:

$$\hat{\theta} = \tan^{-1}\left(\frac{a_{x,\psi}a_{z,\psi} + a_{\tilde{x}}\sqrt{a_{x,\psi}{}^2 + a_{z,\psi}{}^2 - a_{\tilde{x}}{}^2}}{a_{\tilde{z},\psi}{}^2 - a_{\tilde{x}}{}^2}\right) \tag{109}$$

By again rotating the acceleration vector by the newly obtained pitch estimate, a second intermediate acceleration vector, denoted with subscript $\psi\theta$, is defined by

$$\begin{bmatrix} a_{x,\psi\theta} \\ a_{y,\psi\theta} \\ a_{z,\psi\theta} \end{bmatrix} = \begin{bmatrix} a_{x,\psi}\cos\hat{\theta} - a_{z,\psi}\sin\hat{\theta} \\ a_{y,\psi} \\ a_{x,\psi}\sin\hat{\theta} + a_{z,\psi}\cos\hat{\theta} \end{bmatrix} \tag{110}$$

This leaves the roll angle as the only unknown variable:

$$\begin{bmatrix} a_{\tilde{x}} \\ a_{\tilde{y}} \\ a_{\tilde{z}} \end{bmatrix} = \begin{bmatrix} 1 & 0 & 0 \\ 0 & \cos\phi & \sin\phi \\ 0 & -\sin\phi & \cos\phi \end{bmatrix} \begin{bmatrix} a_{x,\psi\theta} \\ a_{y,\psi\theta} \\ a_{z,\psi\theta} \end{bmatrix} \tag{111}$$

which can be solved algebraically to obtain an estimate of the roll angle:

$$\hat{\phi} = \tan^{-1}\left( \frac{-a_{y,\psi\theta}a_{z,\psi\theta} - a_{\tilde{y}}\sqrt{a_{y,\psi\theta}^{\ 2} + a_{z,\psi\theta}^{\ 2} - a_{\tilde{y}}^{\ 2}}}{a_{z,\psi\theta}^{\ 2} - a_{\tilde{y}}^{\ 2}} \right) \tag{112}$$

Within the AVAE algorithm, the GPS acceleration vector is calculated using a numerical backward-difference derivative of the GPS velocity measurement vector. To reduce the noise associated with the numerical derivative, the pitch and roll estimates obtained with the AVAE formulation are smoothed with a first order low-pass Butterworth filter. This section presented a direct calculation method of obtaining an estimate of the aircraft attitude from GPS and IMU accelerations. In the following sections, recursive methods through nonlinear state space formulations are described.

### 3.2.3 3-State GPS/INS Sensor Fusion Formulation

Since attitude estimation is the primary goal, the simplest state vector that can be considered for this problem consists of the three Euler angles, $\mathbf{x} = [\phi \quad \theta \quad \psi]^T$. With these states, the dynamics are determined by (104), with an input vector consisting of the aircraft body angular rates, $\mathbf{u} = [p \quad q \quad r]^T$. The deterministic formulation of these dynamics can be written as

$$\mathbf{x}_k = \begin{bmatrix} \phi_k \\ \theta_k \\ \psi_k \end{bmatrix} = \mathbf{f}\left(\mathbf{x}_{k-1}, \mathbf{u}_k\right) = \begin{bmatrix} \phi_{k-1} \\ \theta_{k-1} \\ \psi_{k-1} \end{bmatrix} + T_s^x \begin{bmatrix} 1 & \sin\phi_{k-1}\tan\theta_{k-1} & \cos\phi_{k-1}\tan\theta_{k-1} \\ 0 & \cos\phi_{k-1} & -\sin\phi_{k-1} \\ 0 & \sin\phi_{k-1}\sec\theta_{k-1} & \cos\phi_{k-1}\sec\theta_{k-1} \end{bmatrix} \begin{bmatrix} p_k \\ q_k \\ r_k \end{bmatrix} \quad (113)$$

Since the IMU is subject to noise uncertainties, the stochastic problem must be considered, and is formulated as follows

$$\begin{aligned} \mathbf{x}_k &= \mathbf{f}\left(\mathbf{x}_{k-1}, \mathbf{u}_k + \mathbf{w}_k\right) \\ \mathbf{w}_k &\sim N(\mathbf{0}, \mathbf{Q}_k) \end{aligned} \quad (114)$$

where **w** is the process noise vector, which is considered to be additive to the inputs. This assumes that all of the uncertainty in the state equations is in the inputs, *i.e.*, the model equation is perfect. Although (102) should not contain any uncertainty since it is derived from kinematics, the discretization process does introduce some error in (104). To compensate for this uncertainty, an additional process noise term can be added to the state vector, as in

$$\begin{aligned} \mathbf{x}_k &= \mathbf{f}\left(\mathbf{x}_{k-1}, \mathbf{u}_k + \mathbf{w}_k^u\right) + \mathbf{w}_k^x \\ \mathbf{w}_k^u &\sim N(\mathbf{0}, \mathbf{Q}_k^u) \\ \mathbf{w}_k^x &\sim N(\mathbf{0}, \mathbf{Q}_k^x) \end{aligned} \quad (115)$$

where $\mathbf{w}_k^x$ is the process noise due to discretization. For this analysis, the discretization error is neglected due to the high sampling rate of the system, and the process noise due to the inputs is assumed constant, and is calculated from static sensor measurements

$$\mathbf{Q}_k = \mathbf{Q} = diag\left[\sigma_p^2 \quad \sigma_q^2 \quad \sigma_r^2\right] \quad (116)$$

The output or observation equations are formulated as follows. The output is considered as the change in velocity between successive time steps, determined by rearranging (103)

$$\mathbf{y}_k = \Delta\mathbf{V} = \mathbf{V}_k - \mathbf{V}_{k-1} = \begin{bmatrix} V_{x,k} \\ V_{y,k} \\ V_{z,k} \end{bmatrix} - \begin{bmatrix} V_{x,k-1} \\ V_{y,k-1} \\ V_{z,k-1} \end{bmatrix} = T_s^y \left( \mathbf{DCM}\left(\phi_{k-1}, \theta_{k-1}, \psi_{k-1}\right) \begin{bmatrix} a_{\tilde{x},k} \\ a_{\tilde{y},k} \\ a_{\tilde{z},k} \end{bmatrix} + \begin{bmatrix} 0 \\ 0 \\ g \end{bmatrix} \right) \quad (117)$$

This equation follows a standard nonlinear form of the deterministic observation equations

$$\mathbf{y}_k = \mathbf{h}\left(\mathbf{x}_k, \mathbf{d}_k\right) \quad (118)$$

where the observation equation input is defined from the IMU accelerations, $\mathbf{d} = \begin{bmatrix} a_{\tilde{x}} & a_{\tilde{y}} & a_{\tilde{z}} \end{bmatrix}^T$. Since again the relationships are derived from kinematics, there are only two primary sources of uncertainty in these equations: uncertainty in the IMU acceleration measurements and uncertainty in the measurement of the output, which is obtained from GPS velocity measurements

$$\mathbf{z} = \begin{bmatrix} V_{x,k} - V_{x,k-1} \\ V_{y,k} - V_{y,k-1} \\ V_{z,k} - V_{z,k-1} \end{bmatrix}_{GPS} \quad (119)$$

To incorporate these uncertainties into the stochastic system, two measurement noise terms are included

$$\begin{aligned} \mathbf{y}_k &= \mathbf{h}\left(\mathbf{x}_k, \mathbf{d}_k + \mathbf{v}_k^d\right) + \mathbf{v}_k^y \\ \mathbf{v}_k^d &\sim N(\mathbf{0}, \mathbf{R}_k^d) \\ \mathbf{v}_k^y &\sim N(\mathbf{0}, \mathbf{R}_k^y) \end{aligned} \quad (120)$$

where the measurement covariance matrices are determined from static sensor measurements, as in

$$\mathbf{R}_k^d = \mathbf{R}^d = diag\begin{bmatrix} \sigma_{a_{\tilde{x}}}^2 & \sigma_{a_{\tilde{y}}}^2 & \sigma_{a_{\tilde{z}}}^2 \end{bmatrix} \tag{121}$$

$$\mathbf{R}_k^y = \mathbf{R}^y = diag\begin{bmatrix} \sigma_{\Delta V_x}^2 & \sigma_{\Delta V_y}^2 & \sigma_{\Delta V_z}^2 \end{bmatrix} \tag{122}$$

To write these uncertainties in the standard form of a nonlinear stochastic equation (44), the measurement noise vectors are combined, such that

$$\begin{aligned} \mathbf{v}_k &= \begin{bmatrix} \mathbf{v}_k^d \\ \mathbf{v}_k^y \end{bmatrix} \sim N(\mathbf{0}, \mathbf{R}_k) \\ \mathbf{R}_k &= \begin{bmatrix} \mathbf{R}_k^d & 0 \\ 0 & \mathbf{R}_k^y \end{bmatrix} \end{aligned} \tag{123}$$

To implement the presented 3-state GPS/INS sensor fusion formulation using an EKF, the following Jacobian matrices must be calculated using (64)

$$\mathbf{A}_k = \begin{bmatrix} 1 + T_s^x \tan\theta(q\cos\phi - r\sin\phi) & T_s^x \sec^2\theta(q\sin\phi + r\cos\phi) & 0 \\ -T_s^x(q\sin\phi + r\cos\phi) & 1 & 0 \\ T_s^x \sec\theta(q\cos\phi - r\sin\phi) & T_s^x \sec\theta\tan\theta(q\sin\phi + r\cos\phi) & 1 \end{bmatrix} \tag{124}$$

$$\begin{aligned} \mathbf{H}_k = \Bigg[ & \begin{matrix} \left(s\psi s\phi + c\psi s\theta c\phi\right)a_{\tilde{y}} + \left(s\psi c\phi - c\psi s\theta s\phi\right)a_{\tilde{z}} & \left(-c\psi s\theta\right)a_{\tilde{x}} + \left(c\psi c\theta s\phi\right)a_{\tilde{y}} + \left(c\psi c\theta c\phi\right)a_{\tilde{z}} \\ \left(-c\psi s\phi + s\psi s\theta c\phi\right)a_{\tilde{y}} + \left(-c\psi c\phi - s\psi s\theta s\phi\right)a_{\tilde{z}} & \left(-s\psi s\theta\right)a_{\tilde{x}} + \left(s\psi c\theta s\phi\right)a_{\tilde{y}} + \left(s\psi c\theta c\phi\right)a_{\tilde{z}} \\ \left(c\theta c\phi\right)a_{\tilde{y}} + \left(-c\theta s\phi\right)a_{\tilde{z}} & \left(-c\theta\right)a_{\tilde{x}} + \left(-s\theta s\phi\right)a_{\tilde{y}} + \left(-s\theta c\phi\right)a_{\tilde{z}} \end{matrix} \\ & \begin{matrix} \left(-s\psi c\theta\right)a_{\tilde{x}} + \left(-c\psi c\phi - s\psi s\theta s\phi\right)a_{\tilde{y}} + \left(c\psi s\phi - s\psi s\theta c\phi\right)a_{\tilde{z}} \\ \left(c\psi c\theta\right)a_{\tilde{x}} + \left(-s\psi c\phi + c\psi s\theta s\phi\right)a_{\tilde{y}} + \left(s\psi s\phi + c\psi s\theta c\phi\right)a_{\tilde{z}} \\ 0 \end{matrix} \Bigg] T_s^y \end{aligned} \tag{125}$$

$$\mathbf{L}_k = T_s^x \begin{bmatrix} 1 & \sin\phi\tan\theta & \cos\phi\tan\theta \\ 0 & \cos\phi & -\sin\phi \\ 0 & \sin\phi\sec\theta & \cos\phi\sec\theta \end{bmatrix} \tag{126}$$

$$\mathbf{M}_k = \begin{bmatrix} T_s^y \mathbf{DCM}(\phi,\theta,\psi) & \mathbf{I} \end{bmatrix} \tag{127}$$

where $s\phi$ and $c\phi$ are used to abbreviate sin $\phi$ and cos $\phi$ respectively, and the states and inputs are evaluated at time step $k$.

### 3.2.4 6-State GPS/INS Sensor Fusion Formulation

For this 6-state sensor fusion formulation, in addition to the attitude of the aircraft, the local Cartesian components of velocity are included as states: $\mathbf{x} = \begin{bmatrix} V_x & V_y & V_z & \phi & \theta & \psi \end{bmatrix}^T$. The state prediction equations for these states are defined by (103) and (104), with the input vector given by all six IMU measurements: $\mathbf{u} = \begin{bmatrix} a_{\tilde{x}} & a_{\tilde{y}} & a_{\tilde{z}} & p & q & r \end{bmatrix}^T$. The output for this formulation is given by extracting the measured states of the system:

$$\mathbf{y}_k = \mathbf{h}(\mathbf{x}_k, \mathbf{d}_k, \mathbf{v}_k) = \mathbf{H}\mathbf{x} + \mathbf{v}_k^y = \begin{bmatrix} V_x & V_y & V_z \end{bmatrix}^T + \mathbf{v}_k^y \tag{128}$$

where the observation function **h** due to linearity can be written using the observation matrix, $\mathbf{H} = \begin{bmatrix} \mathbf{I}_{3x3} & \mathbf{0}_{3x3} \end{bmatrix}$, where **I** is an identity matrix and **0** is a matrix of zeros with given dimensions. Note that for this formulation, there is no input to the output equations, *i.e.*, **d** = 0; therefore there is no component of **R** corresponding to **d**. The measurement vector **z** consists of the velocity measurements provided by GPS: $\mathbf{z} = \begin{bmatrix} V_x & V_y & V_z \end{bmatrix}_{GPS}^T$. The process and measurement noise covariance matrices can be calculated in a similar fashion as the 3-state formulation:

$$\mathbf{Q}_k = \mathbf{Q} = diag\begin{bmatrix} \sigma_{a_{\tilde{x}}}^2 & \sigma_{a_{\tilde{y}}}^2 & \sigma_{a_{\tilde{z}}}^2 & \sigma_p^2 & \sigma_q^2 & \sigma_r^2 \end{bmatrix} \tag{129}$$

$$\mathbf{R}_k^y = \mathbf{R}^y = diag\begin{bmatrix} \sigma_{V_x}^2 & \sigma_{V_y}^2 & \sigma_{V_z}^2 \end{bmatrix} \tag{130}$$

### 3.2.5 9-State GPS/INS Sensor Fusion Formulation

The 9-state formulation expands upon the 6-state formulation to include position states in the filter, thus defining a state vector of $\mathbf{x} = \begin{bmatrix} r_x & r_y & r_z & V_x & V_y & V_z & \phi & \theta & \psi \end{bmatrix}^T$, where $r_x$, $r_y$, and $r_z$ are the position of the aircraft in local Cartesian components. The state prediction equations for the velocity and attitude states remain the same as for the 6-state formulation, while the position dynamics are defined using first order numerical integration of the velocity states, as in:

$$\begin{bmatrix} r_{x,k} \\ r_{y,k} \\ r_{z,k} \end{bmatrix} = \begin{bmatrix} r_{x,k-1} \\ r_{y,k-1} \\ r_{z,k-1} \end{bmatrix} + T_s \begin{bmatrix} V_{x,k-1} \\ V_{y,k-1} \\ V_{z,k-1} \end{bmatrix} \tag{131}$$

The position states are also added to the output vector, since they can be directly measured by GPS, thus leading to the output equations:

$$\mathbf{y}_k = \mathbf{h}(\mathbf{x}_k, \mathbf{d}_k) + \mathbf{v}_k^y = \mathbf{H}\mathbf{x} + \mathbf{v}_k^y = \begin{bmatrix} r_x & r_y & r_z & V_x & V_y & V_z \end{bmatrix}^T + \mathbf{v}_k^y \tag{132}$$

where **h** is the observation function, which for this formulation due to linearity can be written using the observation matrix, $\mathbf{H} = \begin{bmatrix} \mathbf{I}_{6x6} & \mathbf{0}_{6x3} \end{bmatrix}$, where **I** is an identity matrix and **0** is a matrix of zeros with given dimensions.

### 3.2.6 12-State GPS/INS Sensor Fusion Formulation

The 12-state sensor fusion formulation is an extension of the 6-state formulation that includes six additional states that represent time-varying biases associated with the IMU measurements:

$$\mathbf{x} = \begin{bmatrix} V_x & V_y & V_z & \phi & \theta & \psi & b_{a_{\tilde{x}}} & b_{a_{\tilde{y}}} & b_{a_{\tilde{z}}} & b_p & b_q & b_r \end{bmatrix}^T \tag{133}$$

where the $b$ terms denote a sensor bias on each of the 6 IMU measurements, and is represented collectively by $\boldsymbol{b} = \begin{bmatrix} b_{a_{\tilde{x}}} & b_{a_{\tilde{y}}} & b_{a_{\tilde{z}}} & b_p & b_q & b_r \end{bmatrix}^T$, which has associated random walk noise, given by $\mathbf{w}_k^b \sim N(0, \mathbf{Q}_k^b)$. With this state vector, the state prediction equations are equivalent to the 6-state formulation for the first six states, and the biases are predicted using:

$$\mathbf{b}_k = \mathbf{b}_{k-1} + \mathbf{w}_k^b \tag{134}$$

This noise model is a random walk noise model, however other noise models can be used for the bias states such as a Gauss-Markov noise model [83-85]. The components of the process noise covariance matrix corresponding to the biases are obtained using the noise characteristics of each corresponding sensor. Since this formulation is equivalent to the 6-state formulation with the exception of the biases, the same noise covariance matrices are used, with the bias covariance matrix components appended. The measurement update for this formulation is given by extracting the measured states of the system with $\mathbf{H} = \begin{bmatrix} \mathbf{I}_{3x3} & \mathbf{0}_{3x9} \end{bmatrix}$, and measurement vector $\mathbf{z} = \begin{bmatrix} V_x & V_y & V_z \end{bmatrix}_{GPS}^T$.

### 3.2.7 15-State GPS/INS Sensor Fusion Formulation

The 15-state sensor fusion formulation is an extension of the 9-state formulation that includes six additional states that represent time-varying biases associated with the IMU measurements:

$$\mathbf{x} = \begin{bmatrix} r_x & r_y & r_z & V_x & V_y & V_z & \phi & \theta & \psi & b_{a_{\tilde{x}}} & b_{a_{\tilde{y}}} & b_{a_{\tilde{z}}} & b_p & b_q & b_r \end{bmatrix}^T \tag{135}$$

where the *b* terms denote a sensor bias on each of the 6 IMU measurements in the same fashion as the 12-state formulation. The measurement update for the 15-state formulation is the same as for the 9-state formulation, except with additional zeros added to the observation matrix, as in $\mathbf{H} = \begin{bmatrix} \mathbf{I}_{3x3} & \mathbf{0}_{3x12} \end{bmatrix}$.

## 3.3 ALTERNATIVE ATTITUDE ESTIMATION METHODS

While GPS/INS is the most common method for low-cost attitude estimation, other alternative methods were considered during this work. Typical GPS/INS uses a single IMU; however methods for using multiple IMUs for attitude estimation were analyzed. Most Kalman filter based multi-sensor fusion work assumes redundancy only in the measurement update, which can be handled using an information filter [62], or its nonlinear variants such as the Extended Information Filter (EIF) [86] or Unscented Information Filter (UIF) [87]. This work, however, approaches the problem of multi-sensor fusion where the sensor information is used in the prediction stage of a nonlinear estimator. Since the redundancy is in the prediction, the current information filtering tools cannot directly be used, because these methods are formulated only for multiple measurements used in the measurement update stage of the filter. Using previous multi-sensor fusion work as inspiration, three different fusion methods were developed for handling redundant prediction information. Further details and results can be found in [88].

The effectiveness of using multiple Global Positioning System (GPS) antennas for attitude estimation has been well established in the technical community, typically through the use of pseudorange and carrier phase signals. Different applications have been studied for multiple GPS attitude estimation including general aviation aircraft [89-93], ships [94-99], subscale aircraft [100,101], off-road land vehicles [102], micro-satellites [103,104], general test setups [105,106], and simulation studies [107-110]. Loosely-coupled GPS position and velocity calculations can also be effective in extracting attitude information, especially for small low-cost subscale aircraft applications that have limited on-board computational resources. The reduced computational requirements allow for a higher update rate. Various combinations of sensor measurements containing information regarding the attitude of the aircraft were considered. In particular, three sources of attitude information are considered: rate gyroscopes, gravity vector, and the longitudinal axis vector, as illustrated in Figure 4. More details regarding this topic can be found in [111].

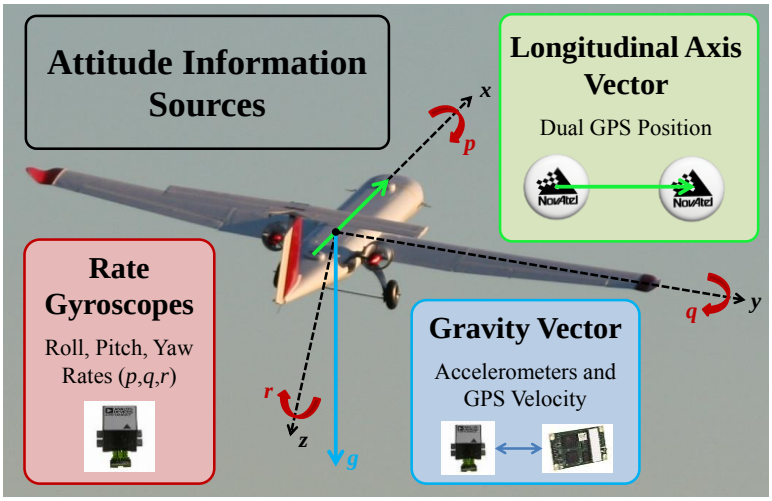


Figure 4. Attitude Information Sources

One problem with the existing work in GPS/INS sensor fusion for attitude estimation is that it implicitly assumes that the angle of attack and sideslip angles of the aircraft are zero, *i.e.* the aircraft is always pointing in the direction of its total velocity. The INS can be used to predict the attitude angles of the aircraft effectively through time integration of the rate gyroscope measurements from an IMU. Since these estimates tend to drift with time due to sensor biases, GPS position and velocity measurements are then used to regulate this drifting phenomenon. However, when using GPS velocity to regulate the attitude angles, current work implicitly makes a simplifying assumption that the orientation of the aircraft is equivalent to the direction of the velocity of the aircraft. While under many operating conditions this approximation can lead to reasonable results, a more theoretically justifiable formulation should consider relative wind information in order to properly relate the INS predicted attitude with the GPS velocity calculations. A new formulation of attitude estimation that includes relative wind information can be found in [112].

Another method of attitude estimation can be provided by the complementary filter [113]. This filter does not require GPS information, and relies solely on measurements from an IMU. Unlike a Kalman-based filter, this technique uses a constant gain to update the states, thus providing a much more computationally efficient algorithm. The basic idea of the complementary filter is to combine low frequency information from the accelerometers with high frequency information from the rate gyroscopes. This is motivated by the idea that the accelerometers provide a good indication of the attitude under static conditions, while the rate gyroscopes provide a

better indication of the attitude under dynamic conditions. This method is relatively simple both in terms of implementation and understanding, but it suffers from some difficulties. If the system dynamics become too significant, such as in a situation where the aircraft is constantly turning, the filter will have trouble providing a stable low-pass estimate of the direction of gravity.

# 4.0 EXPERIMENTAL PLATFORM

The primary subscale aircraft platform that is studied in this work is the West Virginia University (WVU) YF-22, shown in Figure 5. This platform was designed and built by researchers from WVU. The YF-22 has been used for various projects, such as formation flight [114-116] and fault-tolerant flight control [117].

Figure 5. WVU YF-22 Research Platform

Flight data were collected on the three WVU YF-22 aircraft (Green, Blue, and Red) using two different avionics system configurations and four different sensor payloads. Avionics system #1 [114], shown in Figure 6, features a Novatel OEM4® GPS receiver, which reports a 1.8 m Circular Error Probable (CEP) for position measurements and 0.03 m/s root mean square (RMS) accuracy for velocity, and a Crossbow® IMU. A copy of

avionics system #1 was implemented in each of the three aircraft, each with a slightly different version of IMU, as outlined in Table 2. Avionics system #2, shown in Figure 7, was a newer system [118] and was used in the retrofitted „Blue" YF-22 (Blue*). This system also includes a Novatel OEM4® GPS receiver; however, an Analog Devices ADIS-16405® IMU was used. The specifications for the four different IMUs are shown in Table 2.

Table 2. Inertial Measurement Unit (IMU) Specifications

| IMU | WVU YF-22 Aircraft | Accelerometer Dynamic Range (g) | Accelerometer Resolution (mg) | Rate Gyroscope Dynamic Range (deg/sec) | Rate Gyroscope Resolution (deg/sec) |
|---|---|---|---|---|---|
| VG400CA-200 | Green | ± 10 | 1.25 | ± 200 | 0.05 |
| DMU(VG400)-100 | Red | ± 8 | 0.25 | ± 100 | 0.05 |
| IMU400CC-200 | Blue | ± 10 | 1.25 | ± 200 | 0.05 |
| ADIS-16405® | Blue* | ± 18 | 3.33 | ± 150 | 0.025 |

In addition to the IMU and GPS measurements, measurements of the roll and pitch angles were independently recorded using a Goodrich VG34® mechanical vertical gyroscope, which is sampled with 16-bit resolution and has ±90° roll measurement range and ±60° pitch range. The VG34® has a self-erection system, and reported accuracy within 0.25° of true vertical. The mounting plate that holds both the IMU and the vertical gyro is manually leveled before each flight, in order to provide a reference for the pitch and roll angles as close to zero as possible. The mechanical vertical gyroscope measurements are used to establish a baseline „true data" for the sensor fusion study.

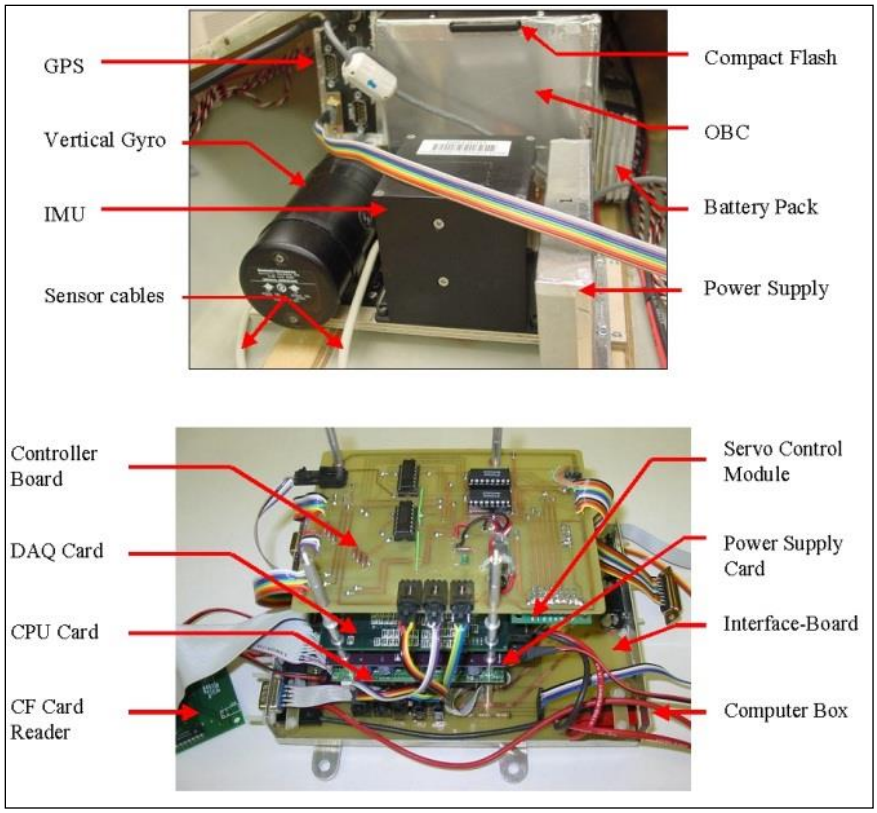


Figure 6. Avionics System #1

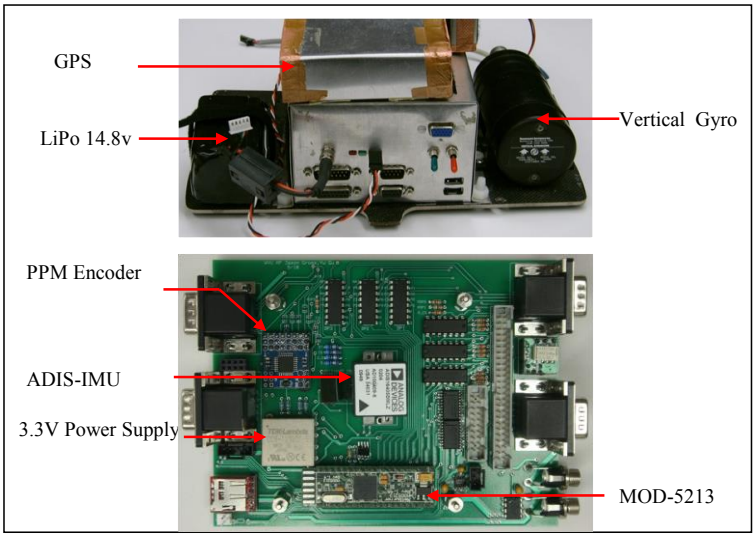


Figure 7. Avionics System #2

## 4.1 FLIGHT DATA SELECTION

Many sets of data were collected from the WVU YF-22 platform. Each data set includes measurements from the IMU, GPS, and vertical gyroscope. For this analysis, 23 flights were selected to obtain data with a variety of sensors and flight conditions. The 23 flights were selected from each aircraft (8 Green, 5 Red, 8 Blue, 2 Blue*), and piloting method (11 mixed manual/autonomous, 12 manual only). The atmospheric temperature and wind speed during the flight were also considered, and the distribution of these conditions is shown in Figure 8.

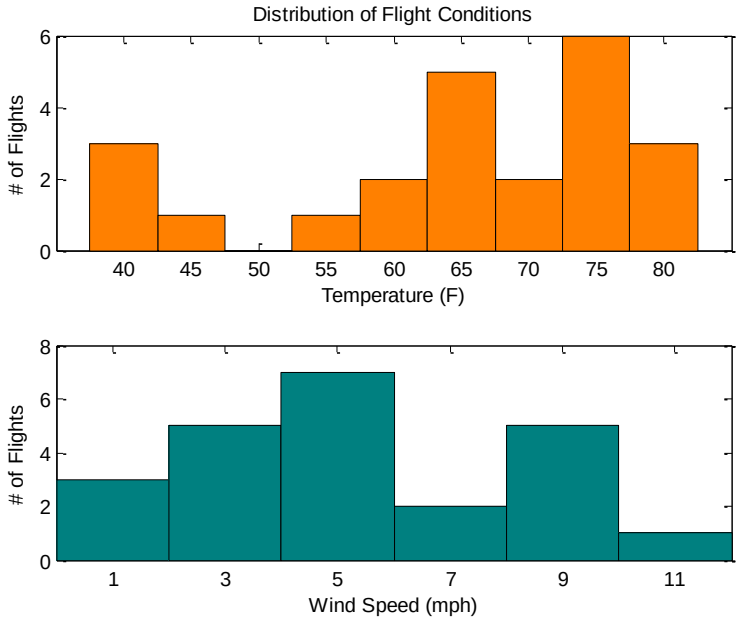


Figure 8. Distribution of Flight Conditions

The flight envelope with respect to the total velocity determined from GPS measurements and the tilt angle is plotted as a contour in Figure 9. The tilt angle is defined as the angle

between the aircraft z-axis and the local z-axis, and is calculated from the roll and pitch measurements from the vertical gyroscope as in:

$$tilt = \cos^{-1}\left(\cos\phi\cos\theta\right) \tag{136}$$

High values of the tilt angle introduce stronger nonlinearity into the attitude estimation. The statistical diversity of the flight data measurements is summarized in Table 3.

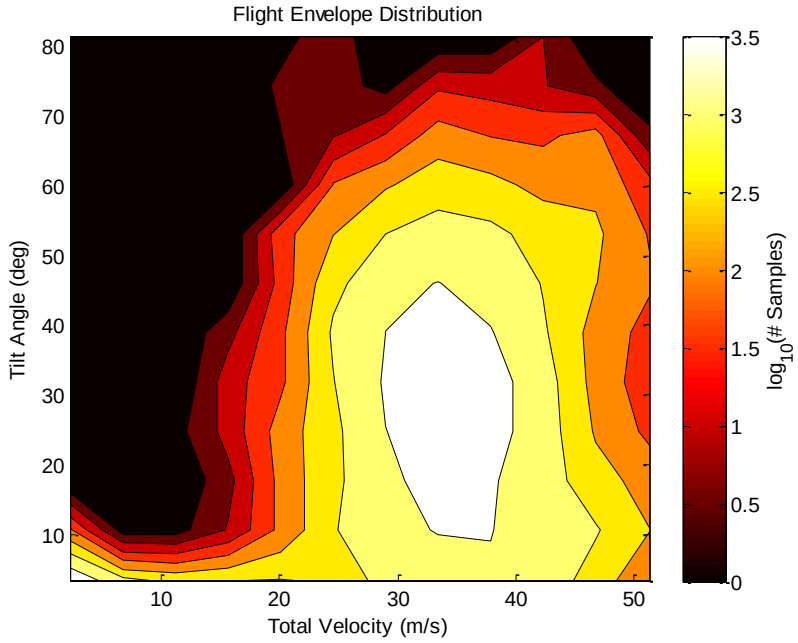


Figure 9. Distribution of Flight Envelope

Table 3. Summary of Flight Envelope Statistics

| Variable | Units | Minimum | Maximum | Mean | Standard Deviation |
|---|---|---|---|---|---|
| Velocity | m/s | 0.00 | 53.5 | 31.1 | 11.5 |
| $a_x$ | $m/s^2$ | -26.8 | 25.8 | 0.878 | 1.35 |
| $a_y$ | $m/s^2$ | -26.3 | 42.0 | -0.145 | 1.04 |
| $a_z$ | $m/s^2$ | -70.9 | 25.5 | -11.4 | 3.34 |
| Roll Angle, $\phi$ | deg | -85.0 | 56.6 | -19.4 | 20.7 |
| Pitch Angle, $\theta$ | deg | -48.5 | 38.8 | 5.33 | 6.73 |
| $p$ | deg/s | -205 | 206 | 0.586 | 15.6 |
| $q$ | deg/s | -100 | 83.1 | 4.90 | 7.17 |
| $r$ | deg/s | -79.0 | 65.0 | -5.32 | 7.14 |

For the use in a sensor fusion algorithm, the stochastic properties of the different sensors also needed to be considered. In order to estimate the random noise properties of the different sensors, the variance was calculated of the measurements from the sensors in a static setting, *i.e.*, when the plane was stationary on the runway prior to flight. These stochastic properties are summarized in Table 4.

Table 4. Stochastic Properties of Sensors

| Component | Sensor | Variance | Units |
|---|---|---|---|
| $a_x$ | IMU | 0.2205 | $(m/s^2)^2$ |
| $a_y$ | IMU | 0.2592 | $(m/s^2)^2$ |
| $a_z$ | IMU | 0.3102 | $(m/s^2)^2$ |
| $p$ | IMU | $1.510 \cdot 10^{-4}$ | $(rad/s)^2$ |
| $q$ | IMU | $1.450 \cdot 10^{-4}$ | $(rad/s)^2$ |
| $r$ | IMU | $1.410 \cdot 10^{-4}$ | $(rad/s)^2$ |
| $\Delta V_x$ | GPS | $0.7024 \cdot 10^{-3}$ | $(m/s)^2$ |
| $\Delta V_y$ | GPS | $0.4744 \cdot 10^{-3}$ | $(m/s)^2$ |
| $\Delta V_z$ | GPS | $2.981 \cdot 10^{-3}$ | $(m/s)^2$ |

# 5.0 SENSITIVITY ANALYSIS

The Unscented Kalman Filter (UKF) [10] is emerging as a popular nonlinear state estimation approach as compared to the commonly used Extended Kalman Filter (EKF) [8]. The theoretical advantage of using an unscented transformation in the UKF instead of analytical linearization in the EKF for recovering statistics after propagating through strong nonlinear equations is documented in a number of simulation based studies [10-13]. However, the advantage of the UKF over the EKF within practical applications is not as obvious, with mixed conclusions reported by different research groups.

VanDyke *et al*. [12], Sadhu *et al*. [13], Orderud [119], Wang *et al*. [120], Won *et al*. [121], and Nick *et al*. [122], reported that the UKF performs significantly and consistently better than the EKF in applications of dual estimation [123] for spacecraft attitude state and parameter estimation, bearing-only tracking, again bearing-only tracking, radar tracking, monocular vision based INS, and localization of Radio Frequency Identification (RFID) tags, respectively. Kandepu *et al*. [124] presented the same conclusions through four different simulation studies of the following problems: Van der Pol oscillator, estimation in an induction machine, state estimation of a reversible reaction, and a solid oxide fuel cell combined gas turbine hybrid system. Stastny *et al*. [125], Akin *et al*. [126], Chowdhary and Jategaonkar [127], Giannitrapani *et al.* [128], and Kim *et al.* [129] concluded that the UKF achieves slightly better performance than the EKF within applications of angles based navigation, state estimation of induction motors, aerodynamic parameter estimation, spacecraft

localization using angle measurements, and spiraling ballistic missile state estimation, respectively. Saulson and Chang [130], and LaViola [131] found insignificant differences in the performance between the EKF and UKF for the ballistic missile tracking problem and for estimation of quaternion motion for human tracking, respectively.

The nonlinear GPS/INS sensor fusion problem was first solved with the EKF and was later replaced with the UKF by several authors, and their performances were compared. The UKF was stated to perform better than the EKF by van der Merwe *et al.* [11]. Although a real flight data example was shown, only simulation results were used to quantify this conclusion [11]. Crassidis [78], Fiorenzani *et al*. [79], and Wendell *et al*. [132], concluded using simulation studies that the UKF performance exceeds that of the EKF only under large initialization errors. El-Sheimy *et al*. reached this same conclusion through experimental tests of the attitude estimation problem for land vehicles [133]. El-Sheimy *et al.* also found that the EKF and UKF performed similarly in terms of position error under GPS outages [133]. St. Pierre and Ing determined from simulation that the UKF performance is slightly better than the EKF for estimating position [134].

The large variance of conclusions on the performance of the EKF against the UKF, especially within similar applications, highlights the need for a systematic evaluation method. Current comparison studies are limited in the consideration of multiple design parameters. Several factors could lead to difficulties in evaluating and assessing state estimation performances for a given problem. First, different nonlinear state-space formulations exist for the same problem; second, the assumptions on the input, process, and measurement noise characteristics might not be realistic; third, the change of operating conditions in the physical world introduces randomness in the

estimation performance. A filtering algorithm may perform well with a particular formulation and a set of particular assumptions under a particular operating environment, but not otherwise. Therefore, the objective of this chapter is to investigate the sensitivity and robustness of EKF and UKF with respect to design parameters and operating conditions.

The GPS/INS attitude estimation problem described in Chapter 3 is used as a case study with the goal of gaining a better understanding of more general properties of nonlinear state estimation algorithms. This analysis uses flight data from the experimental platform described in Chapter 4. First, the metrics that were used to analyze the performance of the attitude estimation are discussed. Next, experimental sensitivity analysis results are provided using flight data. Then, a comparison of matrix square root techniques used in the UKF are explored, followed by an analytical comparison of initialization error and linearization techniques used in the EKF and UKF. Finally, a summary and conclusions of the sensitivity analyses are provided. This chapter consists of a combination of previously published or submitted works [14-19].

## 5.1 PERFORMANCE EVALUATION METRICS

From the flight data, an independent measurement of the roll and pitch angles of the aircraft are provided by the onboard mechanical vertical gyroscope. This sensor provides a fairly accurate measurement of these quantities; therefore these measurements are used as a „truth“ reference to evaluate the performance of the GPS/INS attitude estimation algorithms. After executing a sensor fusion algorithm, the roll and pitch

estimation results were compared with the corresponding vertical gyroscope measurements over the entire flight from take-off to landing. The mean of the absolute value and standard deviation of the errors were calculated. A scalar cost function, *J*, was defined by a weighted average as in:

$$J = 0.3\left[\sigma\left(\hat{\phi}-\phi_{VG}\right)+\sigma\left(\hat{\theta}-\theta_{VG}\right)\right]+0.2\left[mean\left(\left|\hat{\phi}-\phi_{VG}\right|\right)+mean\left(\left|\hat{\theta}-\theta_{VG}\right|\right)\right] \quad (137)$$

The weights for this performance metric were selected such that their sum is unity, equal importance is given to the roll and pitch errors, and less importance is placed on the mean errors because of potential alignment errors between the IMU and vertical gyroscope. Smaller values of *J* represent better performance of the attitude estimation.

## 5.2 EXPERIMENTAL SENSITIVITY ANALYSIS RESULTS

Some of the results from this section were originally published in [15,16]. Pitch and roll angles were estimated for each of the 23 flights using two different assumptions of noise characteristics. The same process and measurement noise matrices were used for the EKF and UKF within each formulation, *i.e.*, the filters were equivalently tuned. The mean of the performance cost function, *J*, over all flights is shown in Figure 10. For comparison purposes, the mean performance of AVAE was approximately 3.7 degrees, which is significantly worse performance than the EKF and UKF formulations.

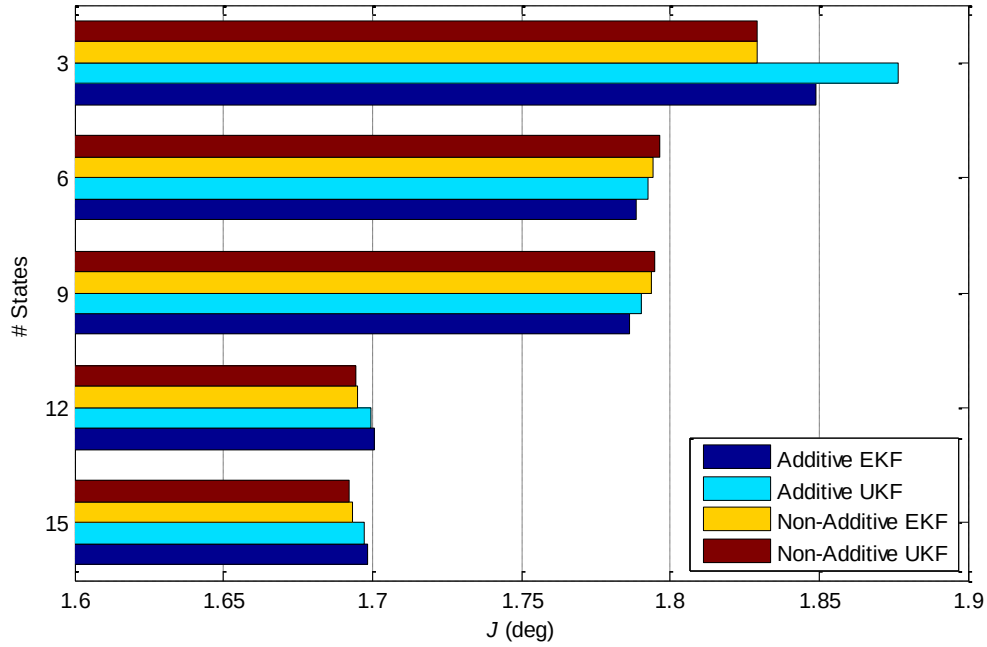


Figure 10. Summary of Mean Performance Cost

Within each formulation and estimator, the differences in performance between additive and non-additive noise is small. For the 3, 12, and 15 state formulations, the non-additive noise case presents better performance results, while the 6 and 9 state formulations show a slight advantage in the additive noise case. It can also be seen in Figure 10 that the EKF and UKF obtain very similar performance results for each formulation, especially for the non-additive case. The non-additive method was selected for further analyses because it involves more correct assumptions about the noise characteristics of the system, and it is more intuitive to implement.

To roughly estimate the computational requirements of each of the considered sensor fusion algorithms, the number of floating point operations (FLOPs) required to process one second of flight data was estimated by manually counting the operations executed in the code. Before counting the FLOPs required for each of the algorithms, the

codes were streamlined to minimize the number of computations fundamentally required by the algorithm. The sampling rates of the IMU and GPS were considered, since they correspond to the execution of the prediction and update stages respectively. The resulting FLOP counts are illustrated in Figure 11. In addition to these theoretical estimates, experimental results were collected for each formulation of the required execution time of the sensor fusion algorithm for the duration of each of the 23 flights. This execution time was measured over the entire length of flight for each data set. Then, the mean of these 23 execution times were calculated, and the results are shown in Table 5. In general similar trends are observed for the FLOP estimates and mean execution times. Note that these estimates are coarse approximations, which were intended only to give a general idea about computational cost.

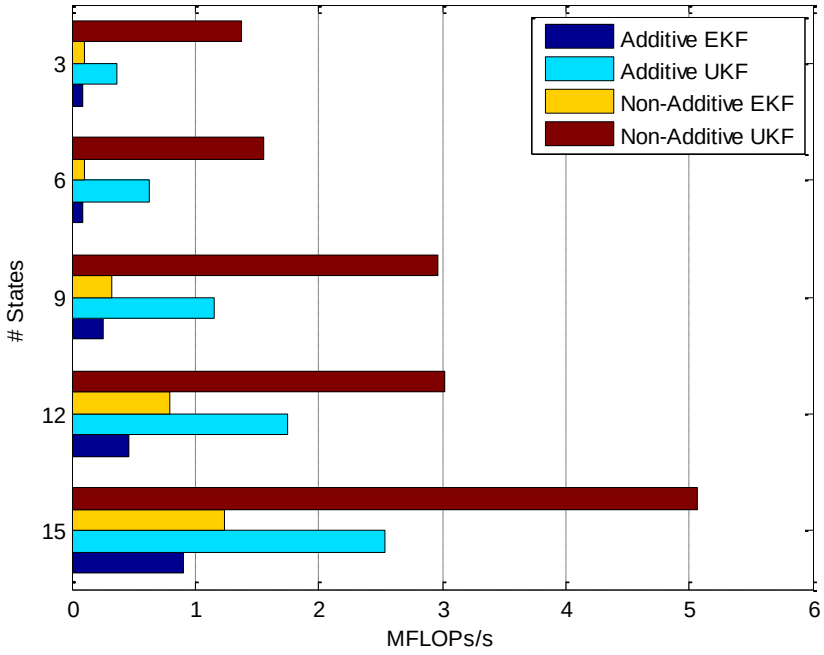


Figure 11. Theoretical Computational Expense of Different Sensor Fusion Algorithms

Table 5. Summary of Computational Expense

| Estimator | Noise Assumption | # States | MFLOPs/sec | Exec. Time (sec) |
|---|---|---|---|---|
| AVAE | N/A | N/A | 0.012 | 0.21 |
| EKF | Additive | 3 | 0.095 | 1.30 |
| EKF | Non-Additive | 3 | 0.101 | 1.35 |
| UKF | Additive | 3 | 0.371 | 8.27 |
| UKF | Non-Additive | 3 | 1.371 | 16.07 |
| EKF | Additive | 6 | 0.088 | 1.56 |
| EKF | Non-Additive | 6 | 0.104 | 1.64 |
| UKF | Additive | 6 | 0.628 | 3.97 |
| UKF | Non-Additive | 6 | 1.557 | 7.04 |
| EKF | Additive | 9 | 0.253 | 2.81 |
| EKF | Non-Additive | 9 | 0.321 | 1.80 |
| UKF | Additive | 9 | 1.161 | 7.58 |
| UKF | Non-Additive | 9 | 2.971 | 7.67 |
| EKF | Additive | 12 | 0.468 | 2.13 |
| EKF | Non-Additive | 12 | 0.799 | 2.25 |
| UKF | Additive | 12 | 1.750 | 27.18 |
| UKF | Non-Additive | 12 | 3.015 | 59.38 |
| EKF | Additive | 15 | 0.901 | 3.51 |
| EKF | Non-Additive | 15 | 1.232 | 4.31 |
| UKF | Additive | 15 | 2.533 | 37.61 |
| UKF | Non-Additive | 15 | 5.060 | 77.06 |

### 5.2.1 Comparison of Baseline Results for Individual Data Sets

Baseline results were calculated for the non-additive noise case of each formulation for each individual data set. The performance results are summarized in Figure 12 and Figure 13.

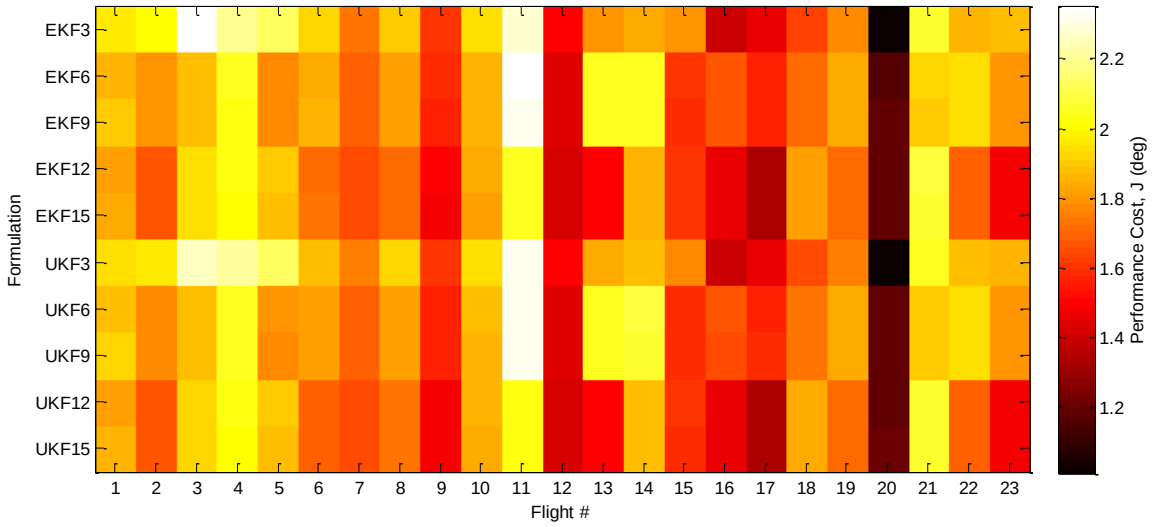


Figure 12. Individual Data Set Performance Summary

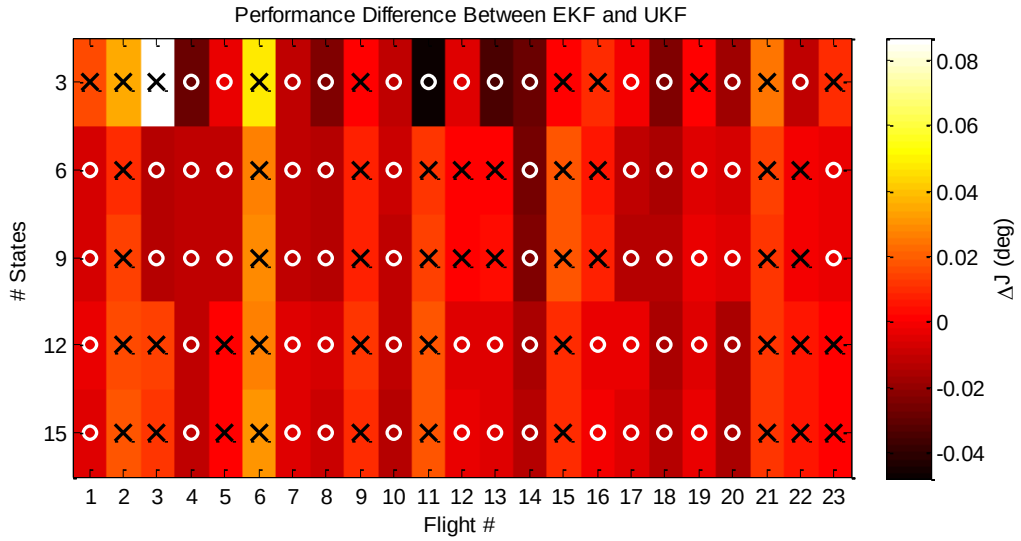


Figure 13. Individual Data Set Performance Comparison

Figure 12 shows the individual results for each formulation and data set with a darker shade indicating better performance, while Figure 13 illustrates the differences between the EKF and UKF for each formulation. In this figure, the black „X"s indicate where the UKF yielded better performance, and the white „O"s mark where the EKF performed better. Although the differences were minor, both the EKF and UKF outperformed one another for different data sets. This observation highlights the importance of considering

multiple sets of diverse data for analysis in order to capture the overall performance of each estimator.

### 5.2.2 Sensitivity to Tuning of Assumed Noise Covariance Matrices

The sensitivity of the assumed process and measurement noise covariance matrices, **Q** and **R** can be evaluated using methods similar to those described in [135,136]. To analyze the effects of changes in these values, two tuning parameters were used. The first tuning parameter, $\gamma_1$, adjusts the ratio of the reliance of the estimation between the prediction and update stages of the nonlinear estimator. Increasing $\gamma_1$ causes the estimation to rely more on the prediction and less on the update, and vice versa. This form of tuning is achieved by:

$$\mathbf{Q} = \mathbf{Q}_0, \quad \mathbf{R}^d = \gamma_1 \mathbf{R}_0^d, \quad \mathbf{R}^y = \gamma_1 \mathbf{R}_0^y \tag{138}$$

where the „0‟ subscripts indicate the baseline covariance matrices. The second tuning parameter, $\gamma_2$, adjusts the ratio of the reliance of the estimation between the IMU and GPS measurements, where increasing $\gamma_2$ causes the estimation to rely more on the IMU measurements and less on the GPS measurements. This tuning parameter is implemented using:

$$\mathbf{Q} = \mathbf{Q}_0, \quad \mathbf{R}^d = \mathbf{R}_0^d, \quad \mathbf{R}^y = \gamma_2 \mathbf{R}_0^y \tag{139}$$

Note that for the 6, 9, 12, and 15-state formulations, these two forms of tuning are equivalent, since $\boldsymbol{R}^d = 0$. The tuning parameters were implemented for each formulation on all 23 flights for EKF and UKF. The performance cost, *J*, was normalized by the case of no tuning for each flight and then averaged over all flights. The mean normalized

results are shown for the 3-State formulation in Figure 14, 6 and 9-State formulations in Figure 15, and 12 and 15-State formulations in Figure 16.

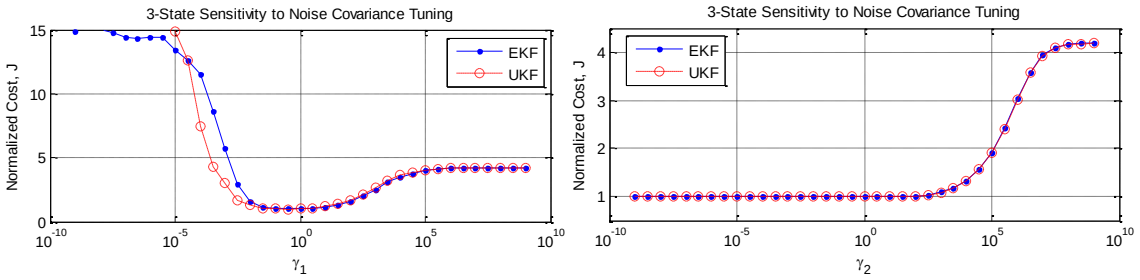


Figure 14. Sensitivity of 3-State Formulation to Noise Covariance Tuning

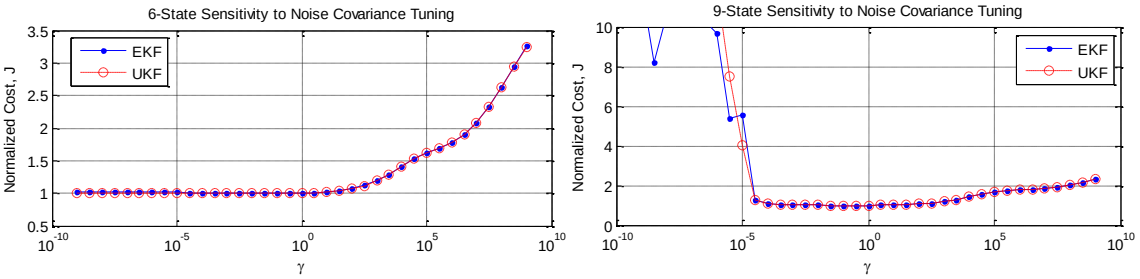


Figure 15. Sensitivity of 6-State (left) and 9-State (right) Formulation to Noise Covariance Tuning

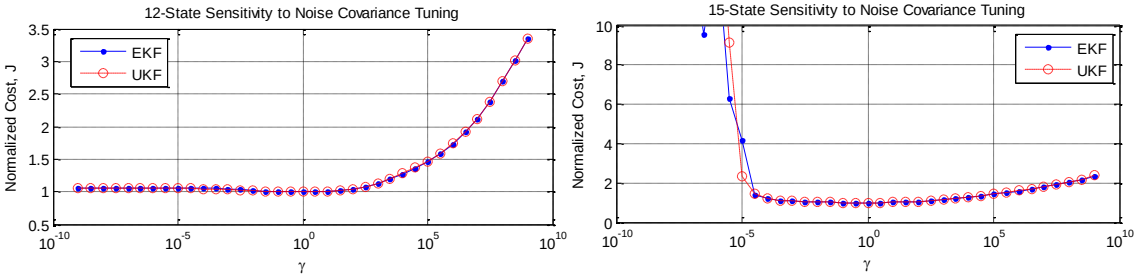


Figure 16. Sensitivity of 12-State (left) and 15-State (right) Formulation to Noise Covariance Tuning

Each of the presented cases in Figure 14, Figure 15, and Figure 16 show similar response to tuning between the EKF and UKF, with the exception of small values of $\gamma_1$ in the 3, 9, and 15-state formulations, where the UKF performance more rapidly degrades as $\gamma_1$ decreases. The similarity between the EKF and UKF indicates that the two nonlinear estimators are comparable with respect to the selection of **Q** and **R** for this application. Since the baseline no tuning case lies around the minimum of the performance cost

curves (*i.e.* the performance curves do not go much below 1), the **Q** and **R** matrices are reasonably tuned at baseline for both the EKF and UKF. It is also interesting to notice the flattening trend for decreasing values of $\gamma_2$ for the 3, 6, and 12-state formulations, which is representative of modeling no uncertainty in the GPS velocity measurements. Since the normalized performance levels off at just over 1, the case of "perfect" GPS velocity yields very reasonable estimation performance.

### 5.2.3 Sensitivity to Sampling Rate

The sampling rates of the IMU and GPS affect the time resolution of the sensor fusion algorithm; in turn, this also affects the quality of the linearization. The prediction step is executed at the sampling rate of the IMU, and the measurement update occurs at the sampling rate of the GPS. In order for the measurement updates to correspond with a prediction, the IMU sampling rate should be a multiple of the GPS sampling rate. Starting with the baseline sampling rates of 50 Hz for the IMU and 20 Hz for the GPS, each signal was down-sampled to appropriate rates in order to analyze the performance effects of using lower sampling rate hardware (*i.e.*, lower cost systems). Estimation results were obtained, normalized by the baseline case of 50 Hz IMU and 10 Hz GPS, and averaged over all 23 flights. To illustrate the results of this analysis, contour plots were generated for each of the formulations for both EKF and UKF, and are shown in Figure 17, Figure 18, Figure 19, Figure 20, and Figure 21.

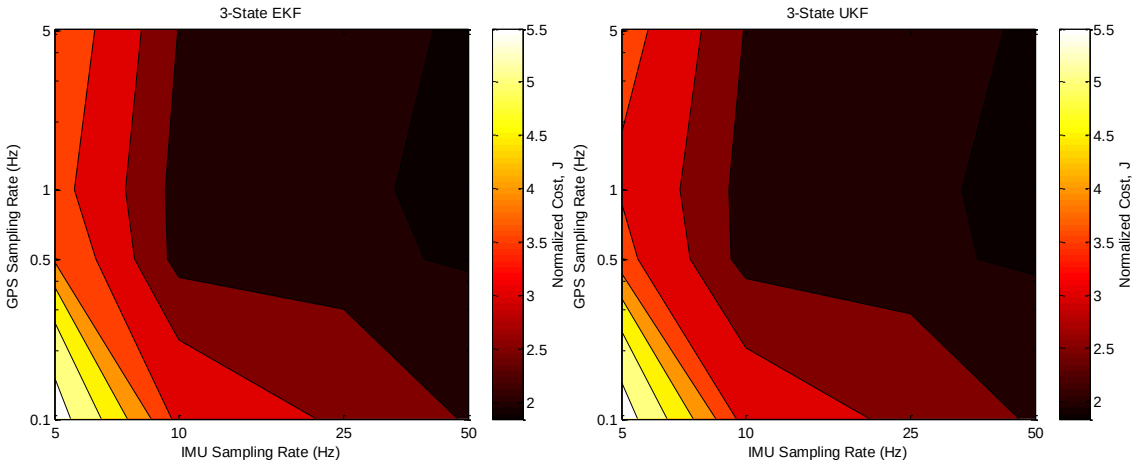


Figure 17. 3-State Sampling Rate Sensitivity of EKF (left) and UKF (right)

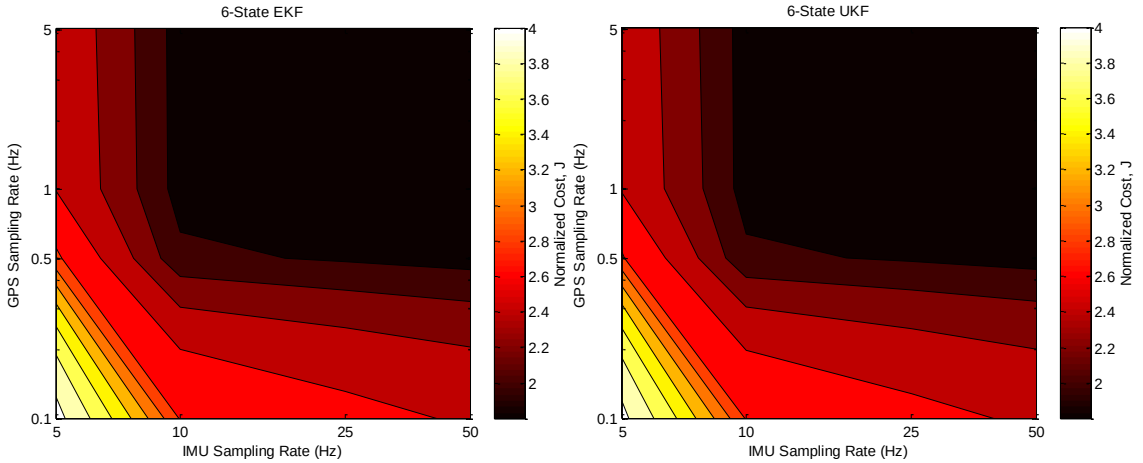


Figure 18. 6-State Sampling Rate Sensitivity of EKF (left) and UKF (right)

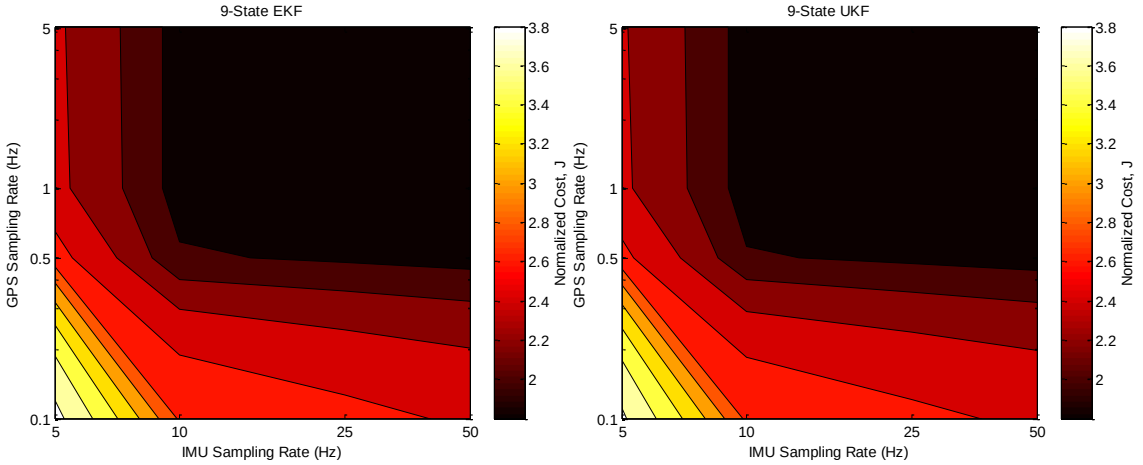


Figure 19. 9-State Sampling Rate Sensitivity of EKF (left) and UKF (right)

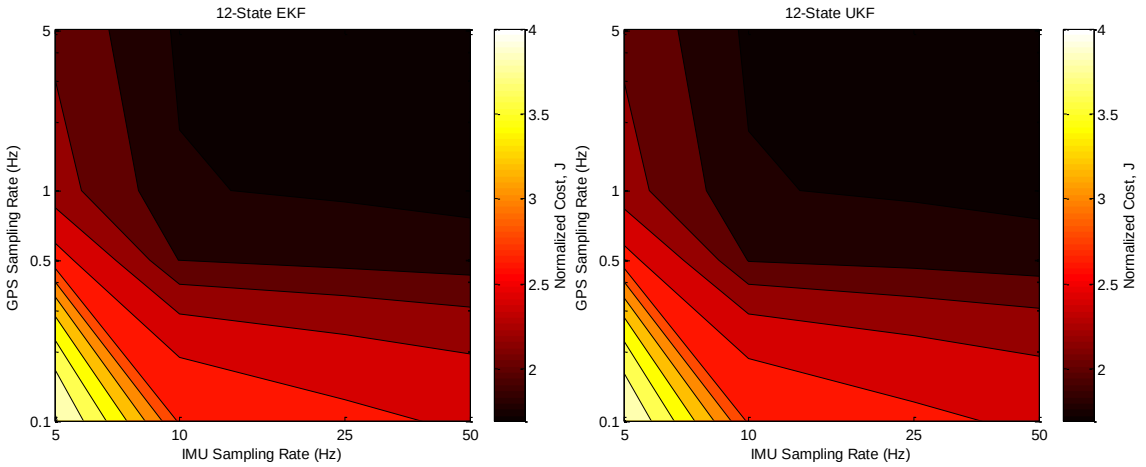


Figure 20. 12-State Sampling Rate Sensitivity of EKF (left) and UKF (right)

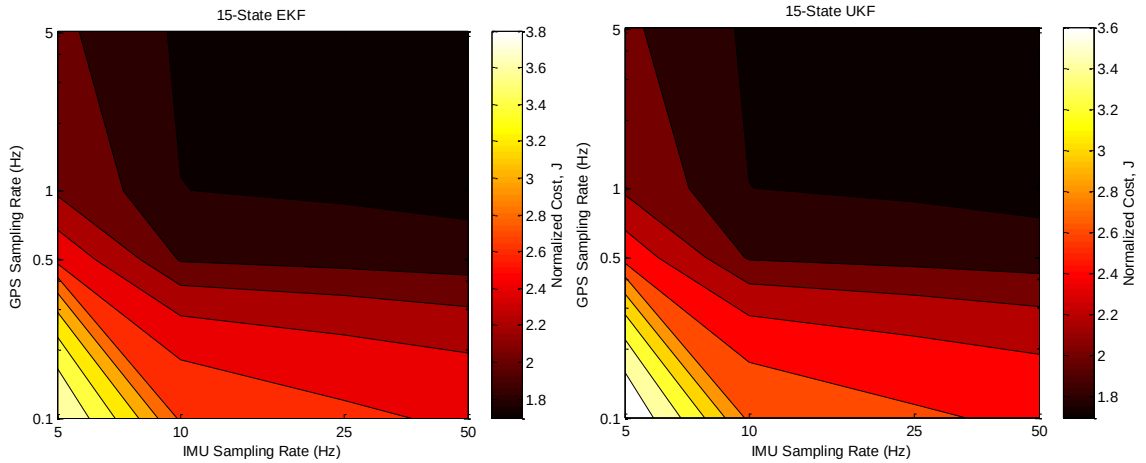


Figure 21. 15-State Sampling Rate Sensitivity of EKF (left) and UKF (right)

In general, for each sensor fusion formulation, lowering either of the sampling rates decreases the attitude estimation performance. Very little difference is shown within each formulation between the EKF and UKF. This demonstrates the comparable sensitivity of the EKF and UKF in response to changes in IMU and GPS sampling rates, which is consistent with the conclusions in [12] for the human motion tracking problem.

### 5.2.4 Sensitivity to Initialization Error

Significant differences between the assumed initial state and the actual initial state could occur in certain applications. Some comparisons have been made for large initialization errors for sensor fusion [78,79,132,133] and tracking [119] problems and found faster convergence in the UKF. To observe this phenomenon for this specific problem, small (5°) and large (60°) initial errors were imposed on the pitch state for each of the 23 flights. The estimation results of these cases were compared to the baseline case of no imposed initialization error. To illustrate the responses of the EKF and UKF in each formulation, the mean over all flights was calculated of the differences of the pitch angle, and the results are shown in Figure 22, Figure 23, Figure 24, Figure 25, and Figure 26.

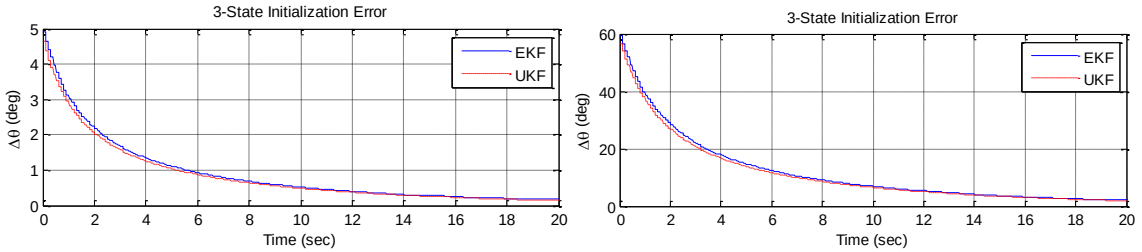


Figure 22. 3-State Response to Small (left) and Large (right) Initialization Error

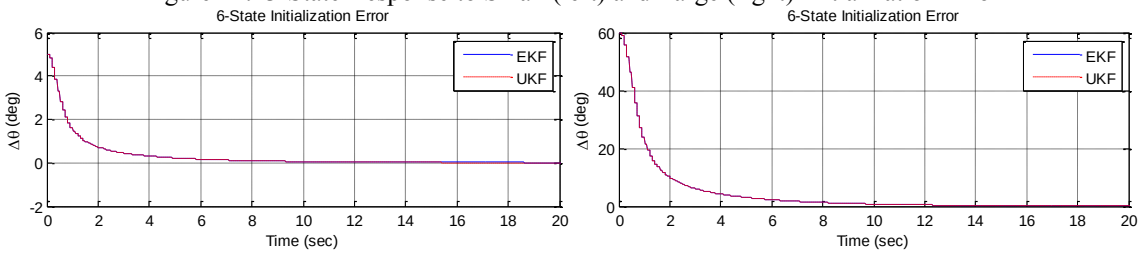


Figure 23. 6-State Response to Small (left) and Large (right) Initialization Error

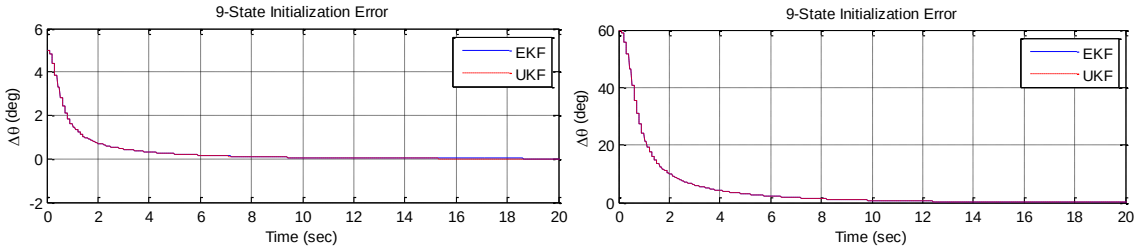


Figure 24. 9-State Response to Small (left) and Large (right) Initialization Error

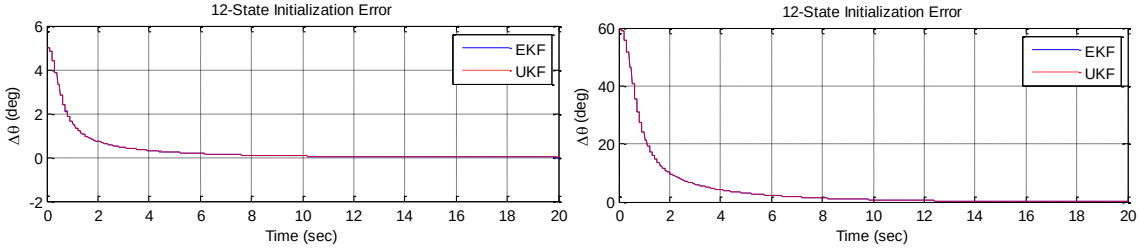


Figure 25. 12-State Response to Small (left) and Large (right) Initialization Error

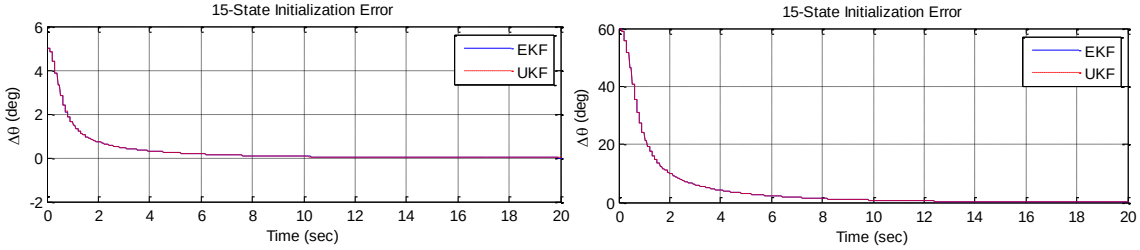


Figure 26. 15-State Response to Small (left) and Large (right) Initialization Error

The above plots show that the EKF and UKF converge in a similar manner in response to both small and large pitch initialization error. Further analysis of the initialization error problem is explored in Section 5.4.

### 5.2.5 Sensitivity to GPS Outages

A practical problem associated with a GPS/INS sensor fusion is the temporary loss of a sufficient number of satellite signals, often referred to as a GPS dropout or GPS outage [137-142]. During a GPS outage, the presented loosely-coupled sensor fusion algorithms rely exclusively on the IMU measurements thus performing dead reckoning

estimation. To simulate this phenomenon, 30 second GPS outages were artificially imposed on the real flight data at 1, 3, and 5 minutes after take-off. Although these times were selected arbitrarily, the state of the aircraft at these times differs from flight to flight. The roll and pitch angles as measured from the vertical gyroscope at the start of each GPS outage for all of the flights is shown in Figure 27.

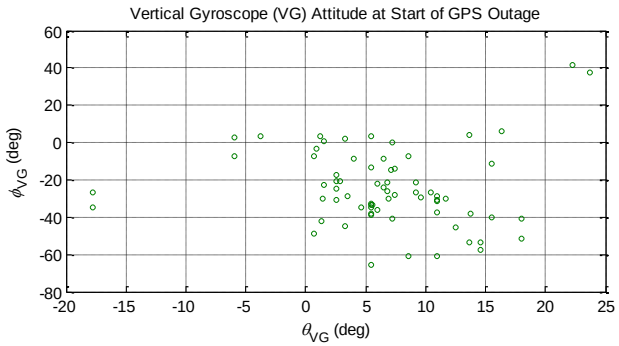


Figure 27. Attitude Envelope at Start of GPS Outages

As done for the initialization error analysis of the previous section, the estimation results of each sensor fusion algorithm with imposed GPS outages was compared with the baseline estimation results. The mean of the differences of the pitch angle for all 23 flights was calculated, and the results are shown in Figure 28, Figure 29, Figure 30, Figure 31, and Figure 32.

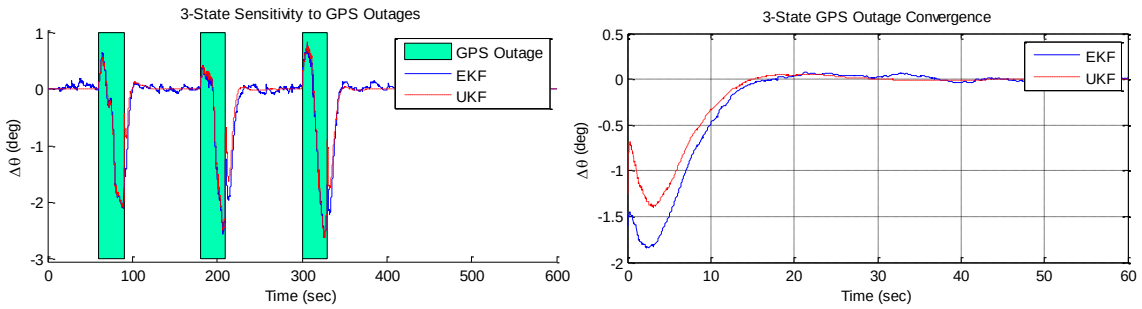


Figure 28. Response of the 3-State Formulation to GPS Outages

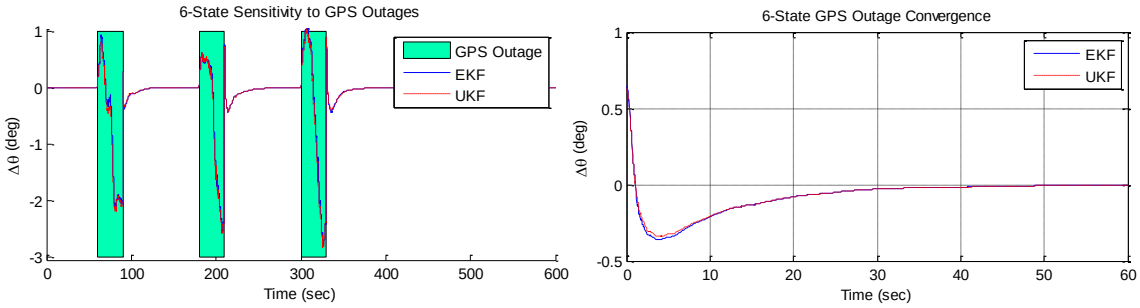


Figure 29. Response of the 6-State Formulation to GPS Outages

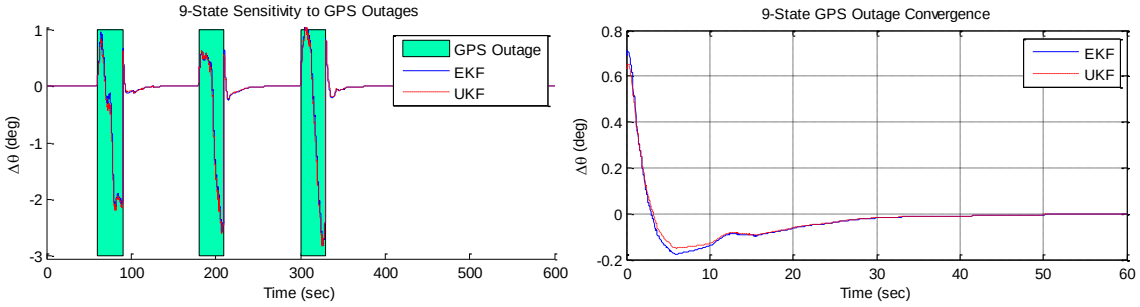


Figure 30. Response of the 9-State Formulation to GPS Outages

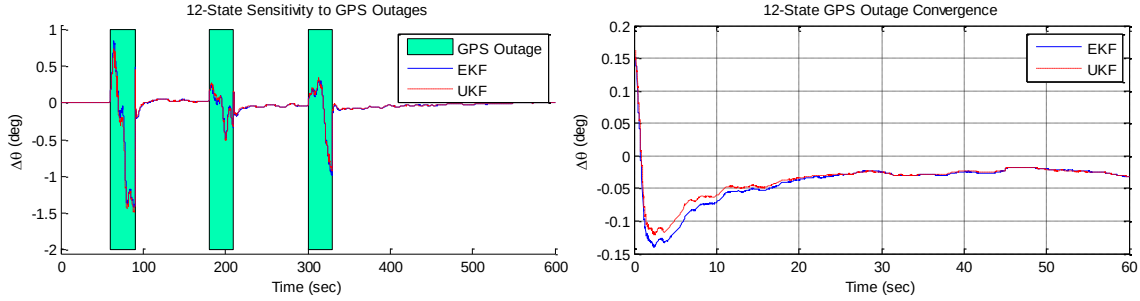


Figure 31. Response of the 12-State Formulation to GPS Outages

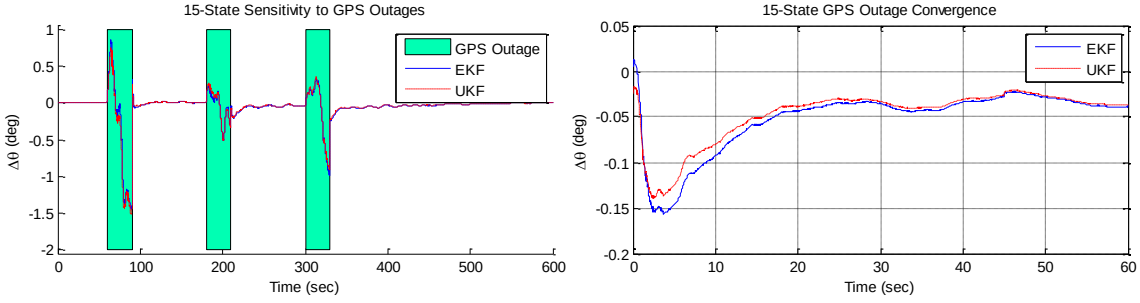


Figure 32. Response of the 15-State Formulation to GPS Outages

The plots on the left show the average difference in the pitch estimation over the entire flight durations; the plots on the right display the average convergence effects for each

time period immediately following a GPS outage. It is shown in these figures that in general the EKF and UKF respond similarly during GPS outages. This is an indication that the prediction stages of the EKF and UKF have very similar performance. Immediately following GPS outages, it is shown that for the 6-state and 12-state formulations, the EKF and UKF converge at comparable rates. However, the 3-state formulation shows some difference between the EKF and UKF.

### 5.2.6 Robustness to Uncertainty in IMU Measurements

In order to analyze the robustness of the different formulations for EKF and UKF, a 250 point Monte Carlo simulation was conducted. In particular, artificial bias and scale factor terms were generated from a uniform distribution across a specified range of values. These terms were applied to a single component of the IMU measurements, and then attitude estimation performance results were calculated for each formulation on a single set of flight data. This process was repeated using different Monte Carlo sampling for each component of the IMU measurements: $a_{\tilde{x}}, a_{\tilde{y}}, a_{\tilde{z}}, p, q, r$. The performance cost, $J$, was calculated for each Monte Carlo point, and was then normalized by the baseline case of no artificial bias or scale factor terms. An example illustration is shown in Figure 33 of the 6-state formulation normalized cost corresponding to artificial bias and scale factor terms on the $p$ measurement.

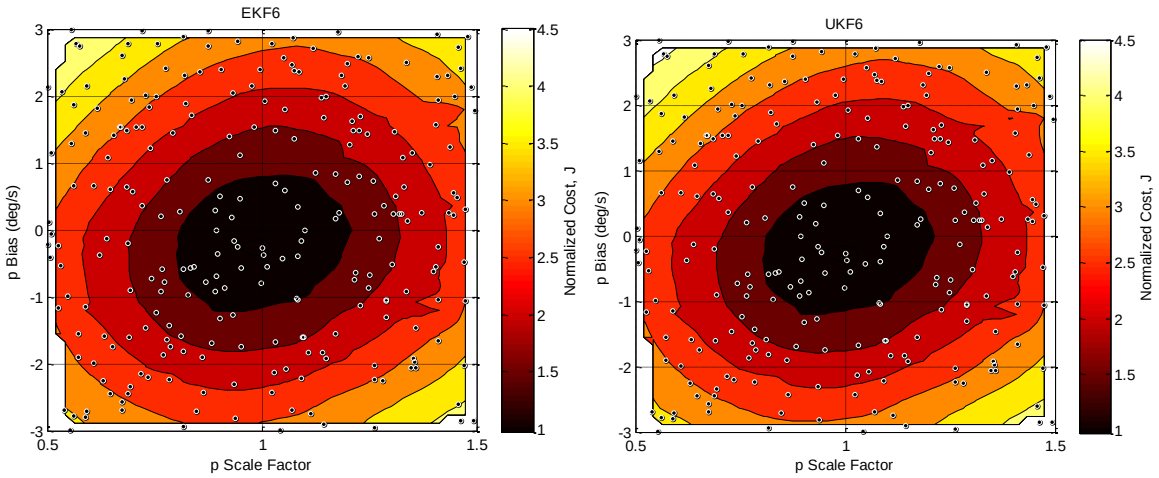


Figure 33. Performance Response to Bias and Scale Factor on Roll Rate for EKF (left) and UKF (right)

Similar overall trends are shown in Figure 33 between the EKF and UKF. As expected, adjusting the scale factor or bias decreases the performance for both the EKF and UKF. To quantify and compare the overall effect of this analysis for the EKF and UKF, the mean of the normalized performance cost for all Monte Carlo points was calculated for each formulation and each IMU component. The percent difference between the EKF and UKF values was evaluated, and the results are summarized in Figure 34. Only three of the cases (marked with „o") showed slightly better performance of the EKF, while the remaining cases showed varying degrees of performance advantage for the UKF. This demonstrates that in general, the UKF is more robust to bias and scaling of the IMU measurements in this application.

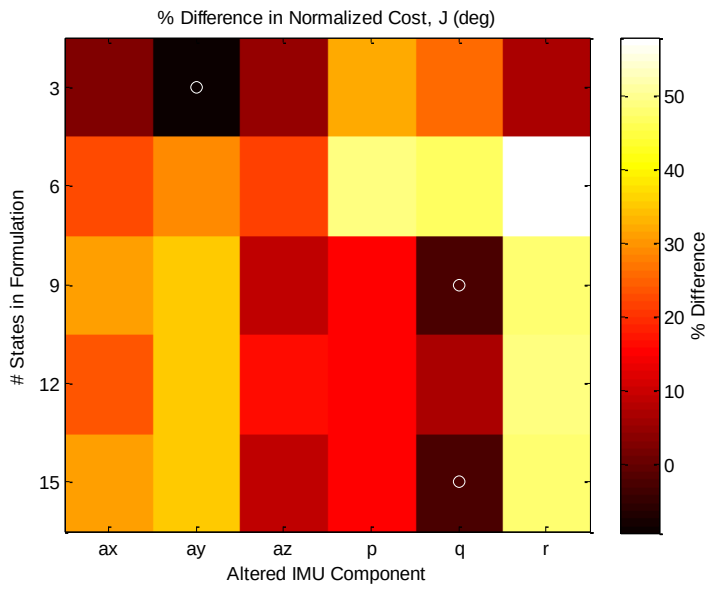


Figure 34. Comparison of Performance of EKF and UKF for IMU Bias and Scaling

### 5.2.7 Comparison of Linearization Techniques

To analyze the differences in the linearization technique of the EKF and UKF, the Hessian norms can be calculated to quantify the nonlinearity of the states as a function of time. A single set of flight data was selected for this analysis to provide a single illustrative example to demonstrate the differences in the linearization techniques of the EKF and UKF. The nonlinearity of the attitude states is quantified by taking the sum of the norms of the Hessian matrices corresponding to each of the 3 attitude states. In Figure 35, the values (left) and distribution (right) of this sum are shown.

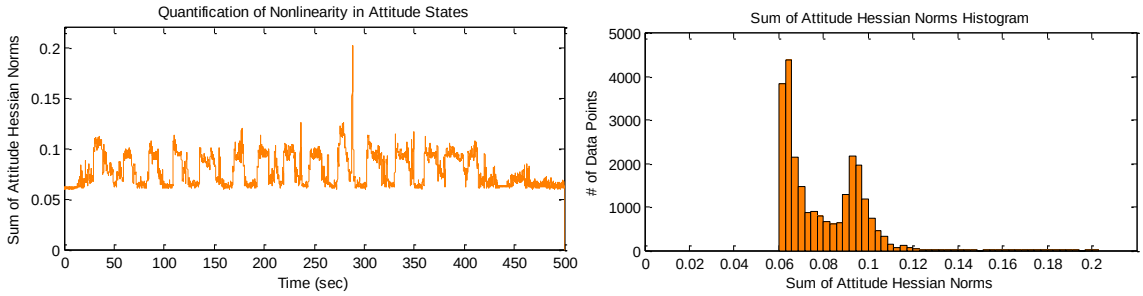


Figure 35. Quantification of Nonlinearity in Attitude States using Hessian Norms

The sum of the Hessian norms for the attitude states can be used to locate discrete time steps which contain high levels of nonlinearity in the attitude. For this single set of flight data, the time step containing the highest level of nonlinearity of the attitude states was determined from the maximum of the attitude Hessian norm sum, occurring at approximately 288.5 seconds into the flight, as demonstrated in Figure 35. At this time step, the accuracy of the linearization technique is especially important. Based on its theoretical derivation, the UKF claims more accurate linearization than the EKF [10]. To analyze the accuracy of linearization of each filter, at the selected time step, the *a priori* information about the mean and covariance of the state are considered for the prediction stage of each filter. A Monte Carlo simulation about the *a priori* information for each filter is used to predict the *a posteriori* mean and covariance to establish an approximate truth. Additionally, the EKF and UKF linearization techniques are used to obtain the *a posteriori* mean and covariance. The results of this analysis are presented in Table 6. The mean values are given in degrees while the covariance values are given in degrees squared. It is shown in Table 6 that the EKF and UKF are both linearizing very closely to the Monte Carlo simulation for the prediction stage. This demonstrates that even for the highest case of nonlinearity of the attitude states, the EKF and UKF are exhibit similar levels of performance in terms of linearization.

Table 6. Comparison of Nonlinearity of Prediction

| **Prediction Estimator** | $\bar{\phi}$ (deg) | $\bar{\theta}$ (deg) | $\bar{\psi}$ (deg) | $\boldsymbol{P}_{\phi\phi}$ (deg$^2$) | $\boldsymbol{P}_{\theta\theta}$ (deg$^2$) | $\boldsymbol{P}_{\psi\psi}$ (deg$^2$) | $\boldsymbol{P}_{\phi\theta}$ (deg$^2$) | $\boldsymbol{P}_{\phi\psi}$ (deg$^2$) | $\boldsymbol{P}_{\theta\psi}$ (deg$^2$) |
|---|---|---|---|---|---|---|---|---|---|
| Prior Conditions | -43.18 | 29.51 | 181.75 | 0.0567 | 0.0263 | 0.1767 | 0.0024 | 0.0365 | 0.0006 |
| EKF | -43.75 | 29.23 | 181.44 | 0.0564 | 0.0263 | 0.1463 | 0.0024 | 0.0360 | 0.0006 |
| UKF | -43.75 | 29.23 | 181.44 | 0.0564 | 0.0263 | 0.1463 | 0.0024 | 0.0360 | 0.0006 |
| Monte Carlo | -43.75 | 29.23 | 181.44 | 0.0564 | 0.0263 | 0.1460 | 0.0024 | 0.0359 | 0.0006 |

### 5.2.8 Sensitivity to GPS Time Offset

In GPS/INS sensor fusion, it is common for the GPS measurements to lag behind the IMU measurements [143-146]. To compensate for this latency in off-line applications, a time offset can be imposed on the GPS measurement in order to properly align the GPS and IMU signals. To analyze the sensitivity of the EKF and UKF to this form of GPS latency compensation, results were calculated for GPS time offset ranging from 0 to 500 ms by 20 ms increments for all of the 23 flights. Only the 9-state formulation was considered for this analysis. The results for each flight were normalized by the baseline case of no latency compensation (GPS time offset is 0). A mean over the 23 flights of the normalized results was taken to establish a generalized result. The results of this analysis are shown in Figure 36.

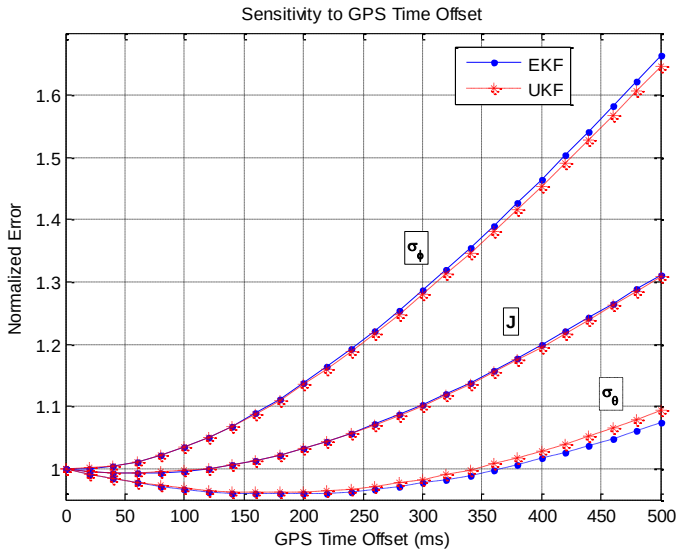


Figure 36. Sensitivity to GPS Time Offset

Figure 36 shows the mean normalized cost function, $J$, standard deviation of roll error, $\sigma_\phi$, and the standard deviation of pitch error, $\sigma_\theta$. The EKF and UKF have similar responses to GPS time offset. Increasing the GPS time offset causes a monotonic increase in roll standard deviation, while the pitch standard deviation improves with GPS time offset until 160 ms and then starts to increase. The overall performance cost decreases with GPS time offset until 60 ms and starts to increase above 60 ms. From this analysis, it was discovered that for this formulation of EKF and UKF, compensating for the GPS latency can improve the pitch performance; however, doing so increases the roll error. Depending on the application, this might be an acceptable effect, since it is possible to decrease the overall cost. For all other sections of this chapter, no GPS latency compensation was introduced.

### 5.2.9 Sensitivity to Acceleration due to Gravity

Acceleration due to gravity, $g$, is often assumed to be constant in many applications. Although this is a reasonable approximation in most cases, the acceleration due to gravity can be derived as a function of various effects. In particular, for this study, acceleration due to gravity can be calculated as a function of the latitude and altitude. The formula used for this calculation is the 1967 Geodetic Reference System Formula [147] using the free air correction (FAC) [148]:

$$g_{\phi} = 9.780327\left(1 + 0.0053024\sin^2\phi_{lat} - 0.0000058\sin^2 2\phi_{lat}\right) - 3.086\cdot 10^{-6} h_{alt} \qquad (140)$$

where $\phi_{lat}$ represents the latitude angle, and $h_{alt}$ represents the height above sea level in meters. In addition to obtaining the latitude and altitude values for the flight testing location for this study, the altitude of the plane is estimated in flight from the nonlinear estimator. Only the 9-state formulation was considered for this analysis. Results were calculated for all 23 flights using a constant nominal $g$ value of 9.80665 m/s$^2$, and a time-varying $g$ value using (140) with flight altitude correction. The results from the time-varying $g$ were normalized by the results from the nominal case and plotted for both the EKF and UKF in Figure 37.

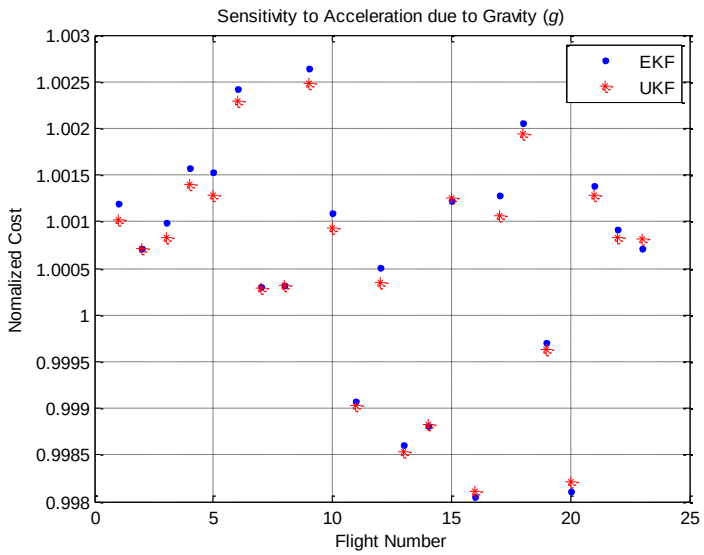


Figure 37. Sensitivity to Acceleration due to Gravity (g)

It is shown in Figure 37 that the EKF and UKF show similar responses to a time-varying value of $g$. The response over the 23 flights from the time-varying case differs only slightly from the constant case, with percent changes in cost function ranging from negative 0.20% (performance improvement) to 0.26% (performance degradation). A mean of these changes over all 23 flights shows that the EKF yields an average cost increase of 0.0058%, while the UKF yields an average cost increase of 0.0050%. Due to the small magnitude of these changes, a time-varying $g$ is not necessary for this formulation. For all other sections of this chapter, a constant $g$ value was used.

### 5.2.10 Experimental Sensitivity Analysis Conclusions

This section presented a sensitivity analysis of the nonlinear state estimation problem using three different GPS/INS sensor fusion attitude estimation formulations with both the EKF and UKF. Two different noise assumptions, additive and non-additive

noise, were considered and compared. Although little differences were found in the baseline case, the non-additive noise assumptions were used because they provide a more intuitive model of the noise in the system. The tuning of the process and measurement noise covariance matrices showed a similar impact on the performance for both the EKF and UKF, which indicated similar requirements on tuning for problem, which does not contain strong nonlinearity, and also demonstrated that the baseline case was well-tuned for all formulations. Additionally, the EKF and UKF showed similar responses to changes in sampling rate. The EKF showed slightly faster convergence than the UKF in response to large initialization error, and similar response to the UKF for small initialization error. Only small differences were found in response to convergence after GPS outages, which were most apparent in the 3-state formulation. Through Monte Carlo simulations, the UKF demonstrated greater robustness to bias and scale factors on the IMU measurements than the EKF. Using the Hessian to locate the time of greatest nonlinearity of the attitude states, the linearization of the prediction stage of the EKF and UKF were both found to be similarly close to their corresponding Monte Carlo estimation of predicted mean and covariance. Overall, in most cases, the EKF and UKF had similar levels of performance for all three considered formulations. The EKF is recommended for use in real-time applications when computation requirement is important, while the UKF is recommended for off-line applications, due to its ease of implementation and lack of Jacobian calculations.

## 5.3 MATRIX SQUARE ROOT OPERATIONS FOR UKF

The results from this section were originally published in [17]. One primary difference between the EKF and UKF is that the UKF requires the calculation of a matrix square root, which is a computationally demanding operation [149]. In particular, computation is an important consideration for small aircraft systems, due to resource limitations onboard the aircraft, *e.g.*, power, weight, and cost [71,72]. The matrix square root computation is also an important consideration when designing a UKF algorithm because there are many different ways to compute the square root of a matrix, potentially with different accuracy and computational requirements [150].

The selection of matrix square root operation in the UKF differs among authors. Julier and Uhlmann state that "*the sigma points capture the same mean and covariance irrespective of the choice of matrix square root which is used. Numerically efficient and stable methods such as the Cholesky decomposition can be used* [10]." Crassidis [78] and Wendel [132] *et al.* also recommended the use of Cholesky decomposition. These claims, however, are provided without any theoretical or empirical justification. Stastny *et al.* found that using the Cholesky decomposition method caused divergence; therefore, they used the Schur method instead [125]. Some authors using the UKF do not explicitly state which matrix square root operation was used [151-153]. A different means of handling the square root operation was developed by van der Merwe and Wan called the "square-root UKF (SR-UKF)" method [149]. This method provides a prediction and update of the square root of the covariance matrix directly at each time-step, which reduces computational requirements of the algorithm [149]. A simulated example was

used to show that the SR-UKF and UKF performances were the same [149]. Since there are inconsistencies in the selected matrix square root method for UKF applications, a detailed comparison of available approaches is necessary. Although some matrix square root comparison studies exist, *e.g.* by Higham [150] and Meini [154], these studies are mostly theoretical, with a few examples using known matrices, such as the Moler, Chebyshev-Vandermonde, and Frobenius matrices. These comparison studies, therefore, do not consider the potential error propagation effects that are introduced by application in a recursive filter such as the UKF.

This analysis aims to expand upon the existing matrix square root comparison studies through an example application of the matrix square root within a UKF-based GPS/INS sensor fusion algorithm for attitude estimation that relies on experimentally collected flight data. By analyzing different matrix square root methods in the context of the UKF, a matrix square root is required at each discrete time step in the algorithm, allowing for a more general comparison since many different matrices are considered. In addition this recursive filtering application introduces the effects of the propagation of uncertainties in the matrix square root computation. Furthermore, the flight data used for this study was selected from a large library of data in order to obtain diversity with respect to different flight conditions, thus providing an additional level of generalization.

### 5.3.1 Matrix Square Root Algorithms

An important requirement of the UKF algorithm is the calculation of the square root of the state covariance matrix, **P**. A covariance matrix by definition is both

symmetric and positive semi-definite. To calculate the square root of a positive semi-definite $n \times n$ matrix, $\mathbf{A}$, various methods can be used. The matrix principal square root, $\mathbf{A}^{1/2}$, exists only for positive semi-definite matrices, and is defined by [150]:

$$\mathbf{A} = \mathbf{A}^{1/2} \cdot \mathbf{A}^{1/2} \tag{141}$$

If $\mathbf{A}$ is symmetric, it can be diagonalized using a similarity transformation [48], and the principal square root can be calculated using the diagonalization method:

$$\mathbf{A}^{1/2} = \mathbf{X}\mathbf{\Lambda}^{1/2}\mathbf{X}^{-1} \tag{142}$$

where $\mathbf{\Lambda}^{1/2}$ is a diagonal matrix with the square roots of the eigenvalues of $\mathbf{A}$ along the main diagonal, and $\mathbf{X}$ is a matrix containing a corresponding set of eigenvectors of $\mathbf{A}$.

Another common matrix square root method is the Schur method, which uses the Schur decomposition:

$$\mathbf{A} = \mathbf{U}\mathbf{T}\mathbf{U}^{*} \tag{143}$$

where $\mathbf{T}$ is an upper triangular matrix and $\mathbf{U}$ is a unitary matrix whose columns form the Schur basis of $\mathbf{A}$ [155], and the (*) denotes the complex conjugate transpose of a matrix. Once in this form, the matrix square root can be calculated from:

$$\mathbf{A}^{1/2} = \mathbf{U}\mathbf{T}^{1/2}\mathbf{U}^{*} \tag{144}$$

where $\mathbf{T}^{1/2}$ can be calculated algebraically since $\mathbf{T}$, and therefore also $\mathbf{T}^{1/2}$, are upper triangular matrices. Let $\mathbf{S} = \mathbf{T}^{1/2}$. The diagonal elements of $\mathbf{S}$ are calculated directly from the diagonal elements of $\mathbf{T}$ such that [150]:

$$s_{ii} = \sqrt{t_{ii}}, \qquad i = 1,...,n \tag{145}$$

The strictly upper triangular elements are then calculated using [150]:

$$s_{ij} = \frac{t_{ij} - \sum_{k=i+1}^{j-1} s_{ik}s_{kj}}{u_{ii} + u_{jj}}, \qquad j = 2,...,n, \qquad i < j \tag{146}$$

In addition to analytical methods for calculating a matrix square root, various iterative methods have been derived. One of the most common iterative methods is Newton‟s method, which can be written as:

$$\mathbf{X}_{k+1} = \frac{1}{2}\left(\mathbf{X}_k + \mathbf{X}_k^{-1}\mathbf{A}\right), \qquad \mathbf{X}_0 = \mathbf{A} \tag{147}$$

where the matrix $\mathbf{X}$ converges quadratically to $\mathbf{A}^{1/2}$ under certain conditions [156]. One variant of Newton‟s method is known as Denman Beavers (DB) iteration, given by [150]:

$$\begin{aligned} \mathbf{X}_{k+1} &= \frac{1}{2}\left(\mathbf{X}_k + \mathbf{Y}_k^{-1}\right), \qquad \mathbf{X}_0 = \mathbf{A} \\ \mathbf{Y}_{k+1} &= \frac{1}{2}\left(\mathbf{Y}_k + \mathbf{X}_k^{-1}\right), \qquad \mathbf{Y}_0 = \mathbf{I} \end{aligned} \tag{148}$$

where the matrix $\mathbf{X}$ converges to $\mathbf{A}^{1/2}$, and the matrix $\mathbf{Y}$ converges to $\mathbf{A}^{-1/2}$. A product form of the Denman-Beavers iteration was identified by Cheng *et al*., which is a more efficient version of the Denman-Beavers iteration [157]:

$$\begin{aligned} \mathbf{M}_{k+1} &= \frac{1}{2}\left(\mathbf{I} + \frac{\mathbf{M}_k + \mathbf{M}_k^{-1}}{2}\right), \qquad \mathbf{M}_0 = \mathbf{A} \\ \mathbf{X}_{k+1} &= \frac{1}{2}\mathbf{X}_k\left(\mathbf{I} + \mathbf{M}_k^{-1}\right), \qquad \mathbf{X}_0 = \mathbf{A} \\ \mathbf{Y}_{k+1} &= \frac{1}{2}\mathbf{Y}_k\left(\mathbf{I} + \mathbf{M}_k^{-1}\right), \qquad \mathbf{Y}_0 = \mathbf{I} \end{aligned} \tag{149}$$

where $\mathbf{M}$ converges to the identity matrix, $\mathbf{I}$, $\mathbf{X}$ converges to $\mathbf{A}^{1/2}$, while $\mathbf{Y}$ converges to $\mathbf{A}^{-1/2}$. Another iterative method is the cyclic reduction (CR) iteration [154]:

$$\begin{aligned} \mathbf{Y}_{k+1} &= -\mathbf{Y}_k\mathbf{Z}_k^{-1}\mathbf{Y}_k, \qquad \mathbf{Y}_0 = \mathbf{I} - \mathbf{A} \\ \mathbf{Z}_{k+1} &= \mathbf{Z}_k + 2\mathbf{Y}_{k+1}, \qquad \mathbf{Z}_0 = 2(\mathbf{I} + \mathbf{A}) \end{aligned} \tag{150}$$

where $\mathbf{Y}$ converges to *0* and $\mathbf{Z}$ converges to $4\mathbf{A}^{1/2}$. A variant of the cyclic reduction iteration is the IN iteration given by [150]:

$$\begin{aligned}\mathbf{X}_{k+1} &= \mathbf{X}_k + \mathbf{E}_k, \qquad \mathbf{X}_0 = \mathbf{A} \\ \mathbf{E}_{k+1} &= -\frac{1}{2}\mathbf{E}_k \mathbf{X}_{k+1}^{-1} \mathbf{E}_k, \qquad \mathbf{E}_0 = \frac{1}{2}(\mathbf{I} - \mathbf{A})\end{aligned} \tag{151}$$

where $\mathbf{X}$ converges to $\mathbf{A}^{1/2}$, and $\mathbf{E}$ converges to *0*.

All of the matrix square root algorithms discussed up to this point are methods of calculating the principle square root of a matrix. Another form of the matrix square root is found using the Cholesky decomposition [158]:

$$\mathbf{A} = \mathbf{L}\mathbf{L}^T \tag{152}$$

where $\mathbf{L}$ is a lower triangular matrix which can be considered as a form of the matrix square root. Although most numerical methods of calculating the Cholesky decomposition of a matrix require positive definiteness, there are ways to calculate this decomposition for positive semi-definite matrices [159,160], although in general this result is not unique. For this application, the state covariance matrix, $\mathbf{P}$, was positive definite at each time step. In general, however, it is possible in a given application for the state covariance matrix to be positive semi-definite, in particular this can occur if some linear combinations of the states are known perfectly, *i.e.*, zero uncertainty in that combination of states.

The computational complexity of the matrix square root operation is important for use in the UKF because it is a significantly expensive part of the UKF algorithm [149]. To analyze the computational complexity of the different matrix square root algorithms, the number of floating point operations (FLOPs) as a function of the matrix dimension, *n*, was determined from various sources [150,158,161]. These results were derived theoretically based on the fundamental requirements of the algorithm, and are summarized in Table 7. Note that number of FLOPs listed for the iterative methods is the

number of FLOPs required for one iteration of the algorithm. It is shown in Table 7 that each of the matrix square root algorithms require computations on the order of $n^3$, but scaled by different factors.

Table 7. Matrix Square Root Algorithm Computational Requirement Summary

| Algorithm | FLOPs |
|---|---|
| Diagonalization | $49n^3/3 - n^2/2 + 43n/6$ |
| Schur | $85n^3/3$ |
| Newton‟s Iteration | $8n^3/3$ (per iteration) |
| Denman-Beavers (DB) Iteration | $4n^3$ (per iteration) |
| Product DB Iteration | $4n^3$ (per iteration) |
| Cyclic Reduction (CR) Iteration | $14n^3/3$ (per iteration) |
| IN Iteration | $14n^3/3$ (per iteration) |
| Cholesky | $n^3/3$ |

### 5.3.3 Sensitivity to UKF Matrix Square Root Calculation

To analyze the sensitivity of this formulation of GPS/INS sensor fusion to the matrix square root operation, the UKF algorithm was executed for each set of flight data using different methods of calculating the matrix square root. In particular, the diagonalization method, Schur method, Cholesky method, and five different iterative methods were implemented. For each of the iterative methods, the UKF was executed for each set of flight data using a set number of iterations throughout the entire flight. This process was repeated for the number of iterations ranging from 5 to 20 by unit increments. For each individual case, results were evaluated based on performance cost, $J$, total execution time of the UKF, and the accuracy of the matrix square root calculation.

A mean was taken of each of these values over all of the 23 flights in order to establish a generalized result. All of the matrix square root operations executed without error, except for certain cases of Newton‟s iteration which incurred matrix square root divergence errors on some flights when the number of iterations exceeded 16. In order to fairly compare the results, these cases of Newton‟s iteration are omitted from the data set. The performance cost of the different algorithms is shown in Figure 38.

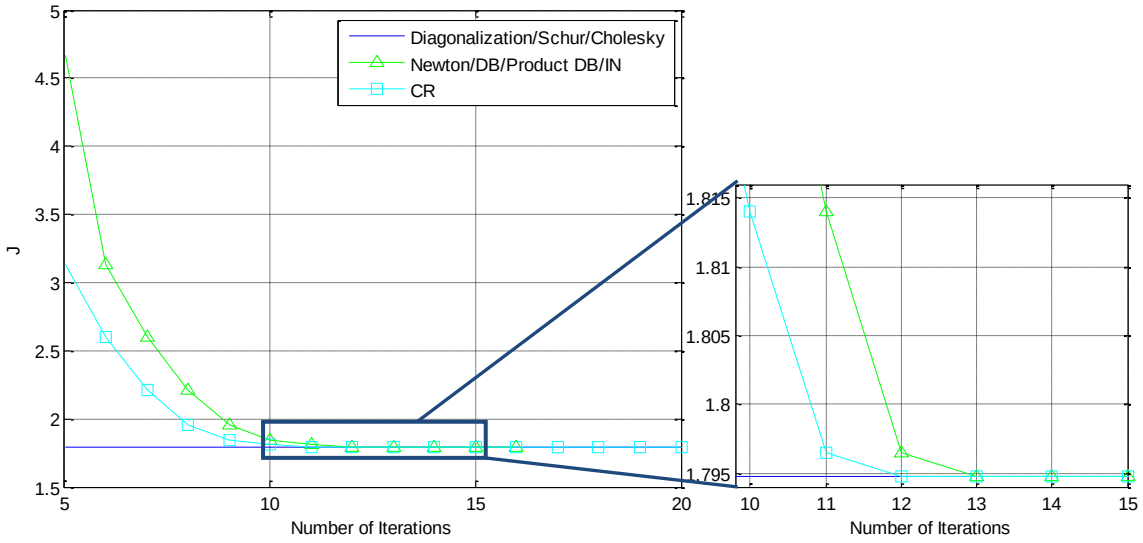


Figure 38. Performance Cost of UKF for Different Matrix Square Root Operations

In Figure 38, the performance curves were combined for some of the algorithms for clarity since those methods yielded nearly identical performance results. The performance of the non-iterative methods is also included in Figure 38 to compare with the iterative methods. The plot on the right in Figure 38 shows a zoomed-in section to show the convergence of the algorithms. In terms of performance, the Cyclic Reduction (CR) algorithm showed the fastest convergence with respect to number of iterations out of the five considered iterative methods. Another interesting observation from these

performance curves is the number of iterations required for each of the iterative algorithms to converge to the same performance as the non-iterative methods. For this application, the CR iteration requires 12 iterations and the other four iterative methods require 13 iterations to achieve similar performance as the non-iterative methods to four significant figures. However, a smaller number of iterations can be used to reduce computations and still achieve reasonable performance. The CR method with 8 iterations could be used, *e.g.*, if performance cost of 2 degrees is acceptable for the application.

Since computational requirements are also important for a matrix square root algorithm, the actual execution time of the entire UKF algorithm was calculated for each of the different methods. These execution times are intended to provide an approximate empirical verification of the theoretical FLOP estimates in order to compare the computational requirements of the different algorithms. All execution time analyses were conducted using the same computer under approximately the same operating conditions. A mean of these execution times over each of the 23 flights is shown in Figure 39 (left). Also shown in Figure 39 (right) are the corresponding estimated number of FLOPs using Table 7.

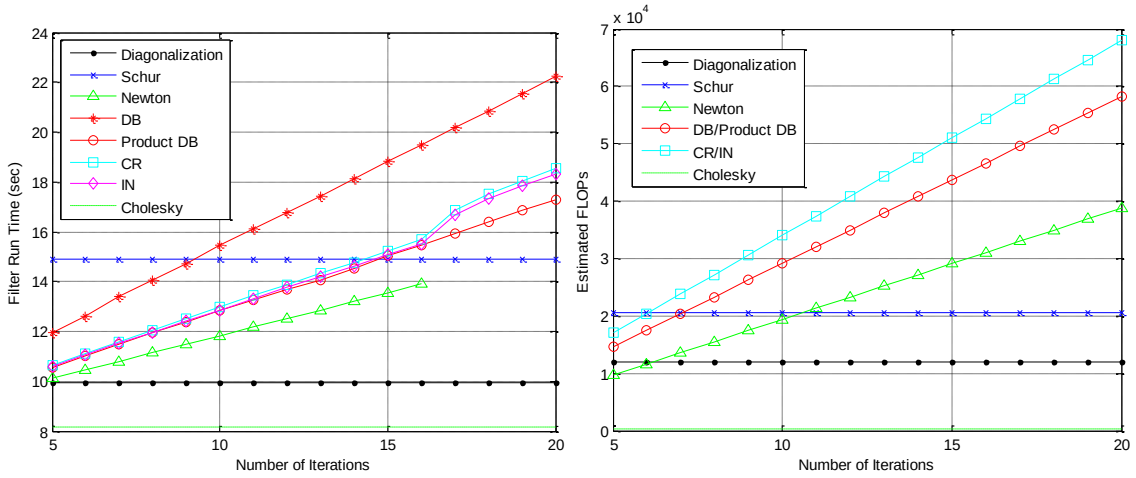


Figure 39. UKF Computational Requirements for Different Matrix Square Root Operations

It is important to note that the number of FLOPs estimate is for the matrix square root operation only, while the execution times represent the run times of the entire sensor fusion algorithm. However, this is representative of the overall trend since the only difference between the curves is the matrix square root operation used. Because the diagonalization, Schur, and Cholesky methods do not require iterations, these algorithms are represented in Figure 39 by horizontal lines. Also, in Figure 39 (right), the Denman-Beavers (DB) and Product DB are represented by a single line, since the estimated FLOPs for these algorithms are the same as listed in Table 7. The CR and IN iterations are similarly combined in Figure 39 (right). Similar trends are observed between the estimated number of FLOPs and the UKF execution time with a few observations. First, the Denman-Beavers (DB) method demonstrates a longer execution time that grows at a steeper rate with the number of iterations than the product DB method, even though the FLOP estimations were the same. Another difference between the FLOP estimates and the UKF execution time is the location of the non-iterative methods with respect to the iterative methods. With respect to the empirical execution time results, the iterative

methods are all found to be more efficient in execution time than the Schur method for cases up to 15 iterations, with the exception of the DB iteration. This is an important result because previously, in Figure 38 it was shown that the iterative methods all achieve performance accuracy to four significant figures by using at most 13 iterations. This indicates the potential value of using iterative methods over the Schur method. It is also shown in Figure 39 that the Cholesky method has the fastest execution time with respect to any of the tested cases.

In order to compare accuracy of the actual matrix square root calculation itself, the $L_1$ norm [53] of the matrix $\left|\mathbf{P}^{1/2}\cdot\mathbf{P}^{1/2}-\mathbf{P}\right|_1$ was calculated as a measure of the accuracy of the matrix square root operation. This norm, which is equal to the maximum of the absolute column sums of the matrix, was calculated at each time step of the UKF algorithm. To analyze the overall accuracy of the matrix square root operation over an entire flight, only the maximum of this norm over all discrete time was considered for each flight. This maximum represents the worst matrix square root estimate that occurred over the entire flight. A mean was taken of each of these maximum norms over all 23 flights, and the results are shown in Figure 40.

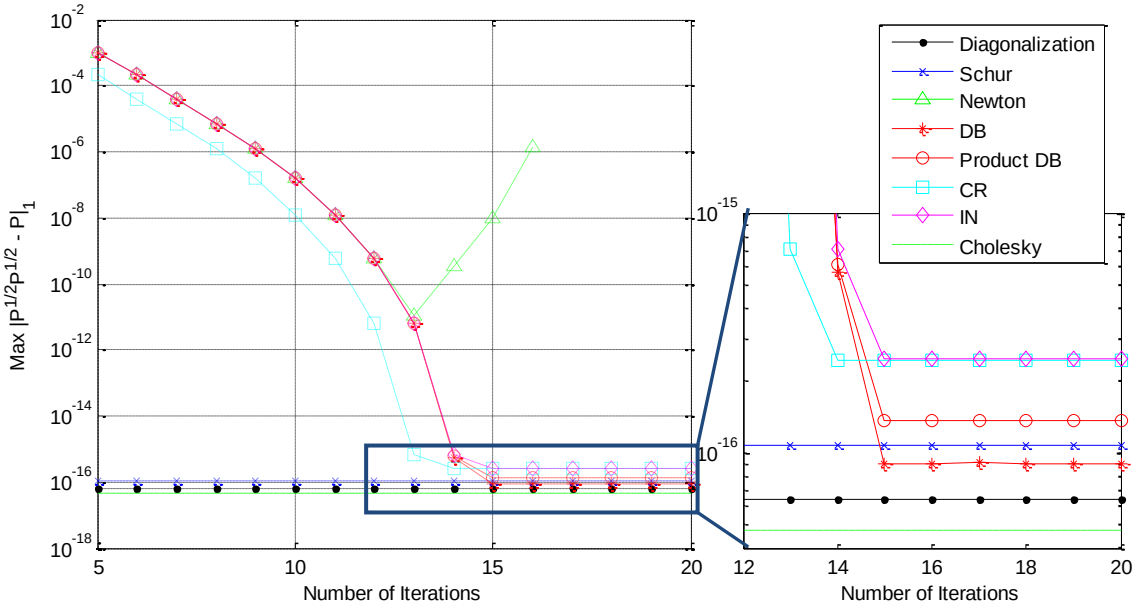


Figure 40. Matrix Square Root Operation Accuracy

Figure 40 shows the convergence of the iterative methods in terms of the matrix square root accuracy. For smaller numbers of iterations, all of the iterative methods except for CR are very close in accuracy. These curves start to separate only at higher numbers of iterations, as shown in the right side plot of Figure 40. All of these algorithms converge to very high matrix square root accuracy after a sufficient number of iterations, with the exception of Newton‟s iteration. Figure 40 demonstrates the divergence of the Newton‟s iteration. After 13 iterations, the matrix square root accuracy starts to degrade and eventually reaches a point where the matrix square root accuracy is too poor to use within the UKF algorithm. Because of the divergence issues associated with Newton‟s iteration, it is not recommended for UKF applications, even though it is the most computationally efficient iterative matrix square root method with respect to both FLOP estimate and execution time. Because the accuracy of the matrix square root operation has a direct effect on the accuracy of the prediction stage of the UKF, the relationship between the

matrix square root accuracy and UKF performance accuracy for all considered matrix square root operations is shown in Figure 41.

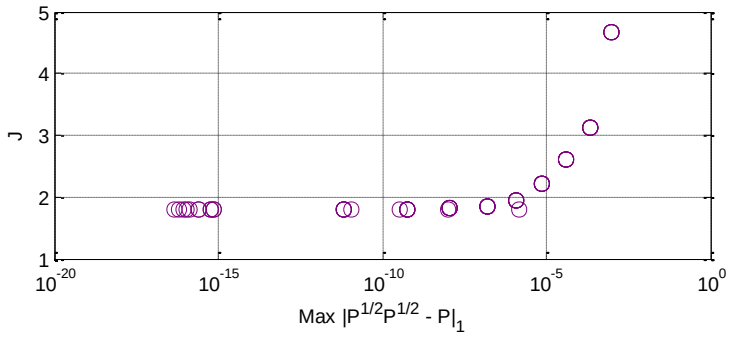


Figure 41. Relationship between Matrix Square Root Accuracy and UKF Performance

As shown in Figure 41, there is a clear nonlinear relationship between the matrix square root accuracy and the UKF performance for this application. This demonstrates the significant effect of the matrix square root accuracy on the performance of the UKF.

### 5.3.3 Comparison of Direct Matrix Square Root Methods to SR-UKF

A different method of handling the square root requirement of the UKF, named the "square-root UKF (SR-UKF)" was suggested by van der Merwe and Wan [149]. In this method, the square root of the state covariance matrix is estimated directly. This eliminates the need to re-factorize the state covariance matrix at each time step, and instead it is updated using Cholesky updates. A significant advantage of this method is a decrease in computational complexity, which leads to a faster run time of the UKF. For comparison purposes, the Cholesky method was selected as a representative case of calculating the matrix square root at each time step from the state covariance estimate.

Performance results were calculated using each of these two methods for each of the 23 flights, and the performance cost is plotted in Figure 42.

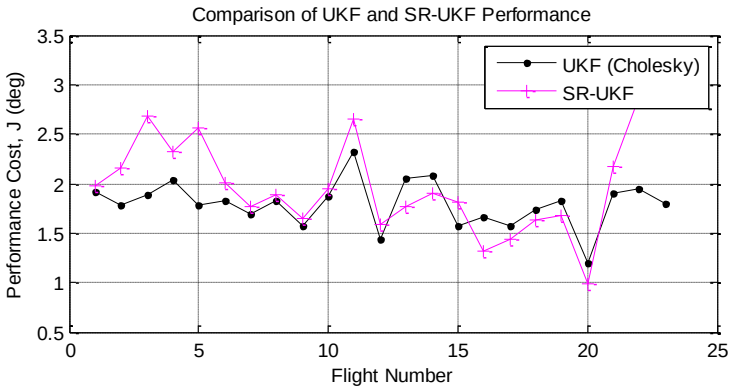


Figure 42. Comparison of UKF and SR-UKF Performance

The mean performance costs of the two different methods are shown in Table 8. To determine if there is a statistically significant performance advantage of the UKF over the SR-UKF, a one-tailed paired samples hypothesis test [53] was done using the *t*-statistic to determine the probability that the SR-UKF has better performance than the UKF. Using this null hypothesis, the probability was calculated to be 1.49%, which is less than the commonly considered 5% null hypothesis rejection criterion. Therefore, the UKF achieves statistically significant better performance than the SR-UKF for this application, at the cost of additional computational complexity. To compare the computational complexity of the two different algorithms, the mean execution time of the algorithms was calculated and is also shown in Table 8.

Table 8. Comparison of UKF and SR-UKF

| **Matrix Square Root Method** | **Mean Performance Cost J (deg)** | **Mean Execution Time (sec)** |
|---|---|---|
| UKF (Cholesky) | 1.795 | 8.16 |
| SR-UKF | 1.996 | 5.73 |

It is also interesting to note from Figure 42 that there are some cases where the SR-UKF method has better performance than the Cholesky method, *e.g.*, flight #16. If this single flight alone was used to analyze results, the opposite conclusion could be drawn about the accuracy of this method. This demonstrates the value of using multiple data sets for comparison.

### 5.3.4 Matrix Square Root Operations for UKF Conclusions

This section presented a comparison of different matrix square root calculations within the UKF. The GPS/INS sensor fusion attitude estimation problem for subscale aircraft applications was used as an example to evaluate the performance with respect to matrix square root accuracy, computational cost, and attitude estimation performance. In terms of attitude estimation performance, the Cholesky, diagonalization and Schur methods yielded the highest accuracy, however this same performance can be reached using a sufficient number of iterations in any of the iterative methods. Newton‟s iteration was found to diverge in certain instances, and is therefore not recommended for UKF applications. The cyclic reduction (CR) iteration demonstrated the fastest performance convergence of the iterative methods. In terms of execution time, the SR-UKF is computationally efficient, but at the cost of performance. Overall, the Cholesky method was found to provide the best compromise in terms of both performance and execution time.

For real-time applications of the UKF, such as attitude estimation for small aircraft, computation is an important consideration factor. For most cases, the Cholesky method is the best suited matrix square root method due to its fast execution and high accuracy. If computational cost is even more important than the accuracy of the filter, the SR-UKF could be considered. The diagonalization and Schur methods are acceptable approaches for off-line applications, because the accuracy is similar to the Cholesky method, although they require more computation time. These methods also might be more desirable than the Cholesky method because they provide a more intuitive representation of the matrix square root, *i.e.* the principle square root. Any of the iterative methods, except for Newton‟s iteration, could also be used with a sufficient number of iterations, though these methods are a bit less intuitive.

## 5.4 ANALYTICAL COMPARISON OF INITIALIZATION ERROR

The analysis in this section was submitted for publication in [19]. Initialization error is an important consideration for nonlinear stochastic filters, such as the EKF and UKF, especially because too large of initial error can lead to divergence of the filter [40,162]. These two nonlinear filters implement different linearization techniques – analytical linearization in the EKF and statistical linearization in the UKF [10] – which lead to differences in the convergence of the initial error, which significantly impacts the estimation performance. Because of this, it is important to understand the initial error convergence rates of the EKF and UKF.

Some authors have commented on the initialization error convergence of the EKF and UKF. Crassidis [78], Fiorenzani *et al.* [79], and Wendell *et al.* [132], concluded using simulation studies that the UKF performance exceeds that of the EKF only under large initialization errors. El-Sheimy *et al.* reached this same conclusion through experimental tests of the attitude estimation problem for land vehicles [133]. It was also shown that the EKF actually performed better in response to large initial errors for a Global Positioning System/Inertial Navigation System (GPS/INS) attitude estimation application [16]. Due to the inconsistency in conclusions regarding the effects of initialization error for EKF and UKF, an analysis of these filters is necessary in order to determine the different conditions under which each filter is advantageous over the other.

This section considers the differences between EKF and UKF in response to initialization error through analysis of an example nonlinear system. This case study thoroughly investigates the initialization error convergence for EKF and UKF of this example system using both theoretical analysis and simulation results. The purpose of this work is to provide a counter example to the general perception of previous work [78,79,132,133] that the UKF is better than the EKF at handling large initialization errors in the system.

Consider a scalar nonlinear system of the form

$$\begin{aligned} x_k &= f\left(x_{k-1}\right) \\ y_k &= x_k + v_k \end{aligned} \tag{153}$$

where $x$ is the state, $y$ is the output, $f$ is the nonlinear state transition function, and $v$ is the measurement noise, which is assumed to be zero-mean Gaussian with variance, $R_k$. Note that this system does not include any input or process noise, and the output equation is

linear. The state of this system can be estimated using either EKF or UKF, which are described in the following sections.

The EKF equations can be found in various sources [62,15], and are presented here for the system described in (153). First, the *a priori* state, $x_{k|k\text{-}1}$, and variance, $P_{k|k\text{-}1}$, are predicted using

$$\begin{aligned} \hat{x}_{k|k-1} &= f\left(\hat{x}_{k-1}\right) \\ P_{k|k-1} &= \left(\partial f\left(\hat{x}_{k-1}\right)/\partial x_{k-1}\right)^2 P_{k-1} \end{aligned} \tag{154}$$

Then, the *a priori* estimates are updated to obtain the *a posteriori* estimates using the Kalman gain, $K_k$, with

$$\begin{aligned} K_k &= P_{k|k-1}/\left(P_{k|k-1}+R_k\right) \\ \hat{x}_k &= \hat{x}_{k|k-1}+K_k\left(y_k-\hat{x}_{k|k-1}\right) \\ P_k &= \left(1-K_k\right)P_{k|k-1} \end{aligned} \tag{155}$$

The UKF equations are simplified here for the system described in (153). Note that because there is no process noise and the measurement noise is additive, no augmentation is required for the state [16]. The primary, secondary, and tertiary scaling parameters for this study are assumed to be $\alpha$=1, $\beta$=2, and $\kappa$=0, respectively [11]. This leads to the spread parameter $\eta$=1, and mean, $\mathbf{w}_m$, and covariance, $\mathbf{w}_c$, weight vectors given by

$$\begin{aligned} \mathbf{w}_m &= \begin{bmatrix} 0 & 0.5 & 0.5 \end{bmatrix}^T \\ \mathbf{w}_c &= \begin{bmatrix} 2 & 0.5 & 0.5 \end{bmatrix}^T \end{aligned} \tag{156}$$

For the scalar UKF with assumed scaling parameters, first, a vector of 3 sigma points is constructed

$$\boldsymbol{\chi}_{k-1} = \begin{bmatrix} \hat{x}_{k-1} & \hat{x}_{k-1}+\eta\sqrt{P_{k-1}} & \hat{x}_{k-1}-\eta\sqrt{P_{k-1}} \end{bmatrix} \tag{157}$$

These sigma points are then each propagated through the nonlinear function to obtain

$$\boldsymbol{\chi}_{k|k-1} = \begin{bmatrix} f\left(\hat{x}_{k-1}\right) & f\left(\hat{x}_{k-1} + \eta\sqrt{P_{k-1}}\right) & f\left(\hat{x}_{k-1} - \eta\sqrt{P_{k-1}}\right) \end{bmatrix} \tag{158}$$

Next, the *a priori* state and variance are predicted through weighted averages, as in

$$\begin{aligned} \hat{x}_{k|k-1} &= \boldsymbol{\chi}_{k|k-1}\mathbf{w}_m \\ P_{k|k-1} &= \left(\boldsymbol{\chi}_{k|k-1} - \hat{x}_{k|k-1}\right)\mathbf{w}_c \end{aligned} \tag{159}$$

Since the output equation is linear, the linear Kalman Filter (KF) measurement update equations in (155) can also be used here.

For this initialization error analysis, the scalar nonlinear system in (153) is used with the nonlinear function, *f*, defined as

$$f\left(x_{k-1}\right) = x_{k-1}^2 \tag{160}$$

Using this simple example system allows for the analytical derivation of the EKF and UKF estimation errors, which leads to the theoretical conditions under which one filter outperforms the other.

The *a priori* state and variance for (160) are calculated for the EKF using (154)

$$\begin{aligned} \hat{x}_{k|k-1}^E &= \hat{x}_{k-1}^2 \\ P_{k|k-1}^E &= 4\hat{x}_{k-1}^2 P_{k-1} \end{aligned} \tag{161}$$

For the UKF, the *a priori* state and variance for (160) are given by

$$\begin{aligned} \hat{x}_{k|k-1}^U &= \hat{x}_{k-1}^2 + P_{k-1} \\ P_{k|k-1}^U &= 4\hat{x}_{k-1}^2 P_{k-1} + 2P_{k-1}^2 \end{aligned} \tag{162}$$

By comparing (161) and (162), it is shown that the UKF contains additional terms that the EKF does not. Next, the measurement update is applied in order to determine the differences in the *a posteriori* state for the EKF, as in

$$\hat{x}_k^E = \frac{\hat{x}_{k-1}^2 R_k + 4\hat{x}_{k-1}^2 P_{k-1} y_k}{4\hat{x}_{k-1}^2 P_{k-1} + R_k} \tag{163}$$

and for the UKF, as in

$$\hat{x}_k^U = \frac{\left(\hat{x}_{k-1}^2 + P_{k-1}\right) R_k + \left(4\hat{x}_{k-1}^2 P_{k-1} + 2P_{k-1}^2\right) y_k}{4\hat{x}_{k-1}^2 P_{k-1} + 2P_{k-1}^2 + R_k} \tag{164}$$

The *a posteriori* estimation errors are then defined by

$$\begin{aligned} \tilde{x}_k^E &= x_k - \hat{x}_k^E = x_{k-1}^2 - \hat{x}_k^E \\ \tilde{x}_k^U &= x_k - \hat{x}_k^U = x_{k-1}^2 - \hat{x}_k^U \end{aligned} \tag{165}$$

and the output is given by

$$y_k = x_k + v_k = x_{k-1}^2 + v_k \tag{166}$$

which after some simplification leads to the *a posteriori* estimation errors of the EKF and UKF

$$\begin{aligned} \tilde{x}_k^E &= \frac{\left(x_{k-1}^2 - \hat{x}_{k-1}^2\right) R_k - 4\hat{x}_{k-1}^2 P_{k-1} v_k}{4\hat{x}_{k-1}^2 P_{k-1} + R_k} \\ \tilde{x}_k^U &= \frac{\left(x_{k-1}^2 - \hat{x}_{k-1}^2 - P_{k-1}\right) R_k - \left(4\hat{x}_{k-1}^2 P_{k-1} + 2P_{k-1}^2\right) v_k}{4\hat{x}_{k-1}^2 P_{k-1} + 2P_{k-1}^2 + R_k} \end{aligned} \tag{167}$$

Now, assuming that the a posteriori estimation error terms for EKF and UKF have the same sign, consider the following ratio

$$\Gamma_k = E\left[\tilde{x}_k^E\right] \Big/ E\left[\tilde{x}_k^U\right] \tag{168}$$

where $E$ is the expectation operator. Note that because of this expectation operator, the following results represent the expected result of the filters, which may differ from the actual results depending on the measurement noise. The ratio $\Gamma_k$ indicates whether the EKF or UKF has better estimation performance, *i.e.*, $\Gamma_k$ greater than 1 means better UKF

performance, while $\Gamma_k$ less than 1 means better EKF performance. Using the definitions of the *a posteriori* errors from (167), $\Gamma_k$ can be calculated

$$\Gamma_k = \frac{\left(x_{k-1}^2 - \hat{x}_{k-1}^2\right)\left(4\hat{x}_{k-1}^2 P_{k-1} + 2P_{k-1}^2 + R_k\right)}{\left(4\hat{x}_{k-1}^2 P_{k-1} + R_k\right)\left(x_{k-1}^2 - \hat{x}_{k-1}^2 - P_{k-1}\right)} \tag{169}$$

This ratio can be reorganized, giving

$$\Gamma_k = \frac{\left(x_{k-1}^2 - \hat{x}_{k-1}^2\right)\left(4\hat{x}_{k-1}^2 P_{k-1} + R_k\right) + \left(x_{k-1}^2 - \hat{x}_{k-1}^2\right)2P_{k-1}^2}{\left(x_{k-1}^2 - \hat{x}_{k-1}^2\right)\left(4\hat{x}_{k-1}^2 P_{k-1} + R_k\right) - P_{k-1}\left(4\hat{x}_{k-1}^2 P_{k-1} + R_k\right)} \tag{170}$$

Then, dividing by the common term in the numerator and denominator gives

$$\Gamma_k = \frac{1 + \dfrac{2P_{k-1}^2}{4\hat{x}_{k-1}^2 P_{k-1} + R_k}}{1 + \dfrac{P_{k-1}}{\hat{x}_{k-1}^2 - x_{k-1}^2}} \triangleq \frac{1+\gamma_k}{1+\delta_k} \tag{171}$$

where $\gamma_k$ and $\delta_k$ are parameters of interest for this analysis. It is clear from its definition that $\gamma_k$ is always positive. The sign of $\delta_k$ however is dependent on the relative magnitude of the true state and the estimated state at time $k$-1. If $\hat{x}_{k-1}^2 < x_{k-1}^2$, $\delta_k$ will be negative, therefore the ratio $\Gamma_k$ will be greater than 1, indicating better performance of the UKF. However, if $\hat{x}_{k-1}^2 > x_{k-1}^2$, $\delta_k$ will be positive, and therefore it must be determined whether $\gamma_k$ or $\delta_k$ is greater, *i.e.*

$$\frac{2P_{k-1}^2}{4\hat{x}_{k-1}^2 P_{k-1} + R_k} < or > \frac{P_{k-1}}{\hat{x}_{k-1}^2 - x_{k-1}^2} \tag{172}$$

Simplifying this relationship gives

$$-2P_{k-1}\left(\hat{x}_{k-1}^2 + x_{k-1}^2\right) < or > R_k \tag{173}$$

Since the left hand side is always negative while the right hand side is always positive, the term $\gamma_k$ is always less than $\delta_k$, therefore the ratio $\Gamma_k$ will be less than 1 for $\hat{x}_{k-1}^2 > x_{k-1}^2$,

indicating better performance of the EKF. It is also interesting to note that larger measurement variance leads to larger performance advantage of the EKF over the UKF for this case. The relative performance characteristics are summarized in Table 9.

Table 9. Theoretical Relative Initial Error Performance

| System Condition | Expected Initial Error Performance |
|---|---|
| $\hat{x}_{k-1}^2 < x_{k-1}^2$ | UKF Better |
| $\hat{x}_{k-1}^2 > x_{k-1}^2$ | EKF Better |

The EKF and UKF were implemented for the considered system and compared with a simulated truth obtained directly from (153). Examples of cases where the EKF performed better in response to the initial error are shown in Figure 43, while examples of cases where the UKF performed better in response to the initial error are shown in Figure 44. These figures show the simulated estimation errors for EKF and UKF, with reported Mean-Square Error (MSE) values taken over 10 discrete time steps. Figure 43 uses an assumed initial state that meets the condition $\hat{x}_{k-1}^2 > x_{k-1}^2$, while Figure 44 assumes an initial state satisfying $\hat{x}_{k-1}^2 < x_{k-1}^2$. Both figures show three different cases of measurement noise variance: 0.01, 1, and 100.

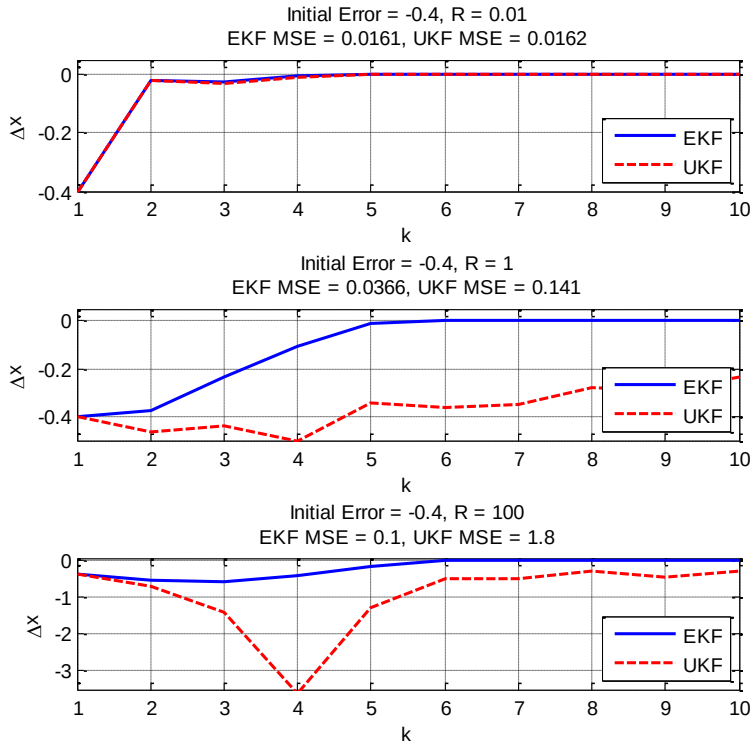


Figure 43. Cases for Better EKF Convergence

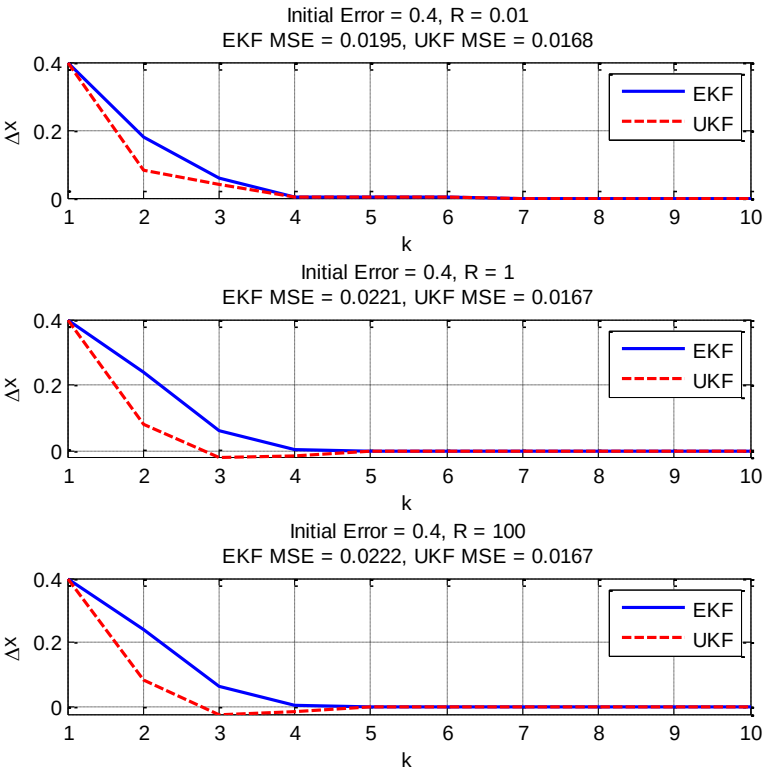


Figure 44. Cases for Better UKF Convergence

The relative performance advantage of the EKF over the UKF displayed in Figure 43 is shown to become more significant as the measurement noise variance is increased. This is especially apparent for the case of $R = 100$, which shows very poor UKF performance. However, for the cases of better UKF performance shown in Figure 44, the different cases of measurement noise variance do not have much of an effect. These simulation results agree with the previous theoretical analysis.

Expanding upon the few selected examples from Figure 43 and Figure 44, various cases of assumed and true initial states were also simulated. The difference in MSE values for EKF and UKF was calculated for each case in order to show which filter performed better. Color scale plots were generated to illustrate these results for $R = 0.01$ in Figure 45, $R = 1$ in Figure 46, and $R = 100$ in Figure 47, where bluer shades indicate better EKF performance while redder shades indicate better UKF performance.

It is interesting to note in Figure 45, Figure 46, and Figure 47 that although it was expected that the UKF should outperform the EKF anywhere that the true initial state was larger than the assumed initial state, the simulation results show that sometimes the EKF still outperforms the UKF in this region, especially for larger measurement noise variance. This identifies the weakness in the theoretical analysis using the expectation operator to remove the stochastic terms, but further justifies the conclusion that larger measurement noise leads to better EKF relative performance.

This section presented a case study that investigated the effects of initialization error for the EKF and UKF. Through a theoretical analysis of an example problem, it was determined that for this particular example, the EKF performs better than the UKF

for cases when the magnitude of the assumed initial state is greater than the actual initial state, *i.e.*, the filter overestimated the initial state. On the contrary, if the filter underestimated the initial state, the UKF was found to have better initial error convergence for the considered example problem. Also, simulation results were used to justify the theoretical conclusions. These results are tied to the example system; however this work demonstrates the possibility of the EKF containing better initial error convergence. Additionally, the EKF performance advantage was found to become more significant as the measurement noise variance increased.

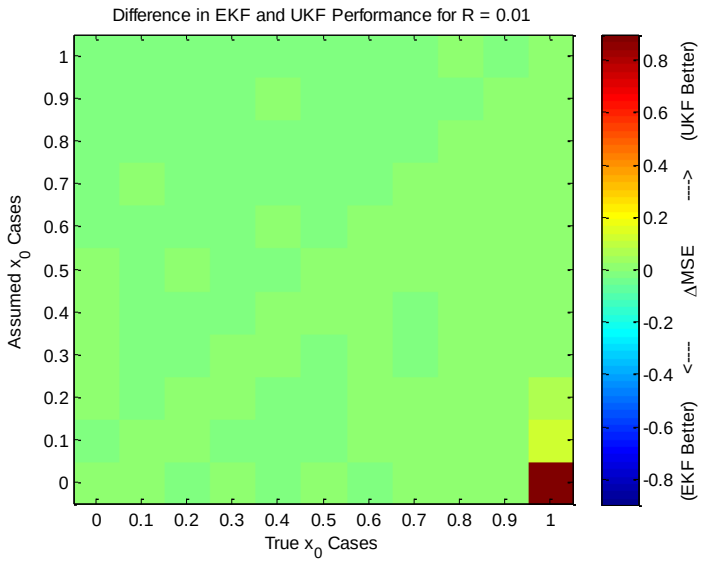


Figure 45. Difference in EKF and UKF Performance for $R = 0.01$

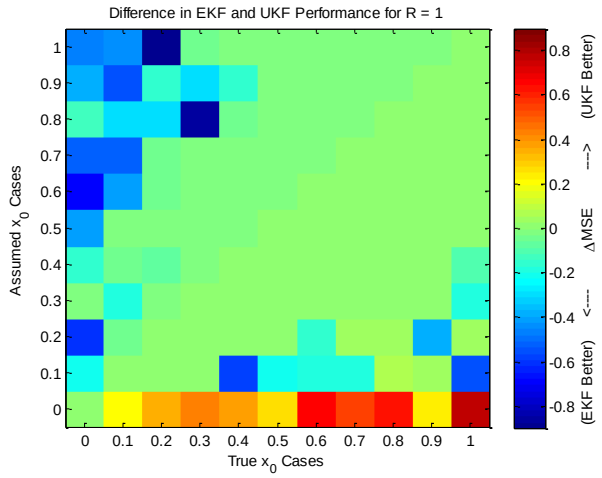


Figure 46. Difference in EKF and UKF Performance for $R = 1$

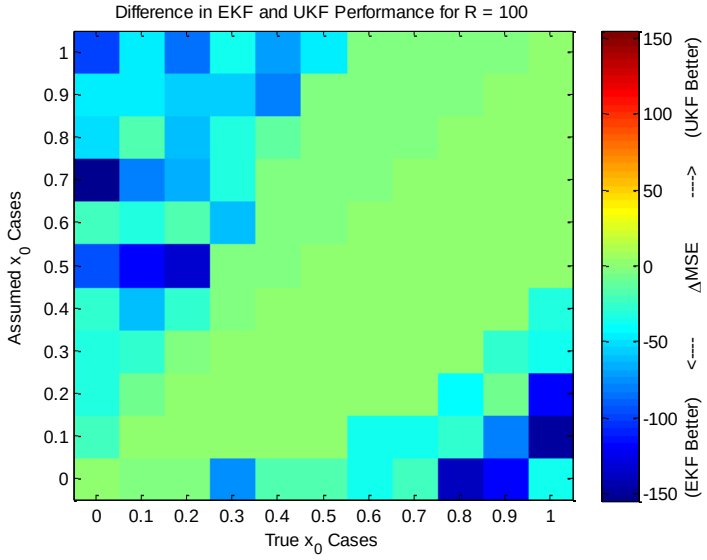


Figure 47. Difference in EKF and UKF Performance for $R = 100$

## 5.5 ANALYTICAL COMPARISON OF LINEARIZATION METHODS

The analysis in this section was originally published in [18]. This section considers the transformation of the mean and variance of a normally distributed random variable through three different nonlinear functions: $\sin(x)$, $\cos(x)$, and $x^k$, where $k$ is

some positive integer. Only Gaussian random variables are considered here, but other nonlinear estimators such as particle filters can be used to approximate other distributions if necessary [163]. The true mean and variance of the random variable after these transformations is theoretically derived and verified with respect to Monte Carlo experiments. These statistics are used as a reference in order to compare the accuracy of two different linearization techniques: analytical linearization used in EKF and statistical linearization used in UKF. First, the statistics for nonlinear transformations of a zero mean Gaussian variable are discussed, and then this derivation is expanded to include non-zero mean variables. Next, the linearization techniques used in EKF and UKF are compared, followed by a nonlinear filtering example to demonstrate the usefulness of the theoretically derived results.

### 5.5.1 Transformations of a Zero Mean Gaussian Variable

Consider a normally distributed random variable, $x$, with zero mean and variance, $\sigma^2$, *i.e.*, $x \sim N\left(0, \sigma^2\right)$. Let $f(x)$ be the probability density function of $x$, and $M(t)$ be the moment generating function of $x$, given by [164]:

$$f(x) = \frac{1}{\sqrt{2\pi\sigma^2}} e^{\frac{-x^2}{2\sigma^2}} \tag{174}$$

$$M(t) = e^{\frac{1}{2}\sigma^2 t^2} \tag{175}$$

Let $y$ be some nonlinear function of $x$, $y = g(x)$. For each of these nonlinear functions, the mean and variance after the nonlinear transformation can be determined using the expectation operator [164]:

$$E\left[g(x)\right]=\int g(x)f(x)dx \tag{176}$$

The nonlinear function $y = x^k$ is considered as a general case to capture the effects of polynomials, where $k$ is some positive integer. For this function, the expectation integral does not need to be evaluated; instead, the moment generating function, $M(t)$, can be used to derive the moments of this function [164]:

$$E\left[x^k\right]=\left.\frac{\partial^k M(t)}{\partial t^k}\right|_{t=0} \tag{177}$$

Thus, the mean of $y$ is given by:

$$\begin{aligned} &E\left[x^{2k-1}\right]=0 \\ &E\left[x^{2k}\right]=(2k-1)!!\sigma^{2k} \\ &k=1,2,3,... \end{aligned} \tag{178}$$

where !! is the double factorial operator [165]. To calculate the variance of $y$, the following equation is used [164]:

$$\sigma_y^2=E\left[y^2\right]-E\left[y\right]^2 \tag{179}$$

Using (178) and (179), the variance of $y = x^k$ is calculated using:

$$\sigma_y^2=\begin{cases}(2k-1)!!\sigma^{2k} & k=1,3,5,... \\ \left[(2k-1)!!-(k-1)!!\right]\sigma^{2k} & k=2,4,6,...\end{cases} \tag{180}$$

Now, consider the nonlinear function $y = \sin(x)$. Solving (176) directly for this function is not a trivial matter. However, if the sine function is expanded using its Taylor series, the expectation becomes:

$$E\left[\sin x\right] = E\left[\sum_{n=0}^{\infty} \frac{(-1)^n x^{2n+1}}{(2n+1)!}\right] = \sum_{n=0}^{\infty} \frac{(-1)^n E\left[x^{2n+1}\right]}{(2n+1)!}$$
$$= E\left[x\right] - \frac{E\left[x^3\right]}{3!} + \frac{E\left[x^5\right]}{5!} - \ldots \tag{181}$$

Using (178), (181) gives $E\left[\sin x\right] = 0$.

For $y = \cos(x)$, a similar procedure is used to calculate the mean of $y$:

$$E\left[\cos x\right] = E\left[\sum_{n=0}^{\infty} \frac{(-1)^n x^{2n}}{(2n)!}\right] = \sum_{n=0}^{\infty} \frac{(-1)^n E\left[x^{2n}\right]}{(2n)!}$$
$$= 1 - \frac{E\left[x^2\right]}{2!} + \frac{E\left[x^4\right]}{4!} - \ldots \tag{182}$$

Using (178), (182) simplifies to:

$$E\left[\cos x\right] = \sum_{n=0}^{\infty} \frac{(-1)^n (2n-1)!!}{(2n)!} \sigma^{2n}$$
$$= \sum_{n=0}^{\infty} \frac{(-1)^n}{(2n)!!} \sigma^{2n} = e^{\frac{-\sigma^2}{2}} \tag{183}$$

Next, the variances for the sine and cosine functions are calculated using (179). The variance of the sine function is given by:

$$\sigma_y^2 = E[\sin^2 x] - E[\sin x]^2$$
$$\sigma_y^2 = E\left[\frac{1-\cos 2x}{2}\right] - 0^2$$
$$\sigma_y^2 = \frac{1}{2} - \frac{1}{2} E\left[\cos 2x\right] \tag{184}$$
$$\sigma_y^2 = \frac{1}{2}\left(1 - e^{-2\sigma^2}\right)$$

The variance of the cosine function is given by:

$$\begin{aligned}
\sigma_y^2 &= E[\cos^2 x] - E[\cos x]^2 \\
\sigma_y^2 &= E\left[\frac{1+\cos 2x}{2}\right] - e^{-\sigma^2} \\
\sigma_y^2 &= \frac{1}{2} + \frac{1}{2}E\left[\cos 2x\right] - e^{-\sigma^2} \\
\sigma_y^2 &= \frac{1}{2}\left(1 - e^{-\sigma^2}\right)^2
\end{aligned} \tag{185}$$

The results of this analysis are summarized in Table 10.

Table 10. Statistics for Transformations of a Zero Mean Gaussian Variable

| $g(x)$ | $E\left[g(x)\right]$ | $\sigma^2\left(g(x)\right)$ |
|---|---|---|
| $x^k$ | $E\left[x^{2k-1}\right] = 0$<br>$E\left[x^{2k}\right] = (2k-1)!!\sigma^{2k}$<br>$k = 1,2,3,...$ | $\begin{cases} (2k-1)!!\sigma^{2k} \\ \quad k = 1,3,5,... \\ \left[(2k-1)!! - (k-1)!!\right]\sigma^{2k} \\ \quad k = 2,4,6,... \end{cases}$ |
| $\sin x$ | $E\left[\sin x\right] = 0$ | $\frac{1}{2}\left(1 - e^{-2\sigma^2}\right)$ |
| $\cos x$ | $E\left[\cos x\right] = e^{\frac{-\sigma^2}{2}}$ | $\frac{1}{2}\left(1 - e^{-\sigma^2}\right)^2$ |

### 5.5.2 Transformations of a Non-Zero Mean Gaussian Variable

Consider a normally distributed random variable, $z$, with mean, $\mu$, and variance, $\sigma^2$, *i.e.*, $z \sim N\left(\mu, \sigma^2\right)$. Note that $z$ is equivalently distributed to $x$, except for a shift in the mean from 0 to $\mu$, *i.e.*, $z = x + \mu$. To take advantage of the relationships from Table 10, this change of variables from $z$ to $x$ will be utilized. Now, let $y$ be some nonlinear function of $z$, $y = g(z)$. Again, the same three different nonlinear functions are considered: $g(z) = \sin(z)$, $g(z) = \cos(z)$, and $g(z) = z^k$, where $k$ is some positive integer.

First the nonlinear function $y = z^k$ is considered. The expected value of $y$ can be obtained using the binomial expansion [164]:

$$\begin{aligned} E\left[z^k\right] &= E\left[(x+\mu)^k\right] = E\left[\sum_{i=0}^{k} \frac{k!}{(k-i)!i!}\mu^{k-i}x^i\right] \\ E\left[z^k\right] &= \sum_{i=0}^{k} \frac{k!}{(k-i)!i!}\mu^{k-i}E\left[x^i\right] \end{aligned} \tag{186}$$

where the expectations of $x$ are given by (178):

$$E\left[z^k\right] = \sum_{i=0}^{k/2} \frac{k!}{(k-2i)!(2i)!!}\mu^{k-2i}\sigma^{2i} \tag{187}$$

The variance is then determined using (179) and (187) to be:

$$\sigma_y^2 = \sum_{i=0}^{k} \frac{(2k)!}{(2k-2i)!(2i)!!}\mu^{2k-2i}\sigma^{2i} - \left(\sum_{j=0}^{k/2} \frac{k!}{(k-2j)!(2j)!!}\mu^{k-2j}\sigma^{2j}\right)^2 \tag{188}$$

Next the nonlinear function $y = \sin(z)$ is considered. The expected value of $y$ can be obtained by taking advantage of the relationship of $z$ to $x$, as well as trigonometric identities:

$$\begin{aligned} E\left[\sin z\right] &= E\left[\sin\left(x+\mu\right)\right] \\ &= E\left[\sin x\cos\mu + \cos x\sin\mu\right] \\ &= E\left[\sin x\right]\cos\mu + E\left[\cos x\right]\sin\mu \end{aligned} \tag{189}$$

Using the previously determined expectations of the sine and cosine functions with respect to $x$ in Table 10, the expected value of $y$ is determined as:

$$E\left[\sin z\right] = \left(\sin\mu\right)e^{\frac{-\sigma^2}{2}} \tag{190}$$

The variance is then derived from (179) and (190), as well as Table 10:

$$\begin{aligned}
\sigma_y^2 &= E[\sin^2(x+\mu)] - E[\sin(x+\mu)]^2 \\
\sigma_y^2 &= E\left[\frac{1}{2} - \frac{1}{2}\cos\big(2(x+\mu)\big)\right] - e^{-\sigma^2}\sin^2\mu \\
\sigma_y^2 &= \frac{1}{2} - \frac{1}{2}E\big[\cos 2x\cos 2\mu - \sin 2x\sin 2\mu\big] - e^{-\sigma^2}\sin^2\mu \\
\sigma_y^2 &= \frac{1}{2} - \frac{1}{2}\cos 2\mu E\big[\cos 2x\big] - e^{-\sigma^2}\sin^2\mu \\
\sigma_y^2 &= \frac{1}{2} - \frac{1}{2}\cos(2\mu)e^{-2\sigma^2} - e^{-\sigma^2}\left[\frac{1-\cos(2\mu)}{2}\right] \\
\sigma_y^2 &= \frac{1}{2}\left(1-e^{-\sigma^2}\right)\left[1+e^{-\sigma^2}\cos(2\mu)\right]
\end{aligned} \tag{191}$$

For the nonlinear function $y = \cos(z)$, similar procedures can be used as for the sine function, and the expected value and variance after the transformation has been found as:

$$E\big[\cos z\big] = (\cos\mu)e^{\frac{-\sigma^2}{2}} \tag{192}$$

$$\sigma_y^2 = \frac{1}{2}\left(1-e^{-\sigma^2}\right)\left[1-e^{-\sigma^2}\cos(2\mu)\right] \tag{193}$$

The results of this analysis are summarized in Table 11.

Table 11. Statistics for Transformations of a Non-Zero Mean Gaussian Variable

| $g(z)$ | $E\big[g(z)\big]$ | $\sigma^2\big(g(z)\big)$ |
|---|---|---|
| $z^k$ | $\displaystyle\sum_{i=0}^{k/2}\frac{k!}{(k-2i)!(2i)!!}\mu^{k-2i}\sigma^{2i}$ | $\displaystyle\sum_{i=0}^{k}\frac{(2k)!}{(2k-2i)!(2i)!!}\mu^{2k-2i}\sigma^{2i} - \left(\sum_{j=0}^{k/2}\frac{k!}{(k-2j)!(2j)!!}\mu^{k-2j}\sigma^{2j}\right)^2$ |
| $\sin z$ | $(\sin\mu)e^{\frac{-\sigma^2}{2}}$ | $\frac{1}{2}\left(1-e^{-\sigma^2}\right)\left[1+e^{-\sigma^2}\cos(2\mu)\right]$ |
| $\cos z$ | $(\cos\mu)e^{\frac{-\sigma^2}{2}}$ | $\frac{1}{2}\left(1-e^{-\sigma^2}\right)\left[1-e^{-\sigma^2}\cos(2\mu)\right]$ |

### 5.5.3 Comparison of Linearization Techniques in Nonlinear Filters

Consider a nonlinear transformation of the form $y = g(z)$, where $z \sim N\left(\mu, \sigma^2\right)$. The Analytical Linearization (AL) method as implemented in the EKF estimates the mean and variance after the transformation as:

$$E\left[g(z)\right] \approx g\left(E\left[z\right]\right) \tag{194}$$

$$\sigma_y^2 \approx \sigma^2 \left(\frac{\partial y}{\partial z}\right)^2 \Bigg|_{z=E[z]} \tag{195}$$

These values were calculated using (194) and (195) for each of the three considered nonlinear transformations and the results are summarized in Table 12.

Table 12. Mean and Variance Estimates from Analytical Linearization

| $y = g(z)$ | $E\left[y\right]$ | $\sigma_y^2$ |
|---|---|---|
| $z^k$<br>$k = 1, 2, 3, \ldots$ | $\mu^k$ | $\sigma^2 k^2 \mu^{2k-2}$ |
| $\sin z$ | $\sin \mu$ | $\sigma^2 \cos^2 \mu$ |
| $\cos z$ | $\cos \mu$ | $\sigma^2 \sin^2 \mu$ |

The Unscented Transformation (UT) is a statistical linearization technique used by the UKF. For the considered scalar case, the UT consists of the calculation of three sigma points:

$$\chi = \left[g(\mu) \quad g(\mu + \alpha\sigma) \quad g(\mu - \alpha\sigma)\right] \tag{196}$$

where $\alpha$ is the primary sigma point scaling parameter, which is suggested to vary between 0.001 and 1 [11]. Weighted averages are taken to recover the mean and variance of these sigma points, as in:

$$E\left[g(z)\right] \approx \tilde{y} = \frac{\alpha^2 - 1}{\alpha^2} g(\mu) + \frac{1}{2\alpha^2}\left[g(\mu + \alpha\sigma) + g(\mu - \alpha\sigma)\right] \tag{197}$$

$$\sigma_y^2 \approx \left(\frac{\alpha^2 - 1}{\alpha^2} + 1 - \alpha^2 + \beta\right)\left[g(\mu) - \tilde{y}\right]^2 + \frac{1}{2\alpha^2}\left\{\left[g(\mu + \alpha\sigma) - \tilde{y}\right]^2 + \left[g(\mu - \alpha\sigma) - \tilde{y}\right]^2\right\} \tag{198}$$

where $\tilde{y}$ is the mean estimate from (197) and $\beta$ is the secondary sigma point scaling parameter. For Gaussian distributions, $\beta = 2$ is optimal [11]; therefore $\beta = 2$ was used for this study. Unlike the AL, the UT does not yield simple explicit form solutions for the transformed mean and variance of the considered nonlinear functions; therefore these explicit solutions are not presented.

Since the linearization process is a function of the prior mean and variance, plots were generated to illustrate the differences between the analytical and statistical linearization techniques. Additionally, the Monte Carlo method was included to verify the theoretically derived results, *i.e.*, $10^5$ points were generated from the prior distribution, propagated through the nonlinear function, and then the mean and variance statistics were calculated. The differences between the Monte Carlo and theoretical estimates for the mean and variance are negligible for all of the considered cases, thus demonstrating the validity of the theoretically derived equations. For the unscented transformation, four different cases of $\alpha$ were considered: 0.25, 0.5, 0.75, and 1.0. These values were selected to represent a few cases in the range of possible values for $\alpha$. Each presented figure shows the error in the transformed mean or variance estimate from the linearization process as compared to the theoretically derived truth from Table 11. These errors are plotted with respect to the prior standard deviation, $\sigma$.

First, two cases of the nonlinear function $y = z^k$ are considered: $k = 2$ and $k = 3$. For both cases, $E[z] = 0.1$. Alternatively, due to the relationship between $z$ and $x$, this

function can be considered as $y = (x+0.1)^k$. For $k = 2$, the mean and variance estimates for each case of $\alpha$ were the same, and therefore only one line is plotted for the UT, as shown in Figure 48.

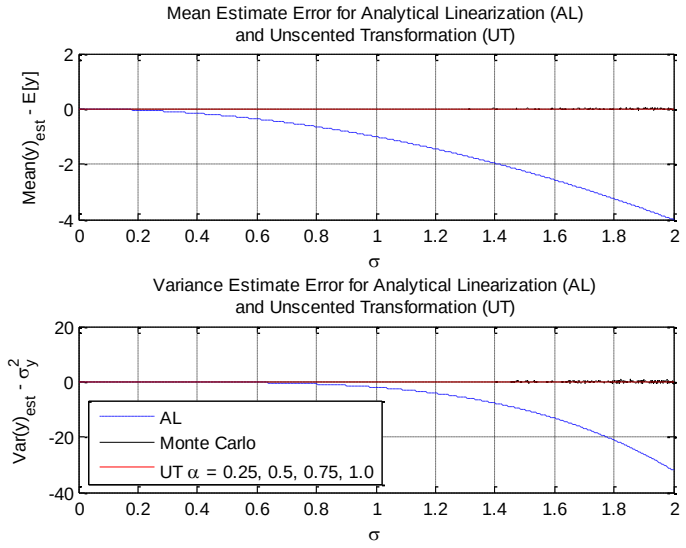


Figure 48. Mean and Variance Estimate Errors for $y = (x + 0.1)^2$

It is shown in Figure 48 that the AL error increases as the prior variance increases, while the UT provides perfect estimation of both the mean and variance. As expected, the Monte Carlo method provides near perfect estimation of the statistics. For $k = 3$, the mean estimate again is not a function of $\alpha$; however, the variance estimate is function of $\alpha$. The results for this case are shown in Figure 49.

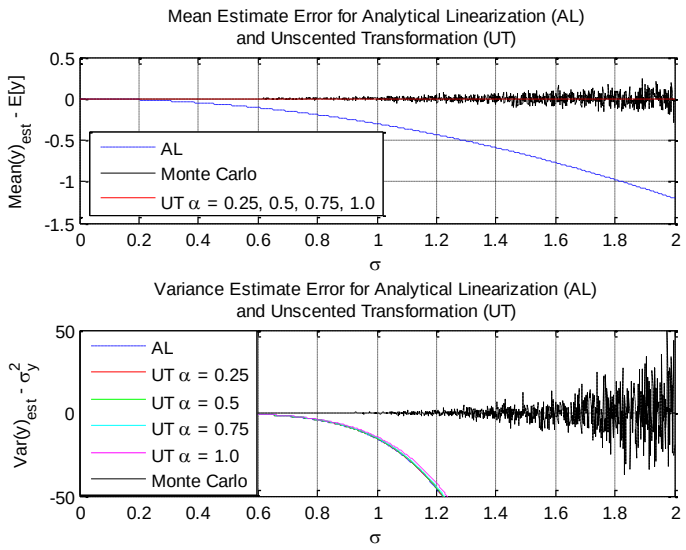


Figure 49. Mean and Variance Estimate Errors for $y = (x + 0.1)^3$

For the case shown in Figure 49, the AL again shows an increasing error trend with prior variance. The UT provides perfect mean estimation, but the variance estimate is now only slightly more accurate than the AL, with $\alpha = 1.0$ giving the greatest accuracy. For this case, errors in the Monte Carlo method become more apparent as the prior variance increases. This indicates that a larger number of points would be required to accurately estimate the statistics. This particular case demonstrates the usefulness of the theoretically derived statistics in Table 11, as the Monte Carlo method can become inaccurate even for a reasonably large number of points. Therefore, using Monte Carlo as a truth reference may be invalid under certain conditions. The derived statistics in Table 11 are clearly advantageous for this case in terms of computation and accuracy.

The next considered case is $y = \sin(x)$. The mean estimate for this case is identically zero for both techniques, therefore it is not shown. The variance estimate,

however, shown in Figure 50, shows that the UT contains greater accuracy than the AL for all cases of $\alpha$, with $\alpha = 1.0$ giving the best variance estimate.

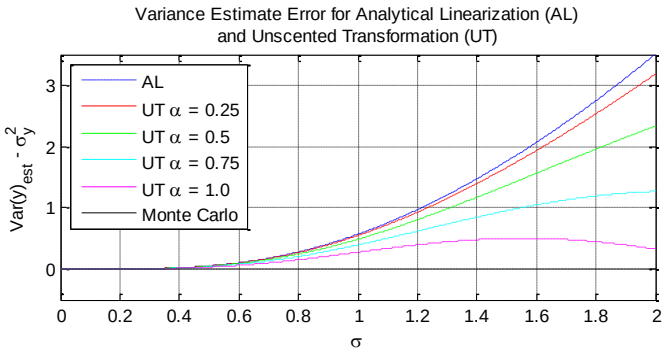


Figure 50. Variance Estimate Error for y = sin(x)

Next, two non-zero mean cases are considered for the sine function. The mean and variance estimates for $y = \sin(z)$ with $E[z] = \pi/4$ are shown in Figure 51, and similarly for $y = \sin(z)$ with $E[z] = \pi/2$ in Figure 52.

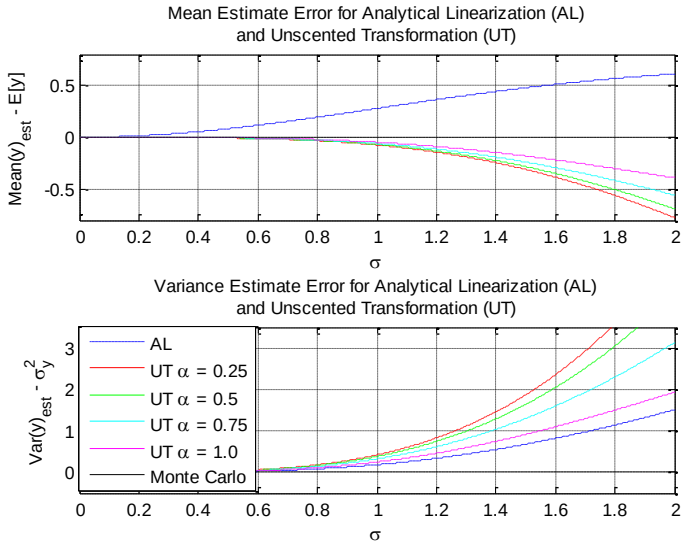


Figure 51. Mean and Variance Estimate Errors for $y = \sin(x+\pi/4)$

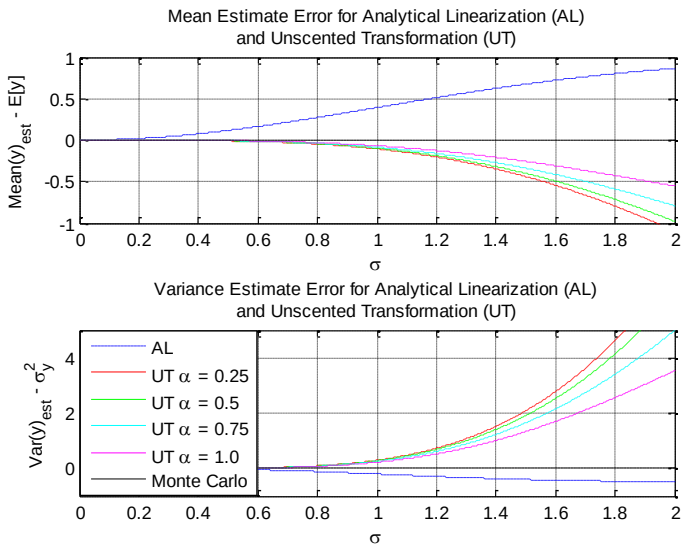


Figure 52. Mean and Variance Estimate Errors for $y = \sin(x+\pi/2)$

For the cases shown in Figure 51 and Figure 52, the UT provides more accurate mean estimation; however, the AL provides a more accurate variance estimate. Comparable cases for the cosine function were generated, and yielded equivalent results as for the sine function as expected, following the co-function identities, *i.e.*, $\cos(x) = \sin(\pi/2 - x)$. For each of the cases for the sine and cosine functions, it is interesting to note that the value of $\alpha = 1.0$ gave the most accurate mean and variance estimates for the UT. Also, the Monte Carlo method provides near perfect estimation of the statistics, as expected.

Figure 51 and Figure 52 show specific cases of the prior mean in order to give snapshots of the performance. To more fully capture the effects of different means, the AL and UT were evaluated for the sine function over a set of values for the standard deviation ranging from 0 to 2 and for the mean ranging from 0 to $\pi/2$. Only the case of $\alpha = 1.0$ was considered here for the UT. The absolute value of the mean estimate error and variance estimate error are displayed for AL in Figure 53 and UT in Figure 54 as

contours. In these figures, the darker areas indicate higher linearization errors with respect to the analytical truth.

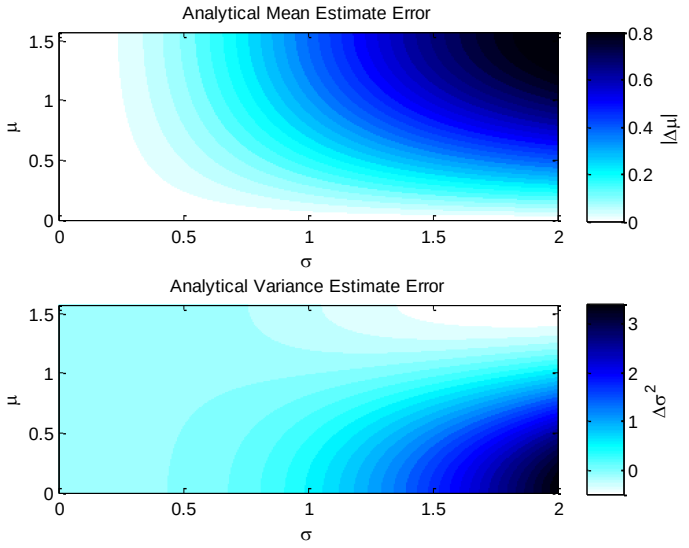


Figure 53. Analytical Linearization Error for $y = \sin(z)$

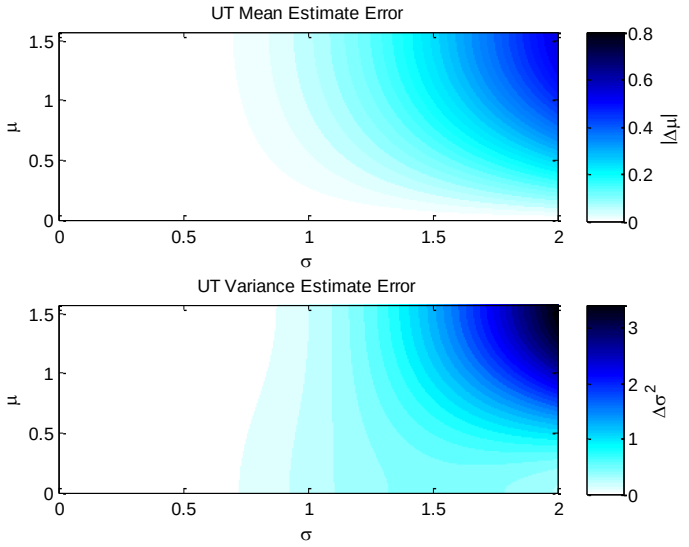


Figure 54. Unscented Transformation Error for $y = \sin(z)$

There are two important observations to recognize in Figure 53 and Figure 54. First, for all cases of prior mean and standard deviation, the UT yields more accurate estimation of the mean. Second, the variance estimate errors of the AL are sometimes better than the UT, and vice versa. This is demonstrated by the different shapes of the contour graphs, with AL having higher errors for smaller means and the UT having higher errors for larger means. Because of this observation, neither the AL nor UT can claim better estimation of the variance for all cases.

### 5.5.4 Nonlinear Filtering Example

In order to demonstrate the usefulness of the derived analytical relationships, an example of a nonlinear filtering problem is considered. Consider the following discrete-time nonlinear system:

$$\begin{aligned} x_k &= \sin x_{k-1} \\ y_k &= x_k + v_k \\ v_k &\sim N(0, R) \end{aligned} \tag{199}$$

where $k$ is the discrete time index, $x$ is the state, $y$ is the output, and $v$ is the measurement noise with known variance, $R$. This problem is approached with EKF, UKF, a theoretical filter which uses the relationships summarized in Table 11, a Monte Carlo based filter, and a particle filter. For this implementation of the UKF, the scaling parameters were set to $\alpha = 1.0$ and $\beta = 2$. The Monte Carlo filter generated $10^6$ points at each time step from the prior distribution to recover the statistics after the nonlinear transformation. Note that this Monte Carlo filter is not a particle filter, but is instead a Kalman filter that uses the Monte Carlo method to determine the *a priori* statistics at each time step. This Monte

Carlo filter is a statistical means of approximating the theoretical filter. A linear Kalman filter measurement update is used for the EKF, UKF, theoretical, and Monte Carlo filters, since the output equation is linear. To provide additional comparison, a simple Sampling Importance Resampling (SIR) particle filter [163] was implemented using $10^6$ particles.

First, the true state trajectory is determined for an initial state, $x_0 = \pi/4$. This trajectory is used to simulate the measurement, with added measurement noise with variance, $R = 0.25$. This measurement is shown with the true state trajectory in Figure 55.

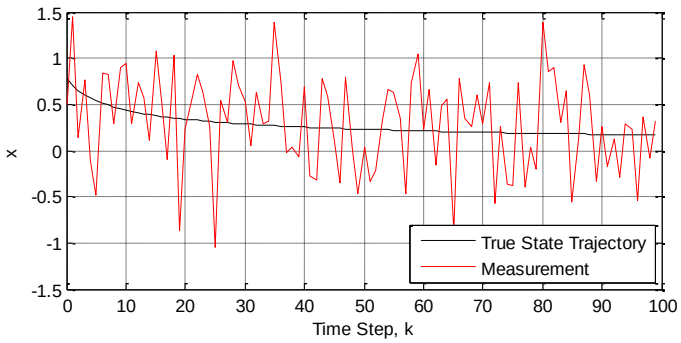


Figure 55. Nonlinear Filtering Example: State and Measurement

Using this measurement, each filter algorithm is executed for 100 discrete time steps, each using assumed initial conditions:

$$\begin{aligned} \tilde{x}_0 &= x_0 + \pi/3 = 7\pi/12 \\ \tilde{P}_0 &= (\pi/3)^2 \end{aligned} \tag{200}$$

where $P$ is the variance of the state. These initial conditions were selected to capture the effects of a reasonably large initialization error. Note that the initial error was selected as

one standard deviation from the assumed initial variance. The state estimation error results of this simulation are shown in Figure 56.

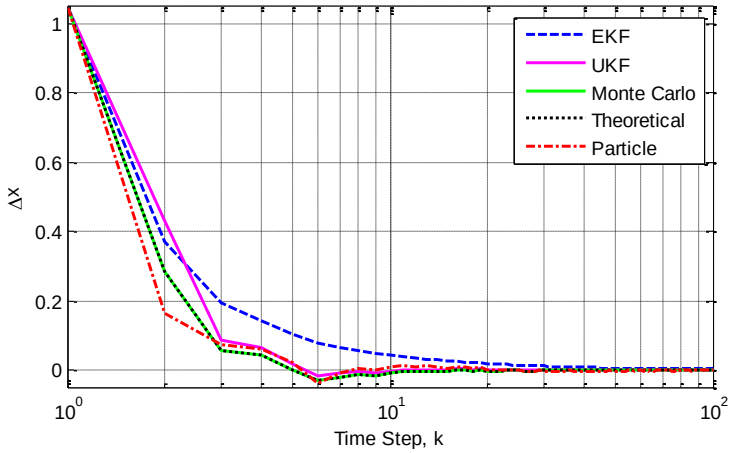


Figure 56. Nonlinear Filtering Example: Estimation Error

Negligible differences are shown in Figure 56 between the Monte Carlo and theoretical filters. To quantify the performance of each filter, the root mean square error (RMSE) was calculated, and is shown in Table 13.

Table 13. Nonlinear Filtering Example: Root Mean Square Error

| **Nonlinear Filter** | **RMSE** |
|---|---|
| EKF | 0.048597 |
| UKF | 0.044619 |
| Monte Carlo | 0.029997 |
| Theoretical | 0.029989 |
| Particle (SIR) | 0.019786 |

From these results, slight performance advantage is demonstrated for the UKF over the EKF, and a more significant performance advantage is shown for the Monte Carlo and theoretical filters over both EKF and UKF. This improvement comes purely from the

removal of the linearization errors that are incurred by EKF and UKF. The particle filter was able to achieve the highest accuracy, due to the removal of the Gaussian noise assumption that is required by the other methods. This indicates that even with perfect linearization, Kalman-based filtering techniques may not be as effective as particle filtering.

### 5.5.5 Analytical Comparison of Linearization Methods Conclusions

This section presented the results of a comparison of analytical linearization and unscented transformation techniques to recover the mean and variance after three different nonlinear transformations. The true statistics were theoretically derived for each of the considered functions in order to compare the errors of the different methods. These theoretical results were verified with respect to Monte Carlo simulations. For all of the considered cases, the unscented transformation yielded equal or greater accuracy in the estimation of the mean. However, mixed conclusions were reached about the accuracy of the variance. For some cases the analytical linearization obtained greater accuracy than the unscented transformation, while for other cases the opposite was noticed. Another interesting observation is that for each function, increasing $\alpha$ in the unscented transformation gave equal or better accuracy. Additionally, a nonlinear filtering example was given to demonstrate the effectiveness of the theoretical estimates in practice, either as a validation tool or for implementation. This example showed that there is room for improvement for both EKF and UKF in terms of linearization errors for

certain applications, and that a particle filter is still able to outperform a Kalman-based filter even with no linearization error.

# 6.0 NONLINEAR KALMAN FILTER STABILITY ANALYSIS

In this chapter, stability is investigated of the considered nonlinear state estimation problem presented in Chapter 3 using experimental data collected with the research platform described in Chapter 4. First, the necessary mathematical and statistical properties are defined. Then, a stochastic stability proof of the linear discrete-time Kalman filter is provided. Next, a preliminary stability analysis is conducted using the existing prior work of other authors [40] directly to derive the required bounds on the system. Then, a method of relaxing these preliminary bounds is presented in detail with results from the considered application of attitude estimation using empirical flight data [162]. Additionally, some analysis is presented for the use of a multiplicative linearization error model. Finally, discussion of the stability analysis is provided.

## 6.1 MATHEMATICAL DEFINITIONS

In order to analyze the stability of the EKF, various mathematical definitions need to be utilized. This section outlines the important mathematical tools that are necessary in the following sections. First, due to the extensive use of matrices for multivariate systems, some linear algebra characteristics are necessary.

An important linear algebra definition is the trace of a matrix, which is defined as the sum of its diagonal elements. This is also equal to the sum of the eigenvalues of the

matrix. The trace operator is denoted by $Tr(.)$. An important and useful property of the trace operator is that the order of matrix multiplication can be changed, as in [53]

$$Tr(\mathbf{AB}) = Tr(\mathbf{BA}) \tag{201}$$

This property is easily derived using the fact that the trace of a matrix is equal to the trace of its transpose [166].

Another important linear algebra property is the matrix inversion lemma [167], which is given by the following formula

$$\left(\mathbf{A}+\mathbf{UCV}\right)^{-1} = \mathbf{A}^{-1} - \mathbf{A}^{-1}\mathbf{U}\left(\mathbf{C}^{-1}+\mathbf{VA}^{-1}\mathbf{U}\right)^{-1}\mathbf{VA}^{-1} \tag{202}$$

where **A**, **U**, **C**, and **V** are matrices with dimensions ($n \times n$), ($n \times m$), ($m \times m$), and ($m \times n$) respectively. If **U** and **V** are taken to be ($n \times n$) identity matrices, the formula simplifies to:

$$\left(\mathbf{A}+\mathbf{C}\right)^{-1} = \mathbf{A}^{-1} - \mathbf{A}^{-1}\left(\mathbf{C}^{-1}+\mathbf{A}^{-1}\right)^{-1}\mathbf{A}^{-1} \tag{203}$$

This simplified form is useful for simplifying various equations in the process of deriving stability.

For stability of the EKF for a stochastic estimation problem, the boundedness of the stochastic process is important. The properties of stochastic boundedness are discussed in the following lemma [64,65].

*Stochastic Stability Lemma*: Assume there is a stochastic process $V_k(\zeta_k)$ such that the following properties are satisfied

$$\begin{aligned} &\nu_1, \nu_2, \mu > 0, \quad 0 < \alpha \le 1 \\ &\nu_1 \left\|\zeta_k\right\|_2^2 \le V_k\left(\zeta_k\right) \le \nu_2 \left\|\zeta_k\right\|_2^2 \\ &E\left[V_{k+1}\left(\zeta_{k+1}\right) \mid \zeta_k\right] - V_k\left(\zeta_k\right) \le \mu - \alpha V_k\left(\zeta_k\right) \end{aligned} \tag{204}$$

then the stochastic process is exponentially bounded in mean square with probability one

$$E\left[\left\|\zeta_k\right\|_2^2\right] \le \frac{\nu_2}{\nu_1} E\left[\left\|\zeta_0\right\|_2^2\right](1-\alpha)^k + \frac{\mu}{\nu_1}\sum_{i=0}^{k-1}(1-\alpha)^i \tag{205}$$

It can be seen from this lemma that the value $\alpha$ is related to the convergence of the estimation error, with greater $\alpha$ corresponding to faster convergence. The summation term of this inequality can be simplified using the property that

$$\sum_{i=0}^{k-1}(1-\alpha)^i \le \sum_{i=0}^{\infty}(1-\alpha)^i = \frac{1}{\alpha} \tag{206}$$

therefore the stochastic process bound can more conservatively be written as

$$E\left[\left\|\zeta_k\right\|_2^2\right] \le \frac{\nu_2}{\nu_1} E\left[\left\|\zeta_0\right\|_2^2\right](1-\alpha)^k + \frac{\mu}{\nu_1\alpha} \tag{207}$$

*Proof*: The proof for the stochastic stability lemma is presented in [65]. Next, modifications are presented to the stochastic stability lemma which use time-varying parameters.

*Modified Stochastic Stability Lemma*: Assume that there is a stochastic process $V(\zeta_k)$ and parameters $b_k, \nu_0, \mu_k > 0$ and $0 < \alpha_k \le 1$ such that the following inequalities are satisfied for all $k$

$$V(\zeta_0) \le \nu_0 \left\|\zeta_0\right\|^2 \tag{208}$$

$$b_k \left\|\zeta_k\right\|^2 \le V(\zeta_k) \tag{209}$$

$$E\left[V(\zeta_k) \mid \zeta_{k-1}\right] - V(\zeta_{k-1}) \le \mu_{k-1} - \alpha_{k-1} V(\zeta_{k-1}) \tag{210}$$

then the random variable $\zeta_k$ is bounded in mean square with probability one by the following inequality

$$E\left[\left\|\zeta_k\right\|^2\right] \le \frac{\nu_0}{b_k} E\left[\left\|\zeta_0\right\|^2\right] \prod_{i=0}^{k-1}\left(1-\alpha_i\right) + \frac{1}{b_k}\sum_{i=0}^{k-1}\left|\mu_{k-i-1}\prod_{j=1}^{i}\left(1-\alpha_{k-j}\right)\right| \tag{211}$$

*Proof:* First, it is important to note the difference between the stochastic stability lemma and the modified stochastic stability lemma. In the modified stochastic stability lemma, the terms $\mu$ and $\alpha$ are time varying quantities, whereas for the stochastic stability lemma, these terms were both considered as constants with respect to the discrete time, $k$. An important property of expectations from statistics is central to this proof [164]

$$E\left[E\left[X \mid Y\right]\right] = E\left[X\right] \tag{212}$$

which can be extended for conditional expectations, as in

$$E\left[E\left[X \mid Y\right] \mid Z\right] = E\left[X \mid Z\right] \tag{213}$$

Rearranging (210) gives

$$E\left[V_{k+1}\left(\zeta_{k+1}\right) \mid \zeta_k\right] \le \mu_k + \left(1-\alpha_k\right)V_k\left(\zeta_k\right) \tag{214}$$

Taking the conditional expectation of this inequality with respect to $\zeta_{k-1}$

$$E\left[E\left[V_{k+1}\left(\zeta_{k+1}\right) \mid \zeta_k\right] \mid \zeta_{k-1}\right] \le E\left[\mu_k + \left(1-\alpha_k\right)V_k\left(\zeta_k\right) \mid \zeta_{k-1}\right] \tag{215}$$

which using (213) simplifies to

$$E\left[V\left(\zeta_{k+1}\right) \mid \zeta_{k-1}\right] \le \mu_k + \left(1-\alpha_k\right)E\left[V\left(\zeta_k\right) \mid \zeta_{k-1}\right] \tag{216}$$

This recursive inequality can be applied repeatedly for $k$-2, $k$-3, …, 0, thus giving

$$\begin{aligned} E\left[V\left(\zeta_{k+1}\right) \mid \zeta_0\right] \le \mu_k + \left(1-\alpha_k\right)\mu_{k-1} + \ldots + \left(1-\alpha_k\right)\left(1-\alpha_{k-1}\right)\ldots\left(1-\alpha_1\right)\mu_0 \\ + \left(1-\alpha_k\right)\left(1-\alpha_{k-1}\right)\ldots\left(1-\alpha_0\right)V\left(\zeta_0\right) \end{aligned} \tag{217}$$

This inequality is rewritten for the discrete time step $k$ as

$$E\left[V\left(\zeta_k\right)|\zeta_0\right] \le \mu_{k-1} + \left(1-\alpha_{k-1}\right)\mu_{k-2} + \ldots + \left(1-\alpha_{k-1}\right)\left(1-\alpha_{k-2}\right)\ldots\left(1-\alpha_1\right)\mu_0 + \left(1-\alpha_{k-1}\right)\left(1-\alpha_{k-2}\right)\ldots\left(1-\alpha_0\right)V\left(\zeta_0\right) \tag{218}$$

which can be written more formally as

$$E\left[V\left(\zeta_k\right)|\zeta_0\right] \le V\left(\zeta_0\right)\prod_{i=0}^{k-1}\left(1-\alpha_i\right) + \sum_{i=0}^{k-1}\left[\mu_{k-i-1}\prod_{j=1}^{i}\left(1-\alpha_{k-j}\right)\right] \tag{219}$$

Taking the expectation and applying (212) gives

$$E\left[V\left(\zeta_k\right)\right] \le E\left[V\left(\zeta_0\right)\right]\prod_{i=0}^{k-1}\left(1-\alpha_i\right) + \sum_{i=0}^{k-1}\left[\mu_{k-i-1}\prod_{j=1}^{i}\left(1-\alpha_{k-j}\right)\right] \tag{220}$$

Using (209) and taking the expectation yields the following useful inequalities

$$\begin{aligned} \nu_1 E\left[\left\|\zeta_k\right\|_2^2\right] &\le E\left[V\left(\zeta_k\right)\right] \\ E\left[V\left(\zeta_0\right)\right] &\le \nu_2 E\left[\left\|\zeta_0\right\|_2^2\right] \end{aligned} \tag{221}$$

Substituting these inequalities into (220) gives the final result of (211), thus completing the proof.

*Remarks*: The modified stochastic stability lemma presents a general case where both the constant term, $\mu$, and the convergence rate, $\alpha$, can be time varying. It is also interesting to note the following two cases, where just one of those two values is time varying

$$E\left[\left\|\zeta_k\right\|_2^2\right] \le \frac{\nu_2}{\nu_1}E\left[\left\|\zeta_0\right\|_2^2\right]\prod_{i=0}^{k-1}\left(1-\alpha_i\right) + \frac{\mu}{\nu_1}\sum_{i=0}^{k-1}\left[\prod_{j=1}^{i}\left(1-\alpha_{k-j}\right)\right] \tag{222}$$

$$E\left[\left\|\zeta_k\right\|_2^2\right] \le \frac{\nu_2}{\nu_1}E\left[\left\|\zeta_0\right\|_2^2\right]\left(1-\alpha\right)^k + \frac{1}{\nu_1}\sum_{i=0}^{k-1}\left[\left(1-\alpha\right)^i\mu_{k-i-1}\right] \tag{223}$$

Note that if both quantities are considered constant, the modified stochastic stability lemma reduces to the stochastic stability lemma. Another difference is that the bounds

for the stochastic process are treated differently. The upper bound of the process is considered only for the initial time step, while the lower bound is considered as a time-varying quantity. The usefulness of the modified stochastic stability lemma is not for stability analysis, but for the on-line monitoring of convergence and estimation error bounds. The consideration of time-varying parameters is the key to the on-line convergence and error analysis of the Kalman filter presented in Section 6.3.

## 6.2 LINEAR KALMAN FILTER STABILITY ANALYSIS

Before considering the stability of the Extended Kalman Filter (EKF), some stability analysis is done for the linear discrete-time Kalman filter. This stability analysis follows a similar analysis as for the EKF, except that there are no linearization errors in the system, therefore the nonlinear part of the problem does not need to be considered. Here, however, the stochastic effects are considered, and therefore the stochastic stability lemma (204) is utilized. First, the error dynamics are derived, followed by a stability analysis of the deterministic system, then the stochastic error is considered.

### 6.2.1 Derivation of Linear Kalman Filter Error Dynamics

The necessary equations for this derivation are recalled from Section 2.4 of this dissertation. Again, the system is assumed to be of the form (45) with noise assumptions given by (46). For this system, the linear Kalman filter can be implemented by using (49) to predict the state and covariance (*a priori*), calculating the Kalman gain matrix with

(50), then updating the predicted state and covariance (*a posteriori*) with (51). This two-step method can be reduced to a one-step method by combining (45), (49), and (51) in order to obtain the dynamics of both the *a priori* and *a posteriori* state and covariance. First, the *a priori* error dynamics are defined, followed by the *a posteriori* error dynamics.

To obtain the *a priori* state dynamics, first insert (51) into (49)

$$\hat{\mathbf{x}}_{k+1|k} = \mathbf{A}_k \left[ \left( \mathbf{I} - \mathbf{K}_k \mathbf{H}_k \right) \hat{\mathbf{x}}_{k|k-1} + \mathbf{K}_k \mathbf{y}_k \right] + \mathbf{B}_k \mathbf{u}_k \tag{224}$$

Substituting the definition of $\mathbf{y}_k$ from (45) gives

$$\hat{\mathbf{x}}_{k+1|k} = \mathbf{A}_k \left[ \left( \mathbf{I} - \mathbf{K}_k \mathbf{H}_k \right) \hat{\mathbf{x}}_{k|k-1} + \mathbf{K}_k \mathbf{H}_k \mathbf{x}_k + \mathbf{K}_k \mathbf{v}_k \right] + \mathbf{B}_k \mathbf{u}_k \tag{225}$$

Defining the *a priori* state error as $\boldsymbol{\xi}_k = \mathbf{x}_k - \hat{\mathbf{x}}_{k|k-1}$, its dynamics can now be defined using

$$\begin{aligned} \boldsymbol{\xi}_{k+1} &= \mathbf{x}_{k+1} - \hat{\mathbf{x}}_{k+1|k} \\ \boldsymbol{\xi}_{k+1} &= \mathbf{A}_k \mathbf{x}_k + \mathbf{B}_k \mathbf{u}_k + \mathbf{w}_k - \mathbf{A}_k \left[ \left( \mathbf{I} - \mathbf{K}_k \mathbf{H}_k \right) \hat{\mathbf{x}}_{k|k-1} + \mathbf{K}_k \mathbf{H}_k \mathbf{x}_k + \mathbf{K}_k \mathbf{v}_k \right] - \mathbf{B}_k \mathbf{u}_k \\ \boldsymbol{\xi}_{k+1} &= \mathbf{A}_k \left( \mathbf{I} - \mathbf{K}_k \mathbf{H}_k \right) \boldsymbol{\xi}_k + \mathbf{w}_k - \mathbf{A}_k \mathbf{K}_k \mathbf{v}_k \end{aligned} \tag{226}$$

To define the *a priori* covariance as a one-step equation, the covariance expressions from (49) and (51) are combined as in

$$\mathbf{P}_{k+1|k} = \mathbf{A}_k \left[ \left( \mathbf{I} - \mathbf{K}_k \mathbf{H}_k \right) \mathbf{P}_{k|k-1} \right] \mathbf{A}_k^T + \mathbf{Q}_k \tag{227}$$

Using the definition of the Kalman gain matrix from (50), this expression can be rewritten as

$$\mathbf{P}_{k+1|k} = \mathbf{A}_k \mathbf{P}_{k|k-1} \mathbf{A}_k^T - \mathbf{A}_k \mathbf{P}_{k|k-1} \mathbf{H}_k^T \left( \mathbf{H}_k \mathbf{P}_{k|k-1} \mathbf{H}_k^T + \mathbf{R}_k \right)^{-1} \mathbf{H}_k \mathbf{P}_{k|k-1} \mathbf{A}_k^T + \mathbf{Q}_k \tag{228}$$

which is a discrete Riccati equation [62]. Using the matrix inversion lemma (202), the a priori covariance dynamics can be rewritten more compactly as

$$\mathbf{P}_{k+1|k} = \mathbf{A}_k \left( \mathbf{P}_{k|k-1}^{-1} + \mathbf{H}_k^T \mathbf{R}_k^{-1} \mathbf{H}_k \right)^{-1} \mathbf{A}_k^T + \mathbf{Q}_k \tag{229}$$

Thus, the error dynamics and covariance have been derived for the *a priori* state vector.

Next, the same procedure is used to derive the error dynamics and covariance of the *a posteriori* state vector. The *a posteriori* state error is defined by $\tilde{\mathbf{x}}_k = \mathbf{x}_k - \hat{\mathbf{x}}_k$. Reorganizing (51) gives

$$\hat{\mathbf{x}}_k = \left( \mathbf{I} - \mathbf{K}_k \mathbf{H}_k \right) \hat{\mathbf{x}}_{k|k-1} + \mathbf{K}_k \mathbf{y}_k \tag{230}$$

Substituting in the definition of $\mathbf{y}_k$ from (45) gives

$$\hat{\mathbf{x}}_k = \left( \mathbf{I} - \mathbf{K}_k \mathbf{H}_k \right) \hat{\mathbf{x}}_{k|k-1} + \mathbf{K}_k \mathbf{H}_k \mathbf{x}_k + \mathbf{K}_k \mathbf{v}_k \tag{231}$$

Now, the *a posteriori* state error can be defined

$$\begin{aligned} \tilde{\mathbf{x}}_k &= \mathbf{x}_k - \hat{\mathbf{x}}_k = \mathbf{x}_k - \left( \mathbf{I} - \mathbf{K}_k \mathbf{H}_k \right) \hat{\mathbf{x}}_{k|k-1} - \mathbf{K}_k \mathbf{H}_k \mathbf{x}_k - \mathbf{K}_k \mathbf{v}_k \\ \tilde{\mathbf{x}}_k &= \left( \mathbf{I} - \mathbf{K}_k \mathbf{H}_k \right) \left( \mathbf{x}_k - \hat{\mathbf{x}}_{k|k-1} \right) - \mathbf{K}_k \mathbf{v}_k \end{aligned} \tag{232}$$

Inserting the state definition from (45) and predicted state estimate from (49) yields

$$\begin{aligned} \tilde{\mathbf{x}}_k &= \left( \mathbf{I} - \mathbf{K}_k \mathbf{H}_k \right) \left[ \left( \mathbf{A}_{k-1} \mathbf{x}_{k-1} + \mathbf{B}_{k-1} \mathbf{u}_{k-1} + \mathbf{w}_{k-1} \right) - \left( \mathbf{A}_{k-1} \hat{\mathbf{x}}_{k-1} + \mathbf{B}_{k-1} \mathbf{u}_{k-1} \right) \right] - \mathbf{K}_k \mathbf{v}_k \\ \tilde{\mathbf{x}}_k &= \left( \mathbf{I} - \mathbf{K}_k \mathbf{H}_k \right) \left( \mathbf{A}_{k-1} \tilde{\mathbf{x}}_{k-1} + \mathbf{w}_{k-1} \right) - \mathbf{K}_k \mathbf{v}_k \end{aligned} \tag{233}$$

For the *a posteriori* covariance, substitute the definition of the *a priori* covariance from (49) into (51), giving

$$\mathbf{P}_k = \left( \mathbf{I} - \mathbf{K}_k \mathbf{H}_k \right) \left( \mathbf{A}_{k-1} \mathbf{P}_{k-1} \mathbf{A}_{k-1}^T + \mathbf{Q}_{k-1} \right) \tag{234}$$

Thus, the *a posteriori* state estimate error dynamics and covariance have each been defined using a single recursive relationship. These equations are important tools that are used to derive different stability characteristics of the system as shown in the following sections.

### 6.2.2 Deterministic Linear Kalman Filter Stability Analysis

As a starting point for the stability analysis, the error dynamics defined by (233) are considered for the deterministic or homogeneous problem, *i.e.*, the stochastic terms are zero, as in

$$\tilde{\mathbf{x}}_k = \left(\mathbf{I} - \mathbf{K}_k \mathbf{H}_k\right) \mathbf{A}_{k-1} \tilde{\mathbf{x}}_{k-1} \tag{235}$$

Consider a candidate Lyapunov function of the form

$$V_k\left(\tilde{\mathbf{x}}_k\right) = \tilde{\mathbf{x}}_k^T \mathbf{P}_k^{-1} \tilde{\mathbf{x}}_k \tag{236}$$

This function is in quadratic form, and is therefore strictly positive since the covariance matrix and also its inverse is positive definite. Substituting in the definition for the error dynamics gives

$$V_k\left(\tilde{\mathbf{x}}_k\right) = \tilde{\mathbf{x}}_{k-1}^T \mathbf{A}_{k-1}^T \left(\mathbf{I} - \mathbf{K}_k \mathbf{H}_k\right)^T \mathbf{P}_k^{-1} \left(\mathbf{I} - \mathbf{K}_k \mathbf{H}_k\right) \mathbf{A}_{k-1} \tilde{\mathbf{x}}_{k-1} \tag{237}$$

Using (49) and (51), the covariance matrix can be rewritten in the following form

$$\mathbf{P}_k = \left(\mathbf{I} - \mathbf{K}_k \mathbf{H}_k\right)\left(\mathbf{A}_{k-1} \mathbf{P}_{k-1} \mathbf{A}_{k-1}^T + \mathbf{Q}_{k-1}\right)\left(\mathbf{I} - \mathbf{K}_k \mathbf{H}_k\right)^T + \mathbf{K}_k \mathbf{H}_k \left(\mathbf{A}_{k-1} \mathbf{P}_{k-1} \mathbf{A}_{k-1}^T + \mathbf{Q}_{k-1}\right)\left(\mathbf{I} - \mathbf{K}_k \mathbf{H}_k\right)^T \tag{238}$$

It can be shown that each of these two terms is positive definite, therefore the following inequality can be written

$$\mathbf{P}_k > \left(\mathbf{I} - \mathbf{K}_k \mathbf{H}_k\right)\left(\mathbf{A}_{k-1} \mathbf{P}_{k-1} \mathbf{A}_{k-1}^T + \mathbf{Q}_{k-1}\right)\left(\mathbf{I} - \mathbf{K}_k \mathbf{H}_k\right)^T \tag{239}$$

Since the covariance matrix is a positive definite matrix by definition, it is invertible. It can also be shown that the matrix $\mathbf{I} - \mathbf{K}_k \mathbf{H}_k$ is invertible, and therefore the following inequality can be written

$$\left(\mathbf{I}-\mathbf{K}_k\mathbf{H}_k\right)^T\mathbf{P}_k^{-1}\left(\mathbf{I}-\mathbf{K}_k\mathbf{H}_k\right)<\left(\mathbf{A}_{k-1}\mathbf{P}_{k-1}\mathbf{A}_{k-1}^T+\mathbf{Q}_{k-1}\right)^{-1} \tag{240}$$

Using this inequality, the Lyapunov function can be written as

$$\begin{aligned} V_k\left(\tilde{\mathbf{x}}_k\right)&=\tilde{\mathbf{x}}_{k-1}^T\mathbf{A}_{k-1}^T\left(\mathbf{I}-\mathbf{K}_k\mathbf{H}_k\right)^T\mathbf{P}_k^{-1}\left(\mathbf{I}-\mathbf{K}_k\mathbf{H}_k\right)\mathbf{A}_{k-1}\tilde{\mathbf{x}}_{k-1}\\ &<\tilde{\mathbf{x}}_{k-1}^T\mathbf{A}_{k-1}^T\left(\mathbf{A}_{k-1}\mathbf{P}_{k-1}\mathbf{A}_{k-1}^T+\mathbf{Q}_{k-1}\right)^{-1}\mathbf{A}_{k-1}\tilde{\mathbf{x}}_{k-1}\end{aligned} \tag{241}$$

Since the matrix **A** is nonsingular, its inverse exists, and therefore the following modification is valid

$$V_k\left(\tilde{\mathbf{x}}_k\right)<\tilde{\mathbf{x}}_{k-1}^T\left(\mathbf{P}_{k-1}+\mathbf{A}_{k-1}^{-1}\mathbf{Q}_{k-1}\mathbf{A}_{k-1}^{-T}\right)^{-1}\tilde{\mathbf{x}}_{k-1} \tag{242}$$

Applying the matrix inversion lemma (203)

$$V_k\left(\tilde{\mathbf{x}}_k\right)<\tilde{\mathbf{x}}_{k-1}^T\left[\mathbf{P}_{k-1}^{-1}-\mathbf{P}_{k-1}^{-1}\left(\mathbf{P}_{k-1}^{-1}+\mathbf{A}_{k-1}^T\mathbf{Q}_{k-1}^{-1}\mathbf{A}_{k-1}\right)^{-1}\mathbf{P}_{k-1}^{-1}\right]\tilde{\mathbf{x}}_{k-1} \tag{243}$$

Recognizing the candidate Lyapunov function on the right hand side

$$V_k\left(\tilde{\mathbf{x}}_k\right)-V_{k-1}\left(\tilde{\mathbf{x}}_{k-1}\right)<\tilde{\mathbf{x}}_{k-1}^T\left[-\mathbf{P}_{k-1}^{-1}\left(\mathbf{P}_{k-1}^{-1}+\mathbf{A}_{k-1}^T\mathbf{Q}_{k-1}^{-1}\mathbf{A}_{k-1}\right)^{-1}\mathbf{P}_{k-1}^{-1}\right]\tilde{\mathbf{x}}_{k-1} \tag{244}$$

Since the matrices **P** and **Q** are both positive definite, the matrix in square brackets is negative definite, therefore the right hand side of the equation is negative. This proves the asymptotic stability of the deterministic problem. Additionally, information about the convergence rate of the estimation can be determined by analyzing the bound on the following matrix

$$\mathbf{P}_{k-1}^{-1}\left(\mathbf{P}_{k-1}^{-1}+\mathbf{A}_{k-1}^T\mathbf{Q}_{k-1}^{-1}\mathbf{A}_{k-1}\right)^{-1}\le\alpha\mathbf{I} \tag{245}$$

where $\alpha$ is the convergence rate and $0 < \alpha \le 1$. By rearranging this inequality, the following matrix bound can alternatively be used to calculate the convergence rate

$$\left(\frac{1-\alpha}{\alpha}\right)\mathbf{I} \le \mathbf{A}_{k-1}^{T}\mathbf{Q}_{k-1}^{-1}\mathbf{A}_{k-1}\mathbf{P}_{k-1} \tag{246}$$

Using this bound, the Lyapunov difference equation can be rewritten as

$$V_k\left(\tilde{\mathbf{x}}_k\right) - V_{k-1}\left(\tilde{\mathbf{x}}_{k-1}\right) < -\alpha V_{k-1}\left(\tilde{\mathbf{x}}_{k-1}\right) \tag{247}$$

This equation can be recognized as taking the form of (204), where no stochastic terms are considered, and with $\mu = 0$. The effect of the stochastic terms is considered separately in the following section.

Before considering the stochastic terms, the uniform stability characteristics of the deterministic system are considered. Since this is a non-autonomous system, the uniform asymptotic stability of the system can be shown by demonstrating that the Lyapunov function is decrescent. From (239), it is shown that there exists a lower bound on the covariance matrix. By definition the covariance matrix is positive definite and the process noise covariance matrix is positive semi-definite for any time $k$, therefore the following inequality is satisfied

$$\mathbf{P}_k > \left(\mathbf{I} - \mathbf{K}_k\mathbf{H}_k\right)\left(\mathbf{A}_{k-1}\mathbf{P}_{k-1}\mathbf{A}_{k-1}^{T} + \mathbf{Q}_{k-1}\right)\left(\mathbf{I} - \mathbf{K}_k\mathbf{H}_k\right)^{T} \ge \beta\mathbf{I} > 0 \tag{248}$$

where $\beta$ is some positive constant. Taking the inverse of this relationship, the inverse of the covariance matrix is bounded as in

$$\mathbf{P}_k^{-1} \le \frac{1}{\beta}\mathbf{I} \tag{249}$$

Thus, the Lyapunov function is bounded as follows

$$V_k\left(\tilde{\mathbf{x}}_k\right)=\tilde{\mathbf{x}}_k^T\mathbf{P}_k^{-1}\tilde{\mathbf{x}}_k\le\tilde{\mathbf{x}}_k^T\frac{1}{\beta}\tilde{\mathbf{x}}_k=\frac{1}{\beta}\left\|\tilde{\mathbf{x}}_k\right\|_2^2$$
$$V_k\left(\tilde{\mathbf{x}}_k\right)\le\frac{1}{\beta}\left\|\tilde{\mathbf{x}}_k\right\|_2^2 \tag{250}$$

Since the Lyapunov function is upper bounded by a class *K* function, it is a decrescent function, and therefore the system is uniformly asymptotically stable.

### 6.2.3 Stochastic Linear Kalman Filter Stability Analysis

Building upon the work of the previous section for the deterministic problem, the stochastic terms are now considered. Using the same Lyapunov function with the stochastic error dynamics, the Lyapunov function can be written as

$$\begin{aligned}V_k\left(\tilde{\mathbf{x}}_k\right)=&\left[\left(\mathbf{I}-\mathbf{K}_k\mathbf{H}_k\right)\left(\mathbf{A}_{k-1}\tilde{\mathbf{x}}_{k-1}+\mathbf{w}_{k-1}\right)-\mathbf{K}_k\mathbf{v}_k\right]^T\mathbf{P}_k^{-1}\\&\times\left[\left(\mathbf{I}-\mathbf{K}_k\mathbf{H}_k\right)\left(\mathbf{A}_{k-1}\tilde{\mathbf{x}}_{k-1}+\mathbf{w}_{k-1}\right)-\mathbf{K}_k\mathbf{v}_k\right]\end{aligned} \tag{251}$$

Since the process and measurement noise vectors are zero mean and independent from the other terms, when taking the expectation, terms containing only **w** or **v** are zero, thus simplifying the equation to

$$\begin{aligned}&E\left[V_k\left(\tilde{\mathbf{x}}_k\right)\mid\tilde{\mathbf{x}}_{k-1}\right]=\tilde{\mathbf{x}}_{k-1}^T\mathbf{A}_{k-1}^T\left(\mathbf{I}-\mathbf{K}_k\mathbf{H}_k\right)^T\mathbf{P}_k^{-1}\left(\mathbf{I}-\mathbf{K}_k\mathbf{H}_k\right)\mathbf{A}_{k-1}\tilde{\mathbf{x}}_{k-1}+\Gamma_k\\&\Gamma_k\equiv E\left[\left\{\left(\mathbf{I}-\mathbf{K}_k\mathbf{H}_k\right)\mathbf{w}_{k-1}-\mathbf{K}_k\mathbf{v}_k\right\}^T\mathbf{P}_k^{-1}\left\{\left(\mathbf{I}-\mathbf{K}_k\mathbf{H}_k\right)\mathbf{w}_{k-1}-\mathbf{K}_k\mathbf{v}_k\right\}\right]\end{aligned} \tag{252}$$

where Γ is defined to represent the stochastic terms in the Lyapunov equation. The other term in the equation can be recognized as the term corresponding to the deterministic problem. Using the assumption that **w** and **v** are uncorrelated, *i.e.*,

$$E\left[\mathbf{w}_{k-1}^T\mathbf{v}_k\right]=E\left[\mathbf{v}_k^T\mathbf{w}_{k-1}\right]=0 \tag{253}$$

the process and measurement noise terms can be separated

$$\begin{aligned}\Gamma_k &= \Gamma_k^w + \Gamma_k^v \\ \Gamma_k^w &\equiv E\left[\mathbf{w}_{k-1}^T\left(\mathbf{I}-\mathbf{K}_k\mathbf{H}_k\right)^T\mathbf{P}_k^{-1}\left(\mathbf{I}-\mathbf{K}_k\mathbf{H}_k\right)\mathbf{w}_{k-1}\right] \\ \Gamma_k^v &\equiv E\left[\mathbf{v}_k^T\mathbf{K}_k^T\mathbf{P}_k^{-1}\mathbf{K}_k\mathbf{v}_k\right]\end{aligned} \tag{254}$$

First the process noise term is considered. Since this equation is scalar, the trace can be taken without affecting the equality, as in

$$\Gamma_k^w = Tr\left\{\Gamma_k^w\right\} = Tr\left\{E\left[\mathbf{w}_{k-1}^T\left(\mathbf{I}-\mathbf{K}_k\mathbf{H}_k\right)^T\mathbf{P}_k^{-1}\left(\mathbf{I}-\mathbf{K}_k\mathbf{H}_k\right)\mathbf{w}_{k-1}\right]\right\} \tag{255}$$

Using the trace property (201), the terms are reordered, and the deterministic terms are removed from the expectation

$$\Gamma_k^w = Tr\left\{\left(\mathbf{I}-\mathbf{K}_k\mathbf{H}_k\right)^T\mathbf{P}_k^{-1}\left(\mathbf{I}-\mathbf{K}_k\mathbf{H}_k\right)E\left[\mathbf{w}_{k-1}\mathbf{w}_{k-1}^T\right]\right\} \tag{256}$$

Using (239), the following inequality can be established

$$\Gamma_k^w < Tr\left\{\left(\mathbf{A}_{k-1}\mathbf{P}_{k-1}\mathbf{A}_{k-1}^T+\mathbf{Q}_{k-1}\right)^{-1}E\left[\mathbf{w}_{k-1}\mathbf{w}_{k-1}^T\right]\right\} \tag{257}$$

Since both terms inside of the matrix inverse are positive definite, the following inequality is also satisfied

$$\left(\mathbf{A}_{k-1}\mathbf{P}_{k-1}\mathbf{A}_{k-1}^T+\mathbf{Q}_{k-1}\right)^{-1} < \mathbf{Q}_{k-1}^{-1} \tag{258}$$

Using this relationship as well as the definition of the covariance of the process noise, this term can be simplified

$$\Gamma_k^w < Tr\left\{\mathbf{Q}_{k-1}^{-1}E\left[\mathbf{w}_{k-1}\mathbf{w}_{k-1}^T\right]\right\} = Tr\left\{\mathbf{Q}_{k-1}^{-1}\mathbf{Q}_{k-1}\right\} = n_w \tag{259}$$

where $n_w$ is the size of the process noise vector, $\mathbf{w}$. Next, the measurement noise term is considered.

Similarly to the process noise term, the trace is considered in order to utilize the reordering property (201), thus giving

$$\Gamma_k^v = Tr\left\{\mathbf{K}_k^T\mathbf{P}_k^{-1}\mathbf{K}_k E\left[\mathbf{v}_k\mathbf{v}_k^T\right]\right\} \tag{260}$$

To simplify the measurement noise term, an alternative definition of the Kalman gain matrix is considered [62]

$$\mathbf{K}_k = \mathbf{P}_k\mathbf{H}_k^T\mathbf{R}_k^{-1} \tag{261}$$

Inserting this into the measurement noise term yields

$$\begin{aligned}\Gamma_k^v &= Tr\left\{\mathbf{R}_k^{-1}\mathbf{H}_k\mathbf{P}_k\mathbf{P}_k^{-1}\mathbf{P}_k\mathbf{H}_k^T\mathbf{R}_k^{-1}E\left[\mathbf{v}_k\mathbf{v}_k^T\right]\right\}\\ \Gamma_k^v &= Tr\left\{\mathbf{R}_k^{-1}\mathbf{H}_k\mathbf{P}_k\mathbf{H}_k^T\mathbf{R}_k^{-1}E\left[\mathbf{v}_k\mathbf{v}_k^T\right]\right\}\end{aligned} \tag{262}$$

Considering the definition of the measurement noise covariance

$$\Gamma_k^v = Tr\left\{\mathbf{R}_k^{-1}\mathbf{H}_k\mathbf{P}_k\mathbf{H}_k^T\right\} \tag{263}$$

Using the trace property (201) again to reorder the matrix multiplication

$$\Gamma_k^v = Tr\left\{\mathbf{H}_k^T\mathbf{R}_k^{-1}\mathbf{H}_k\mathbf{P}_k\right\} \tag{264}$$

From the information filtering form of the covariance update equation [62]

$$\mathbf{P}_k^{-1} = \mathbf{P}_{k|k-1}^{-1} + \mathbf{H}_k^T\mathbf{R}_k^{-1}\mathbf{H}_k \tag{265}$$

Substituting this relationship in for the $\mathbf{H}_k^T\mathbf{R}_k^{-1}\mathbf{H}_k$ term yields

$$\Gamma_k^v = Tr\left\{\left(\mathbf{P}_k^{-1} - \mathbf{P}_{k|k-1}^{-1}\right)\mathbf{P}_k\right\} = Tr\left\{\mathbf{I} - \mathbf{P}_{k|k-1}^{-1}\mathbf{P}_k\right\} \tag{266}$$

Since both the *a priori* and *a posteriori* covariance matrices are positive definite, the following inequality is satisfied

$$\begin{aligned}&\mathbf{P}_{k|k-1}^{-1}\mathbf{P}_k > 0\\ &\mathbf{I} - \mathbf{P}_{k|k-1}^{-1}\mathbf{P}_k < \mathbf{I}\end{aligned} \tag{267}$$

This effectively establishes a bound for the measurement noise covariance term as in

$$\Gamma_k^v < Tr\{\mathbf{I}\} = n_v \tag{268}$$

where $n_v$ is the size of the measurement noise vector.

Combining the results of the previous section with this one, the following bound can be written for the stochastic system

$$E\left[V_k(\tilde{\mathbf{x}}_k) \mid \tilde{\mathbf{x}}_{k-1}\right] - V_{k-1}(\tilde{\mathbf{x}}_{k-1}) < -\alpha V_{k-1}(\tilde{\mathbf{x}}_{k-1}) + n_w + n_v \tag{269}$$

which follows the form of (204) with $\mu = n_w + n_v$.

## 6.3 LINEAR KALMAN FILTER ON-LINE CONVERGENCE ANALYSIS

When the Linear Kalman Filter (LKF) is implemented in real-time applications, it is often difficult to quantify the performance of the filter without access to some reference „truth". Off-line simulations can provide some indication of the filter performance; however accurate mathematical models are not always available. There is a need to analyze the performance of the LKF on-line by quantifying the convergence rate and steady state error bounds of the real system. Such a tool could benefit many safety or performance critical systems, such as the aircraft health management system. Existing techniques for on-line performance analysis of the LKF include outlier detection [168], performance reliability prediction [169], and confidence bounds from the covariance matrix, *e.g.* see [170]. Confidence bounds can also be established through use of the Chebyshev inequality [171], although these bounds tend to be too large for practical use [172]. Some other investigations for confidence bounds on the Kalman filter consider the non-Gaussian case using enhancements to the Chebyshev inequality [172] or the Kantorovich inequality [173]. The work presented herein offers a novel on-line method

for monitoring the performance of the LKF by providing an upper bound on the estimation error.

An important and useful tool for analyzing the stochastic stability of a system is the stochastic stability lemma which was described in Section 6.1. This lemma has been used to approach the stability of the Extended Kalman Filter (EKF) [40] and later for a general class of nonlinear filters including EKF and UKF [35,36]. A common problem with existing convergence analysis techniques for nonlinear state estimators is extremely loose bounds on the system and noise matrices, leading to very conservative and unrealistic requirements on the initial error and noise of the system [40]. A method for the relaxation of these conditions for EKF was considered in a related work [162], and is also discussed further in Section 6.4. Using the stochastic stability lemma, these works [40,162] perform an off-line prediction of the stability of the state estimation. This process involves the calculation of a convergence rate and steady state error which establish an upper bound on the estimation error.

In addition to its previous uses for nonlinear systems, the stochastic stability lemma can also be used to establish important results for the LKF. Since the LKF is an adaptive process even for Linear Time-Invariant (LTI) systems, it becomes useful to analyze the convergence rate and steady state error as a function of time. Using the modified stochastic stability lemma, the convergence properties of the LKF are evaluated, thus providing a more realistic bound on the estimation error. Determining a bound on the estimation error is useful for applications where a reference „truth" value is not available for validation. This technique provides an upper bound on the filter

performance, which can be used to represent the worst case scenario for the LKF estimation results.

Using the modified stochastic stability lemma, the main result of this section can be stated.

*Kalman Filter Convergence Theorem*: Consider a linear stochastic system of the form (45) with no input using the standard LKF equations. Let the following assumptions hold.

1) The system matrix, $\mathbf{F}_k$, is nonsingular (invertible) for all $k$.

2) The assumed initial covariance is bounded by:

$$\tilde{\mathbf{x}}_0^T \mathbf{P}_0^{-1} \tilde{\mathbf{x}}_0 \le \nu_0 \left\| \tilde{\mathbf{x}}_0 \right\|^2 \tag{270}$$

3) The state error covariance matrix is bounded by the following inequality for all $k$:

$$\tilde{\mathbf{x}}_k^T \mathbf{P}_k^{-1} \tilde{\mathbf{x}}_k \ge b_k \left\| \tilde{\mathbf{x}}_k \right\|^2 \tag{271}$$

4) The assumed process and measurement noise covariance matrices are conservative, *i.e.*:

$$\mathbf{Q}_{k-1} \ge E\left\lfloor \mathbf{w}_{k-1} \mathbf{w}_{k-1}^T \right\rfloor \tag{272}$$

$$\mathbf{R}_k \ge E\left\lfloor \mathbf{v}_k \mathbf{v}_k^T \right\rfloor \tag{273}$$

Then the expected value of the estimation error is bounded in mean square with probability one by

$$E\left[ \left\| \tilde{\mathbf{x}}_k \right\|^2 \right] \le \frac{\nu_0}{b_k} E\left[ \left\| \tilde{\mathbf{x}}_0 \right\|^2 \right] \prod_{i=0}^{k-1} \left(1 - \alpha_i\right) + \frac{1}{b_k} \sum_{i=0}^{k-1} \left[ \mu_{k-i-1} \prod_{j=1}^{i} \left(1 - \alpha_{k-j}\right) \right] \tag{274}$$

where the time varying parameters $\alpha_{k\text{-}1}$, $\mu_{k\text{-}1}$, and $b_k$ are given by

$$\alpha_{k-1} = \lambda_{\min}\left[\left(\mathbf{P}_{k|k-1} + \mathbf{P}_{k|k-1}\mathbf{H}_k^T\mathbf{R}_k^{-1}\mathbf{H}_k\mathbf{P}_{k|k-1}\right)^{-1}\left(\mathbf{Q}_{k-1} + \mathbf{P}_{k|k-1}\mathbf{H}_k^T\mathbf{R}_k^{-1}\mathbf{H}_k\mathbf{P}_{k|k-1}\right)\right] \tag{275}$$

$$\mu_{k-1} = Tr\left\{\left(\mathbf{P}_{k|k-1} + \mathbf{P}_{k|k-1}\mathbf{H}_k^T\mathbf{R}_k^{-1}\mathbf{H}_k\mathbf{P}_{k|k-1}\right)^{-1}\left(\mathbf{Q}_{k-1} + \mathbf{P}_{k|k-1}\mathbf{H}_k^T\mathbf{R}_k^{-1}\mathbf{H}_k\mathbf{P}_{k|k-1}\right)\right\} \tag{276}$$

$$b_k = \lambda_{\min}\left(\mathbf{P}_k^{-1}\right) \tag{277}$$

*Proof*: The proof of this theorem is detailed in the following sections.

*Remarks*:

1) The bound in (270) only matters for the assumed initial covariance matrix. Since this has a known value, the constant $v_0$ should be selected as the minimum eigenvalue of the inverse of the assumed initial covariance matrix and this bound will be automatically satisfied.

2) It is worth noting in (271) that if the error covariance approaches infinity (divergence) then the term $b_k$ will approach zero, which would lead to an infinite bound on the estimation error, thus indicating divergence of the filter as expected. For a stable system however, the error covariance matrix has an upper bound, which can be determined from the stochastic controllability and observability properties of the system [4,5].

3) The parameters $\alpha$ and $\mu$ are both functions of the same matrix, where $\alpha$ is the minimum eigenvalue and $\mu$ is the trace of the matrix. Since the eigenvalues of this matrix lie between 0 and 1 (the *a priori* covariance is always greater than or equal to the process noise covariance matrix) and recalling that the trace of a matrix is equal to the sum of its eigenvalues [53], the parameter $\mu$ will satisfy $0 < \alpha_{k-1} < \mu_{k-1} < n$ for all $k$, where $n$ is the number of states in the filter. From here, it is interesting to note that

increasing the parameter $\alpha$, which corresponds to the convergence of the stochastic process, will in turn also increase the parameter $\mu$, which corresponds to the steady state error bound due to noise. This introduces a trade-off in convergence and steady state error, which can be tuned through the selection of the process and measurement noise covariance matrices.

4) Using the modified stochastic stability lemma for analysis of the LKF convergence leads to three important time-varying parameters: $\alpha_k$, $\mu_k$, and $b_k$. The parameter $\alpha_k$ represents the convergence of the stochastic process, as defined in the following section by (278), while the parameter $b_k$ represents the convergence of the error covariance. The parameter $\mu_k$ corresponds to the steady state error bound on the filter due to the process and measurement noise. *I.e.*, in (274) it is shown that the initial error term will vanish as $k$ increases, thus leaving the term containing $\mu_k$ in the steady state. This makes sense because as a LKF progresses in time, eventually the performance will converge within a region determined from the process and measurement noise, since these phenomena do not disappear with time. Together, these three parameters determine a bound on the convergence and steady state error of the filter using (274). Due to the time-varying nature of these parameters, the bound must be determined on-line, and therefore cannot provide an off-line prediction of the filter convergence as in [40,162].

The proof of the Kalman Filter Convergence Theorem is provided in the following sections.

### 6.3.1 Defining and Decomposing the Estimation Error Analysis

As recommended in other works, *e.g.* [7,40], a candidate Lyapunov function is selected to define the stochastic process using a quadratic form of the estimation error and inverse error covariance matrix, as in

$$V\left(\tilde{\mathbf{x}}_k\right) = \tilde{\mathbf{x}}_k^T \mathbf{P}_k^{-1} \tilde{\mathbf{x}}_k \tag{278}$$

Note that this function is used in the context of the modified stochastic stability lemma, not using traditional Lyapunov stability theorems; therefore it is only being used as a tool for analyzing the convergence, not to prove the stability of the filter. Inserting the error dynamics from (233) into this function gives

$$V\left(\tilde{\mathbf{x}}_k\right) = \left[\left(\mathbf{I} - \mathbf{K}_k \mathbf{H}_k\right)\left(\mathbf{F}_{k-1}\tilde{\mathbf{x}}_{k-1} + \mathbf{w}_{k-1}\right) - \mathbf{K}_k \mathbf{v}_k\right]^T \mathbf{P}_k^{-1} \left[\left(\mathbf{I} - \mathbf{K}_k \mathbf{H}_k\right)\left(\mathbf{F}_{k-1}\tilde{\mathbf{x}}_{k-1} + \mathbf{w}_{k-1}\right) - \mathbf{K}_k \mathbf{v}_k\right] \tag{279}$$

Taking the conditional expectation with respect to $\tilde{\mathbf{x}}_{k-1}$ and using the assumption that the process and measurement noise are uncorrelated gives

$$E\left[V\left(\tilde{\mathbf{x}}_k\right)|\,\tilde{\mathbf{x}}_{k-1}\right]=\Gamma_k^x+\Gamma_k^w+\Gamma_k^v \tag{280}$$

$$\Gamma_k^x \triangleq \tilde{\mathbf{x}}_{k-1}^T\mathbf{F}_{k-1}^T\left(\mathbf{I}-\mathbf{K}_k\mathbf{H}_k\right)^T\mathbf{P}_k^{-1}\left(\mathbf{I}-\mathbf{K}_k\mathbf{H}_k\right)\mathbf{F}_{k-1}\tilde{\mathbf{x}}_{k-1} \tag{281}$$

$$\Gamma_k^w \triangleq E\left[\mathbf{w}_{k-1}^T\left(\mathbf{I}-\mathbf{K}_k\mathbf{H}_k\right)^T\mathbf{P}_k^{-1}\left(\mathbf{I}-\mathbf{K}_k\mathbf{H}_k\right)\mathbf{w}_{k-1}\right] \tag{282}$$

$$\Gamma_k^v \triangleq E\left[\mathbf{v}_k^T\mathbf{K}_k^T\mathbf{P}_k^{-1}\mathbf{K}_k\mathbf{v}_k\right] \tag{283}$$

Now the problem of analyzing the LKF estimation error has been divided into three parts: the homogeneous problem in (281), the process noise problem in (282), and the measurement noise problem in (283). The homogeneous problem considers the deterministic part of the filter, *i.e.* no noise. The process and measurement noise problems consider the effects of the stochastic uncertainty in the prediction and measurement equations respectively. Each of these three parts is considered separately in the following sections.

### 6.3.2 The Homogeneous Problem

The homogeneous part of the problem is defined by (281). This part of the problem is related to the convergence rate of the filter. For this part of the analysis, a bound is desired in the form

$$\Gamma_k^x \le \left(1-\alpha_{k-1}\right)V\left(\tilde{\mathbf{x}}_{k-1}\right) \tag{284}$$

This inequality is desired as it is the assumption given by (210) ignoring for now the noise terms and assuming that $\mu_k = 0$ for all $k$. Substituting in for (278) and (281) gives

$$\tilde{\mathbf{x}}_{k-1}^T\mathbf{F}_{k-1}^T\left(\mathbf{I}-\mathbf{K}_k\mathbf{H}_k\right)^T\mathbf{P}_k^{-1}\left(\mathbf{I}-\mathbf{K}_k\mathbf{H}_k\right)\mathbf{F}_{k-1}\tilde{\mathbf{x}}_{k-1} \le \left(1-\alpha_{k-1}\right)\tilde{\mathbf{x}}_{k-1}^T\mathbf{P}_{k-1}^{-1}\tilde{\mathbf{x}}_{k-1} \tag{285}$$

This scalar inequality is equivalent to the matrix inequality

$$\mathbf{F}_{k-1}^{T}\left(\mathbf{I}-\mathbf{K}_{k}\mathbf{H}_{k}\right)^{T}\mathbf{P}_{k}^{-1}\left(\mathbf{I}-\mathbf{K}_{k}\mathbf{H}_{k}\right)\mathbf{F}_{k-1}\leq\left(1-\alpha_{k-1}\right)\mathbf{P}_{k-1}^{-1} \tag{286}$$

The following relationship can be derived from (51)

$$\mathbf{I}-\mathbf{K}_{k}\mathbf{H}_{k}=\mathbf{P}_{k}\mathbf{P}_{k|k-1}^{-1} \tag{287}$$

Substituting this into the matrix inequality

$$\mathbf{F}_{k-1}^{T}\mathbf{P}_{k|k-1}^{-1}\mathbf{P}_{k}\mathbf{P}_{k|k-1}^{-1}\mathbf{F}_{k-1}\leq\left(1-\alpha_{k-1}\right)\mathbf{P}_{k-1}^{-1} \tag{288}$$

Taking the inverse of this inequality gives

$$\mathbf{F}_{k-1}^{-1}\mathbf{P}_{k|k-1}\mathbf{P}_{k}^{-1}\mathbf{P}_{k|k-1}\mathbf{F}_{k-1}^{-T}\geq\left(1-\alpha_{k-1}\right)^{-1}\mathbf{P}_{k-1} \tag{289}$$

Note that this operation requires that the system matrix, **F**, be nonsingular for all *k* (Assumption 1). The covariance matrices are invertible because they are positive definite by definition. Starting from the covariance prediction equation in (49) and rearranging gives

$$\mathbf{P}_{k-1}=\mathbf{F}_{k-1}^{-1}\left(\mathbf{P}_{k|k-1}-\mathbf{Q}_{k-1}\right)\mathbf{F}_{k-1}^{-T} \tag{290}$$

Substituting this equation into the matrix inequality yields

$$\mathbf{F}_{k-1}^{-1}\mathbf{P}_{k|k-1}\mathbf{P}_{k}^{-1}\mathbf{P}_{k|k-1}\mathbf{F}_{k-1}^{-T}\geq\left(1-\alpha_{k-1}\right)^{-1}\mathbf{F}_{k-1}^{-1}\left(\mathbf{P}_{k|k-1}-\mathbf{Q}_{k-1}\right)\mathbf{F}_{k-1}^{-T} \tag{291}$$

Now, the system matrix can be removed from the inequality

$$\mathbf{P}_{k|k-1}\mathbf{P}_{k}^{-1}\mathbf{P}_{k|k-1}\geq\left(1-\alpha_{k-1}\right)^{-1}\left(\mathbf{P}_{k|k-1}-\mathbf{Q}_{k-1}\right) \tag{292}$$

The covariance update equation from (51) is used to relate the *a posteriori* covariance and *a priori* covariance, as in

$$\mathbf{P}_{k|k-1}\left(\mathbf{P}_{k|k-1}^{-1}+\mathbf{H}_{k}^{T}\mathbf{R}_{k}^{-1}\mathbf{H}_{k}\right)\mathbf{P}_{k|k-1}\geq\left(1-\alpha_{k-1}\right)^{-1}\left(\mathbf{P}_{k|k-1}-\mathbf{Q}_{k-1}\right) \tag{293}$$

Rearranging this inequality results in the following simplifications

$$
\begin{aligned}
&(1-\alpha_{k-1})\left(\mathbf{P}_{k|k-1}+\mathbf{P}_{k|k-1}\mathbf{H}_k^T\mathbf{R}_k^{-1}\mathbf{H}_k\mathbf{P}_{k|k-1}\right)\geq \mathbf{P}_{k|k-1}-\mathbf{Q}_{k-1}\\
&\mathbf{P}_{k|k-1}\mathbf{H}_k^T\mathbf{R}_k^{-1}\mathbf{H}_k\mathbf{P}_{k|k-1}-\alpha_{k-1}\left(\mathbf{P}_{k|k-1}+\mathbf{P}_{k|k-1}\mathbf{H}_k^T\mathbf{R}_k^{-1}\mathbf{H}_k\mathbf{P}_{k|k-1}\right)\geq -\mathbf{Q}_{k-1}\\
&\alpha_{k-1}\left(\mathbf{P}_{k|k-1}+\mathbf{P}_{k|k-1}\mathbf{H}_k^T\mathbf{R}_k^{-1}\mathbf{H}_k\mathbf{P}_{k|k-1}\right)\leq \mathbf{Q}_{k-1}+\mathbf{P}_{k|k-1}\mathbf{H}_k^T\mathbf{R}_k^{-1}\mathbf{H}_k\mathbf{P}_{k|k-1}\\
&\alpha_{k-1}\mathbf{I}\leq\left(\mathbf{P}_{k|k-1}+\mathbf{P}_{k|k-1}\mathbf{H}_k^T\mathbf{R}_k^{-1}\mathbf{H}_k\mathbf{P}_{k|k-1}\right)^{-1}\left(\mathbf{Q}_{k-1}+\mathbf{P}_{k|k-1}\mathbf{H}_k^T\mathbf{R}_k^{-1}\mathbf{H}_k\mathbf{P}_{k|k-1}\right)
\end{aligned}
\tag{294}
$$

Therefore the time-varying parameter, $\alpha$, can be determined as the minimum eigenvalue of the matrix, as in (275). From the covariance prediction equation in (49), it is clear that the *a priori* covariance is greater than the process noise covariance matrix, therefore $\alpha$ is always between 0 and 1. Note that increasing $\mathbf{Q}$ will increase $\alpha$. Alternatively, increasing $\mathbf{R}$ will decrease $\alpha$. If the parameter $\alpha$, is selected as in (275), the desired inequality (284) is satisfied, thus satisfying the homogeneous part of the problem. Next, the process noise is considered.

### 6.3.3 The Process Noise Problem

For the process noise problem, the quantity of interest is given by (282). Since this is a scalar equation, the trace can be taken without changing the value

$$
\Gamma_k^w = Tr\left\{\Gamma_k^w\right\} = Tr\left\{E\left[\mathbf{w}_{k-1}^T\left(\mathbf{I}-\mathbf{K}_k\mathbf{H}_k\right)^T\mathbf{P}_k^{-1}\left(\mathbf{I}-\mathbf{K}_k\mathbf{H}_k\right)\mathbf{w}_{k-1}\right]\right\} \tag{295}
$$

Using the trace property (201) and removing the deterministic terms from the expectation yields

$$
\Gamma_k^w = Tr\left\{\left(\mathbf{I}-\mathbf{K}_k\mathbf{H}_k\right)^T\mathbf{P}_k^{-1}\left(\mathbf{I}-\mathbf{K}_k\mathbf{H}_k\right)E\left[\mathbf{w}_{k-1}\mathbf{w}_{k-1}^T\right]\right\} \tag{296}
$$

Using (287) simplifies the equation to

$$\Gamma_k^w = Tr\left\{\mathbf{P}_{k|k-1}^{-1}\mathbf{P}_k\mathbf{P}_{k|k-1}^{-1}E\left[\mathbf{w}_{k-1}\mathbf{w}_{k-1}^T\right]\right\} \tag{297}$$

Inserting the covariance update equation from (51) gives

$$\Gamma_k^w = Tr\left\{\mathbf{P}_{k|k-1}^{-1}\left(\mathbf{P}_{k|k-1}^{-1} + \mathbf{H}_k^T\mathbf{R}_k^{-1}\mathbf{H}_k\right)^{-1}\mathbf{P}_{k|k-1}^{-1}E\left[\mathbf{w}_{k-1}\mathbf{w}_{k-1}^T\right]\right\} \tag{298}$$

which simplifies to

$$\Gamma_k^w = Tr\left\{\left(\mathbf{P}_{k|k-1} + \mathbf{P}_{k|k-1}\mathbf{H}_k^T\mathbf{R}_k^{-1}\mathbf{H}_k\mathbf{P}_{k|k-1}\right)^{-1}E\left[\mathbf{w}_{k-1}\mathbf{w}_{k-1}^T\right]\right\} \tag{299}$$

Since the process noise covariance matrix can be chosen freely for the LKF, it is assumed that the assumed process noise covariance matrix is greater than the actual covariance of the process noise, as in (272). This bound is motivated by the idea that it is better to assume greater rather than less noise than there actually is in the system. This leads to the bound on the process noise term

$$\Gamma_k^w \le Tr\left\{\left(\mathbf{P}_{k|k-1} + \mathbf{P}_{k|k-1}\mathbf{H}_k^T\mathbf{R}_k^{-1}\mathbf{H}_k\mathbf{P}_{k|k-1}\right)^{-1}\mathbf{Q}_{k-1}\right\} \tag{300}$$

While increasing **Q** was shown to increase the convergence rate in the previous section, it is clear here that this increase in convergence comes at the expense of a larger bound on the process noise term. This selection of **Q** becomes a trade-off between the convergence and the accuracy of the estimate, *i.e.* assuming an unnecessarily large **Q** will lead to faster convergence but larger steady state errors of the filter due to process noise. Next, the measurement noise problem is considered.

### 6.3.4 The Measurement Noise Problem

For the measurement noise problem, the quantity of interest is given by (283). Since this is a scalar equation, the trace can be taken without changing the value

$$\Gamma_k^v = Tr\left\{\Gamma_k^v\right\} = Tr\left\{E\left[\mathbf{v}_k^T\mathbf{K}_k^T\mathbf{P}_k^{-1}\mathbf{K}_k\mathbf{v}_k\right]\right\} \tag{301}$$

Using the trace property (201) and removing the deterministic terms from the expectation yields

$$\Gamma_k^v = Tr\left\{\mathbf{K}_k^T\mathbf{P}_k^{-1}\mathbf{K}_k E\left[\mathbf{v}_k\mathbf{v}_k^T\right]\right\} \tag{302}$$

Using the second equation for the Kalman gain yields

$$\Gamma_k^v = Tr\left\{\mathbf{R}_k^{-1}\mathbf{H}_k\mathbf{P}_k\mathbf{H}_k^T\mathbf{R}_k^{-1}E\left[\mathbf{v}_k\mathbf{v}_k^T\right]\right\} \tag{303}$$

Inserting the covariance update equation from (51) gives the relationship in terms of the *a priori* covariance

$$\Gamma_k^v = Tr\left\{\mathbf{R}_k^{-1}\mathbf{H}_k\left(\mathbf{P}_{k|k-1}^{-1} + \mathbf{H}_k^T\mathbf{R}_k^{-1}\mathbf{H}_k\right)^{-1}\mathbf{H}_k^T\mathbf{R}_k^{-1}E\left[\mathbf{v}_k\mathbf{v}_k^T\right]\right\} \tag{304}$$

Using the matrix inversion lemma (202), this term can be rewritten as

$$\Gamma_k^v = Tr\left\{\left[\mathbf{R}_k^{-1} - \left(\mathbf{R}_k + \mathbf{H}_k\mathbf{P}_{k|k-1}\mathbf{H}_k^T\right)^{-1}\right]E\left[\mathbf{v}_k\mathbf{v}_k^T\right]\right\} \tag{305}$$

Similarly as for the process noise, the assumed measurement noise covariance matrix is selected as an upper bound on the actual measurement noise covariance, as in (273), which determines the bound for the measurement noise term

$$\Gamma_k^v \le Tr\left\{\left[\mathbf{R}_k^{-1} - \left(\mathbf{R}_k + \mathbf{H}_k\mathbf{P}_{k|k-1}\mathbf{H}_k^T\right)^{-1}\right]\mathbf{R}_k\right\} \tag{306}$$

This inequality can be simplified to the following form

$$\Gamma_k^{\nu} \le Tr\left\{\left(\mathbf{R}_k + \mathbf{H}_k\mathbf{P}_{k|k-1}\mathbf{H}_k^T\right)^{-1}\mathbf{H}_k\mathbf{P}_{k|k-1}\mathbf{H}_k^T\right\} \tag{307}$$

From here, it is shown that increasing the assumed measurement noise covariance matrix, **R**, will in fact lead to a smaller bound on the estimation error due to measurement noise. Now that each part of the problem has been considered separately, the results are combined and the modified stochastic stability lemma is applied.

### 6.3.5 Final Result from the Modified Stochastic Stability Lemma

Combining the results from the previous sections gives the following inequality

$$\begin{aligned} E\left[V\left(\tilde{\mathbf{x}}_k\right)|\,\tilde{\mathbf{x}}_{k-1}\right] \le (1-\alpha_{k-1})V\left(\tilde{\mathbf{x}}_{k-1}\right) + Tr\left\{\left(\mathbf{P}_{k|k-1} + \mathbf{P}_{k|k-1}\mathbf{H}_k^T\mathbf{R}_k^{-1}\mathbf{H}_k\mathbf{P}_{k|k-1}\right)^{-1}\mathbf{Q}_{k-1}\right\} \\ + Tr\left\{\left(\mathbf{R}_k + \mathbf{H}_k\mathbf{P}_{k|k-1}\mathbf{H}_k^T\right)^{-1}\mathbf{H}_k\mathbf{P}_{k|k-1}\mathbf{H}_k^T\right\} \end{aligned} \tag{308}$$

which is equivalent to (210) with

$$\mu_{k-1} = Tr\left\{\left(\mathbf{P}_{k|k-1} + \mathbf{P}_{k|k-1}\mathbf{H}_k^T\mathbf{R}_k^{-1}\mathbf{H}_k\mathbf{P}_{k|k-1}\right)^{-1}\mathbf{Q}_{k-1}\right\} + Tr\left\{\left(\mathbf{R}_k + \mathbf{H}_k\mathbf{P}_{k|k-1}\mathbf{H}_k^T\right)^{-1}\mathbf{H}_k\mathbf{P}_{k|k-1}\mathbf{H}_k^T\right\} \tag{309}$$

This term can be simplified further. First, the trace property (201) is used to obtain

$$\mu_{k-1} = Tr\left\{\left(\mathbf{P}_{k|k-1} + \mathbf{P}_{k|k-1}\mathbf{H}_k^T\mathbf{R}_k^{-1}\mathbf{H}_k\mathbf{P}_{k|k-1}\right)^{-1}\mathbf{Q}_{k-1} + \mathbf{H}_k^T\left(\mathbf{R}_k + \mathbf{H}_k\mathbf{P}_{k|k-1}\mathbf{H}_k^T\right)^{-1}\mathbf{H}_k\mathbf{P}_{k|k-1}\right\} \tag{310}$$

Then, applying the matrix inversion lemma (202) gives

$$\mu_{k-1} = Tr\left\{\left(\mathbf{P}_{k|k-1} + \mathbf{P}_{k|k-1}\mathbf{H}_k^T\mathbf{R}_k^{-1}\mathbf{H}_k\mathbf{P}_{k|k-1}\right)^{-1}\mathbf{Q}_{k-1} + \left[\mathbf{P}_{k|k-1}^{-1} - \mathbf{P}_{k|k-1}^{-1}\left(\mathbf{P}_{k|k-1}^{-1} + \mathbf{H}_k^T\mathbf{R}_k^{-1}\mathbf{H}_k\right)^{-1}\mathbf{P}_{k|k-1}^{-1}\right]\mathbf{P}_{k|k-1}\right\} \tag{311}$$

Further simplification yields

$$\mu_{k-1} = Tr\left\{\left(\mathbf{P}_{k|k-1} + \mathbf{P}_{k|k-1}\mathbf{H}_k^T\mathbf{R}_k^{-1}\mathbf{H}_k\mathbf{P}_{k|k-1}\right)^{-1}\mathbf{Q}_{k-1} + \mathbf{I} - \left(\mathbf{P}_{k|k-1} + \mathbf{P}_{k|k-1}\mathbf{H}_k^T\mathbf{R}_k^{-1}\mathbf{H}_k\mathbf{P}_{k|k-1}\right)^{-1}\mathbf{P}_{k|k-1}\right\} \tag{312}$$

Then, combining the terms gives (276). Thus, the inequality in (210) has been satisfied.

In order to apply the modified stochastic stability lemma, the inequalities (208) and (209) also need to be satisfied. These inequalities are guaranteed by the assumptions (270) and (271) in the Kalman Filter Convergence Theorem. Thus, the necessary conditions for the modified stochastic stability lemma have been satisfied, therefore the estimation error of the LKF is bounded in mean square with probability one, and the bound is given by (274). This completes the proof of the Kalman Filter Convergence Theorem. In the following section, a LKF example is provided to illustrate the usefulness of the Kalman Filter Convergence Theorem for LKF convergence analysis.

### 6.3.6 Illustrative Example of the Kalman Filter Convergence Theorem

To demonstrate the use of Kalman Filter Convergence Theorem, a simple LKF example is presented. This example problem was adapted from Example 5.1 in [62] to include process noise. The system equations are defined in the form of (45) with no input and system matrices defined by

$$\begin{aligned} \mathbf{F}_k = \mathbf{F} &= \begin{bmatrix} 1 & T & T^2/2 \\ 0 & 1 & T \\ 0 & 0 & 1 \end{bmatrix} \\ \mathbf{H}_k = \mathbf{H} &= \begin{bmatrix} 1 & 0 & 0 \end{bmatrix} \end{aligned} \tag{313}$$

and the true process and measurement noise covariance matrices are given by

$$\begin{aligned} E\left[\mathbf{w}_k \mathbf{w}_k^T\right] &= 10^{-8}\mathbf{I} \\ E\left[\mathbf{v}_k \mathbf{v}_k^T\right] &= 10^{-8} \end{aligned} \tag{314}$$

where $T$ is the sampling time, which for this example is considered to be 0.02. The initial conditions are assumed to be

$$\hat{\mathbf{x}}_0 = \begin{bmatrix} 1.5 & 1.5 & -0.3 \end{bmatrix}^T$$
$$\mathbf{P}_0 = \mathbf{I} \tag{315}$$

while the true initial state for the system is actually

$$\mathbf{x}_0 = \begin{bmatrix} 1 & 0.5 & 0.2 \end{bmatrix}^T \tag{316}$$

Note that this considers a case of reasonably large initialization error.

In order to apply the Kalman Filter Convergence Theorem, certain assumptions need to be satisfied. From the definition of **F**, it is clear that this matrix is invertible. Four different cases of assumed process and measurement covariance matrices were considered, as summarized in Table 14.

Table 14. Cases of Assumed Covariance Matrices

| Case # | Q | R |
|---|---|---|
| 1 | $E\lfloor \mathbf{w}_k \mathbf{w}_k^T \rfloor$ | $E\lfloor \mathbf{v}_k \mathbf{v}_k^T \rfloor$ |
| 2 | $100\, E\lfloor \mathbf{w}_k \mathbf{w}_k^T \rfloor$ | $E\lfloor \mathbf{v}_k \mathbf{v}_k^T \rfloor$ |
| 3 | $E\lfloor \mathbf{w}_k \mathbf{w}_k^T \rfloor$ | $100\, E\lfloor \mathbf{v}_k \mathbf{v}_k^T \rfloor$ |
| 4 | $100\, E\lfloor \mathbf{w}_k \mathbf{w}_k^T \rfloor$ | $100\, E\lfloor \mathbf{v}_k \mathbf{v}_k^T \rfloor$ |

It is clear from Table 14 that (272) and (273) are satisfied. Note that these cases vary the assumed noise properties, not the actual noise. The true nose covariance matrices are given by (314) for all cases. The value for the initial Lyapunov function upper bound, $v_0$, is calculated from the assumed initial covariance matrix with (270). Additionally, the values for the time-varying convergence rate, $\alpha_k$, noise parameter, $\mu_k$, and Lyapunov function bound $b_k$ are defined using (275), (276), and (271) respectively. These values are calculated on-line at each time step of the filter. Using these equations, the convergence properties can be calculated on-line with (274).

For the given example, the presented convergence analysis technique is applied, and the results are given as follows. Since the initial covariance is the identity matrix, $v_0 = 1$. The time-varying convergence and error parameters are shown in Figure 57 for each of the considered cases of assumed process and measurement noise covariance.

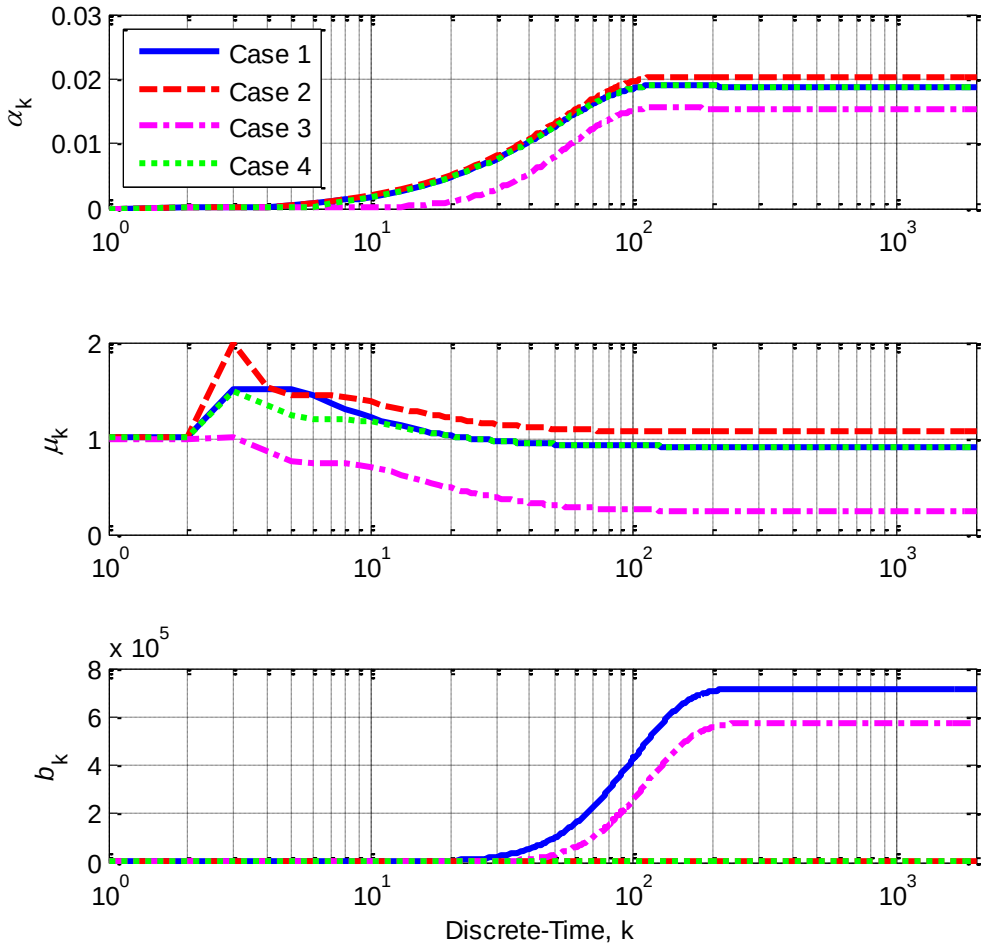


Figure 57. LKF Example: Time-Varying Convergence and Error Parameters

The parameter $\alpha_k$ represents the convergence rate of the stochastic process, $\mu_k$ represents the steady state error of the stochastic process, and $b_k$ represents the convergence of the error covariance. From these time-varying parameters, the bound on the expected value

of the norm of the estimation error squared can be determined from (274). This bound is verified with respect to the actual estimation error which was determined from simulation as shown in Figure 58.

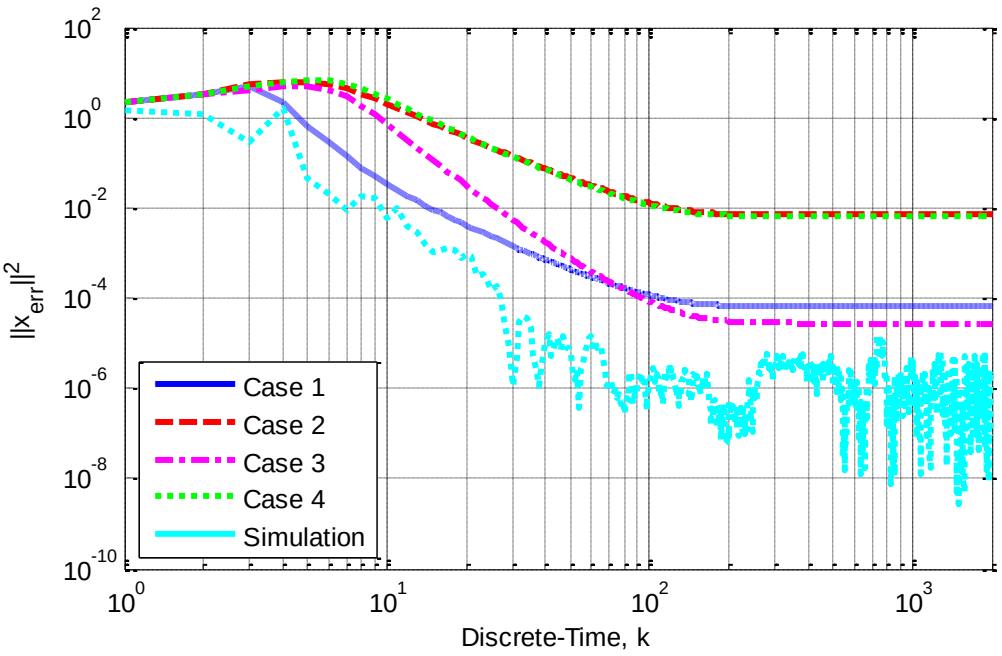


Figure 58. LKF Example: Estimation Error with Bounds

It is shown in Figure 58 that the estimation error does not exceed the theoretical bounds. The on-line bounds are relatively close to the estimation error, thus providing a reasonable guide to the convergence and steady-state error of the filter performance. This is useful because a reference truth is not available to evaluate the performance of a filter in most practical applications. This method provides a means of calculating an upper bound on the performance of the filter using only known values from the filtering process.

There are some interesting observations to make from Figure 57 and Figure 58 regarding the different noise covariance assumptions. Case 1, which represents perfect knowledge of the simulated noise properties, offers a very good approximation to the convergence and steady state error of the example filter. Increasing the assumption on the process noise (Case 2) leads to an increase in $\alpha_k$, but also an increase in $\mu_k$, as predicted. However, this increase in assumed process noise significantly increased the parameter $b_k$, thus leading to a slowly converging, loose bound on the estimation error. A similar performance bound was seen for Case 4 due to the dominant effect of the parameter $b_k$, however the parameters $\alpha_k$ and $\mu_k$ were similar to Case 1. This makes sense because the ratio between the assumed **Q** and **R** remained the same for Cases 1 and 4. For Case 3, increasing the assumed measurement noise decreased the parameters $\alpha_k$ and $\mu_k$ as expected, but the parameter $b_k$ also decreased, further decreasing the convergence of the estimation error. This lead to a slower converging bound, but a tighter bound on the steady state error. This demonstrates a trade-off in the selection of the measurement noise covariance, which could be used for filter tuning depending on the application and desired convergence properties.

The predicted estimation error bound from off-line analysis [40,162] using the stochastic stability lemma is also provided as a reference to demonstrate the effectiveness of using this new on-line method. To relate the time-varying parameters to previous off-line work using the stochastic stability lemma [40,162], the following relations are used

$$\begin{aligned} \alpha &= \min\left(\alpha_k\right) \\ \mu &= \max\left(\mu_k\right) \\ \nu_1 &= \min\left(b_k\right) \end{aligned} \tag{317}$$

The bound from Case 1 is used for this comparison, as shown in Figure 59.

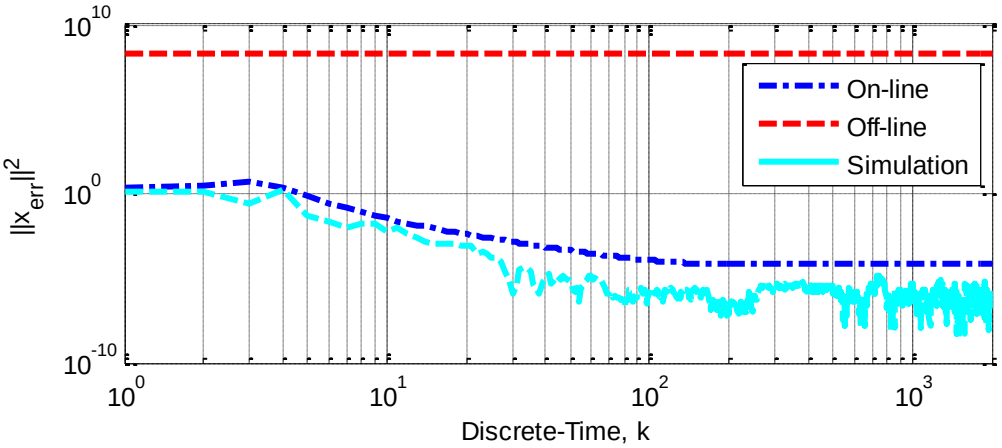


Figure 59. LKF Example: On-line vs. Off-line Estimation Error Bounds

While the off-line estimation error bound is valid, it is extremely loose, and does not provide a realistic portrayal of the convergence of the estimation error. This shows that the presented on-line method is useful for more closely determining the convergence and steady state error of the LKF, but is limited in that it cannot predict these bounds prior to the filtering process and it cannot be used for off-line stability analysis.

## 6.4 PRELIMINARY EKF STABILITY ANALYSIS

The work from this section was previously published in [162]. As a starting point for the stability analysis, the methodology of Reif *et al*. [40] is used directly for the 3-state GPS/INS attitude estimation formulation. In order to use this method, the bounds in (69) must be determined. Before this is done, however, certain bounds must be considered for the states and inputs. These bounds were selected based on observations from flight data, as in Table 3

$$\left.\begin{array}{l} -26.8 \le a_x \le 25.8 \\ -26.3 \le a_y \le 42.0 \\ -70.9 \le a_z \le 25.5 \end{array}\right\} \frac{m}{s^2}$$
$$\left.\begin{array}{l} -205 \le p \le 206 \\ -100 \le q \le 83.1 \\ -79.0 \le r \le 65.0 \end{array}\right\} \frac{\deg}{s} \qquad (318)$$
$$\left.\begin{array}{l} -85.0 \le \phi \le 56.6 \\ -48.5 \le \theta \le 38.8 \\ 0 \le \psi \le 360 \end{array}\right\} \deg$$

Additionally, the sampling rate of the prediction, 50 Hz ($T_s^x = 0.02s$), and measurement update, 10 Hz ($T_s^y = 0.1s$), are required. Using this information, the upper bounds of the matrices **A** and **H** are determined by calculating the values of the matrix spectral norm, as in (70), for (124) and (125) over the range of all possible values defined by (318)

$$\begin{array}{l} a_2 = 1.0676 \\ h_2 = 11.4192 \end{array} \qquad (319)$$

Since Reif *et al.* [40] formulate the EKF using additive noise, the additive **Q** and **R** matrices are defined by including the appropriate sampling time and the static sensor variances defined in Table 4 [15].

$$\mathbf{Q} = \left(T_s^x\right)^2 \begin{bmatrix} 1.51 & 0 & 0 \\ 0 & 1.45 & 0 \\ 0 & 0 & 1.41 \end{bmatrix} \cdot 10^{-4} = \begin{bmatrix} 6.04 & 0 & 0 \\ 0 & 5.80 & 0 \\ 0 & 0 & 5.64 \end{bmatrix} \cdot 10^{-8}$$

$$\mathbf{R}^d = \left(T_s^y\right)^2 \begin{bmatrix} 0.2205 & 0 & 0 \\ 0 & 0.2592 & 0 \\ 0 & 0 & 0.3102 \end{bmatrix} = \begin{bmatrix} 0.2205 & 0 & 0 \\ 0 & 0.2592 & 0 \\ 0 & 0 & 0.3102 \end{bmatrix} \cdot 10^{-2}$$

$$\mathbf{R}^y = \begin{bmatrix} 0.7022 & 0 & 0 \\ 0 & 0.4744 & 0 \\ 0 & 0 & 2.981 \end{bmatrix} \cdot 10^{-3} \tag{320}$$

$$\mathbf{R} = \mathbf{R}^d + \mathbf{R}^y = \begin{bmatrix} 0.2907 & 0 & 0 \\ 0 & 0.3066 & 0 \\ 0 & 0 & 0.6083 \end{bmatrix} \cdot 10^{-2}$$

Using these **Q** and **R** matrices, the lower bounds are given by

$$\begin{aligned} q_1 &= 5.64 \cdot 10^{-8} \\ r_1 &= 0.2907 \cdot 10^{-2} \end{aligned} \tag{321}$$

Determining the bounds of the state covariance matrix, **P**, is not as simple, since the dynamics of the filter are complex, and the difference equation for **P** is coupled with difference equation for the state estimate. To determine an estimate for the upper and lower bounds of this matrix, the 3-state GPS/INS sensor fusion formulation was implemented for each of the 23 sets of flight data. The maximum and minimum eigenvalues of this matrix over all 23 flights were then selected as the upper and lower bounds

$$\begin{aligned} p_1 &= 1.3554 \cdot 10^{-5} \\ p_2 &= 3.9031 \cdot 10^{-4} \end{aligned} \tag{322}$$

In order to determine the linearization error bounds, as in (71), the Hessian [1] can be calculated for the nonlinear prediction and observation functions with respect to the

state vector. The Hessian is defined as the second derivative of a ($n_x \times 1$) vector valued function, **f**, by

$$\mathbf{F}_{xx} = \frac{\partial^2 \mathbf{f}(\mathbf{x})}{\partial \mathbf{x}^2} \tag{323}$$

where $\mathbf{F}_{xx}$ is the Hessian, which is a third order tensor ($n_x \times n_x \times n_x$), which can be considered as a set of $n_x$ matrices with dimensions ($n_x \times n_x$). When calculated for a nonlinear prediction or observation function, these matrices can be used to quantify the nonlinearity of the corresponding state or observation [16]. As remarked in [40], the maximums of the spectral norms of the Hessian matrices for the prediction and observation functions are equal to the constants $\kappa_\varphi, \kappa_\chi$ respectively, in (71). For the 3-state GPS/INS sensor fusion formulation prediction, the Hessian was calculated to be

$$\mathbf{F}_{xx}^{\phi} = T_s^x \begin{bmatrix} -(q\sin\phi + r\cos\phi)\tan\theta & (q\cos\phi - r\sin\phi)\sec^2\theta & 0 \\ (q\cos\phi - r\sin\phi)\sec^2\theta & 2(q\sin\phi + r\cos\phi)\tan\theta\sec^2\theta & 0 \\ 0 & 0 & 0 \end{bmatrix} \tag{324}$$

$$\mathbf{F}_{xx}^{\theta} = T_s^x \begin{bmatrix} -(q\cos\phi - r\sin\phi) & 0 & 0 \\ 0 & 0 & 0 \\ 0 & 0 & 0 \end{bmatrix} \tag{325}$$

$$\mathbf{F}_{xx}^{\psi} = T_s^x \begin{bmatrix} -(q\sin\phi + r\cos\phi)\sec\theta & (q\cos\phi - r\sin\phi)\tan\theta\sec\theta & 0 \\ (q\cos\phi - r\sin\phi)\tan\theta\sec\theta & (q\sin\phi + r\cos\phi)\sec\theta(\tan^2\theta + \sec^2\theta) & 0 \\ 0 & 0 & 0 \end{bmatrix} \tag{326}$$

where the superscripts $\phi$, $\theta$, and $\psi$ denote the Hessian matrix corresponding to the roll, pitch, and yaw states respectively, and the discrete time dependence is implied for all variables, *i.e.*, $q = q_k$, $\phi = \phi_k$, etc. Similarly for the 3-state GPS/INS sensor fusion formulation observation function, the Hessian is given by

$$\mathbf{F}_{xx}^{\Delta V_x} = \begin{bmatrix} \frac{\partial^2 V_{x,k}}{\partial \phi^2} & \frac{\partial^2 V_{x,k}}{\partial \phi \partial \theta} & \frac{\partial^2 V_{x,k}}{\partial \phi \partial \psi} \\ \frac{\partial^2 V_{x,k}}{\partial \phi \partial \theta} & \frac{\partial^2 V_{x,k}}{\partial \theta^2} & \frac{\partial^2 V_{x,k}}{\partial \theta \partial \psi} \\ \frac{\partial^2 V_{x,k}}{\partial \phi \partial \psi} & \frac{\partial^2 V_{x,k}}{\partial \theta \partial \psi} & \frac{\partial^2 V_{x,k}}{\partial \psi^2} \end{bmatrix}, \quad \vec{a} = \begin{bmatrix} a_{\tilde{x}} \\ a_{\tilde{y}} \\ a_{\tilde{z}} \end{bmatrix}$$

$$\frac{\partial^2 V_{x,k}}{\partial \phi^2} = \begin{bmatrix} 0 & c\phi s\psi - s\phi s\theta c\psi & -s\phi s\psi - c\phi s\theta c\psi \end{bmatrix} \vec{a}$$

$$\frac{\partial^2 V_{x,k}}{\partial \theta^2} = T_s^y \begin{bmatrix} c\theta c\psi & -s\phi s\theta c\psi & -c\phi s\theta c\psi \end{bmatrix} \vec{a} \tag{327}$$

$$\frac{\partial^2 V_{x,k}}{\partial \psi^2} = T_s^y \begin{bmatrix} -c\theta c\psi & c\phi s\psi - s\phi s\theta c\psi & -s\phi s\psi - c\phi s\theta c\psi \end{bmatrix} \vec{a}$$

$$\frac{\partial^2 V_{x,k}}{\partial \phi \partial \theta} = T_s^y \begin{bmatrix} 0 & c\phi c\theta c\psi & -s\phi c\theta c\psi \end{bmatrix} \vec{a}$$

$$\frac{\partial^2 V_{x,k}}{\partial \phi \partial \psi} = T_s^y \begin{bmatrix} 0 & s\phi c\psi - c\phi s\theta s\psi & c\phi c\psi + s\phi s\theta s\psi \end{bmatrix} \vec{a}$$

$$\frac{\partial^2 V_{x,k}}{\partial \theta \partial \psi} = T_s^y \begin{bmatrix} s\theta s\psi & -s\phi c\theta s\psi & -c\phi c\theta s\psi \end{bmatrix} \vec{a}$$

$$\mathbf{F}_{xx}^{\Delta V_y} = \begin{bmatrix} \frac{\partial^2 V_{y,k}}{\partial \phi^2} & \frac{\partial^2 V_{y,k}}{\partial \phi \partial \theta} & \frac{\partial^2 V_{y,k}}{\partial \phi \partial \psi} \\ \frac{\partial^2 V_{y,k}}{\partial \phi \partial \theta} & \frac{\partial^2 V_{y,k}}{\partial \theta^2} & \frac{\partial^2 V_{y,k}}{\partial \theta \partial \psi} \\ \frac{\partial^2 V_{y,k}}{\partial \phi \partial \psi} & \frac{\partial^2 V_{y,k}}{\partial \theta \partial \psi} & \frac{\partial^2 V_{y,k}}{\partial \psi^2} \end{bmatrix}, \quad \vec{a} = \begin{bmatrix} a_{\tilde{x}} \\ a_{\tilde{y}} \\ a_{\tilde{z}} \end{bmatrix}$$

$$\frac{\partial^2 V_{y,k}}{\partial \phi^2} = T_s^y \begin{bmatrix} 0 & -c\phi c\psi - s\phi s\theta s\psi & s\phi c\psi - c\phi s\theta s\psi \end{bmatrix} \vec{a}$$

$$\frac{\partial^2 V_{y,k}}{\partial \theta^2} = T_s^y \begin{bmatrix} -c\theta s\psi & -s\phi s\theta s\psi & -c\phi s\theta s\psi \end{bmatrix} \vec{a} \tag{328}$$

$$\frac{\partial^2 V_{y,k}}{\partial \psi^2} = T_s^y \begin{bmatrix} -c\theta s\psi & -c\phi c\psi - s\phi s\theta s\psi & s\phi c\psi - c\phi s\theta s\psi \end{bmatrix} \vec{a}$$

$$\frac{\partial^2 V_{y,k}}{\partial \phi \partial \theta} = T_s^y \begin{bmatrix} 0 & c\phi c\theta s\psi & -s\phi c\theta s\psi \end{bmatrix} \vec{a}$$

$$\frac{\partial^2 V_{y,k}}{\partial \phi \partial \psi} = T_s^y \begin{bmatrix} 0 & s\phi s\psi + c\phi s\theta c\psi & c\phi s\psi - s\phi s\theta c\psi \end{bmatrix} \vec{a}$$

$$\frac{\partial^2 V_{y,k}}{\partial \theta \partial \psi} = T_s^y \begin{bmatrix} -s\theta c\psi & s\phi c\theta c\psi & c\phi c\theta c\psi \end{bmatrix} \vec{a}$$

$$\mathbf{F}_{xx}^{\Delta V_z} = \begin{bmatrix} \frac{\partial^2 V_{z,k}}{\partial \phi^2} & \frac{\partial^2 V_{z,k}}{\partial \phi \partial \theta} & \frac{\partial^2 V_{z,k}}{\partial \phi \partial \psi} \\ \frac{\partial^2 V_{z,k}}{\partial \phi \partial \theta} & \frac{\partial^2 V_{z,k}}{\partial \theta^2} & \frac{\partial^2 V_{z,k}}{\partial \theta \partial \psi} \\ \frac{\partial^2 V_{z,k}}{\partial \phi \partial \psi} & \frac{\partial^2 V_{z,k}}{\partial \theta \partial \psi} & \frac{\partial^2 V_{z,k}}{\partial \psi^2} \end{bmatrix}, \quad \vec{a} = \begin{bmatrix} a_{\tilde{x}} \\ a_{\tilde{y}} \\ a_{\tilde{z}} \end{bmatrix}$$

$$\frac{\partial^2 V_{z,k}}{\partial \phi^2} = T_s^y \begin{bmatrix} 0 & -s\phi c\theta & -c\phi c\theta \end{bmatrix} \vec{a} \tag{329}$$

$$\frac{\partial^2 V_{z,k}}{\partial \theta^2} = T_s^y \begin{bmatrix} s\theta & -s\phi c\theta & -c\phi c\theta \end{bmatrix} \vec{a}$$

$$\frac{\partial^2 V_{z,k}}{\partial \phi \partial \theta} = T_s^y \begin{bmatrix} 0 & -c\phi s\theta & s\phi s\theta \end{bmatrix} \vec{a}$$

$$\frac{\partial^2 V_{z,k}}{\partial \psi^2} = \frac{\partial^2 V_{z,k}}{\partial \phi \partial \psi} = \frac{\partial^2 V_{z,k}}{\partial \theta \partial \psi} = 0$$

where $s\phi$ and $c\phi$ are used to abbreviate sin $\phi$ and cos $\phi$ respectively, and the states and inputs are evaluated at time step $k$.

Using these equations in conjunction with the bounds defined in (318), the maximum value of the Hessian for the prediction and observation was determined, thus defining the linearization error bounds

$$\begin{aligned} \kappa_{\phi} &= 0.4256 \\ \kappa_{\chi} &= 8.6787 \end{aligned} \tag{330}$$

The assumed bounds from (319), (321), (322), and (330) establish the necessary conditions in order to calculate the initialization error and noise bounds as determined by Reif *et al*. [40] in (73)

$$\begin{aligned} \alpha &= 3.7011 \cdot 10^{-7} \\ \kappa_{nonl} &= 5.8454 \cdot 10^{7} \\ \kappa_{noise} &= 1.4074 \cdot 10^{6} \\ \varepsilon &= 8.1112 \cdot 10^{-12} \\ \delta &= 2.2164 \cdot 10^{-32} \end{aligned} \tag{331}$$

Clearly, these bounds are too strict for the given problem, and further analysis needs to be done in order to demonstrate the stability of the system under more practical initialization error and noise bound requirements.

## 6.5 RELAXATION OF STABILITY BOUNDS

The work from this section was previously published in [162]. With the goal of relaxing the bounds derived using the methodology of Reif *et al*. [40], the stability problem is reconsidered here with respect to the specific 3-state GPS/INS attitude estimation problem. One primary difference between Reif *et al.* [40] and the work presented here is that Reif *et al*. presented an analysis of the one-step EKF, while here the two-step EKF is considered. It is remarked in [29] that while performance and transient

behavior may differ, the convergence properties are the same. For the two-step formulation, the estimation error and its dynamics are derived as follows. Assume a nonlinear discrete-time system

$$\begin{aligned}\mathbf{x}_{k+1} &= \mathbf{f}(\mathbf{x}_k, \mathbf{u}_k) + \mathbf{w}_k \\ \mathbf{y}_k &= \mathbf{h}(\mathbf{x}_k, \mathbf{u}_k) + \mathbf{v}_k\end{aligned} \tag{332}$$

where **f** and **h** are the nonlinear prediction and observation functions respectively, and **w** and **v** are zero-mean, uncorrelated, white, Gaussian noise processes with assumed covariance matrices **Q** and **R** respectively. Note that the true covariance of these processes is typically unknown, and for stochastic stability of this system these covariance matrices will need to be bounded. This noise bounding is discussed later in this dissertation. Using the EKF, the state estimate can be obtained using

$$\hat{\mathbf{x}}_{k+1} = \mathbf{f}(\hat{\mathbf{x}}_k, \mathbf{u}_k) + \mathbf{K}_k \left[ \mathbf{y}_k - \mathbf{h}\left(\mathbf{f}(\hat{\mathbf{x}}_k, \mathbf{u}_k), \mathbf{u}_k\right) \right] \tag{333}$$

where **K** is the Kalman gain matrix, and the ^ indicates that the corresponding value is an estimate. The state estimate error, denoted by ~, can now be defined using (332) and (333)

$$\begin{aligned}\tilde{\mathbf{x}}_k &= \mathbf{x}_k - \hat{\mathbf{x}}_k \\ \tilde{\mathbf{x}}_{k+1} &= \mathbf{f}(\mathbf{x}_k, \mathbf{u}_k) + \mathbf{w}_k - \mathbf{f}(\hat{\mathbf{x}}_k, \mathbf{u}_k) - \mathbf{K}_k \left[ \mathbf{y}_k - \mathbf{h}\left(\mathbf{f}(\hat{\mathbf{x}}_k, \mathbf{u}_k), \mathbf{u}_k\right) \right] \\ \tilde{\mathbf{x}}_{k+1} &= \mathbf{f}(\mathbf{x}_k, \mathbf{u}_k) + \mathbf{w}_k - \mathbf{f}(\hat{\mathbf{x}}_k, \mathbf{u}_k) - \mathbf{K}_k \left[ \mathbf{h}(\mathbf{x}_k, \mathbf{u}_k) + \mathbf{v}_k - \mathbf{h}\left(\mathbf{f}(\hat{\mathbf{x}}_k, \mathbf{u}_k), \mathbf{u}_k\right) \right]\end{aligned} \tag{334}$$

Next, the linearization errors are defined using

$$\begin{aligned}\mathbf{f}(\mathbf{x}_k, \mathbf{u}_k) - \mathbf{f}(\hat{\mathbf{x}}_k, \mathbf{u}_k) &= \mathbf{A}_k \left( \mathbf{x}_k - \hat{\mathbf{x}}_k \right) + \boldsymbol{\varphi}\left( \mathbf{x}_k, \hat{\mathbf{x}}_k, \mathbf{u}_k \right) \\ \mathbf{h}(\mathbf{x}_k, \mathbf{u}_k) - \mathbf{h}\left(\mathbf{f}(\hat{\mathbf{x}}_k, \mathbf{u}_k), \mathbf{u}_k\right) &= \mathbf{H}_k \mathbf{A}_k \left( \mathbf{x}_k - \hat{\mathbf{x}}_k \right) + \boldsymbol{\chi}\left( \mathbf{x}_k, \hat{\mathbf{x}}_k, \mathbf{u}_k \right)\end{aligned} \tag{335}$$

where $\boldsymbol{\varphi}$ and $\boldsymbol{\chi}$ are the unknown prediction and observation linearization error functions respectively. Using these definitions, the error dynamics can be rewritten as

$$\tilde{\mathbf{x}}_{k+1} = \mathbf{A}_k \tilde{\mathbf{x}}_k + \boldsymbol{\varphi}\left(\mathbf{x}_k, \hat{\mathbf{x}}_k, \mathbf{u}_k\right) + \mathbf{w}_k - \mathbf{K}_k \left[\mathbf{H}_k \mathbf{A}_k \tilde{\mathbf{x}}_k + \boldsymbol{\chi}\left(\mathbf{x}_k, \hat{\mathbf{x}}_k, \mathbf{u}_k\right) + \mathbf{v}_k\right] \tag{336}$$

These dynamics can be separated into three parts, the homogeneous or linearized problem, the nonlinearity problem, and the stochastic problem. A summary of the error dynamics is given by

$$\begin{aligned} \tilde{\mathbf{x}}_k &= \mathbf{x}_k - \hat{\mathbf{x}}_k \\ \tilde{\mathbf{x}}_{k+1} &= (\mathbf{I} - \mathbf{K}_k \mathbf{H}_k)\mathbf{A}_k \tilde{\mathbf{x}}_k + \mathbf{r}_k + \mathbf{s}_k \\ \mathbf{r}_k &= \boldsymbol{\varphi}(\mathbf{x}_k, \hat{\mathbf{x}}_k, \mathbf{u}_k) - \mathbf{K}_k \boldsymbol{\chi}(\mathbf{x}_k, \hat{\mathbf{x}}_k, \mathbf{u}_k) \\ \mathbf{s}_k &= \mathbf{w}_k - \mathbf{K}_k \mathbf{v}_k \end{aligned} \tag{337}$$

where the **r** term corresponds to linearization error, the **s** term corresponds to stochastic error, and the remaining term represents the homogeneous problem (linearized deterministic system). With this error definition, the following function is considered as the candidate Lyapunov function

$$V_k\left(\tilde{\mathbf{x}}_k\right) = \tilde{\mathbf{x}}_k^T \mathbf{P}_k^{-1} \tilde{\mathbf{x}}_k \tag{338}$$

In order to analyze the stability of the EKF using these definitions, the problem can be decomposed into three components: homogeneous problem, linearization error problem, and noise problem. These individual components are considered separately in the following sections.

### 6.5.1 Analysis of Homogenous Problem

To consider the homogeneous part of the stability problem, we set the linearization error term, $\mathbf{r}_k$, and noise term, $\mathbf{s}_k$, to zero. Then the candidate Lyapunov function at time $k$+1 can be written as

$$V_{k+1}\left(\tilde{\mathbf{x}}_{k+1}\right)=\tilde{\mathbf{x}}_{k+1}^{T}\mathbf{P}_{k+1}^{-1}\tilde{\mathbf{x}}_{k+1}=\tilde{\mathbf{x}}_{k}^{T}\mathbf{A}_{k}^{T}\left(\mathbf{I}-\mathbf{K}_{k}\mathbf{H}_{k}\right)^{T}\mathbf{P}_{k+1}^{-1}\left(\mathbf{I}-\mathbf{K}_{k}\mathbf{H}_{k}\right)\mathbf{A}_{k}\tilde{\mathbf{x}}_{k} \tag{339}$$

Starting from (65), the covariance difference equation is given by

$$\mathbf{P}_{k+1}=\left(\mathbf{I}-\mathbf{K}_{k}\mathbf{H}_{k}\right)\left(\mathbf{A}_{k}\mathbf{P}_{k}\mathbf{A}_{k}^{T}+\mathbf{Q}_{k}\right) \tag{340}$$

Then, the inverse is taken, leading to

$$\mathbf{P}_{k+1}^{-1}=\left(\mathbf{A}_{k}\mathbf{P}_{k}\mathbf{A}_{k}^{T}+\mathbf{Q}_{k}\right)^{-1}\left(\mathbf{I}-\mathbf{K}_{k}\mathbf{H}_{k}\right)^{-1} \tag{341}$$

Rearranging, multiplying on the left by $\mathbf{A}_{k}^{T}\left(\mathbf{I}-\mathbf{K}_{k}\mathbf{H}_{k}\right)^{T}$ and on the right by $\mathbf{A}_{k}$ gives

$$\mathbf{A}_{k}^{T}\left(\mathbf{I}-\mathbf{K}_{k}\mathbf{H}_{k}\right)^{T}\mathbf{P}_{k+1}^{-1}\left(\mathbf{I}-\mathbf{K}_{k}\mathbf{H}_{k}\right)\mathbf{A}_{k}=\mathbf{A}_{k}^{T}\left(\mathbf{I}-\mathbf{K}_{k}\mathbf{H}_{k}\right)^{T}\left(\mathbf{A}_{k}\mathbf{P}_{k}\mathbf{A}_{k}^{T}+\mathbf{Q}_{k}\right)^{-1}\mathbf{A}_{k} \tag{342}$$

Next, the inverse term on the right hand side is reorganized

$$\mathbf{A}_{k}^{T}\left(\mathbf{I}-\mathbf{K}_{k}\mathbf{H}_{k}\right)^{T}\mathbf{P}_{k+1}^{-1}\left(\mathbf{I}-\mathbf{K}_{k}\mathbf{H}_{k}\right)\mathbf{A}_{k}=\mathbf{A}_{k}^{T}\left(\mathbf{I}-\mathbf{K}_{k}\mathbf{H}_{k}\right)^{T}\mathbf{A}_{k}^{-T}\left(\mathbf{I}+\mathbf{P}_{k}^{-1}\mathbf{A}_{k}^{-1}\mathbf{Q}_{k}\mathbf{A}_{k}^{-T}\right)^{-1}\mathbf{P}_{k}^{-1} \tag{343}$$

Following the work of Reif *et al*. [40], the following bound is desired

$$\mathbf{A}_{k}^{T}\left(\mathbf{I}-\mathbf{K}_{k}\mathbf{H}_{k}\right)^{T}\mathbf{P}_{k+1}^{-1}\left(\mathbf{I}-\mathbf{K}_{k}\mathbf{H}_{k}\right)\mathbf{A}_{k}\leq\left(1-\alpha\right)\mathbf{P}_{k}^{-1} \tag{344}$$

where $\alpha$ is some constant between 0 and 1. Therefore the following upper bound is desired

$$\mathbf{A}_{k}^{T}\left(\mathbf{I}-\mathbf{K}_{k}\mathbf{H}_{k}\right)^{T}\mathbf{A}_{k}^{-T}\left(\mathbf{I}+\mathbf{P}_{k}^{-1}\mathbf{A}_{k}^{-1}\mathbf{Q}_{k}\mathbf{A}_{k}^{-T}\right)^{-1}\leq\left(1-\alpha\right)\mathbf{I} \tag{345}$$

Using the definition of $\mathbf{K}$ from (65), the following is written

$$\mathbf{K}_{k}\mathbf{H}_{k}=\mathbf{P}_{k|k-1}\mathbf{H}_{k}^{T}\left(\mathbf{H}_{k}\mathbf{P}_{k|k-1}\mathbf{H}_{k}^{T}+\mathbf{R}_{k}\right)^{-1}\mathbf{H}_{k}>0 \tag{346}$$

This matrix is positive definite by definition, since the predicted covariance and measurement noise covariance are both positive definite. Since a similarity transformation does not change the eigenvalues of a matrix [48], it will also not change the positive definiteness of the matrix, therefore

$$\mathbf{A}_k^{-1}\mathbf{K}_k\mathbf{H}_k\mathbf{A}_k > 0 \tag{347}$$

Because of this property, the following bound is written

$$\mathbf{A}_k^T\left(\mathbf{I}-\mathbf{K}_k\mathbf{H}_k\right)^T\mathbf{A}_k^{-T} = \left(\mathbf{I}-\mathbf{A}_k^{-1}\mathbf{K}_k\mathbf{H}_k\mathbf{A}_k\right)^T < \mathbf{I} \tag{348}$$

Now, the desired bound is reduced to the following condition

$$\left(\mathbf{I}+\mathbf{P}_k^{-1}\mathbf{A}_k^{-1}\mathbf{Q}_k\mathbf{A}_k^{-T}\right)^{-1} \le (1-\alpha)\mathbf{I} \tag{349}$$

To simplify the calculation of this bound, the following steps are used

$$\begin{aligned}
&\left(\frac{1}{1-\alpha}\right)\mathbf{I} \le \mathbf{I}+\mathbf{P}_k^{-1}\mathbf{A}_k^{-1}\mathbf{Q}_k\mathbf{A}_k^{-T} \\
&\left(\frac{1}{1-\alpha}-1\right)\mathbf{I} \le \mathbf{P}_k^{-1}\mathbf{A}_k^{-1}\mathbf{Q}_k\mathbf{A}_k^{-T} \le \frac{1}{p_1}\mathbf{A}_k^{-1}\mathbf{Q}_k\mathbf{A}_k^{-T} \\
&\mathbf{A}_k^{-1}\mathbf{Q}_k\mathbf{A}_k^{-T} \ge p_1\left(\frac{1}{1-\alpha}-1\right)\mathbf{I} \equiv \alpha_1\mathbf{I}
\end{aligned} \tag{350}$$

where $\alpha_1$ is an intermediate bound, which can be calculated as the minimum eigenvalue of $\mathbf{A}_k^{-1}\mathbf{Q}_k\mathbf{A}_k^{-T}$ over all possible values in (318) using (124) and (320)

$$\alpha_1 = 5.1729\cdot 10^{-8} \tag{351}$$

From this intermediate bound, the desired bound, $\alpha$, can be calculated using

$$\begin{aligned}
&\alpha = 1-\left(1+\frac{\alpha_1}{p_1}\right)^{-1} \\
&\alpha = 3.8020\cdot 10^{-3}
\end{aligned} \tag{352}$$

This larger value indicates a faster convergence of the estimation error than the preliminary analysis. Using this new value for $\alpha$ but keeping the same nonlinearity and noise assumptions, the bounds on the initialization error and noise are recalculated. These results are compared with the original preliminary analysis in Table 15.

Table 15. Comparison of Preliminary Analysis and Relaxed Homogeneous Problem

| Value | Variable | Preliminary Analysis | Relaxed Homogeneous Problem |
|---|---|---|---|
| Convergence Rate | $\alpha$ | $3.7011 \cdot 10^{-7}$ | $3.8020 \cdot 10^{-3}$ |
| Initialization Error Bound | $\varepsilon$ | $8.1112 \cdot 10^{-12}$ | $8.3322 \cdot 10^{-8}$ |
| Noise Bound | $\delta$ | $2.2164 \cdot 10^{-32}$ | $2.4026 \cdot 10^{-20}$ |

A clear improvement in the convergence rate and bounds is shown in Table 15. The relaxation of the homogeneous problem shown here also provides potential reduction in the noise and nonlinearity problems as well. These problems are considered in the following sections.

### 6.5.2 Analysis of Noise Problem

When considering the noise problem, the important corresponding term in the candidate Lyapunov function is defined by

$$\mathbf{s}_k^T \mathbf{P}_{k+1}^{-1} \mathbf{s}_k = \left( \mathbf{w}_k - \mathbf{K}_k \mathbf{v}_k \right)^T \mathbf{P}_{k+1}^{-1} \left( \mathbf{w}_k - \mathbf{K}_k \mathbf{v}_k \right) \tag{353}$$

Since this represents the stochastic part of the problem, the expectation operator is applied to the equation. Since the process noise and measurement noise are uncorrelated, terms in the expectation containing both $\mathbf{w}_k$ and $\mathbf{v}_k$ are zero. Thus, the noise term is simplified

$$E\left[ \mathbf{s}_k^T \mathbf{P}_{k+1}^{-1} \mathbf{s}_k \right] = E\left[ \mathbf{w}_k^T \mathbf{P}_{k+1}^{-1} \mathbf{w}_k \right] + E\left[ \mathbf{v}_k^T \mathbf{K}_k^T \mathbf{P}_{k+1}^{-1} \mathbf{K}_k \mathbf{v}_k \right] \tag{354}$$

Now, the process and measurement noise components can be handled separately.

The process noise term is considered first

$$E\left[\mathbf{w}_k^T\mathbf{P}_{k+1}^{-1}\mathbf{w}_k\right]=E\left[\mathbf{w}_k^T\left\{\left(\mathbf{A}_k\mathbf{P}_k\mathbf{A}_k^T+\mathbf{Q}_k\right)^{-1}+\mathbf{H}_k^T\mathbf{R}_k^{-1}\mathbf{H}_k\right\}\mathbf{w}_k\right] \tag{355}$$

Since this is a scalar equation, the trace operator can be applied to both sides

$$Tr\left\{E\left[\mathbf{w}_k^T\mathbf{P}_{k+1}^{-1}\mathbf{w}_k\right]\right\}=Tr\left\{E\left[\mathbf{w}_k^T\left\{\left(\mathbf{A}_k\mathbf{P}_k\mathbf{A}_k^T+\mathbf{Q}_k\right)^{-1}+\mathbf{H}_k^T\mathbf{R}_k^{-1}\mathbf{H}_k\right\}\mathbf{w}_k\right]\right\} \tag{356}$$

Using the well-known trace property (201), the equation is reordered, and the expectation is simplified by pulling out the non-random terms

$$E\left[\mathbf{w}_k^T\mathbf{P}_{k+1}^{-1}\mathbf{w}_k\right]=Tr\left(\left\{\left(\mathbf{A}_k\mathbf{P}_k\mathbf{A}_k^T+\mathbf{Q}_k\right)^{-1}+\mathbf{H}_k^T\mathbf{R}_k^{-1}\mathbf{H}_k\right\}E\left[\mathbf{w}_k\mathbf{w}_k^T\right]\right) \tag{357}$$

Next, it is assumed that there exists a constant upper bound, $\delta_w>0$, on the stochastic term such that

$$E\left\lfloor\mathbf{w}_k\mathbf{w}_k^T\right\rfloor\le\delta_w\mathbf{I} \tag{358}$$

Therefore the process noise term is bounded as in

$$E\left[\mathbf{w}_k^T\mathbf{P}_{k+1}^{-1}\mathbf{w}_k\right]\le Tr\left(\left(\mathbf{A}_k\mathbf{P}_k\mathbf{A}_k^T+\mathbf{Q}_k\right)^{-1}+\mathbf{H}_k^T\mathbf{R}_k^{-1}\mathbf{H}_k\right)\delta_w \tag{359}$$

The trace term is calculated for all possible values in (318), and the maximum value is taken to determine the following upper bound

$$\begin{aligned}&E\left[\mathbf{w}_k^T\mathbf{P}_{k+1}^{-1}\mathbf{w}_k\right]\le w_2\delta_w\\&w_2=2.9371\cdot10^5\end{aligned} \tag{360}$$

Now, the measurement noise term is considered. First, some simplifications are made to the following term

$$
\begin{aligned}
\mathbf{K}_k^T\mathbf{P}_{k+1}^{-1}\mathbf{K}_k &= \mathbf{K}_k^T\left\{\left(\mathbf{A}_k\mathbf{P}_k\mathbf{A}_k^T+\mathbf{Q}_k\right)^{-1}+\mathbf{H}_k^T\mathbf{R}_k^{-1}\mathbf{H}_k\right\}\\
&\quad\times\left(\mathbf{A}_k\mathbf{P}_k\mathbf{A}_k^T+\mathbf{Q}_k\right)\mathbf{H}_k^T\left\{\mathbf{H}_k\left(\mathbf{A}_k\mathbf{P}_k\mathbf{A}_k^T+\mathbf{Q}_k\right)\mathbf{H}_k^T+\mathbf{R}_k\right\}^{-1}\\
\mathbf{K}_k^T\mathbf{P}_{k+1}^{-1}\mathbf{K}_k &= \mathbf{K}_k^T\left\{\mathbf{I}+\mathbf{H}_k^T\mathbf{R}_k^{-1}\mathbf{H}_k\left(\mathbf{A}_k\mathbf{P}_k\mathbf{A}_k^T+\mathbf{Q}_k\right)\right\}\\
&\quad\times\mathbf{H}_k^T\left\{\mathbf{H}_k\left(\mathbf{A}_k\mathbf{P}_k\mathbf{A}_k^T+\mathbf{Q}_k\right)\mathbf{H}_k^T+\mathbf{R}_k\right\}^{-1}\\
\mathbf{K}_k^T\mathbf{P}_{k+1}^{-1}\mathbf{K}_k &= \mathbf{K}_k^T\left\{\mathbf{I}+\mathbf{H}_k^T\mathbf{R}_k^{-1}\mathbf{H}_k\left(\mathbf{A}_k\mathbf{P}_k\mathbf{A}_k^T+\mathbf{Q}_k\right)\right\}\\
&\quad\times\left\{\left(\mathbf{A}_k\mathbf{P}_k\mathbf{A}_k^T+\mathbf{Q}_k\right)+\mathbf{H}_k^{-1}\mathbf{R}_k\mathbf{H}_k^{-T}\right\}^{-1}\mathbf{H}_k^{-1}\\
\mathbf{K}_k^T\mathbf{P}_{k+1}^{-1}\mathbf{K}_k &= \mathbf{K}_k^T\mathbf{H}_k^T\mathbf{R}_k^{-1}\mathbf{H}_k\left\{\mathbf{H}_k^{-1}\mathbf{R}_k\mathbf{H}_k^{-T}+\left(\mathbf{A}_k\mathbf{P}_k\mathbf{A}_k^T+\mathbf{Q}_k\right)\right\}\\
&\quad\times\left\{\left(\mathbf{A}_k\mathbf{P}_k\mathbf{A}_k^T+\mathbf{Q}_k\right)+\mathbf{H}_k^{-1}\mathbf{R}_k\mathbf{H}_k^{-T}\right\}^{-1}\mathbf{H}_k^{-1}\\
\mathbf{K}_k^T\mathbf{P}_{k+1}^{-1}\mathbf{K}_k &= \mathbf{K}_k^T\mathbf{H}_k^T\mathbf{R}_k^{-1}\\
\mathbf{K}_k^T\mathbf{P}_{k+1}^{-1}\mathbf{K}_k &= \left\{\mathbf{H}_k\left(\mathbf{A}_k\mathbf{P}_k\mathbf{A}_k^T+\mathbf{Q}_k\right)\mathbf{H}_k^T+\mathbf{R}_k\right\}^{-1}\mathbf{H}_k\left(\mathbf{A}_k\mathbf{P}_k\mathbf{A}_k^T+\mathbf{Q}_k\right)\mathbf{H}_k^T\mathbf{R}_k^{-1}\\
\mathbf{K}_k^T\mathbf{P}_{k+1}^{-1}\mathbf{K}_k &= \left\{\mathbf{I}+\mathbf{H}_k^{-T}\left(\mathbf{A}_k\mathbf{P}_k\mathbf{A}_k^T+\mathbf{Q}_k\right)^{-1}\mathbf{H}_k^{-1}\mathbf{R}_k\right\}^{-1}\mathbf{R}_k^{-1}\\
\mathbf{K}_k^T\mathbf{P}_{k+1}^{-1}\mathbf{K}_k &= \left\{\mathbf{R}_k+\mathbf{R}_k\mathbf{H}_k^{-T}\left(\mathbf{A}_k\mathbf{P}_k\mathbf{A}_k^T+\mathbf{Q}_k\right)^{-1}\mathbf{H}_k^{-1}\mathbf{R}_k\right\}^{-1}
\end{aligned}
\tag{361}
$$

Using this simplification, the expectation of the measurement noise is given by

$$
E\left[\mathbf{v}_k^T\mathbf{K}_k^T\mathbf{P}_{k+1}^{-1}\mathbf{K}_k\mathbf{v}_k\right] = E\left[\mathbf{v}_k^T\left\{\mathbf{R}_k+\mathbf{R}_k\mathbf{H}_k^{-T}\left(\mathbf{A}_k\mathbf{P}_k\mathbf{A}_k^T+\mathbf{Q}_k\right)^{-1}\mathbf{H}_k^{-1}\mathbf{R}_k\right\}^{-1}\mathbf{v}_k\right] \tag{362}
$$

Applying the trace operator to both sides of this scalar equation

$$
Tr\left\{E\left[\mathbf{v}_k^T\mathbf{K}_k^T\mathbf{P}_{k+1}^{-1}\mathbf{K}_k\mathbf{v}_k\right]\right\} = Tr\left\{E\left[\mathbf{v}_k^T\left\{\mathbf{R}_k+\mathbf{R}_k\mathbf{H}_k^{-T}\left(\mathbf{A}_k\mathbf{P}_k\mathbf{A}_k^T+\mathbf{Q}_k\right)^{-1}\mathbf{H}_k^{-1}\mathbf{R}_k\right\}^{-1}\mathbf{v}_k\right]\right\} \tag{363}
$$

Reordering with the trace property (201), and moving the non-random terms outside of the expectation operator

$$
E\left[\mathbf{v}_k^T\mathbf{K}_k^T\mathbf{P}_{k+1}^{-1}\mathbf{K}_k\mathbf{v}_k\right] = Tr\left(\left\{\mathbf{R}_k+\mathbf{R}_k\mathbf{H}_k^{-T}\left(\mathbf{A}_k\mathbf{P}_k\mathbf{A}_k^T+\mathbf{Q}_k\right)^{-1}\mathbf{H}_k^{-1}\mathbf{R}_k\right\}^{-1}E\left[\mathbf{v}_k\mathbf{v}_k^T\right]\right) \tag{364}
$$

Next, it is assumed that there exists a constant upper bound, $\delta_v$>0, on the stochastic term such that

$$E\left\lfloor \mathbf{v}_k \mathbf{v}_k^T \right\rfloor \leq \delta_v \mathbf{I} \tag{365}$$

Therefore the measurement noise term is bounded as in

$$E\left[\mathbf{v}_k^T \mathbf{K}_k^T \mathbf{P}_{k+1}^{-1} \mathbf{K}_k \mathbf{v}_k\right] \leq Tr\left(\left\{\mathbf{R}_k + \mathbf{R}_k \mathbf{H}_k^{-T}\left(\mathbf{A}_k \mathbf{P}_k \mathbf{A}_k^T + \mathbf{Q}_k\right)^{-1} \mathbf{H}_k^{-1} \mathbf{R}_k\right\}^{-1}\right)\delta_v \tag{366}$$

The trace term is calculated for all possible values in (318), and the maximum value is taken to determine the following upper bound

$$\begin{aligned} &E\left[\mathbf{v}_k^T \mathbf{P}_{k+1}^{-1} \mathbf{v}_k\right] \leq v_2 \delta_v \\ &v_2 = 0.001176 \end{aligned} \tag{367}$$

Following the framework of Reif *et al*. [40], the following bound is desired

$$E\left[\mathbf{s}_k^T \mathbf{P}_{k+1}^{-1} \mathbf{s}_k\right] \leq \kappa_{noise} \delta \tag{368}$$

This bound assumes the same restriction on process and measurement noise. However, from this analysis it is seen that the bounds on process and measurement noise differ greatly. Based on the assumptions (358) and (365), the bound in (368) is modified to be

$$\begin{aligned} &E\left[\mathbf{s}_k^T \mathbf{P}_{k+1}^{-1} \mathbf{s}_k\right] \leq w_2 \delta_w + v_2 \delta_v \\ &\kappa_{noise} \delta = w_2 \delta_w + v_2 \delta_v \\ &\delta_v = \frac{\delta}{2} \\ &\delta_w = \frac{v_2}{w_2} \frac{\delta}{2} \\ &\kappa_{noise} = v_2 \end{aligned} \tag{369}$$

Using these new definitions, the process and measurement noise bounds are given by

$$\begin{aligned} \delta_w &= 5.7565 \cdot 10^{-20} \\ \delta_v &= 1.4383 \cdot 10^{-12} \end{aligned} \tag{370}$$

Comparing to the previous value from the relaxed homogeneous problem of $\delta = 2.4026 \cdot 10^{-20}$, a small improvement is seen in the process noise restriction; however a

significant improvement is achieved in the measurement noise restriction. Although these restrictions may still be too strict for application, they can be improved further by relaxing the conditions on the linearization error, which is discussed next.

### 6.5.3 Analysis of Linearization Error Problem

The linearization error problem introduces a great amount of difficulty into the stability analysis. In fact, it is this part of the problem that separates EKF stability analysis from the well-established linear KF stability. A major issue surrounding this problem is that the true state is not known, and therefore it becomes difficult to quantify the linearization error. Instead, the linearization error is analyzed by investigating theoretical bounds on the linearization error. This error is a function of the considered nonlinear function as well as the estimation error, which is also unknown since the true state is unknown. Currently, there are two primary methods of modeling the linearization error. Reif *et al*. [40] consider an additive linearization error term as in (67), while the work of Boutayeb *et al.* [34,46] and Xiong *et al*. [35] formulate the linearization error using a multiplicative linearization error term as in (81). Each of these methods then places bounds on the additive or multiplicative linearization error, although it is not clear how these bounds are determined. The estimation of these bounds is a critical part of the stability analysis.

Following the additive linearization error model of (67) as considered by Reif *et al*. [40], the bounds on the linearization error are determined using calculations of the Hessian, as described in the preliminary analysis in Section 6.4. In an effort to relax

these linearization error bounds, an alternative method was considered. This method is first described through a simple scalar nonlinear function for illustrative purposes, and then it is extended to the attitude estimation problem.

Consider the nonlinear function $f(x) = \sin(x)$. The additive linearization error can be written for this function as

$$\begin{aligned} \varphi(x_k, \hat{x}_k) &= f(x_k) - f(\hat{x}_k) - A_k(x_k - \hat{x}_k) \\ \varphi(x_k, \hat{x}_k) &= \sin(x_k) - \sin(\hat{x}_k) - \cos(\hat{x}_k)(x_k - \hat{x}_k) \end{aligned} \tag{371}$$

To approach this problem, a set of cases for both the true and estimated states are evaluated over a set interval, and the linearization error is calculated for each of these cases. In doing so, a two-dimensional grid on linearization error was constructed over the interval $-\pi$ to $\pi$ for both the true and estimated states, as shown in Figure 60.

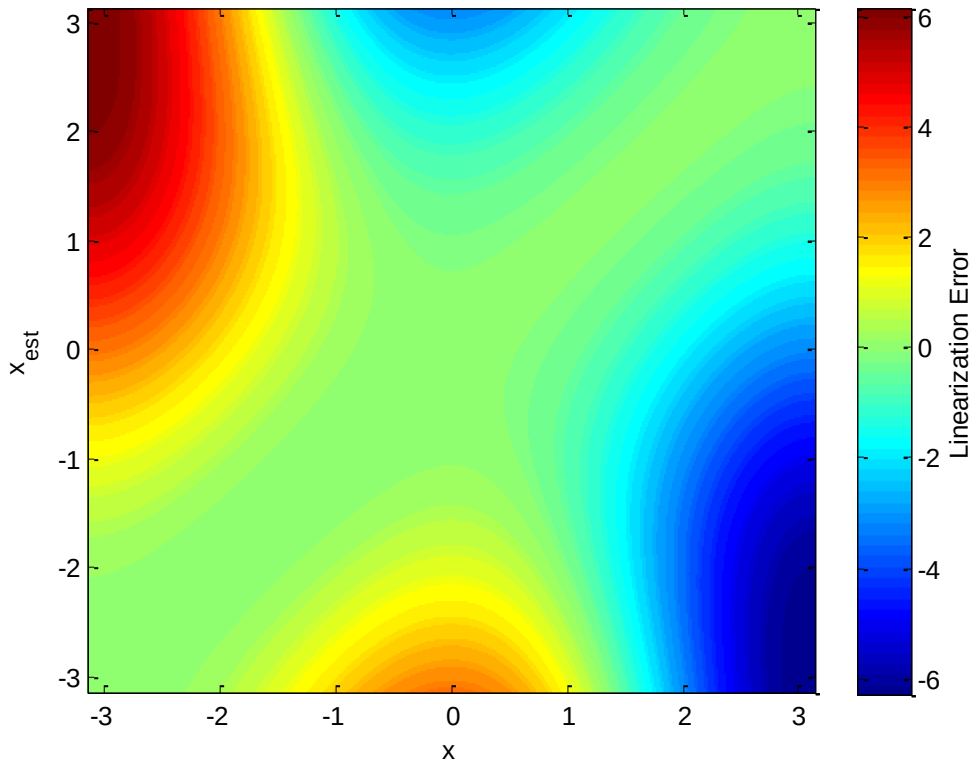


Figure 60. Linearization Error Map for $f(x) = \sin(x)$

In order to fit the linearization error bound structure of Reif *et al*. [40], the linearization error must be represented as a function of the estimation error only. Towards this end, each case of estimation error from the linearization error map in Figure 60 is calculated, and is shown in Figure 61.

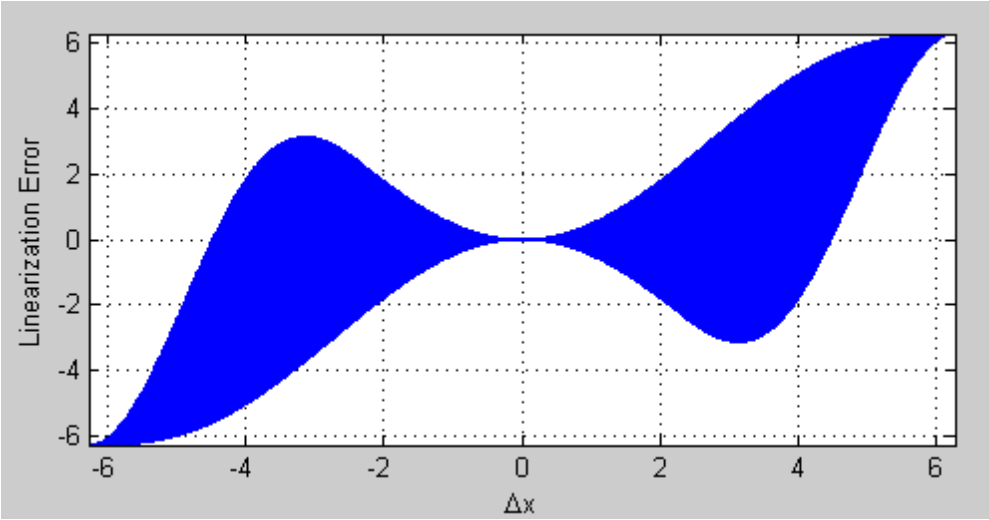


Figure 61. Linearization Error as Function of Estimation Error for $f(x) = \sin(x)$

Figure 61 shows the region of possible values of linearization error given the estimation error. The reason this is a region and not a single curve is due to the fact that the curvature of the function will lead to different values of linearization error based on the point of linearization. When considering a bound for linearization error as a function of the estimation error, the worst case of linearization error must be considered to ensure that the bound is always valid. For this purpose, the absolute value of the linearization error is considered. Additionally, it is desired to obtain a bound for the linearization error which is a function of the estimation error norm squared, as in (71). Therefore, the linearization error bound can be determined by selecting the smallest possible value of $\kappa_\varphi$

such that the linearization error remains bounded by (71). A visual representation of this procedure is shown in Figure 62.

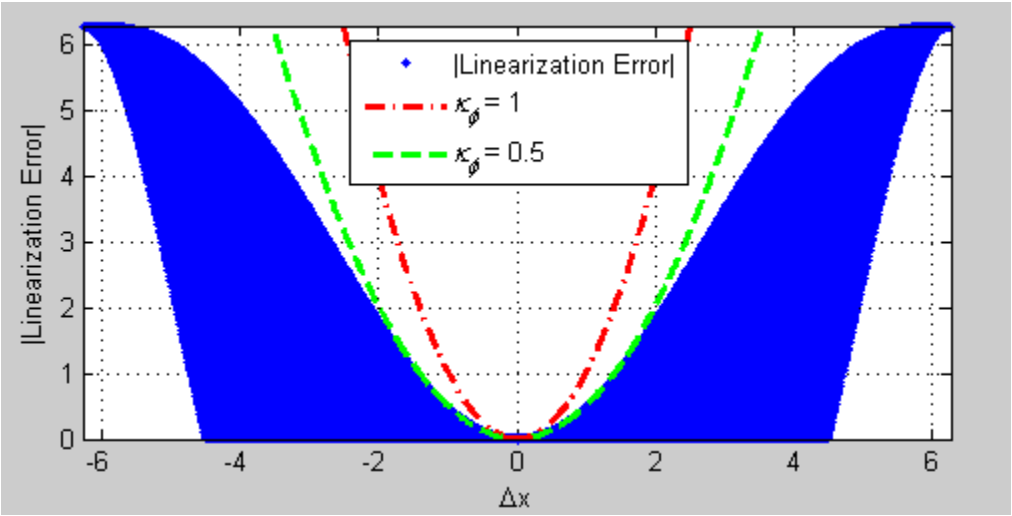


Figure 62. Linearization Error Bound Determination for $f(x) = \sin(x)$

From this method, the value of $\kappa_\varphi$ was determined to be 0.5. For comparison, the method of using the Hessian to determine the linearization error bound is also considered for this example. The Hessian for the sine function is given by the negative of the sine function, which is bounded in absolute value by 1, thus giving a value of $\kappa_\varphi$ of 1. Therefore, this new method of obtaining the linearization error bound was found to be less restrictive than using the Hessian for this example.

This new method can also be applied to higher order systems. In order to consider the relaxation of the linearization error bounds for the attitude estimation problem, this new method is applied to evaluate the linearization error over a set of possible cases of the true and estimated attitude states. First, the linearization error in the prediction is considered, using

$$\boldsymbol{\varphi}(\mathbf{x},\hat{\mathbf{x}},\mathbf{u}) = \mathbf{f}(\mathbf{x},\mathbf{u}) - \mathbf{f}(\hat{\mathbf{x}},\mathbf{u}) - \mathbf{A}(\mathbf{x}-\hat{\mathbf{x}}) \tag{372}$$

Inserting the definition of the state prediction function and Jacobian matrix leads to

$$\begin{aligned}\boldsymbol{\varphi}(\mathbf{x},\hat{\mathbf{x}},\mathbf{u}) = \mathbf{x}-\hat{\mathbf{x}} + T_s\left(\begin{bmatrix}1 & \sin\phi\tan\theta & \cos\phi\tan\theta\\ 0 & \cos\phi & -\sin\phi\\ 0 & \sin\phi\sec\theta & \cos\phi\sec\theta\end{bmatrix} - \begin{bmatrix}1 & \sin\hat{\phi}\tan\hat{\theta} & \cos\hat{\phi}\tan\hat{\theta}\\ 0 & \cos\hat{\phi} & -\sin\hat{\phi}\\ 0 & \sin\hat{\phi}\sec\hat{\theta} & \cos\hat{\phi}\sec\hat{\theta}\end{bmatrix}\right)\begin{bmatrix}p\\ q\\ r\end{bmatrix}\\ -\left(I + T_s\begin{bmatrix}\tan\hat{\theta}\left(q\cos\hat{\phi}-r\sin\hat{\phi}\right) & \sec^2\hat{\theta}\left(q\sin\hat{\phi}+r\cos\hat{\phi}\right) & 0\\ -\left(q\sin\hat{\phi}+r\cos\hat{\phi}\right) & 0 & 0\\ \sec\hat{\theta}\left(q\cos\hat{\phi}-r\sin\hat{\phi}\right) & \sec\hat{\theta}\tan\hat{\theta}\left(q\sin\hat{\phi}+r\cos\hat{\phi}\right) & 0\end{bmatrix}\right)\left(\mathbf{x}-\hat{\mathbf{x}}\right)\end{aligned} \tag{373}$$

After some simplification, the linearization error can be written as

$$\boldsymbol{\varphi}(\mathbf{x},\hat{\mathbf{x}},\mathbf{u}) = \begin{bmatrix} y\tan\theta - \hat{y}\tan\hat{\theta} - \hat{z}\tan\hat{\theta}\left(\phi-\hat{\phi}\right) - \hat{y}\sec^2\hat{\theta}\left(\theta-\hat{\theta}\right)\\ z-\hat{z}+\hat{z}\left(\theta-\hat{\theta}\right)\\ y\sec\theta - \hat{y}\sec\hat{\theta} - \sec\hat{\theta}\hat{z}\left(\phi-\hat{\phi}\right) - \hat{y}\sec\hat{\theta}\tan\hat{\theta}\left(\theta-\hat{\theta}\right)\end{bmatrix} \tag{374}$$

where

$$\begin{aligned} y &= q\sin\phi + r\cos\phi, \quad \hat{y} = q\sin\hat{\phi} + r\cos\hat{\phi}\\ z &= q\cos\phi - r\sin\phi, \quad \hat{z} = q\cos\hat{\phi} - r\sin\hat{\phi}\end{aligned} \tag{375}$$

From this relationship, it is shown that the linearization error is only a function of the true and estimated roll and pitch angles and the pitch and yaw rate inputs. The linearization error is not a function of the roll rate or the yaw angle. The possible cases of linearization error are plotted with respect to the estimation error norm in Figure 63.

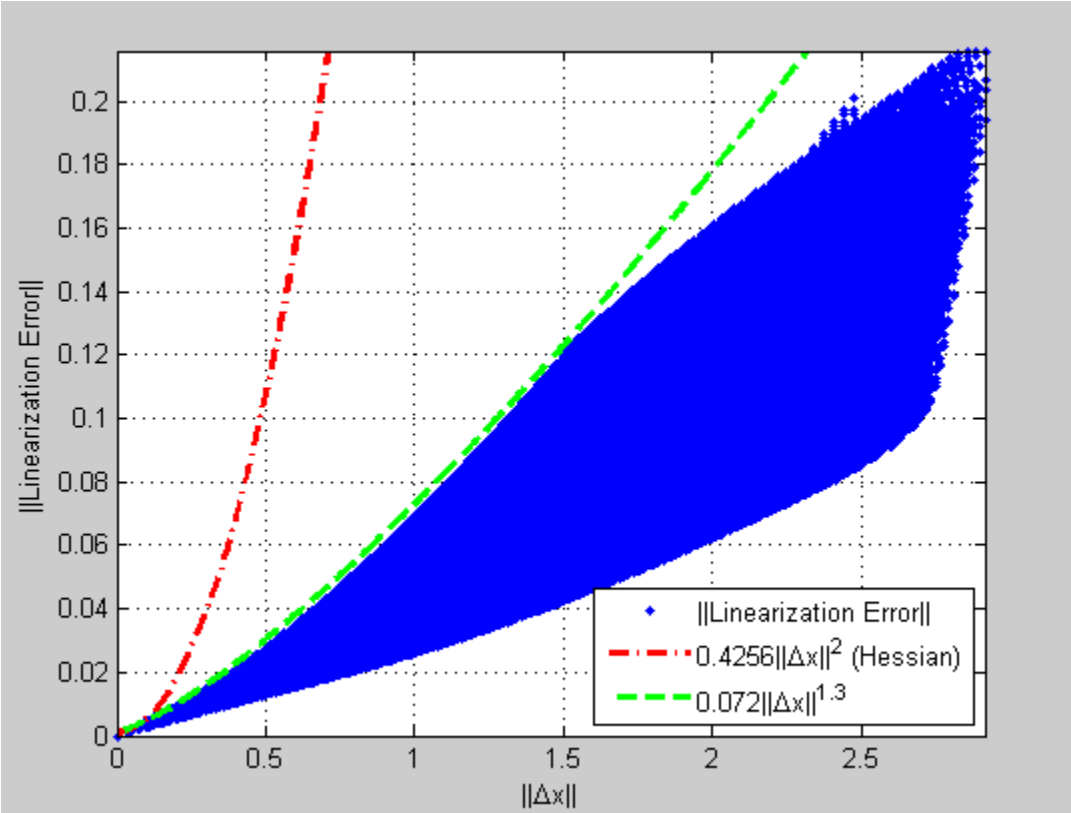


Figure 63. Prediction Linearization Error Bound Determination for Attitude Estimation

Figure 63 also shows the bound determined from using the Hessian as in the preliminary analysis in Section 6.4, as well as a new bound which was empirically fitted to the linearization error data set. When determining this new bound, the curvature of the linearization error was recognized to follow a slower rate than a quadratic function of the estimation error. This led to the new exponent for the estimation error norm of 1.3. As noted in [40], the stability proof can be modified for estimation error norm exponents that are greater than 1 and less than or equal to 2.

Next, the linearization error in the observation equations is considered, using the form

$$\boldsymbol{\chi}(\mathbf{x},\hat{\mathbf{x}},\mathbf{u}) = \mathbf{h}\left(\mathbf{x},\mathbf{u}\right) - \mathbf{h}\left(\hat{\mathbf{x}},\mathbf{u}\right) - \mathbf{H}(\mathbf{x}-\hat{\mathbf{x}}) \tag{376}$$

Inserting the definition of the observation function and Jacobian matrix leads to

$$\begin{aligned}
\boldsymbol{\chi}(\mathbf{x},\hat{\mathbf{x}},\mathbf{u}) = T_s^y \left(\mathbf{DCM}\left(\phi,\theta,\psi\right) - \mathbf{DCM}\left(\hat{\phi},\hat{\theta},\hat{\psi}\right)\right)\begin{bmatrix} a_{\tilde{x}} \\ a_{\tilde{y}} \\ a_{\tilde{z}} \end{bmatrix} \\
-\begin{bmatrix}
\left(s\hat{\psi}s\hat{\phi}+c\hat{\psi}s\hat{\theta}c\hat{\phi}\right)a_{\tilde{y}} + \left(s\hat{\psi}c\hat{\phi}-c\hat{\psi}s\hat{\theta}s\hat{\phi}\right)a_{\tilde{z}} & \left(-c\hat{\psi}s\hat{\theta}\right)a_{\tilde{x}} + \left(c\hat{\psi}c\hat{\theta}s\hat{\phi}\right)a_{\tilde{y}} + \left(c\hat{\psi}c\hat{\theta}c\hat{\phi}\right)a_{\tilde{z}} \\
\left(-c\hat{\psi}s\hat{\phi}+s\hat{\psi}s\hat{\theta}c\hat{\phi}\right)a_{\tilde{y}} + \left(-c\hat{\psi}c\hat{\phi}-s\hat{\psi}s\hat{\theta}s\hat{\phi}\right)a_{\tilde{z}} & \left(-s\hat{\psi}s\hat{\theta}\right)a_{\tilde{x}} + \left(s\hat{\psi}c\hat{\theta}s\hat{\phi}\right)a_{\tilde{y}} + \left(s\hat{\psi}c\hat{\theta}c\hat{\phi}\right)a_{\tilde{z}} \\
\left(c\hat{\theta}c\hat{\phi}\right)a_{\tilde{y}} + \left(-c\hat{\theta}s\hat{\phi}\right)a_{\tilde{z}} & \left(-c\hat{\theta}\right)a_{\tilde{x}} + \left(-s\hat{\theta}s\hat{\phi}\right)a_{\tilde{y}} + \left(-s\hat{\theta}c\hat{\phi}\right)a_{\tilde{z}}
\end{bmatrix} \\
\begin{bmatrix}
\ldots & \left(-s\hat{\psi}c\hat{\theta}\right)a_{\tilde{x}} + \left(-c\hat{\psi}c\hat{\phi}-s\hat{\psi}s\hat{\theta}s\hat{\phi}\right)a_{\tilde{y}} + \left(c\hat{\psi}s\hat{\phi}-s\hat{\psi}s\hat{\theta}c\hat{\phi}\right)a_{\tilde{z}} \\
\ldots & \left(c\hat{\psi}c\hat{\theta}\right)a_{\tilde{x}} + \left(-s\hat{\psi}c\hat{\phi}+c\hat{\psi}s\hat{\theta}s\hat{\phi}\right)a_{\tilde{y}} + \left(s\hat{\psi}s\hat{\phi}+c\hat{\psi}s\hat{\theta}c\hat{\phi}\right)a_{\tilde{z}} \\
\ldots & 0
\end{bmatrix}\begin{bmatrix} \phi-\hat{\phi} \\ \theta-\hat{\theta} \\ \psi-\hat{\psi} \end{bmatrix} T_s^y
\end{aligned} \tag{377}$$

where „*s*“ and „*c*“ denote the sine and cosine functions respectively. Similarly as for the prediction linearization error, the linearization error for the observation is shown in Figure 64.

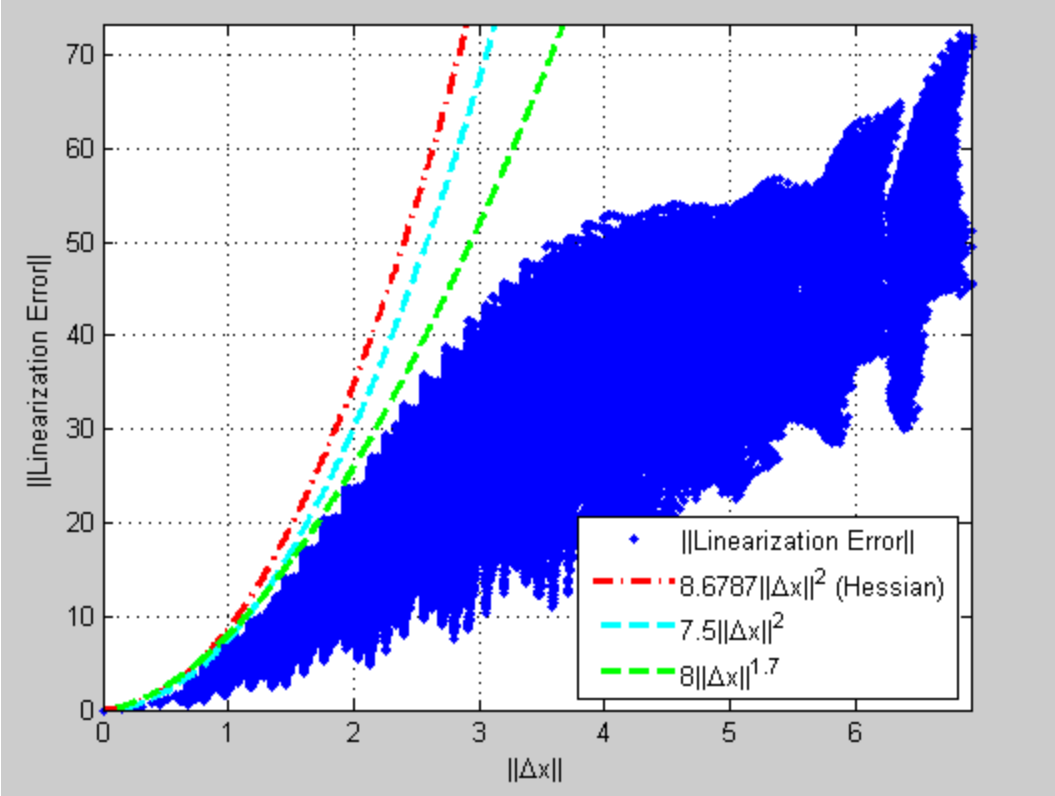


Figure 64. Observation Linearization Error Bound Determination for Attitude Estimation

Figure 64 also shows the bound determined from using the Hessian as in the preliminary analysis in Section 6.4, as well as two new bounds which were empirically fitted to the linearization error data set. The first new bound is given as a quadratic function of the linearization error with a reduced value of $\kappa_\chi$ from the Hessian method. The second new bound was determined using a smaller exponent of 1.7 in order to more closely match the trend of the linearization error. For the analysis, it is necessary for both exponents to match. Therefore, the larger exponent of 1.7 was selected, and the prediction linearization error was reconsidered, as shown in Figure 65.

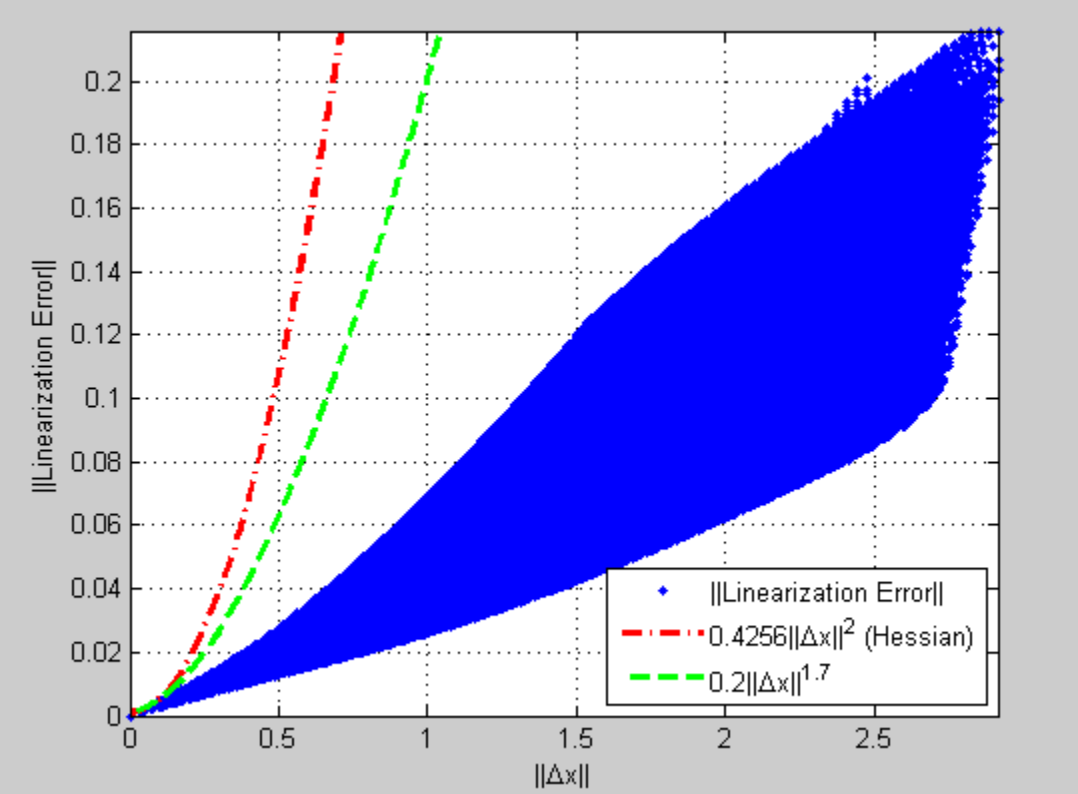


Figure 65. Modified Prediction Linearization Error Bound Determination for Attitude Estimation

Using this modified version, the linearization error is now represented by the following

$$\begin{aligned} &\left\|\boldsymbol{\varphi}(\mathbf{x},\hat{\mathbf{x}},\mathbf{u})\right\| \le \kappa_{\varphi}\left\|\tilde{\mathbf{x}}\right\|^{1+\beta} \\ &\left\|\boldsymbol{\chi}(\mathbf{x},\hat{\mathbf{x}},\mathbf{u})\right\| \le \kappa_{\chi}\left\|\tilde{\mathbf{x}}\right\|^{1+\beta} \\ &\kappa_{\varphi}=0.2, \quad \kappa_{\chi}=8.0, \quad \beta=0.7 \end{aligned} \tag{378}$$

This leads to the following modifications to (73)

$$\begin{aligned} \kappa_{nonl} &= \frac{\kappa'}{p_1}\left[2\left(a_2+\frac{a_2 p_2 h_2}{r_1}h_2\right)+\kappa'\left(\varepsilon'\right)^{\beta}\right] \\ \varepsilon &= \min\left(\varepsilon', \left(\frac{\alpha}{2p_2\kappa_{nonl}}\right)^{\beta}\right) \end{aligned} \tag{379}$$

Using the new bounds for the linearization error, the initial error and noise bounds are reduced to

$$\begin{aligned} \varepsilon &= 1.2057 \cdot 10^{-5} \\ \delta_w &= 2.4108 \cdot 10^{-15} \\ \delta_v &= 6.0235 \cdot 10^{-8} \end{aligned} \tag{380}$$

This completes the relaxation of bounds for EKF stability. The results from this analysis are summarized in Figure 66 and Table 16. Note that Figure 66 uses a logarithmic scale to represent the bounds, which are all less than 1. Therefore, for this figure, smaller bounds are represented by longer bars, *i.e.*, the shorter the bar, the less conservative the bound.

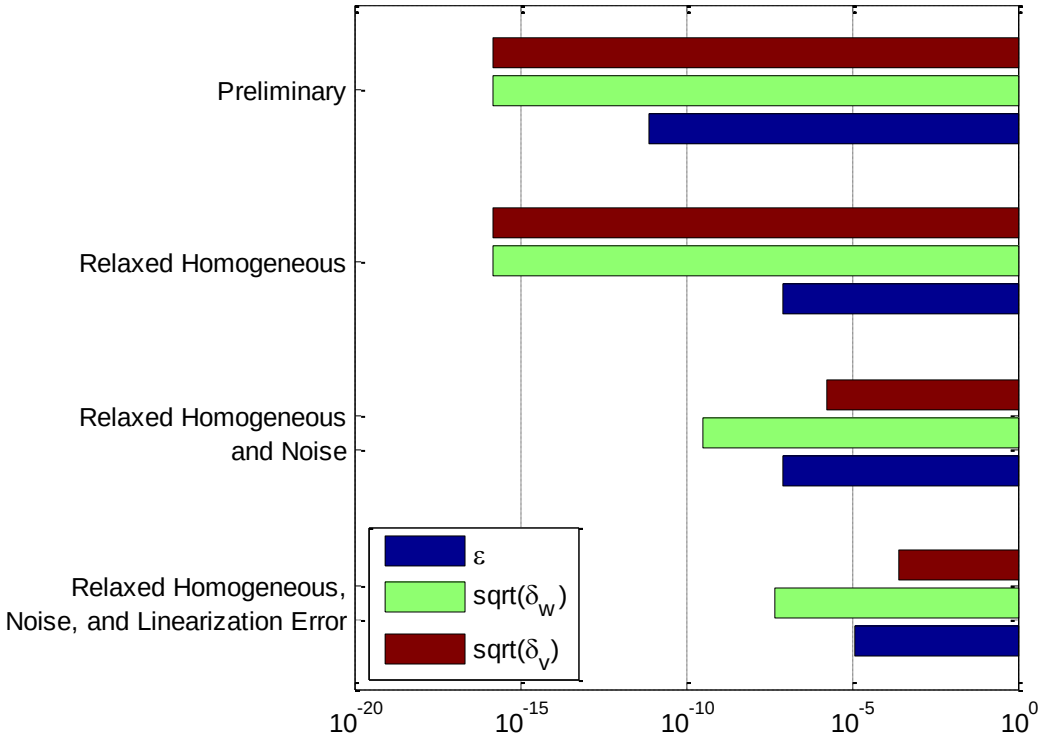


Figure 66. Summary of Relaxation of Stability Bounds

Table 16. Summary of Relaxation of Stability Bounds

| **Analysis** | $\varepsilon$ | $\delta_w$ | $\delta_v$ |
|---|---|---|---|
| Preliminary Analysis | $8.1112 \cdot 10^{-12}$ | $2.2164 \cdot 10^{-32}$ | $2.2164 \cdot 10^{-32}$ |
| Relaxed Homogeneous | $8.3322 \cdot 10^{-8}$ | $2.2164 \cdot 10^{-32}$ | $2.2164 \cdot 10^{-32}$ |
| Relaxed Homogenous and Noise | $8.3322 \cdot 10^{-8}$ | $1.1513 \cdot 10^{-19}$ | $2.8765 \cdot 10^{-12}$ |
| Relaxed Homogeneous, Noise, and Linearization Error | $1.2057 \cdot 10^{-5}$ | $2.4108 \cdot 10^{-15}$ | $6.0235 \cdot 10^{-8}$ |

This analysis presented a means of reducing the bounds on the initial error and noise terms required in order to guarantee the stability of an EKF. An example problem of attitude estimation was considered, which demonstrated significant reduction in the initial error and noise bounds over the existing methods. Unfortunately, even these greatly reduced bounds are not large enough for realistic application of the problem. However, this work has made significant improvement on the existing work in order to get closer to realistic application of EKF stability.

## 6.6 MULTIPLICATIVE LINEARIZATION ERROR ANALYSIS

Due to the overly strict bounds for stability using the additive linearization error model, the multiplicative linearization error model was also considered. Additionally, a linear measurement model was considered to help simplify the equations. Following the previous analyses using the stochastic stability lemma but using a multiplicative linearization model leads to the following Lyapunov difference equation

$$\tilde{\mathbf{x}}_{k-1}^T \mathbf{F}_{k-1}^T \boldsymbol{\beta}_{k-1}^T \left(\mathbf{I}-\mathbf{K}_k\mathbf{H}_k\right)^T \mathbf{P}_k^{-1} \left(\mathbf{I}-\mathbf{K}_k\mathbf{H}_k\right) \boldsymbol{\beta}_{k-1} \mathbf{F}_{k-1} \tilde{\mathbf{x}}_{k-1} \leq \left(1-\alpha_{k-1}\right) \tilde{\mathbf{x}}_{k-1}^T \mathbf{P}_{k-1}^{-1} \tilde{\mathbf{x}}_{k-1} \qquad (381)$$

This inequality can be simplified using the following steps

$$
\begin{aligned}
&\mathbf{F}_{k-1}^T\boldsymbol{\beta}_{k-1}^T\mathbf{P}_{k|k-1}^{-1}\mathbf{P}_k\mathbf{P}_{k|k-1}^{-1}\boldsymbol{\beta}_{k-1}\mathbf{F}_{k-1} \le \left(1-\alpha_{k-1}\right)\mathbf{F}_{k-1}^T\left(\mathbf{P}_{k|k-1}-\mathbf{Q}_{k-1}\right)^{-1}\mathbf{F}_{k-1}\\
&\boldsymbol{\beta}_{k-1}^T\mathbf{P}_{k|k-1}^{-1}\mathbf{P}_k\mathbf{P}_{k|k-1}^{-1}\boldsymbol{\beta}_{k-1} \le \left(1-\alpha_{k-1}\right)\left(\mathbf{P}_{k|k-1}-\mathbf{Q}_{k-1}\right)^{-1}\\
&\boldsymbol{\beta}_{k-1}^T\left(\mathbf{P}_{k|k-1}+\mathbf{P}_{k|k-1}\mathbf{H}_k^T\mathbf{R}_k^{-1}\mathbf{H}_k\mathbf{P}_{k|k-1}\right)^{-1}\boldsymbol{\beta}_{k-1}\left(\mathbf{P}_{k|k-1}-\mathbf{Q}_{k-1}\right) \le \left(1-\alpha_{k-1}\right)\mathbf{I}\\
&\alpha_{k-1}\mathbf{I} \le \mathbf{I}-\boldsymbol{\beta}_{k-1}^T\left(\mathbf{P}_{k|k-1}+\mathbf{P}_{k|k-1}\mathbf{H}_k^T\mathbf{R}_k^{-1}\mathbf{H}_k\mathbf{P}_{k|k-1}\right)^{-1}\boldsymbol{\beta}_{k-1}\left(\mathbf{P}_{k|k-1}-\mathbf{Q}_{k-1}\right)\\
&\alpha_{k-1}\mathbf{I} \le \left(\mathbf{P}_{k|k-1}+\mathbf{P}_{k|k-1}\mathbf{H}_k^T\mathbf{R}_k^{-1}\mathbf{H}_k\mathbf{P}_{k|k-1}\right)^{-1}\\
&\qquad\qquad \times\left[\mathbf{P}_{k|k-1}+\mathbf{P}_{k|k-1}\mathbf{H}_k^T\mathbf{R}_k^{-1}\mathbf{H}_k\mathbf{P}_{k|k-1}-\boldsymbol{\beta}_{k-1}\left(\mathbf{P}_{k|k-1}-\mathbf{Q}_{k-1}\right)\boldsymbol{\beta}_{k-1}^T\right]
\end{aligned}
\tag{382}
$$

Now, from this form, the requirement that the convergence rate be between 0 and 1, and the positive definiteness of various terms in the inequality leads to the following reduced inequality

$$
\mathbf{P}_{k|k-1}+\mathbf{P}_{k|k-1}\mathbf{H}_k^T\mathbf{R}_k^{-1}\mathbf{H}_k\mathbf{P}_{k|k-1} > \boldsymbol{\beta}_{k-1}\left(\mathbf{P}_{k|k-1}-\mathbf{Q}_{k-1}\right)\boldsymbol{\beta}_{k-1}^T \tag{383}
$$

This inequality is a function of the unknown diagonal matrix $\boldsymbol{\beta}$ and other matrices which are known for the system at any given time step. Therefore, at any given time step, this inequality can be evaluated in order to determine acceptable values for $\boldsymbol{\beta}$. Additionally, for each acceptable value of $\boldsymbol{\beta}$, the convergence rate $\alpha$ can be calculated by taking the minimum eigenvalue of the right hand side matrix in the last inequality of (382).

As a starting point, consider the first time step of the filter, *i.e.* $k = 1$. At this time step, the assumed initial state and covariance are known, the noise covariance matrices are known, and the other matrices of interest can be calculated from these terms with the exception of $\boldsymbol{\beta}$, as in

$$
\begin{aligned}
\mathbf{F}_{k-1} &= \left.\frac{\partial \mathbf{f}}{\partial \mathbf{x}}\right|_{\hat{\mathbf{x}}_{k-1}} \\
\mathbf{P}_{k|k-1} &= \mathbf{F}_{k-1}\mathbf{P}_{k-1}\mathbf{F}_{k-1}^{T} + \mathbf{Q}_{k-1} \\
\hat{\mathbf{x}}_{k|k-1} &= \mathbf{f}\left(\hat{\mathbf{x}}_{k-1}\right) \\
\mathbf{H}_{k} &= \left.\frac{\partial \mathbf{h}}{\partial \mathbf{x}}\right|_{\hat{\mathbf{x}}_{k|k-1}}
\end{aligned}
\tag{384}
$$

Since $\boldsymbol{\beta}$ is the only unknown in the inequality, it can be evaluated for a given problem in order to determine the acceptable values of $\boldsymbol{\beta}$ to guarantee the Lyapunov difference equation, thus demonstrating the stability of the estimation. Once the acceptable values of $\boldsymbol{\beta}$ have been determined, using the definition of the multiplicative linearization error, various cases of initial error can be used to calculate the actual value of $\boldsymbol{\beta}$ for that level of error. *I.e.*, the following equation is solved for $\boldsymbol{\beta}$ over many different cases of initial error

$$
\mathbf{f}\left(\hat{\mathbf{x}}_{k-1} + \tilde{\mathbf{x}}_{k-1}\right) - \mathbf{f}\left(\hat{\mathbf{x}}_{k-1}\right) = \boldsymbol{\beta}_{k-1}\mathbf{F}_{k-1}\tilde{\mathbf{x}}_{k-1} \tag{385}
$$

This vector valued equation is easy to solve for $\boldsymbol{\beta}$, since $\boldsymbol{\beta}$ is a diagonal matrix, as in

$$
\boldsymbol{\beta}_{k-1}^{(i)} = \frac{\left[\mathbf{f}\left(\hat{\mathbf{x}}_{k-1} + \tilde{\mathbf{x}}_{k-1}\right) - \mathbf{f}\left(\hat{\mathbf{x}}_{k-1}\right)\right]^{(i)}}{\left[\mathbf{F}_{k-1}\tilde{\mathbf{x}}_{k-1}\right]^{(i)}} \tag{386}
$$

where the superscript $(i)$ denotes the $i^{\text{th}}$ element of the vector or diagonal component of the matrix. This calculation represents the true value of the multiplicative linearization error term, $\boldsymbol{\beta}$, as a function of the initial error. This function is then compared with the allowable values of $\boldsymbol{\beta}$ from the Lyapunov difference equation in order to select the largest allowable case of initial error in order for the estimation to be stable. To help illustrate this method an example problem is used.

The considered example problem is taken from Reif *et al.* [40]. The example problem is summarized as follows

$$\begin{aligned}\mathbf{f}\left(\mathbf{x}_k\right) &= \begin{bmatrix} x_{1,k} + \tau x_{2,k} \\ x_{2,k} + \tau\left(-x_{1,k} + \left(x_{1,k}^2 + x_{2,k}^2 - 1\right)x_{2,k}\right) \end{bmatrix} \\ h\left(\mathbf{x}_k\right) &= x_{1,k}\end{aligned} \tag{387}$$

where $\tau = 0.001$, and the assumed noise and initial conditions are given by

$$\begin{aligned}\mathbf{Q}_k &= \tau\mathbf{I} \\ R_k &= \tau^{-1} \\ \mathbf{P}_0 &= \mathbf{I} \\ \hat{\mathbf{x}}_0 &= \begin{bmatrix} 0.5 & 0.5 \end{bmatrix}^T\end{aligned} \tag{388}$$

First, the inequality in (383) is evaluated over a range of possible values for **β**. This leads to cases where the inequality is satisfied (acceptable **β** for stability) or cases when the inequality is not satisfied (unacceptable **β** for stability). To provide a visual representation of this result for this example problem, a color map is provided in Figure 67, where white indicates the region of acceptable values for **β**, while the black region represents the unacceptable values for **β**.

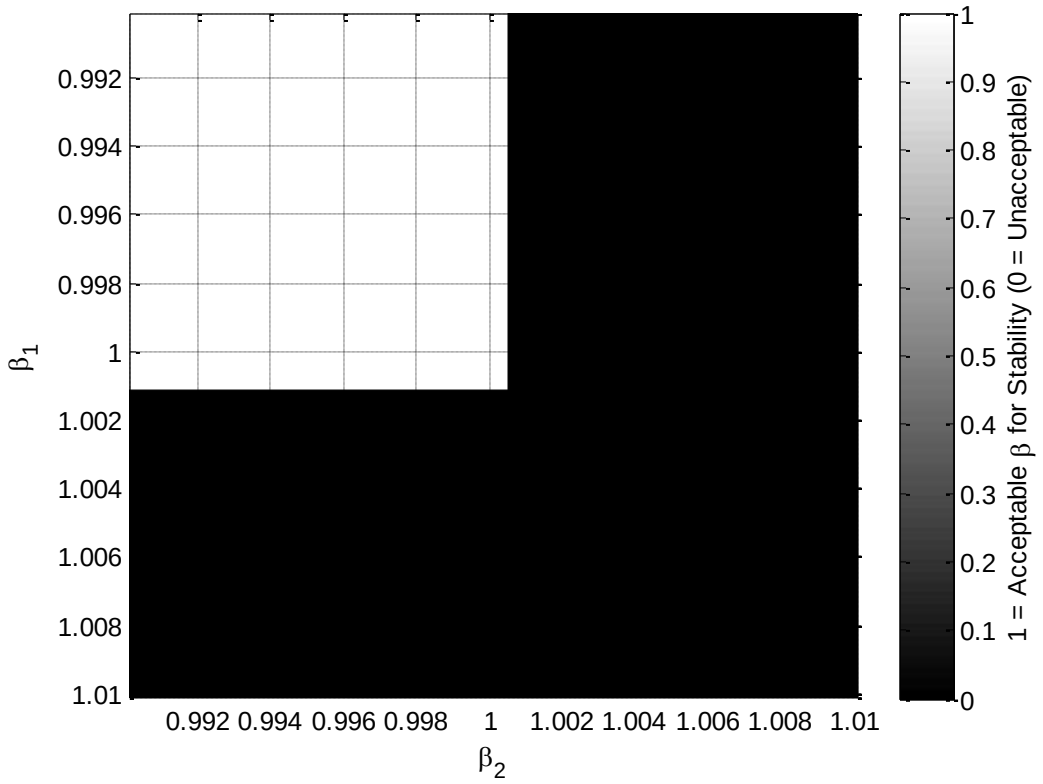


Figure 67. Acceptable Values of Multiplicative Linearization Error, **β**

An additional color map was generated in Figure 68 in order to illustrate the corresponding convergence rate, $\alpha$, for each case of **β**.

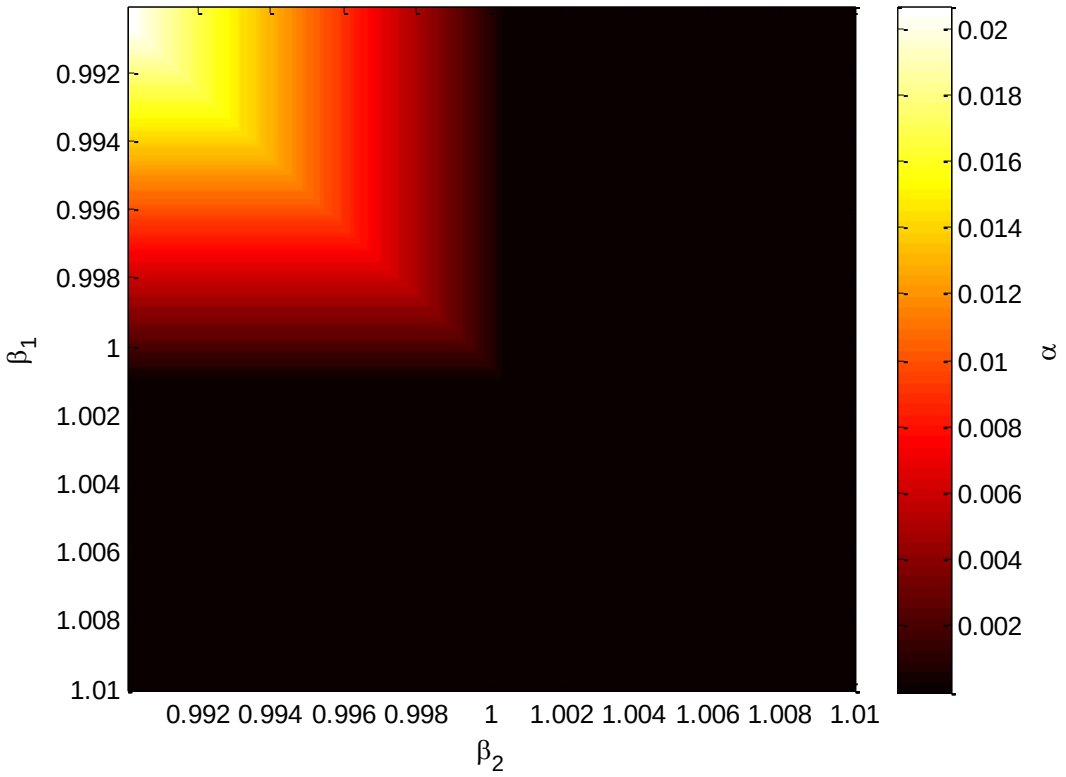


Figure 68. Convergence Rate as a Function of Multiplicative Linearization Error

In Figure 68, it is shown that smaller values of **β** lead to a larger (better) convergence rate of the estimation, as expected. Next, **β** is calculated as a function of possible cases of initial error using (386). From this calculation, and the observation that the dynamics of the first state are linear, the first component of **β** is always 1 for any case of initial error. This value lies in the acceptable region of **β** from the Lyapunov difference equation, as long as the second component of **β** is less than 1.004 (obtained from Figure 67). This simplifies the problem to examining the second component of **β** as a function of initial error, which is shown in Figure 69.

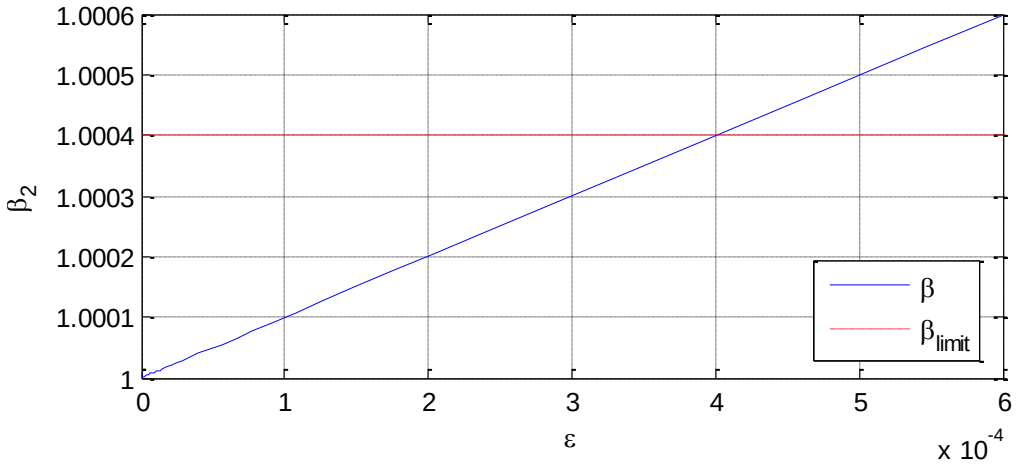


Figure 69. Multiplicative Linearization Error as a Function of Initial Error

From Figure 69 it is shown that in order for the multiplicative linearization error term, **β**, to be acceptable for stability, the norm of the initial error must be less than or equal to 0.0004. This value is very small, even smaller than the reported value from Reif *et al.* [40] of 0.005. Some other limitations of this method are that:

1. Knowledge of the error covariance and Jacobian matrices at the current time step are required, thus limiting this analysis to a step-wise approach;
2. This analysis could be repeated at each time step, but it is computationally expensive, and therefore not practical for real-time application;
3. Linear measurement equations are required.

Because of these problems, this method is not practical for use in proving the stability of the EKF. However, this analysis is useful in that it reveals some analytical justification using (383) for the following observations regarding the conditions for stability:

1. Smaller assumed measurement noise covariance, **R**, tends to improve stability;
2. Larger assumed process noise covariance, **Q**, tends to improve stability;
3. Larger assumed initial error covariance, $\mathbf{P}_0$, tends to improve stability.

It is important to note that these observations are for the assumed noise characteristics, not necessarily the true noise characteristics. Each of these observations makes intuitive sense and agrees with results seen in practice.

## 6.7 STABILITY ANALYSIS DISCUSSION

This chapter presented a detailed stability analysis of the EKF through the context of the attitude estimation problem and other simulated example problems. First, the state of the art stability analysis techniques were applied, yielding unrealistically strict bounds on the initial error and noise terms in order to prove the stability of the estimation. Significant effort was put into relaxing these strict bounds with reasonable success. However, even the significantly relaxed bounds were still too strict for practical use. Based on this analysis, it seems that the considered stability framework using the stochastic stability lemma and a quadratic form Lyapunov function may not be sufficient in order to analyze the estimation stability of the EKF for practical application. Further effort should be placed on the determination of other possible Lyapunov functions as well as other stochastic stability analysis techniques to apply to this problem.

One of the major difficulties with the current EKF stability framework is the requirement of constant bounds on the covariance and Jacobian matrices of the system. Because the EKF is a dynamic system, these bounds are forced to represent the worst possible case of each quantity, rather than the typical values. For example, the upper bound on the state error covariance matrix is typically given by the assumed initial error covariance matrix, which is often selected to be unnecessarily large in order to obtain

reasonable convergence of the filter. This large estimate tends to decrease in magnitude very quickly in order to converge to a more reasonable estimate of the expected errors at that time. Since this typical operating condition is much lower than the absolute maximum, the bound for the quantity is unnecessarily large, which effectively leads to unnecessarily strict bounds on other conditions for the system. While constant bounds have these issues, a time-varying bound suffers from other problems. Particularly, it becomes very difficult to demonstrate that quantities will remain bounded absolutely if this bound is allowed to change with time. This is a possible approach for on-line stability and performance monitoring, as discussed in Section 6.3, but does not offer a robust off-line approach for guaranteeing the stability of an estimation algorithm.

Another major difficulty regarding the current EKF stability analysis is the stochastic stability lemma framework, which is similar to Lyapunov stability analysis. For discrete-time, these techniques require a difference equation, which relates the stochastic process or Lyapunov function between two successive time steps. While it is relatively simple to relate these terms for linear systems, when considering a nonlinear estimation algorithm like the EKF, the error dynamics are given as a nonlinear function of the previous error. Because of this nonlinearity, it is difficult to relate the values between the two time steps. This issue could potentially be alleviated through the selection of an alternative Lyapunov function. Also, a new theoretical stability framework that could evaluate the error dynamics without using a standard difference equation is highly desired, and would greatly benefit this analysis.

# 7.0 CONCLUSIONS

This dissertation presented a thorough analysis of the nonlinear state estimation problem using the Kalman filtering framework. Most of the work was considered through an example application problem of low-cost aircraft attitude estimation for subscale aircraft. This example problem was considered due to the vast availability of experimental flight data within the research group. The experimental results were supported with simulation studies when necessary. There are two major topics within this dissertation. The first topic is comparison and sensitivity analysis, which offered a detailed analysis of two nonlinear Kalman filters (EKF and UKF) with respect to various design parameters. This study allowed for a comprehensive comparison of these two filters in order to determine their differences and relative advantages. The primary conclusion of this sensitivity analysis was that there are little differences between the EKF and UKF when the nonlinearities are small, which is the case for the considered attitude estimation problem. For this application problem, either filter could be used with similar results. The EKF has less computational load, so it is better suited for online applications, while the UKF is easier to implement for offline applications since no Jacobian matrices need to be calculated.

This sensitivity analysis led the research direction towards the topic of estimation stability, which is the second major topic of this dissertation. The stability and convergence properties of both the linear Kalman Filter and the EKF were considered from both theoretical and practical perspectives. The existing stability research concepts

were first applied to our example problem and experimental data, thus yielding unrealistic requirements on the system in order to guarantee the stability of the estimation. This prompted an effort to relax these strict conditions in order to demonstrate the stability under more realistic situations. This effort allowed for significant reduction in the required bounds on the initial error and noise disturbances; however these values were still too strict for realistic application. This stability analysis utilized the stochastic stability lemma and a quadratic Lyapunov function of the estimation error and the inverse covariance matrix with an additive linearization error model. A multiplicative linearization error model was also considered, thus providing an alternative method to analyzing the stability of an EKF. This method, however, did not provide any additional benefit in terms of required stability conditions.

This work provided an initial study of nonlinear state estimation stability and convergence, thus discovering more knowledge about the intricacies of this problem. This research, however, requires further effort in order to satisfy the desired goal of understanding the theoretical stability requirements for real engineering applications. The work in this dissertation is limited to the use of the stochastic stability lemma in conjunction with the quadratic form Lyapunov function that is commonly considered for estimation stability analysis. Based on the conclusions of this work, it seems that in order to gain significant ground regarding realistic conditions for nonlinear estimation stability, other Lyapunov functions should be considered. Additionally, different stability analysis techniques should be considered, since the stochastic stability lemma may also be limiting the analysis.

## REFERENCES


[1] F. L. Lewis and V. L. Syrmos, *Optimal Control*, 2nd Ed., Wiley, NY, 1995.

[2] R. E. Kalman, "A New Approach to Linear Filtering and Prediction Problems," *Trans. of the ASME – Journal of Basic Engineering*, March 1960, pp. 35-45.

[3] R. E. Kalman, "New methods in Wiener filtering theory," *Proc. 1st Symp. on Engr. Applications of Random Function Theory and Probability*, J. L. Bogdanoff and F. Kozin, Eds. Wiley, New York, 1963.

[4] J. J. Deyst, Jr. and C. F. Price, "Conditions for Asymptotic Stability of the Discrete Minimum-Variance Linear Estimator," *IEEE Trans. on Automatic Control*, December, 1968.

[5] J. J. Deyst, Jr., "Correction to „Conditions for Asymptotic Stability of the Discrete Minimum-Variance Linear Estimator"," *IEEE Trans. on Automatic Control*, October, 1973.

[6] A. H. Jazwinski, *Stochastic Processes and Filtering Theory*, Academic, New York, 1970.

[7] J. L. Crassidis and J. L. Junkins, *Optimal Estimation of Dynamic Systems*, CRC Press, Boca Raton, 2004, Chap. 5.

[8] R. E. Kalman and R. S. Bucy, "New Results in Linear Filtering and Prediction Theory," *Journal of Basic Engineering (Trans. of ASME)*, Vol. 83, 1961, pp. 95-108.

[9] L. Perea, J. How, L. Breger, and P. Elosegui, "Nonlinearity in Sensor Fusion: Divergence Issues in EKF, modified truncated SOF, and UKF," *AIAA Guidance, Navigation and Control Conference and Exhibit*, Hilton Head, SC, Aug., 2007.

[10] S. Julier and J. Uhlmann, "A New Extension of the Kalman Filter to Nonlinear Systems," *SPIE Proceedings Series*, Vol. 3068, 1997, pp. 182-193.

[11] R. van der Merwe, E. Wan, and S. Julier, "Sigma-Point Kalman Filters for Nonlinear Estimation and Sensor Fusion- Applications to Integrated Navigation." *AIAA Guidance, Navigation and Control Conference*, Providence, RI, 2004.

[12] M. C. VanDyke, J. L. Schwartz, and C. D. Hall, "Unscented Kalman Filtering for Spacecraft Attitude State and Parameter Estimation," *AAS/AIAA Space Flight Mechanics Meeting*, Maui, HI, Feb. 2004.

[13] S. Sadhu, S. Mondal, M. Srinivasan, and T. K. Ghoshal, "Sigma point Kalman filter for bearing only tracking," *Signal Processing*, vol. 86, no. 12, April 2006, pp. 3769-3777.

[14] J. Gross, Y. Gu, M. Rhudy, S. Gururajan, and M. Napolitano, "Flight Test Evaluation of Sensor Fusion Algorithms for Attitude Estimation," *IEEE Trans. on Aerospace Electronic Systems*, Vol. 48, No. 3, July 2012, pp. 2128-2139.

[15] M. Rhudy, Y. Gu, J. Gross, and M. Napolitano, "Sensitivity Analysis of EKF and UKF in GPS/INS Sensor Fusion," *AIAA Guidance, Navigation and Control Conference*, Portland, OR, 2011.

[16] M. Rhudy, Y. Gu, J. Gross, S. Gururajan, and M. R. Napolitano, "Sensitivity Analysis of Extended and Unscented Kalman Filters for Attitude Estimation,"

*AIAA Journal of Aerospace Information Systems*, Vol. 10, No. 3, March 2013, pp. 131-143.

[17] M. Rhudy, Y. Gu, J. Gross, and M. R. Napolitano, "Evaluation of Matrix Square Root Operations for UKF within a UAV GPS/INS Sensor Fusion Application," *International Journal of Navigation and Observation*, Vol. 2011, Article ID 416828, 11 pages, Dec. 2011. doi:10.1155/2011/416828.

[18] M. Rhudy, Y. Gu, and M. R. Napolitano, "An Analytical Approach for Comparing Linearization Methods in EKF and UKF," *International Journal of Advanced Robotic Systems*, Vol. 10, No. 208, 2013.

[19] M. Rhudy, Y. Gu, and M. R. Napolitano, "Does the Unscented Kalman Filter Converge Faster than the Extended Kalman Filter? A Counter Example," *AIAA Guidance, Navigation, and Control Conference*, Boston, MA, August 2013.

[20] R. J. Fitzgerald, "Divergence of the Kalman Filter," *IEEE Trans. on Automatic Control*, Vol. AC-16, No. 6, December, 1971.

[21] H. W. Sorenson, "On the Error Behavior in Linear Minimum Variance Estimation Problems," *IEEE Trans. on Automatic Control*, Vol. AC-12, No. 5, October, 1967.

[22] K. L. Hitz, T. E. Fortmann, and B. D. O. Anderson, "A Note on Bounds on Solutions of the Riccati Equation," *IEEE Trans. on Automatic Control*, Vol. AC-17, February, 1972.

[23] E. Tse, "Observer-Estimators for Discrete-Time Systems," *IEEE Trans. on Automatic Control*, Vol. AC-18, No. 1, February 1973.

[24] L. Guo, "Estimating Time-Varying Parameters by the Kalman Filter Based Algorithm: Stability and Convergence," *IEEE Trans. on Automatic Control*, Vol. 35, No. 2, February, 1990.

[25] S. W. Chan, G. C. Goodwin, and K. S. Sin, "Convergence Properties of the Riccati Difference Equation in Optimal Filtering of Nonstabilizable Systems," *IEEE Trans. on Automatic Control*, Vol. AC-29, No. 2, February, 1984.

[26] E. F. Costa and A. Astolfi, "On the Stability of the Recursive Kalman Filter for Linear Time-Invariant Systems," *American Control Conference*, Seattle, WA, June, 2008.

[27] J. B. Moore and B. D. O. Anderson, "Coping with singular transition matrices in estimation and control stability theory," Int. J. Control, Vol. 31, No. 3, 1980, pp. 571-586.

[28] L. Ljung, "Analysis of Recursive Stochastic Algorithms," *IEEE Trans. on Automatic Control*, Vol. AC-22, No. 4, August, 1977.

[29] L. Ljung, "Asymptotic Behavior of the Extended Kalman Filter as a Parameter Estimator for Linear Systems," *IEEE Trans. on Automatic Control*, Vol. AC-24, No. 1, February, 1979.

[30] J. S. Baras, A. Bensoussan, and M. R. James, "Dynamic Observers as Asymptotic Limits of Recursive Filters: Special Cases," SIAM J. Appl. Math., Vol. 48, No. 5, October, 1988, pp. 1147-1158.

[31] J. W. Grizzle and P. E. Moraal, "Newton, Observers and Nonlinear Discrete-time Control," *Proc. of the 29th Conference on Decision and Control*, Honolulu, HI, December, 1990.

[32] Y. Song and J. W. Grizzle, "The Extended Kalman Filter as a Local Asymptotic Observer for Discrete-Time Nonlinear Systems," *Journal of Mathematical Systems, Estimation, and Control*, Vol. 5, No. 1, 1995, pp. 59-78.

[33] B. F. La Scala, R. R. Bitmead, and M. R. James, "Conditions for Stability of the Extended Kalman Filter and Their Application to the Frequency Tracking Problem," *Math. Controls Signals Systems*, Vol. 8, 1995.

[34] M. Boutayeb, H. Rafaralahy, and M. Darouach, "Convergence Analysis of the Extended Kalman Filter Used as an Observer for Nonlinear Deterministic Discrete-Time Systems," *IEEE Trans. on Automatic Control*, Vol. 42, No. 4, April, 1997.

[35] K. Xiong, H. Y. Zhang, and C. W. Chan, "Performance Evaluation of UKF-based nonlinear filtering," *Automatica*, Vol. 42, 2006, pp. 261-270.

[36] Y. Wu, D. Hu, and X. Hu, Comments on "Performance Evaluation of UKF-based nonlinear filtering," *Automatica*, Vol. 43, 2007, pp. 567-568.

[37] J. Xu, G. M. Dimirovski, Y. Jing, and C. Shen, "UKF Design and Stability for Nonlinear Stochastic Systems with Correlated Noises," *Proc. of the 46th IEEE Conference on Decision and Control*, New Orleans, LA, Dec. 12-14, 2007, pp. 6226-6231.

[38] K. Reif, F. Sonnemann, and R. Unbehauen, "Modification of the Extended Kalman Filter with an Additive Term of Instability," *Proc. of the 35th Conference on Decision and Control*, Kobe, Japan, December, 1996.

[39] K. Reif, F. Sonnemann, and R. Unbehauen, "An EKF-Based Nonlinear Observer with a Prescribed Degree of Stability," *Automatica*, Vol. 34, No. 9, 1998, pp. 1119-1123.

[40] K. Reif, S. Günther, E. Yaz, and R. Unbehauen, "Stochastic Stability of the Discrete-Time Extended Kalman Filter," *IEEE Trans. on Automatic Control*, Vol. 44, No. 4, April, 1999.

[41] K. Reif and R. Unbehauen, "The Extended Kalman Filter as an Exponential Observer for Nonlinear Systems," *IEEE Trans. on Signal Processing*, Vol. 47, No. 8, August, 1999.

[42] K. Reif, S. Günther, E. Yaz, and R. Unbehauen, "Stochastic Stability of the Continuous-Time Extended Kalman Filter," *IEEE Proc. Control Theory Applications*, Vol. 147, No. 1, January, 2000.

[43] S. Kluge, K. Reif, and M. Brokate, "Stochastic Stability of the Extended Kalman Filter With Intermittent Observations," *IEEE Trans. on Automatic Control*, Vol. 55, No. 2, 2010, pp. 514-518.

[44] T. L. Song and J. L. Speyer, "A Stochastic Analysis of a Modified Gain Extended Kalman Filter with Applications to Estimation with Bearings Only Measurements," *IEEE Trans. on Automatic Control*, Vol. AC-30, No. 10, October 1985, pp. 940-949.

[45] E. K. Babacan, L. Ozbek, and M. Efe, "Stability of the Extended Kalman Filter When the States are Constrained," *IEEE Trans. on Automatic Control*, Vol. 53, No. 11, December, 2008.

[46] M. Boutayeb and D. Aubry, "A Strong Tracking Extended Kalman Observer for Nonlinear Discrete-Time Systems," *IEEE Trans. on Automatic Control*, Vol. 44, No. 8, Aug., 1999.

[47] J. E. Slotine and W. Li, *Applied Nonlinear Control*, Prentice Hall, NJ, 1991.
[48] D. A. McQuarrie, *Mathematical Methods for Scientists and Engineers*, University Science Books, CA, 2003.
[49] C. Chen, *Linear System Theory and Design*, 3rd Ed., Oxford University Press, NY, 1999.
[50] W. M. Haddad and V. Chellaboina, *Nonlinear Dynamical Systems and Control: A Lyapunov-Based Approach*, Princeton University Press, 2008.
[51] X. Liao, L. Wang, and P. Yu, *Stability of Dynamical Systems*, 1st Ed., Elsevier, 2007.
[52] W. E. Boyce and R. C. DiPrima, *Elementary Differential Equations and Boundary Value Problems*, 8th Ed., John Wiley & Sons, 2005.
[53] E. Kreyszig, *Advanced Engineering Mathematics*, 9th Ed., Wiley, NY, 2006.
[54] B. T. Kulakowski, J. F. Gardner, and J. L. Shearer, *Dynamic Modeling and Control of Engineering Systems*, 3rd Ed., Cambridge University Press, 2007.
[55] M. Vidyasagar, *Nonlinear Systems Analysis*, 2nd Ed., Prentice-Hall, 2002.
[56] R. P. Agarwal and D. O'Regan, *An Introduction to Ordinary Differential Equations*, 1st Ed., Springer, 2008.
[57] R. E. Kalman and J. E. Bertram, "Control System Analysis and Design via the Second Method of Lyapunov, II Discrete-Time Systems," *Journal of Basic Engineering (Trans. of ASME),* June, 1960, pp. 394.
[58] V. M. Popov, *Hyperstability of control systems*. Springer-Verlag, NY, 1973.
[59] K. S. Narendra and A. M. Annaswamy, *Stable Adaptive Systems*. Prentice-Hall, NJ, 1989.
[60] N. Hovakimyan and C. Cao, *$L_1$ Adaptive Control Theory: Guaranteed Robustness with Fast Adaptation*, SIAM, PA, 2010.
[61] W. S. Slaughter, *The Linearized Theory of Elasticity*, Birkhäuser, Boston, 2002.
[62] D. Simon, *Optimal State Estimation*, Wiley, New York, 2006.
[63] M. S. Grewal and A. P. Andrews, *Kalman Filtering: Theory and Practice Using MATLAB*, 2nd Ed., Wiley, New York, 2001.
[64] R. G. Agniel and E. I. Jury, "Almost Sure Boundedness of Randomly Sampled Systems," *SIAM J. Control*, Vol. 9, No. 3, August 1971, pp. 372-384.
[65] T. Tarn and Y. Rasis, "Observers for Nonlinear Stochastic Systems," *IEEE Trans. on Automatic Control*, Vol. AC-21, No. 4, August 1976, pp. 441-448.
[66] B. D. O. Anderson, R. R. Bitmead, C. R. Johnson, Jr., P. V. Kokotovic, R. L. Kosut, I. M. Y. Mareels, L. Praly, and B. D. Riedle. *Stability of Adaptive Systems: Passivity and Averaging Analysis*. M.I.T. Press, Cambridge, MA, 1986.
[67] L. Changchun, S. Li, W. Hai-bo, L. Tianjie, "The Research on Unmanned Aerial Vehicle Remote Sensing and Its Applications," *Proc. of the IEEE 2010 International Conference on Advanced Computer Control (ICACC)*, Shenyang, 2010, pp. 644-647.
[68] A. Jensen, M. Baumann, and Y. Chen, "Low-Cost Multispectral Aerial Imaging using Autonomous Runway-Free Small Flying Wing Vehicles,". *of the IEEE International Geoscience and Remote Sensing Symposium (IGARSS)*, Boston, 2008, pp.506-509.

[69] M. Nagai, T. Chen, R. Shibasaki, H. Kumagai, and A. Ahmed, "UAV-Borne 3-D Mapping System by Multisensor Integration," *IEEE Trans. on Geoscience and Remote Sensing*, March 2009, Issue 3, Vol. 47, pp. 701-708.

[70] T. Suzuki, Y. Amano, and T. Hashizym, "Vision Based Localization of a Small UAV for Generating a Large Mosaic Image," *Proc. of 2010 SICE Annual Conference*, Taipei, 2010, pp. 2960-2964.

[71] S. Dascalu, "Remote Sensing Using Autonomous UAVs Suitable for Less Developed Countries," *The International Archives of the Photogrammetry, Remote Sensing and Spatial Information Sciences*, Enschede, Netherlands, May 2006, Issue XXX, Vol. 34.

[72] G. Zhou and D. Zang, "Civil UAV System for Earth Observation," *Proc. of the IEEE International Geoscience and Remote Sensing Symposium (IGARSS)*, Barcelona, 2007.

[73] J. Everaerts, "The Use of Unmanned Aerial Vehicles (UAVs) for Remote Sensing and Mapping," *The International Archives of the Photogrammetry, Remote Sensing and Spatial Information Sciences*, Beijing, 2008, Issue B1, Vol. XXXVI, pp. 1187-1192.

[74] M. S. Grewal, L. R. Weill, and A. P. Andrew, *Global Positioning, Inertial Navigation & Integration*, 2nd Ed, Wiley, NY, 2007.

[75] E. Kaplan and C. Heagarty, *Understanding GPS Principles and Applications*, 2nd Ed., Arttech House, Norwood, MA, 2006.

[76] M. S. Arulampalam, S. Maskell, N. Gordon, and T. Clapp, "A Tutorial on Particle Filters for Online Nonlinear/Non-Gaussian Bayesian Tracking," IEEE Trans. on Signal Processing, Vol. 50, No. 2, Feb. 2002, pp. 174-188.

[77] F. Gustafsson, F. Gunnarsson, N. Bergman, U. Forssel, J. Jansson, R. Karlsson, and P. Nordlund, "Particle Filters for Positioning, Navigation, and Tracking," IEEE Trans. on Signal Processing, Vol. 50, No. 2, Feb. 2002, pp. 425-437.

[78] J. L. Crassidis, "Sigma-Point Kalman Filtering for Integrated GPS and Inertial Navigation," *AIAA Guidance, Navigation and Control Conference and Exhibit*, San Francisco, CA, 2005.

[79] T. Fiorenzani, C. Manes, G. Oriolo, and P. Peliti, "Comparative Study of Unscented Kalman Filter and Extended Kalman Filter for Position/Attitude Estimation in Unmanned Aerial Vehicles," *IASI-CNR*, R. 08-08, 2008.

[80] B. L. Stevens and F. L. Lewis, *Aircraft Control and Simulation*, 2nd Ed., Wiley, NJ, 2003.

[81] J. Roskam, *Airplane Flight Dynamics and Automatic Flight Controls*, DARcorporation, Lawrence, KS, 2003.

[82] D. B., Kingston and R. W. Beard, "Real-Time Attitude and Position Estimation for Small UAVs Using Low-Cost Sensors," *AIAA 3rd Unmanned Unlimited Systems Conference and Workshop*, AIAA-2004-6488, Chicago, IL, Sept. 2004.

[83] J. N. Gross, Y. Gu, M. Rhudy, F. J. Barchesky, and M. R. Napolitano, "On-line Modeling and Calibration of Low-Cost Navigation Sensors," *AIAA Modeling and Simulation Technologies Conference*, Portland, 2011.

[84] Z. Xing and D. Gebre-Egziabher, "Modeling and Bounding Low Cost Inertial Sensor Errors," IEEE/ION Position, Location and Navigation Symposium, Monterey, CA, 2008, pp. 1122-1132.

[85] Z. Xing, "Over-bounding Integrated INS/GNSS Output Errors," PhD Dissertation, The University of Minnesota, Minneapolis, 2010.

[86] A. G. O. Mutambara and H. F. Durrant-Whyte, "Estimation and Control for a Modular Wheeled Mobile Robot," *IEEE Trans. on Control Systems Technology*, Vol. 8, No. 1, January, 2000.

[87] D. Lee, "Nonlinear Estimation and Multiple Sensor Fusion Using Unscented Information Filtering," *IEEE Signal Processing Letters*, 2008.

[88] M. Rhudy, J. Gross, Y. Gu, and M. R. Napolitano, "Fusion of GPS and Redundant IMU Data for Attitude Estimation," *AIAA Guidance Navigation and Control Conference*, AIAA-2012-5030, Minneapolis, MN, August 2012.

[89] C. E. Cohen, B. D. McNally, and B. W. Parkinson, "Flight Tests of Attitude Determination Using GPS Compared Against an Inertial Navigation Unit," *Proc. of the Institute of Navigation National Technical Meeting*, San Francisco, CA, Jan. 1993, pp. 579-587.

[90] D. Gebre-Egziabher, R. C. Hayward, and J. D. Powell, "A Low-Cost GPS/Inertial Attitude Heading Reference System (AHRS) for General Aviation Purposes," *Proc. of the IEEE Position, Location, and Navigation Symposium*, April 1998, pp. 518-525.

[91] R. C. Hayward, D. Gebre-Egziabher, M. Schwall, J. D. Powell, and J. Wilson, "Inertially Aided GPS Based Attitude Heading Reference System (AHRS) for General Aviation Aircraft," *Proc. of the Institute of Navigation ION-GPS Conference*, Kansas City, MO, Sept. 1997, pp. 289-298.

[92] A. K. Barows, D. Gebre-Egziabher, R. Hayward, R. Xia, and J. D. Powell, "GPS-Based Attitude and Guidance Displays for General Aviation," *IEEE Emerging Technologies and Factory Automation*, 1996, pp. 423-428.

[93] Y. Li, K. Zhang, C. Roberts, and M. Murata, "On-the-fly GPS-based attitude determination using single- and double-differenced carrier phase measurements," *GPS Solutions*, Vol. 8, 2004, pp. 93-102.

[94] G. Lachapelle, M. E. Cannon, G. Lu, and B. Loncarevic, "Shipborne GPS Attitude Determination During MMST-93," *IEEE Journal of Oceanic Engineering*, Vol. 21, No. 1, Jan. 1996, pp. 100-105.

[95] G. Lu, M. E. Cannon, and G. Lachapelle, "Attitude Determination in a Survey Launch Using Multi-Antenna GPS Technologies," *Proc. of the Institute of Navigation National Technical Meeting*, San Francisco, CA, Jan. 1993, pp. 251-260.

[96] G. Lu, "Development of a GPS Multi-Antenna System for Attitude Determination," *PhD Thesis*, University of Calgary, Jan. 1995.

[97] H. Bian, Z. Jin, and W. Tian, "Study on GPS attitude determination system aided INS using adaptive Kalman Filter," *Institute of Physics Publishing: Measurement Science*, Vol. 16, 2005, pp. 2072-2079.

[98] J. C. McMillan, D. A. G. Arden, G. Lachapelle, and G. Lu, "Dynamic GPS Attitude Performance Using INS/GPS Reference," *ION GPS*, Salt Lake City, UT, Sept. 1994.

[99] J. C. McMillan, "A GPS Attitude Error Model for Kalman Filtering," *Proc. of the Position Location and Navigation Symposium*, Las Vegas, NV, April 1994.

[100] C. Hide, J. Pinchin, and D. Park, "Development of a Low Cost Multiple GPS Antenna Attitude System," *Proc. of the 20th International Technical Meeting of the Satellite Division of the Institute of Navigation*, Fort Worth, TX, Sept. 2007, pp. 88-95.

[101] J. Jan and C. Kee, "Flight Test of Attitude Determination System using Multiple GPS Antennae," *Journal of Navigation*, Vol. 59, No. 01, 2006, pp. 119-133.

[102] D. M. Bevly, A. Rekow, and B. Parkinson, "Comparison of INS vs Carrier-phase DGPS for Attitude Determination in the Control of Off-Road Vehicles," *Journal of Navigation*, Vol. 47, No. 4, 2001, pp. 257-266.

[103] D. Lin, L. Keck Voon, H. Guo Rong, and N. Nagarajan, "GPS-based Attitude Determination for Microsatellite Using Three-Antenna Technology," *IEEE Aerospace Conference Proceedings*, Vol. 2, 2004, pp. 1024-1029.

[104] M. Ziebart and P. Cross, "LEO GPS attitude determination algorithm for a micro-satellite using boom-arm deployed antennas," *GPS Solutions*, Vol. 6, 2003, pp. 242-256.

[105] B. Wang, L. Miao, S. Wang, and J. Shen, "A Constrained LAMBDA method for GPS attitude determination," *GPS Solutions*, Vol. 13, 2009, pp. 97-106.

[106] J. Xu, T. Arslan, D. Wan, and Q. Wang, "GPS Attitude Determination Using a Genetic Algorithm," *Congress on Evolutionary Computation*, Vol. 1, May 2002, pp. 998-1002.

[107] S. Hong, J. Y. Choi, C. S. Kim, M. H. Lee, and J. Speyer, "Estimation Errors in INS with Multiple GPS Antennas," *The 27th Annual Conference of the IEEE Industrial Electronics Society*, 2001, pp. 410-415.

[108] S. Hong, M. H. Lee, J. Rios, and J. Speyer, "Observability Analysis of GPS Aided INS," *Proc. of the Institute of Navigation ION-GPS Conference*, Salt Lake City, UT, Sept. 2000, pp. 2618-2624.

[109] A. Morales-Reyes, N. Haridas, A. T. Erdogan, and T. Arslan, "Fault Tolerant and Adaptive GPS Attitude Determination System," *IEEE Aerospace Conference Proceedings*, March 2009.

[110] J. Xu, T. Arslan, Q. Wang, and D. Wan, "An EHW Architecture for Real-Time GPS Attitude Determination Based on Parallel Genetic Algorithm," *Conference on Evolvable Hardware NASA/DoD*, Vol. 1, 2002, pp. 133-141.

[111] M. Rhudy, Y. Gu, and M. R. Napolitano, "Low-Cost Loosely-Coupled Dual GPS/INS for Attitude Estimation with Application to a Small UAV," *AIAA Guidance, Navigation, and Control Conference*, Boston, MA, August 2013.

[112] M. Rhudy, T. Larrabee, H. Chao, Y. Gu, and M. R. Napolitano, "UAV Attitude Heading, and Wind Estimation Using GPS/INS and Relative Wind Measurements," *AIAA Guidance Navigation and Control Conference*, Boston, MA, August, 2013.

[113] M. Euston, P. Coote, R. Mahony, J. Kim, and T. Hamel, "A Complementary Filter for Attitude Estimation of a Fixed-Wing UAV," IEEE International Conference on Intelligent Robots and Systems, Sept. 2008, pp. 340-345.

[114] Y. Gu, B. Seanor, G. Campa, M. R. Napolitano, S. Gururajan, and L. Rowe, "Autonomous Formation Flight: Hardware Development." *Mediterranean Control Conference*, Ancona, Italy, 2006.

[115] B. Seanor, Y. Gu, M. R. Napolitano, G. Campa, S. Gururajan, and L. Rowe, "3 Aircraft Formation Flight Experiment." *Mediterranean Control Conference*, Ancona, Italy, 2006.

[116] Y. Gu, *et al.*, "Design and Flight Testing Evaluation of Formation Flight Control Laws." *IEEE Transactions on Control Systems Technology*, 2006, pp. 1105-1112.

[117] M. Perhinschi, J. Burken, and G. Campa, "Comparison of Different Neural Augmentations for the Fault Tolerant Control Laws of the WVU YF-22 Model Aircraft." *Mediterranean Control Conference*, Ancona, Italy, 2006.

[118] J. Gross, Y. Gu, B. Seanor, S. Gururajan, and M. R. Napolitano, "Advanced Research Intergrated Avionics (ARIA) System for Fault-Tolerant Flight Research." *AIAA Guidance, Navigation and Controls Conference and Exhibit*, Chicago, 2009.

[119] F. Orderud, "Comparison of Kalman Filter Estimation Approaches for State Space Models with Nonlinear Measurements," *Proc. of Scandinavian Conference on Simulation and Modeling*, 2005.

[120] W. Wang, S. Liao, and T. Xing, "The Unscented Kalman Filter for State Estimation of 3-Dimension Bearing-Only Tracking," International Conference on Information Engineering and Computer Science (ICIECS), Wuhan, China, Dec. 2009.

[121] D. H. Won, S. Yun, Y. J. Lee, and S. Sung, "System Modeling and Non-linear Estimation Performance Comparison of Monocular Vision Based Integrated Navigation System," *Appl. Math. Inf. Sci.*, Vol. 6, No. xx, Jan. 2012.

[122] T. Nick, J. Goetze, W. John, and G. Stoenner, "Comparison of Extended and Unscented Kalman Filter for Localization of Passive UHF RFID Labels," *General Assembly and Scientific Symposium 2011 XXXth URSI*, Aug. 2011.

[123] S. S. Haykin, "The Unscented Kalman Filter," in *Kalman Filtering and Neural Networks*, New York: Wiley, 2001.

[124] R. Kandepu, B. Foss, and L. Imsland, "Applying the unscented Kalman filter for nonlinear state estimation," *Journal of Process Control*, Vol. 18, no. 7/8, Aug. 2008, pp. 753-768.

[125] N. B. Stastny, R. A. Bettinger, and F. R. Chavez, "Comparison of the Extended and Unscented Kalman Filters for Angles Based Relative Navigation," *AIAA/AAS Astrodynamics Specialist Conf. and Exhibit*, Honolulu, HI, 2008, pp. 2270-2279.

[126] B. Akin, U. Orguner, and A. Ersak, "State Estimation of Induction Motor Using Unscented Kalman Filter," *IEEE Trans. on Control Applications*, Jan. 2003, pp. 915-919.

[127] G. Chowdhary, and R. Jategaonkar, "Aerodynamic parameter estimation from flight data applying extended and unscented Kalman filter," *Aerospace Science and Technology*, Vol. 14, 2010, pp. 106-117

[128] A. Giannitrapani, N. Ceccarelli, F. Scortecci, and A. Garulli, "Comparison of EKF and UKF for spacecraft localization via angle measurements," *IEEE Trans. on Aerospace and Electronic Systems*, Vol. 47, No. 1, pp. 75-84, Jan. 2011.

[129] J. Kim, S. S. Vaddi, P. K. Menon, and E. J. Ohlmeyer, "Comparison Between Nonlinear Filtering Techniques for Spiraling Ballistic Missile State Estimation," *IEEE Trans. on Aerospace and Electronic Systems*, Vol. 48, No. 1, Jan. 2012.

[130] B. Saulson and K. C. Chang, "Comparison of Nonlinear Estimation for Ballistic Missile Tracking," *Signal Processing, Sensor Fusion, and Target Recognition XII*, Vol. 5096, pp. 13-24, 2003.

[131] J. J. LaViola Jr., "A Comparison of Unscented and Extended Kalman Filtering for Estimating Quaternion Motion," *Proc. of the American Control Conference*, Denver, CO, June, 2003, pp. 2435-2440.

[132] J. Wendel, J. Metzger, R. Moenikes, A. Maier, and G. F. Trommer, "A Performance Comparison of Tightly Coupled GPS/INS Navigation Systems Based on Extended and Sigma Point Kalman Filters." *Journal of the Institute of Navigation*, Vol. 53, No. 1, 2006.

[133] N. El-Sheimy, E. Shin, and X. Niu, "Kalman Filter Face-Off: Extended vs. Unscented Kalman Filters for Integrated GPS and MEMS Inertial," *Inside GNSS*, 2006, pp. 48-54.

[134] M. St. Pierre and D. Ing, "Comparison between the unscented Kalman filter and the extended Kalman filter for the position estimation module of an integrated navigation information system" *IEEE Intelligent Vehicles Symposium*, Parma, Italy, June 2004.

[135] J. L. Crassidis and F. L. Markley, "Unscented Filtering for Spacecraft Attitude Estimation," *Journal of Guidance, Control, and Dynamics*, Vol. 26, No. 4, 2003, pp. 536-542.

[136] Gelb, "Suboptimal Filter Design and Sensitivity Analysis," in *Applied Optimal Estimation*, MIT Press, Cambridge, MA, 1974.

[137] A. Noureldin, R. Sharaf, A. Osman, and N. El-Sheimy, "INS/GPS Data Fusion Technique Utilizing Radial Basis Functions Neural Networks," *Proc. of IEEE Position, Location, and Navigation Symposium*, Monterey, CA, 2004, pp. 280-284.

[138] U. Iqbal, A. F. Okou, and A. Noureldin, "An Integrated Reduced Inertial Sensor System – RISS/GPS for Land Vehicle," *Proc. of IEEE/ION Position, Location, and Navigation Symposium*, Monterey, CA, May 2008, pp. 1014-1021.

[139] O. S. Salychev, V. V. Voronov, M. E. Cannon, R. Nayak, and G. Lachapelle, "Low Cost INS/GPS Integration: Concepts and Testing," *Institute of Navigation National Technical Meeting*, Anaheim, CA, Jan., 2000.

[140] B. M. Scherzinger, "Precise Robust Positioning with Inertial/GPS RTK," *Proc. of the ION-GPS-2000*, Salt Lake City, UT, Sept. 2000.

[141] J. Wendel, O. Meister, C. Schlaile, and G. F. Trommer, "An integrated GPS/MEMS-IMU navigation system for an autonomous helicopter," *Aerospace Science and Technology*, vol. 10, no. 1016, 2006, pp. 527-533.

[142] C. Boucher, A. Lahrech, and J. C. Noyer, "Non-linear filtering for land vehicle navigation with GPS outage," *IEEE International Conference on Systems, Man, and Cybernetics*, 2004, pp. 1321-1325.

[143] M. G. Petovello, *et al.*, "Development and Testing of a Real-Time GPS/INS Reference System for Autonomous Automobile Navigation," *Proceedings of ION GPS-01*, Salt Lake City, UT, 2001.

[144] J. Ryu and J. C. Gerdes, "Integrating Inertial Sensors With Global Positioning System (GPS) for Vehicle Dynamics Control," *ASME Journal of Dynamic Systems, Measurement, and Control*, Vol. 126, 2004, pp. 243-254.

[145] D. M. Bevly, J. Ryu, and J. C. Gerdes, "Integrating INS Sensors With GPS Measurements for Continuous Estimation of Vehicle Sideslip, Roll, and Tire Cornering Stiffness," *IEEE Transactions on Intelligent Transportation Systems*, Vol. 7, No. 4, 2006, pp. 483-493.

[146] J. Ryu, E. J. Rossetter, and J. C. Gerdes, "Vehicle Sideslip and Roll Parameter Estimation using GPS," *AVEC 2002 6th Int. Symposium on Advanced Vehicle Control*, Hiroshima, Japan, 2002.

[147] International Association of Geodesy, 1971, *Geodetic Reference System 1967: International Association of Geodesy Special Publication*, No. 3, pp. 116.

[148] R. J. Blakely, *Potential Theory in Gravity and Magnetic Applications*, Cambridge University Press, New York, NY, 1996, pp. 140.

[149] R. van der Merwe and E. A. Wan, "The Square-Root Unscented Kalman Filter for State and Parameter Estimation," *Proceedings of the International Conference on Acoustics, Speech, and Signal Processing*, Salt Lake City, UT, 2001.

[150] N. J. Higham, *Functions of Matrices: Theory and Computation, Society for Industrial and Applied Mathematics (SIAM)*, Philadelphia, PA, 2008.

[151] Y. Wu, D. Hu, M. Wu, and X. Hu, "Unscented Kalman Filtering for Additive Noise Case: Augmented vs. Non-augmented," *American Control Conference*, Portland, OR, 2005.

[152] F. Sun, G. Li, and J. Wang, "Unscented Kalman Filtering using Augmented State in the Presence of Additive Noise," *IITA International Conference on Control, Automation, and Systems Engineering*, Zhangjiajie, China, 2009.

[153] S. A. Banani and M. A. Masnadi-Shirazi, "A New Version of Unscented Kalman Filter," *World Academy of Science, Engineering, and Technology*, Vol. 20, 2007, pp. 192-197.

[154] B. Meini, "The Matrix Square Root from a New Functional Perspective: Theoretical Results and Computational Issues," *SIAM J. Matrix Anal. Appl.*, Vol. 26, No. 2, pp. 362-376, 2004.

[155] M. M. Konstantinov, *Perturbation Theory for Matrix Equations*, Elsevier Science B.V., Amsterdam, The Netherlands, 2003, pp. 350.

[156] N. J. Higham, "Newton‟s Method for the Matrix Square Root," *Mathematics of Computation*, Vol. 46, No. 174, 1986, pp. 537-549.

[157] S. H. Cheng, N. J. Higham, C. S. Kenney, and A. J. Laub, "Approximating the Logarithm of a Matrix to Specified Accuracy," *SIAM J. Matrix Anal. Appl.*, Vol. 22, No. 4, pp. 1112-1125, 2001.

[158] L. N. Trefethen and D. Bau, *Numerical Linear Algebra*. 1st ed., SIAM, Philadelphia, PA, 1997.

[159] N. J. Higham, "Analysis of the Cholesky Decomposition of a Semi-definite Matrix," *Reliable Numerical Computation*, Oxford University Press, Oxford, pp. 161-185, 1990.

[160] N. J. Higham, *Accuracy and Stability of Numerical Algorithms*, 2nd Ed., Society for Industrial and Applied Mathematics (SIAM), Philadelphia, PA, 2002.

[161] D. W. Tufts and C. D. Melissinos, "Simple, Effective Computation of Principal Eigenvectors and Their Eigenvalues and Application to High-Resolution Estimation of Frequencies," *IEEE Transactions of Acoustics, Speech, and Signal Processing*, Vol. ASSP-34, No. 5, October 1986.

[162] M. Rhudy, Y. Gu, and M. R. Napolitano, "Relaxation of Initial Error and Noise Bounds for Stability of GPS/INS Attitude Estimation," *AIAA Guidance Navigation and Control Conference*, AIAA-2012-5031, Minneapolis, MN, August 2012.

[163] M. S. Arulampalam, S. Maskell, N. Gordon, and T. Clapp, "A Tutorial on Particle Filters for Online Nonlinear/Non-Gaussian Bayesian Tracking," *IEEE Trans. on Signal Processing*, Vol. 50, No. 2, Feb. 2002, pp. 174-188.

[164] R. V. Hogg, J. W. McKean, and A. T. Craig, *Introduction to Mathematical Statistics, Pearson Education*, 2005.

[165] B. E. Meserve, "Double Factorials," *Amer. Math. Monthly*, Vol. 55, pp. 425-426, 1948.

[166] B. D. O. Anderson and J. B. Moore, *Optimal Filtering*, Prentice-Hall, NJ, 1979.

[167] F. L. Lewis, *Optimal Estimation*, Wiley, NY, 1986.

[168] H. Liu, S. Shah, and W. Jiang, "On-line outlier detection and data cleaning," *Computers and Chemical Engineering*, Vol. 28, 2004, pp. 1635-1647.

[169] S. Lu, H. Lu, and W. J. Kolarik, "Multivariate performance reliability prediction in real-time," *Reliability Engineering and System Safety*, Vol. 72, 2001, pp. 39-45.

[170] D. Jwo and T. Cho, "A practical note on evaluating Kalman filter performance optimality and degradation," *Applied Mathematics and Computation*, Vol. 193, 2007, pp. 482-505.

[171] J. G. Saw, M. C. K. Yang, and T. C. Mo, "Chebyshev Inequality with Estimated Mean and Variance," *The American Statistician*, Vol. 38, No. 2, May 1984, pp. 130-132.

[172] J. L. Maryak, J. C. Spall, and B. D. Heydon, "Use of the Kalman Filter for Inference in State-Space Models with Unknown Noise Distributions," *American Control Conference*, Albuquerque, NM, June 1997, pp. 2127-2132.

[173] J. C. Spall, "The Kantorovich Inequality for Error Analysis of the Kalman Filter with Unknown Noise Distributions," *Automatica*, Vol. 31, No. 10, 1995, pp. 1513-1517.